



2019-03-01

Selective Catalysis by Polymer-Supported Ruthenium Nanoparticles AND New Ligand Design for Cooperative and Bimetallic Catalysis

Seyed Hadi Nazari
Brigham Young University

Follow this and additional works at: <https://scholarsarchive.byu.edu/etd>

BYU ScholarsArchive Citation

Nazari, Seyed Hadi, "Selective Catalysis by Polymer-Supported Ruthenium Nanoparticles AND New Ligand Design for Cooperative and Bimetallic Catalysis" (2019). *All Theses and Dissertations*. 7386.
<https://scholarsarchive.byu.edu/etd/7386>

This Dissertation is brought to you for free and open access by BYU ScholarsArchive. It has been accepted for inclusion in All Theses and Dissertations by an authorized administrator of BYU ScholarsArchive. For more information, please contact scholarsarchive@byu.edu, ellen_amatangelo@byu.edu.

Selective Catalysis by Polymer-Supported Ruthenium Nanoparticles

AND

New Ligand Design for Cooperative and Bimetallic Catalysis

Seyed Hadi Nazari

A dissertation submitted to the faculty of
Brigham Young University
in partial fulfillment of the requirements for the degree of

Doctor of Philosophy

David J. Michaelis, Chair
Steven L. Castle
Joshua L. Price
Daniel H. Ess
Roger G. Harrison

Department of Chemistry and Biochemistry

Brigham Young University

Copyright © 2019 Seyed Hadi Nazari

All Rights Reserved

ABSTRACT

Selective Catalysis by Polymer-Supported Ruthenium Nanoparticles AND New Ligand Design for Cooperative and Bimetallic Catalysis

Seyed Hadi Nazari
Department of Chemistry and Biochemistry, BYU
Doctor of Philosophy

The abstract is the summary of three different projects all centered around the general idea of catalysis which is the general theme of research in the Michaelis laboratory. The first project focuses on development of a new heterogeneous catalyst for selective catalysis. In the Michaelis lab, we were interested in the potential of nanoparticle catalysts for regioselective transformations. We showed that polymer supported ruthenium nanoparticles performed as a reliable catalyst for regioselective reduction of azide to amine. In our study of regioselective reduction of multiple azide containing substrates, we observed that in presence of our ruthenium nanoparticle catalysts, the least sterically hindered azide group reduced to amine functional group. The results were complementary to the conventional methods that employ triphenyl phosphine (Staudinger reaction) as the reductant and target the most electronically active azide group.

In the second project, we were looking to develop a new class of hetero-bimetallic Nickel-Titanium complexes as an efficient catalyst for organic transformations. We designed and synthesized numerous bidentate ligands including NHC-Phosphine ligand. Our kinetic studies on the Suzuki cross coupling of allylic alcohols and phenyl boronic esters showed that the bidentate nature of the ligand was necessary for the success of the catalytic process. The ligand was proved to stabilize the catalyst in the solution by increasing the lifetime of the nickel (0) in the reaction medium. We also discovered a new cooperative titanium-nickel system for mild allylic amination of allyl alcohols. The system also represents an ideal catalyst for tandem cyclization amination process.

In the Michaelis lab, we were also interested to explore the ability of bimetallic complexes in C-H functionalization process. Our efforts in this project led to the discovery of new Palladium dimer complexes with two palladium centers in oxidation state of (I). The catalyst showed unique reactivity in C-C bond activation/functionalization. We have also discovered that in presence of catalytic amount of triflic acid and stoichiometric amount of phenyl boronic acid, cinnamyl alcohol undergoes a boron template dimerization/cyclization. The reaction represents a great synthetic pathway for the synthesis of bis homoallylic alcohols.

Keywords: nanoparticle catalysis, nickel catalyst, regioselective reduction, C-H activation

ACKNOWLEDGEMENTS

I would like to express my sincere appreciation and gratitude to all those who helped me to finish this work and write this dissertation at Brigham Young University.

I am indebted to my family for their support without which I could not have moved through this tortuous path. I would like to thank my parents for their prayers and warm support.

Particular thanks to Prof. David J. Michaelis for his guidance during my research. Prof. Michaelis helped me to think independently, and be a better writer and researcher. The energy, enthusiasm, and encouragement I received from him have been key factors in my success.

I would also like to thank all the committee members, Dr. Josh L. Price, Steven L. Castle, Roger G. Harrison, Daniel H. Ess, and David J. Michaelis for their support and inspiring suggestions and comments through my dissertation, proposal, and annual evaluations.

I am very grateful to all the students, technicians, and Professors including, Shenglou Deng, Venkata Reddy Udumula, Ankur Jalan, Marjan Hashemi, Concordia Lo, Michael Kinghorn, Chloe Ence, Karissa Kenney, Gabriel Valdivia, Yu Cai, Erin Martinez, Jordan Tretbar, Jacob Parkman, Kari Van Sickel, Dr. Matt. A. Linford and Dr. Scott R. Burt who provided assistance during my research.

This work was mainly supported by the PRF, NSF, and Brigham Young University.

TABLE OF CONTENTS

TITLE PAGE.....	i
ABSTRACT.....	ii
ACKNOWLEDGEMENTS.....	iii
TABLE OF CONTENTS.....	iv
LIST OF FIGURES.....	viii
LIST OF TABLES.....	xiii
Chapter 1 Catalysis by Polystyrene-Supported Ruthenium Nanoparticle Catalysts.....	1
1.1 Introduction.....	1
1.2 Synthesis of Nanoparticle Catalysts: A General Overview.....	2
1.3 The Impact of Nanoparticle Shape on Catalytic Activity.....	3
1.4 The Impact of Nanoparticle Size on Catalytic Activity.....	5
1.5 Application of Polymer Incarcerated Nanoparticles in Organic Reactions.....	6
1.5.1 Asymmetric transformations with chiral modified ligand nanoparticle catalysts:	8
1.5.2 Chemo- and regioselective transformations by nanoparticle catalysts:	10
1.6 Site-Selective Alkyl and Azide Reductions with Heterogeneous Nanoparticle Catalysts	11
1.7 Results and Discussion	12
1.8 Synthesis of Aryl-Hydroxylamines via Partial Reduction of Nitroaryls with Soluble Nanoparticles	18
1.8.1 Results and discussion	18
1.9 Experimental Procedures and Supporting Data for Chemo and Site Selective Azide Reduction with Heterogeneous Nanoparticle Catalysts.	21

1.9.1	General information	21
1.9.2	Synthesis and characterization of Ru NP's@polystyrene	21
1.9.3	Preparation of the sample for ICP-analysis	22
1.9.4	Characterization of Ru/polystyrene nanoparticles	22
1.9.5	Experimental procedures	23
1.9.5.1	General procedure: reduction of (E)-1-azidohex-3-ene	23
1.9.5.2	Reuse experiments of Ru NP's@polystyrene	24
1.9.5.3	Experimental procedures and spectral data	24
1.10	Experimental Procedures and Supporting Data for the Synthesis of Arylhydroxylamines via Partial Reduction of Nitroarenes with Nanoparticle Catalysts	56
1.10.1	General information	56
1.10.2	Synthesis and characterization of Ru NP's in polystyrene	57
1.10.3	Preparation of the sample for ICP-analysis	58
1.10.4	Characterization of Ru/polystyrene nanoparticles	58
1.10.5	Experimental procedures	58
1.10.5.1	General procedure for the synthesis of N- aryl hydroxylamines:	58
1.10.5.2	Large scale reaction.....	59
1.10.5.3	Reaction time course study.....	59
1.11	References.....	68
 Chapter 2 Nickel-Catalyzed Suzuki Cross Couplings with Unprotected Allylic Alcohols Enabled by Bidentate N-Heterocyclic Carbene (NHC)/Phosphine Ligands		
2.1	Introduction.....	77
2.2	Transition Metal Catalyzed Suzuki Cross Coupling Reactions	78
2.2.1	Palladium catalyzed Suzuki cross-coupling reactions	78

2.3	Nickel-Catalyzed Suzuki Cross Couplings with Unprotected Allylic Alcohols Enabled by Bidentate N-Heterocyclic Carbene (NHC)/Phosphine Ligands.....	82
2.3.1	Results and discussion	83
2.3.2	Experimental data and supporting information for Nickel-catalyzed Suzuki cross couplings with unprotected allylic alcohols enabled by bidentate N-heterocyclic carbene (NHC)/phosphine ligands.....	88
2.3.2.1	General information	88
2.4	Synthesis of Ligands	89
2.5	References.....	105
Chapter 3 C-N Bond Formation from Allylic Alcohols via Cooperative Nickel and Titanium Catalysis		
3.1	Introduction.....	109
3.2	Results and Discussions.....	111
3.3	Experimental Procedures and Supporting Information for C–N Bond Formation from Allylic Alcohols via Cooperative Nickel and Titanium Catalysis	117
3.3.1	General information	117
3.3.1.1	Synthesis of the substrates.....	117
3.3.1.2	Optimization studies:.....	119
3.4	References.....	133
Chapter 4 Boron-Templated Dimerization of Allylic Alcohols Catalyzed by Strong Acid: Formal Difunctionalization Of Alkenes		
4.1	Introduction.....	137

4.2	Results and Discussion	140
4.3	References.....	144
Chapter 5	New Ligand Design for Bimetallic Catalysis.....	147
5.1	Introduction.....	147
5.1.1	New ligand design for regioselective transformations.....	152
5.2	References.....	158
Appendix A	Spectral images for chapter 1, 2, and 3	162

LIST OF FIGURES

Figure 1.1 Different facets of metals they crystallize in	4
Figure 1.2 Tetrahedral PdNPs catalyzed Suzuki-Miyaura coupling reaction.....	4
Figure 1.3 Tetrahedral PtNPs catalyzed Suzuki-Miyaura coupling reaction.....	5
Figure 1.4 Effect of nanoparticle size on the reactivity	5
Figure 1.5 Aerobic oxidation of alcohols by polymer incarcerated gold NPs.....	6
Figure 1.6 Synthesis and application of Pd and Ni nanoparticle catalysts in cross coupling reactions.....	7
Figure 1.7 Polymer incarcerated (PI) Au/Co NPs for amide synthesis from alcohols and amine.....	8
Figure 1.8 Selectivity of the product under different nanoparticle catalysts	8
Figure 1.9 Chemoselectivity in nitroreduction with Ru:Co (A) and electronic effects on reactivity of the catalyst (B).....	9
Figure 1.10 Asymmetric hydrogenation of amide (A) and the concept of the immobilized chiral catalyst (B).....	9
Figure 1.11 One pot sequential reaction catalyzed by two nanoparticle catalysts.....	10
Figure 1.12 Iron nanoparticle catalyzed asymmetric and regioselective addition of indoles to epoxides.....	11
Figure 1.13 Chemoselective reduction of aromatic azides	13
Figure 1.14 Chemoselective reduction of aliphatic azides	14
Figure 1.15 Chemoselective azide reduction in biomolecule synthesis.....	14
Figure 1.16 Regioselective monoazide reduction. (a) Conditions: 2mol% RuNPs Catalyst, 4eq NH ₂ NH ₂ .H ₂ O in EtOH (0.13M), 0 °C to r.t, 16h. Regioselectivity determined by HNMR analysis of the crude reaction mixture (b) Ratio of 11a:11b determined by isolated yield of each isomer.....	16

Figure 1.17 Regioselective azide reduction of polysaccharides. Conditions: 4-7mol% RuNPs Catalyst, 4-5eq NH ₂ NH ₂ .H ₂ O in EtOH (0.13M), 0 °C to r.t, 7-10h. Regioselectivity determined by HNMR analysis of the crude reaction mixture.	17
Figure 1.18 Site-selective azide reduction in aminoglycoside antibiotic derivatives including (a) Kanamycin tetraazide and (b) neamine tetraazide.	17
Figure 1.19 Substrate scope of hydroxylamine formation.....	20
Figure 1.20 Substrate scope for heteroaryl hydroxylamine formation	20
Figure 1.21 EDS spectrum of the Ru nanoparticles showing the presence of the main components Ru. Cu and C peak are background from the TEM support grid.....	22
Figure 1.22 STEM image of Ru NPs on polystyrene catalyst. (a) STEM Image and statistical analysis of original polymer-encapsulated nanoparticles. (b) STEM Image and statistical analysis of nanoparticle size of the same catalyst after recycling.....	23
Figure 1.23 <i>STEM image of Ru NPs in polystyrene catalyst. (a) STEM Image of polymer-encapsulated nanoparticles. (b) Statistical analysis of nanoparticle size (average size: 1.33 nm). STEM Scale bar = 10nm.</i>	58
Figure 1.24 Time dependent conversion of nitrobenzene to hydroxyl amine product or aniline.....	59
Figure 2.1 Application of Buchwald's ligand in Synthesis	78
Figure 2.2 Nickel-catalyzed cross coupling of aryl ethers.....	79
Figure 2.3 Nickel catalyzed cross coupling of aryl fluorides (A) late state synthesis of poly aryl ketones (B).....	80
Figure 2.4 Allylic arylation with noble metals (A) enantioselective synthesis of 1,5 diene	81
Figure 2.5 New NHC/Phosphine ligands for Suzuki cross coupling reactions	82
Figure 2.6 Synthetic route and the structures of bidentate NHC ligands	83
Figure 2.7 Crystal structure of allyl nickel complex.....	85

Figure 2.8 Substrate scope for allylic alcohol partner: (a) reaction run with 2.5 mol% Ni and 2.5 mol% L ₃ , (b) 1-propyl-2-propen-1-ol was used as starting material, and (c) reaction run with 5mol% Ni and 5mol% L ₃	85
Figure 2.9 Substrate scope for boronic ester coupling partner: (a) reaction run with 2.5 mol% Ni and 2.5 mol% L ₃ , (b) reaction run with 5mol% Ni and 5mol% L ₃	86
Figure 2.10 Tandem cyclization/cross coupling reaction: (a) run with Ni(COD) ₂ and (b) ligand L ₂ was employed in MeCN.....	87
Figure 3.1 The concept of cooperative catalysis.....	109
Figure 3.2 Regioselectivity of allylic amination with Rh, Ru, or Ir (A). regioselectivity with Ni or Pd(B).....	110
Figure 3.3 Advances in allylic amination; withPd/new ligand (A). with Nickel at lower catalyst loading (B).....	111
Figure 3.4 Allylic amination under mild conditions (A) Tandem cyclization/Amination (B).....	111
Figure 3.5 Plausible reaction mechanism for cooperative Ni/Ti catalyst.....	112
Figure 3.6 Amination of various primary and secondary alcohol substrates. (a) Reaction run with 2 mol% of Ni and 0.5 eq of Ti(O- <i>i</i> Pr) ₄ . (b) Reaction run with 5 mol% of Ni and 1eq of Ti(O- <i>i</i> Pr).....	114
Figure 3.7 Substrate scope for the amine nucleophile. (a) Reaction run with 2 mol% of Ni and 1 eq of Ti(O- <i>i</i> Pr) ₄ . (b) Reaction run with 1eq of Ti(O- <i>i</i> Pr) ₄	115
Figure 3.8 Tandem cyclization amination of diene containing substrates.....	116
Figure 4.1 Cascade polyolefine cyclization in the total synthesis of progesterone.	137
Figure 4.2 Bronsted acid catalyzed cascade reaction for the synthesis of tetrahydropyridine.....	138

Figure 4.3 Comparison of two different strategies in cyclizations; Radical Cascade (A) Bronsted acid catalyzed (B)	138
Figure 4.4 Comparison of the strategies towards the synthesis of 2-cyanoacrylamide; (A) Transition meta catalyzed hydration reaction. (B) Bronsted acid catalyzed tandem coupling hydrolysis	139
Figure 4.5 Double C(SP ³)-H bond functionalization in alkyl phenylether derivatives	140
Figure 4.6 Bronsted acid catalyzed dimerization of allyl alcohol (A) Application in natural product synthesis (B)	140
Figure 4.7 Crystal structure of the dimerization product	141
Figure 4.8 Plausible mechanism of acid catalyzed dimerization of cinnamyl alcohols	143
Figure 4.9 Substrate scope of dimerization of various allyl alcohols	143
Figure 4.10 Hydrolysis of the cyclic boronic ester product to diol.....	144
Figure 5.1 Early examples of C-H activation	147
Figure 5.2 The first example of site selective C(sp ²)-H activation	148
Figure 5.3 Regioselective cross dehydrogenative coupling.....	148
Figure 5.4 Regioselective arylation of heteroaryls using ancillary thioether ligands.....	149
Figure 5.5 Auxiliary directed C-H functionalization at Ortho (A) and metha (B) positions.....	149
Figure 5.6 Distal C-H functionalization of aliphatic amide.....	150
Figure 5.7 Distal beta C-H functionalization using removable directing group.....	150
Figure 5.8 Late stage beta C-H functionalization of oligopeptide.....	151
Figure 5.9 Beta functionalization of ketones using catalytic amount of transient directing group.....	151
Figure 5.10 Enantioselective gamma functionalization desymmetrization using auxiliary ligand	151

Figure 5.11 Cooperative heterobimetallic approach for C-H activation.....	152
Figure 5.12 New ligand design for heterobimetallic catalysis.....	153
Figure 5.13 Synthesis pathway for newly designed ligands	154
Figure 5.14 Crystal structure of the ligands (C) and (J)	155
Figure 5.15 Activity of the ligand (G) in C(SP ³)-H activation	155
Figure 5.16 Activity of the ligand (J) in C(SP ³)-H functionalization	156
Figure 5.17 Synthetic route and the crystal structure of the bimetallic complexes using ligand (J) and different metal precursors (A) Pd(OAc) ₂ , (B) PdCl ₂ , and (C) phosphinoimidazole	157
Figure 5.18 Activity of the ligand J in the Heck reaction and comparison with conventional methods	158

LIST OF TABLES

Table 1.1 Optimization studies of alkyl azide reduction.....	13
Table 1.2 Regioselective Azide Reduction	15
Table 1.3 Optimization studies of nitro arene reduction to hydroxylamine.....	19
Table 2.1 Optimization studies.....	84
Table 3.1 Optimization of the cooperative catalysis system.....	113
Table 4.1 Optimization studies of dimerization of allylic alcohols	142

Chapter 1 Catalysis by Polystyrene-Supported Ruthenium Nanoparticle Catalysts

1.1 Introduction

Catalysis is a term coined by Berzelius in 1835 to describe the properties of substances that facilitate chemical reactions without being consumed in them. It is a critical pursuit for modern chemistry and improvements in catalytic processes increase the efficiency of chemical transformations while reducing waste and decreasing environmental footprints¹. The development of modular catalytic systems, in which different parameters can be tuned for optimization of catalytic properties and reaction scope is highly desirable. Generally, there are two types of catalytic systems: heterogeneous and homogeneous catalysts. In homogeneous catalysis, the catalyst is soluble and all the reactants and the catalyst are present in the same phase. In this type of catalysts, the properties of the transition metal can be tuned by the coordinatin ligands. Therefore, selective processes are viable by using appropriate ligands. However, thermal instability and sensitivity to the air and oxygen limits their industrial applications. A heterogeneous catalytic reaction involves adsorption of reactants from a fluid phase onto a solid surface, surface reaction of adsorbed species, and then desorption of products into the liquid phase. The main advantage of using a heterogeneous catalyst is the relative ease of catalyst separation from the product stream that aids in the creation of continuous chemical processes². Additionally, heterogeneous catalysts are typically more tolerant of extreme operating conditions than their homogeneous analogues³. Also, when the structure of the catalyst surface is designed wisely, the catalyst can demonstrate selectivity that is not seen with homogeneous catalysts⁴. Nanoparticle catalysis is often described as a bridge between traditional heterogeneous and homogeneous catalysis because the reactivity and selectivity of the heterogeneous metal nanoparticles can be optimized by varying their size, shape, or solid support material⁵. This optimization process is similar to what is accomplished in homogeneous catalysis with catalyst design. Polymer-supported nanoparticles introduce a new element for catalyst optimization because the nanoparticle is known to directly interact with the polymer structure⁶. The strength of the polymer-nanoparticle interaction can be optimized by changing the structure of the polymer, providing a way to predictably alter the properties and reactivity of the nanoparticles⁷. Nanoparticle catalysts are as robust as heterogeneous catalysts and can often be recovered and recycled. In addition, nanoparticle catalysts can display the same reactivity and selectivity seen in homogeneous catalysts. Replacing homogeneous catalysts with their heterogeneous nanoparticle catalysts will enhance the sustainability of the catalytic

system, providing a highly recyclable, scalable and efficient setup. An understanding of the underlying principles for polymer-nanoparticle interactions will also aid in the development of more efficient and selective nanoparticle catalysts. A broader understanding of polymer-nanoparticle interfaces could also have widespread implications for the design and synthesis of electronically unique nanostructured materials.

The purpose of this chapter is to show that by our polymer-supported nanoparticles we can enable unprecedented reactivity and selectivity in organic reactions that is difficult to achieve with homogeneous catalysts and that take place with different regioselectivities. Specifically, the synthesis and application of polymer-incarcerated nanoparticles in organic transformations will be discussed, followed by our work in regioselective reductions with polyazide starting materials.

Keywords: Heterogeneous Catalysis, Nanoparticles, Polymer, Regioselective, Aminoglycoside, Ruthenium

1.2 Synthesis of Nanoparticle Catalysts: A General Overview

For the past several decades there have been numerous reports on the synthesis of heterogeneous nanoparticle catalysts⁸. Since the size of nanoparticles is a determining factor in their catalytic activity (smaller particles have higher overall surface area), efforts have focused on development of new strategies that reduce the size distribution and agglomeration of metal nanoparticles⁹. This requirement has imposed application of various supports including TiO₂, Al₂O₃, SiO₂, CeO₂, ZrO₂, porous zeolites or carbon nanotubes in the synthesis of nanocatalysts¹⁰⁻¹¹. In all these approaches, a strong support has been used to seat metal nanoparticles on the surface. In a typical procedure, supported metal nanoparticles are made by soaking a porous support like Al₂O₃ in an aqueous solution of a metal salt, followed by heating in air (calcination) and reduction with hydrogen gas¹². The resultant cluster consists of metal particles that spread all over the surface of the support. The exact structure of the supported nanoparticle catalysts made by this method is difficult to determine because the support surface and the size of the nanoparticles are not uniform.

Several techniques have been developed to improve the impregnation process in order to enhance the quality of the catalyst¹³. For instance, co-precipitation and deposition-precipitation techniques for the synthesis of oxide-support nanoparticles have been reported¹⁴. In a representative recipe, single-atom metal precursors are either co-precipitated with oxide precursors or directly deposited on an oxide surface¹⁴. Although the nanoparticles produced by

this method are more uniform, their size and size-distribution highly depend on the pH, the oxide support, and the temperature¹⁵. Pre-synthesized metal colloidal particles have also been used as precursors to make oxide-supported metal nanoparticle catalysts¹⁶. The colloidal nanoparticles have a broad particle-size distribution and generally precipitate on the oxide supports through mechanical mixing followed by evaporation¹⁷. As a result, the nanoparticles are not homogeneously dispersed on the oxide surface. To overcome this problem, Stucky and coworkers proposed milder reaction conditions that use weak reducing reagents like amine-borane complexes instead of strong reductants such as sodium borohydride¹⁸.

The idea of using polymers as a support for nanoparticles has been pursued for the last decade¹⁹. Specifically, polystyrene has been introduced as an electronically rich support that holds the metal through nonbonding interactions²⁰. An important advantage of polymer supports over other metal oxide sources is the ability to tune the structure of polymer. This modification includes incorporation of donating or withdrawing groups that enhances or decreases the extent of that electronic interaction respectively²¹. It is also possible to bind different ligands to the polymer and make a tailored catalyst for a variety of organic transformations²². The synthesis of polymer supported nanoparticle catalysts is also much easier compared to other supports and doesn't require harsh conditions. Recent advances in the synthesis of polymer-supported nanoparticles includes the incarceration of nanoparticles in the structure of a polymer after reducing the metal precursor with a reducing reagent²³. In a typical procedure, a mixture of a polymer and a metal ion in a higher oxidation state are mixed in a protic solvent. After addition of the reducing reagent (sodium or lithium borohydride) the mixture stirs at room temperature for several hours. Evaporation of the solvent and trituration of the solid with water and hexanes gives the polymer incarcerated metal nanoparticles. The nanoparticles made by this method have much smaller size and lower size distributions compared to other methods. Polymer-supported nanoparticles prepared in this manner have also shown regio- and chemoselectivity not observed with homogeneous catalysts.

1.3 The Impact of Nanoparticle Shape on Catalytic Activity

Catalysis by transition metal nanoparticles requires that the nanoparticle maintain a specific shape in order to maximize its catalytic activity²⁴. Shape control is crucial for tuning the properties of the nanoparticles as it controls the number of atoms located in different spots in the structure²⁵. Since metals crystallize in different crystalline structures, they form different

shapes during nanoparticle growth. Moreover, thermodynamic considerations dictate specific shapes during the crystallization process in order to minimize the surface energy. So, the actual

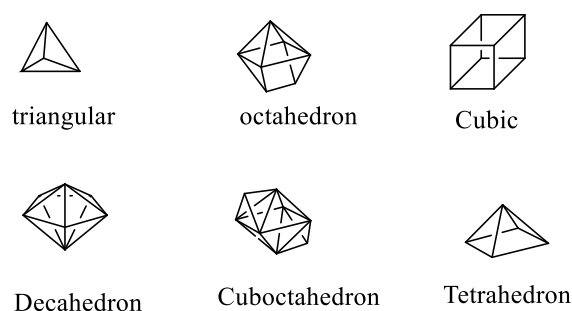


Figure 1.1 Different facets of metals they crystallize in

shape of the nanoparticles relies on the conditions under which the crystals grow. Based on thermodynamic requirements and crystallization conditions, crystals of different shapes have been grown including spheres, octahedrons, cubes, rods, wires, and prisms²⁶. For example, palladium nanoparticles with different morphologies (cubic, cuboctahedral, and octahedral) have been made²⁷ (Figure 1.1). McGlacken and coworkers²⁸ tested the catalytic activity of various palladium nanoparticles with different shapes in Suzuki-Miyaura cross coupling reactions. After some optimization studies, they realized that the activity of the nanoparticles are in the order of Octahedral > Cuboctahedral > Cube (Figure 1.2).

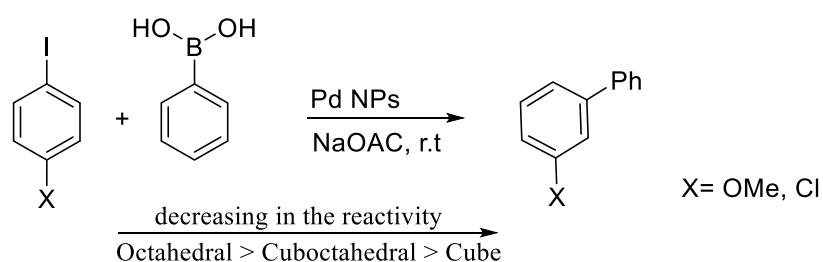


Figure 1.2 Tetrahedral PdNPs catalyzed Suzuki-Miyaura coupling reaction

In similar studies, various platinum nanoparticles were synthesized and tested in the Suzuki cross coupling reaction²⁹. The tetrahedral shape proved to be the best for this reaction (Figure 1.3). While some nanostructures with special shapes show better reactivity in certain reactions, they still suffer from loss of reactivity over time in the course of the reaction³⁰. The issue is that the shape of the nanoparticles does not remain constant during the reaction and their performance changes as the reaction proceeds.

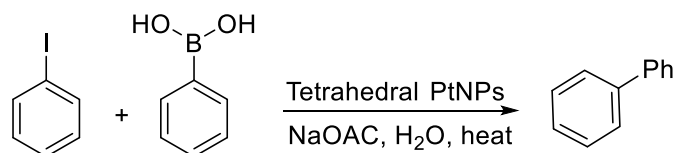


Figure 1.3 Tetrahedral PtNPs catalyzed Suzuki-Miyaura coupling reaction

1.4 The Impact of Nanoparticle Size on Catalytic Activity

The unique catalytic performance of nanoparticles stems from their nanometer size, which gives them higher surface-to-volume ratio. However, the size of nanoparticles changes over the course of a chemical reaction and the development of methods to study the relation between their size and reactivity is pivotal³¹. Recent technological advances make the study of single nanoparticles possible and has uncovered the dynamic behavior of individual nanoparticles³². Using single molecule fluorescence microscopy, Chen and coworkers⁹ studied the catalytic activity of gold nanoparticles. Their kinetic studies showed that smaller nanoparticles have increased catalytic activity and turn over numbers. However, smaller nanoparticles also have lower substrate binding rate constants. In a parallel study, the activity of gold nanoparticles was tested in CO oxidation reaction³³. The highest activity of the catalyst was observed when the size of the particles was about 3 nm. The best correlation between size and reactivity can be seen in Yang's work where he studied the impact of size on the reactivity of platinum nanoparticles³⁴ (Figure 1.4). His studies on the reduction of ethylene and pyrrole confirmed that the size of the platinum nanoparticles can also impact the selectivity of the reaction. Using platinum nanoparticles of about 2 nm diameter, he was able to selectively reduce pyrrole to pyrrolidine (Figure 1.4 a,b). Despite all the drawbacks associated with

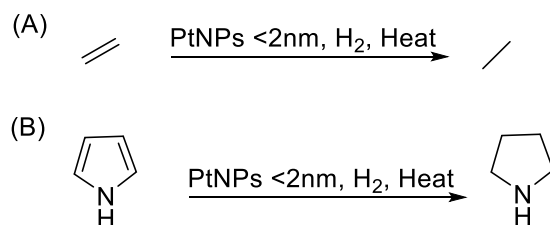


Figure 1.4 Effect of nanoparticle size on the reactivity

nanoparticles, the value of nanoparticle catalysts is well appreciated in the pharmaceutical industry. Their ease of separation and novel selectivity make them an invaluable tool for large

scale synthesis. So, efforts will continue to introduce nanoparticle catalysts as a solid replacement for homogeneous catalysts.

1.5 Application of Polymer Incarcerated Nanoparticles in Organic Reactions

Polymer-supported nanoparticles have attracted much attention among organic chemists due to their valuable advantages over other supported nanoparticles³⁵. Polystyrene has been the support of choice because of its numerous practical merits³⁶. It can be easily modified to tune the electronic and steric properties of the metal nanoparticle. It is also possible to functionalize the styrene by incorporating donating ligands into the monomer structure of the polymer. Moreover, crosslinking is feasible by adding small amounts of divinylbenzene, generating less soluble nanoparticle supports that can be separated from the reaction solution very easily³⁷. The concept that the nanoparticle forms electronic interactions with the polystyrene support was proposed by Somorjai³⁸ in 1993 where he discovered the interaction of benzene rings with gold surfaces. Later, Kobayashi³⁹ and coworkers validated the ability of polymer supports to stabilize gold nanoparticles. They used AuClPPh₃ as the nanoparticle precursor and sodium borohydride as reducing reagent. Reduction of gold in absence of polymer support formed a black agglomerate. However, addition of polystyrene formed a nice red color, indicating the formation of polystyrene-supported nanoparticles.

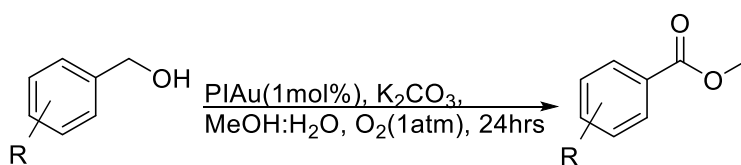


Figure 1.5 Aerobic oxidation of alcohols by polymer incarcerated gold NPs

This experiment represents the first practical evidence of π -interaction between benzene rings and a nanoparticle surface. Using cross-linked polystyrene, Kobayashi and co-workers were then able to develop a highly active catalyst for a tandem aerobic oxidation of alcohols to esters (Figure 1.5). The crosslinking property of the polymer gives heterogeneous character to the catalyst in the reaction and creates a highly active catalyst. Since their initial report on gold-nanoparticle catalyzed oxidation, the Kobayashi group has also demonstrated that functionalized polystyrene polymers can enable a variety of nanoparticle-catalyzed reactions. By incorporating phosphine ligands and a cross-linkable styrene in the structure of their polymer, they were able to make a variety of palladium and nickel nanoparticle catalysts

(Figure 1.6a). These catalysts proved to be highly active in cross-coupling reactions, including for Suzuki and Kumada cross-couplings (Figure 1.6b and 1.6c respectively). In additional work from the Kobayashi group, they demonstrated that introduction of a second metal into the structure of their nanoparticle catalysts makes a bimetallic catalyst⁴². This new catalyst exhibits

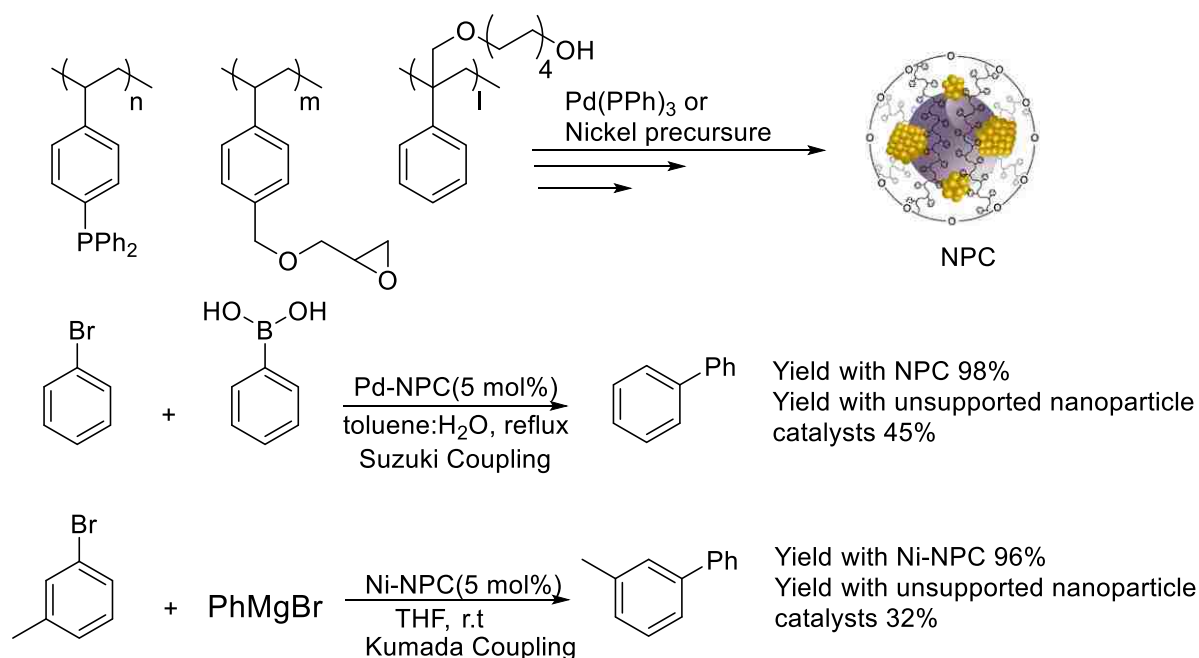


Figure 1.6 Synthesis and application of Pd and Ni nanoparticle catalysts in cross coupling reactions

catalytic activity that is unique from either of the monometallic nanoparticle catalysts and opens new doors to organic chemists for nanoparticle catalyst design. Typically, when two metals mix to make a bimetallic catalyst, a mixture of bimetallic and two distinct monometallic catalysts will form. The Kobayashi group demonstrated that the synthesis of various bimetallic Au catalysts provided only the alloyed bimetallic nanoparticles. Studies after the synthesis of bimetallic complex focused on reactivity and selectivity of these catalysts. Using carbon black as support, Kobayashi studied the reactivity of heterobimetallic gold-nickel, gold-cobalt, and gold-iron complexes. In a representative study, he compared their reactivity in amide bond formation from the reaction between an alcohol and an amine under aerobic oxidation conditions (Figure 1.7). Oxidation of alcohols to aldehydes and ketones were also investigated under aerobic conditions using heterobimetallic gold/palladium and gold/platinum nanoparticles⁴³. The interesting aspect of this study is the different selectivity observed with different catalysts. Under Au/Pd nanoparticles the alcohol oxidized to the ester, while switching to the Pt/Au catalyst provided the aldehyde as the major product (Figure 1.8). More recently, the Michaelis group reported an intimate connection between the cobalt nanoparticle

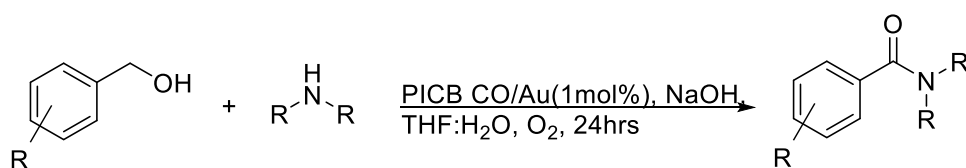
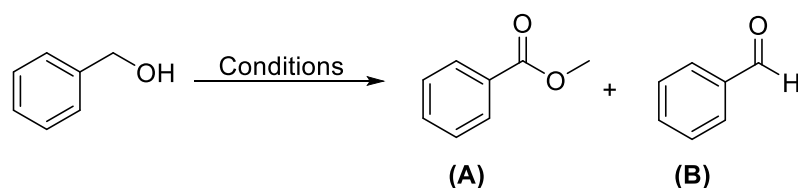


Figure 1.7 Polymer incarcerated (PI) Au/Co NPs for amide synthesis from alcohols and amines

catalysts for nitroarene reductions to anilines⁷. In their work, they demonstrated that varying the electronic properties of the aromatic groups on polystyrene dramatically impacted the activity of the catalyst (Figure 1.9). For example, making the aromatic groups more electron-deficient by introduction of para-CF₃ groups greatly increased catalytic activity in the reduction. In contrast, introduction of electron-donating para-methyl or para-OMe groups decreased catalytic activity with respect to the parent phenyl group of polystyrene. This result supports the notion that the aromatic rings of the polymer are indeed interacting with the nanoparticle surface and can potentially influence catalytic activity.



Conditions	Product A	Product B
Au/Pd MeOH, K ₂ CO ₃	80%	0
Au/Pt BTF	trace	92%

Figure 1.8 Selectivity of the product under different nanoparticle catalysts

1.5.1 Asymmetric transformations with chiral modified ligand nanoparticle catalysts:

Asymmetric transformations are desired in pharmaceutical synthesis as most of the drug candidates have at least one stereogenic center in their structure. Conventional methods for the introduction of chiral centers employ homogeneous catalysts. However, the cost, toxicity, and inefficiency of bulk metals in solution requires development of a robust catalyst that can be reused without loss of reactivity. Initial reports on asymmetric catalysis by heterogeneous nanoparticles have focused on stabilization of a homogeneous chiral catalyst on a solid support.

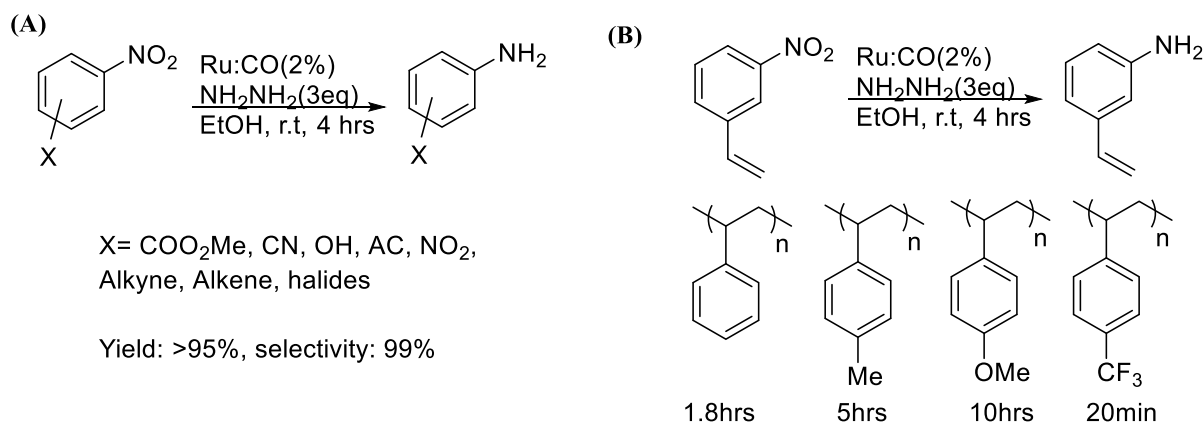


Figure 1.9 Chemoselectivity in nitroreduction with Ru:Co (A) and electronic effects on reactivity of the catalyst (B)

The first example of this strategy was reported by Akabori in 1956 using palladium Pd catalyst immobilized on silk fibroin fiber for the asymmetric hydrogenation of imines⁴⁴ (Figure 1.10a). Later, more examples were reported using immobilized chiral nickel catalysts and these studies confirmed that asymmetric catalysis by immobilized chiral catalysts is possible. The first example of an asymmetric C-C bond-forming reaction catalyzed by nanoparticle catalysts was reported by Gomez and coworkers using colloidal palladium nanoparticles⁴⁵. More recently, Kobayashi and coworkers reported that polystyrene-supported palladium nanoparticles catalyze the asymmetric allylic alkylation⁴⁶. Other C-C bond forming reactions such as Suzuki

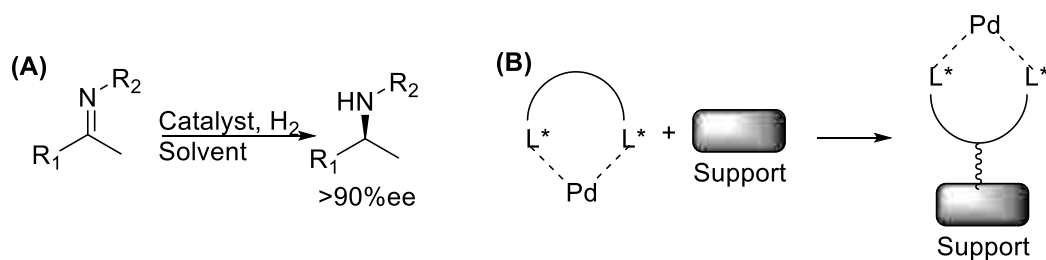


Figure 1.10 Asymmetric hydrogenation of amide (A) and the concept of the immobilized chiral catalyst (B)

cross-couplings⁴⁷, rhodium-catalyzed hydroformylations⁴⁸, and Pauson-Khand⁴⁹ reactions were also reported but in general had limited substrate scope.

To improve asymmetric catalysis by nanoparticle catalysts, several mechanisms have been proposed. McBreen⁵⁰ suggested that the chirality in the nanoparticle-catalyzed reactions is induced through two different pathways. First, it was suggested that the chiral ligand can bind to the nanoparticle surface and enable enantioselective reactions at the nanoparticle surface. Second, the chiral ligand structures can cause the metal in the nanoparticle to leach

into the reaction solution and perform enantioselective catalysis with a homogeneous metal catalyst. Extensive control experiments have in general favored the first mechanism where enantioinduction occurs at the surface of the nanoparticle⁵¹. New advances in the synthesis of polymer supports have enabled incorporation of diverse chiral ligands in the structure of nanoparticle catalysts⁵²⁻⁵³. Moreover, introduction of a second metal into the composition of nanoparticles can improve reactivity and selectivity of the catalyst⁵⁴ (see figure 1.9 above). As an example, Kobayashi and coworkers reported the an enantioselective one pot reaction that

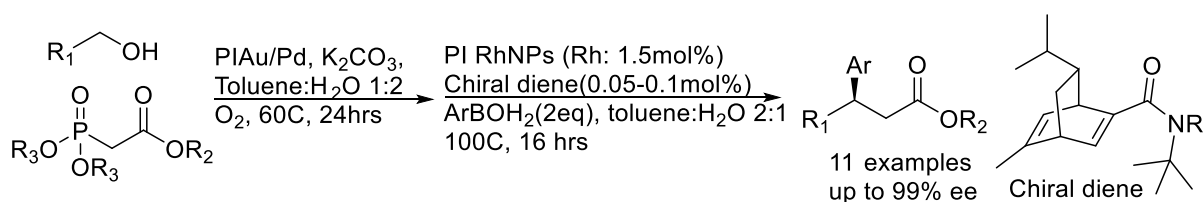


Figure 1.11 One pot sequential reaction catalyzed by two nanoparticle catalysts.

involves oxidation of an alcohol to an aldehyde, subsequent olefination with triethylphosphonoacetates to generate an enone, followed by enantioselective 1,4 addition (Figure 1.11). In the presence of polymer-incarcerated Au/Pd bimetallic catalyst (PI/CB Au/Pd), the tandem aerobic oxidation and Horner–Wadsworth–Emmons olefination were performed. Then addition of Rhodium nanoparticles, phenylboronic acid, and a chiral diene ligand created a β -aryl ester⁵⁵. After this report by Kobayashi, several additional asymmetric nanoparticle-catalyzed reactions have been reported, including conjugate additions to unsaturated amides⁵⁶ and allylations of benzaldehydes⁵⁷. In all these reactions, a positive nonlinear effect was observed in the heterogeneous nanoparticle systems, indicating that the catalysis occurs at the surface of the nanoparticles.

1.5.2 Chemo- and regioselective transformations by nanoparticle catalysts:

The development of efficient methods that employ a reusable catalyst for regio- and chemoselective organic transformations is highly desirable. Babu⁵⁸ reported the first regioselective nucleophilic addition of indoles to epoxides using nano-iron catalysts under solvent-free conditions (Figure 1.12). Although the reaction proceeds with retention of chirality, it did not show great reactivity with less reactive aliphatic epoxides. Wang and coworkers reported regioselective hydrosilylation of alkynes using polymer-supported platinum nanoparticles⁵⁹. In their study, they compared the activity and regioselectivity of platinum nanoparticles on polyaniline- support versus carbon black as the support.

Although the supported platinum nanoparticle catalyst was relatively slow compared to the commercially available Pt/C hydrosilylation catalyst, the polyaniline supported nano catalyst exhibited enhanced regioselectivity and excellent yields.

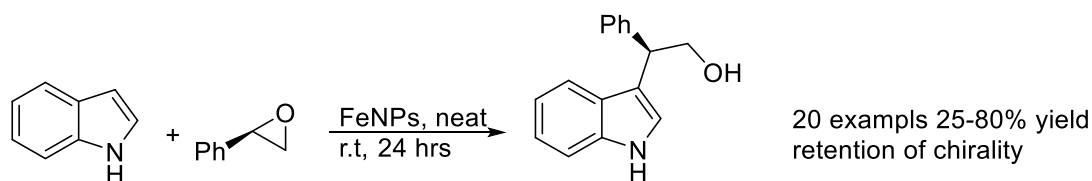


Figure 1.12 Iron nanoparticle catalyzed asymmetric and regioselective addition of indoles to epoxides

The Michaelis laboratory recently reported a nanoparticle-catalyzed azide reduction reaction that also proceeds with unique regioselectivity when compared to homogeneous catalysts⁶⁰. Using ruthenium nanoparticles, they also applied this method to the site-selective reduction of azides in the context of aminoglycosides. In addition, extensions of this work led to the development of polystyrene-supported ruthenium nanoparticle catalysts for the selective reduction of nitroarene to hydroxylamine products. The development of these new catalysts and their application to selective reactions will be the subject of the remainder of this chapter in nanoparticle catalysis and comprises the initial original work of this dissertation.

1.6 Site-Selective Alkyl and Azide Reductions with Heterogeneous Nanoparticle Catalysts

Site-selective modification of natural products is a viable strategy for derivatization of existing analogues. This approach to drug development is a promising way to develop new classes of antibiotics by generating unique structural derivatives that are not easily accessed via chemical synthesis⁶¹. This approach also provides a way to develop new antibiotics and help address the problem of multi-drug resistance in bacteria. Several methods toward site-selective derivatization of antibiotics have been reported and used in the context of polyol natural product diversification, including site-selective acylation and lipidation⁶², phosphorylation⁶³, halogenation⁶⁴, and thiocarbonylation⁶⁵. Regioselective amine functionalization introduces an alternative way for diversification of polyamine natural products for the potential generation of new aminoglycoside antibiotics⁶⁶. Because of the prevalence of azides in synthetic routes toward polyamines, site-selective azide reduction is one potential approach to selective amine functionalization⁶⁷. Conventional methods for site-selective azide reduction employ phosphine reductants (Staudinger reaction) that target the

most electronically activated azide⁶⁸ (electron-deficient).

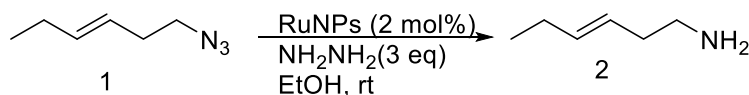
In our laboratory, we developed a highly chemoselective heterogeneous nanoparticle catalyst that enables site-selective reduction of the least hindered azide in polyazido substrates as a complementary method for site-selective azide reductions in antibiotic synthesis⁶⁰. During our studies on nanoparticle-catalyzed nitroarene reduction, we found that azide groups can be reduced in the presence of other active functional groups. This discovery suggested the potential of nanoparticle catalysts for chemoselective late stage azide reduction in the presence of other sensitive functional groups. Our studies showed that polystyrene-supported ruthenium nanoparticles act as highly chemoselective catalysts for the reduction of both aryl and alkyl azides. More importantly, we demonstrated that the nanoparticle catalysts provide high regioselectivity in late-stage reductions of polyazides, where selectivity is principally governed by sterics.

1.7 Results and Discussion

The importance of alkyl azides as vital intermediates en route to amines encouraged us to start our optimization studies on these substrates. Our polystyrene-supported ruthenium nanoparticles (~2 nm particle size) were prepared in a single step from commercial materials via NaBH₄ reduction of RuCl₃ in the presence of polystyrene. Our optimization studies confirmed that the reaction works best with only 2 mol% of catalyst and 3 equivalent of hydrazine monohydride in ethanol as solvent. An olefin containing alkyl azide (**1**) was used as a model substrate for our optimization studies (Table 1.1). Remarkably, the reduction occurred within one hour at room temperature and the olefin functional group remained intact (entry 1). No product was observed in the absence of our ruthenium nanoparticles or when hydrazine monohydride was left out (entry 2, 3). Decreasing the catalyst loading or equivalents of hydrazine monohydrate gave the same conversion and yield at the cost of higher reaction time (entry 5-7). Also, employing our heterobimetallic nanoparticle catalyst (Ru-Co) did not improve the reaction conditions (entry 8).

Using our optimal conditions, we next tested the functional group tolerance of our reaction conditions for a variety of substrates containing different functional groups. Aromatic azides are chemoselectively reduced in the presence of numerous other functional groups, including halides (**3a-3c**), anilines (**3d**), phenols (**3e**), carboxylic acids (**3f**), ketones (**3g**), cyanides (**3h**), nitro groups (**3i**), and esters (**3j**) (Figure 1.13). In addition, alkynes and alkenes were not reduced under our standard conditions (**3k-3l**). An aromatic bis (azide) substrate was

Table 1.1 Optimization studies of alkyl azide reduction



entry ^a	conditions	time	Yield ^b (%)
1	standard	1 h	98
2	No Ru catalyst	24 h	0
3	No NH ₂ NH ₂ ·H ₂ O	24 h	0
4	3% RuNPs	1 h	99
5	1% RuNPs	3 h	94
6	2 eq NH ₂ NH ₂ ·H ₂ O	1.5 h	97
7	1.5 eq NH ₂ NH ₂	2 h	98
8 ^c	2% Ru-Co catalyst	2 h	98

^aReactions run using 0.4 mmol **3**, 3 mol% Ru nanocatalyst, 0.41 mmol/gramin polystyrene) and 3 equivalent Hydrazine monohydrate in 1 ml of ethanol, unless otherwise notified.

^bIsolated yield, ^cRun with 2 eq of NH₂NH₂·H₂O.

also cleanly reduced in nearly quantitative yield to generate dianiline product **3m**. In all cases, the product was isolated in exceptional purity without the need for chromatography.

Polyfunctional alkyl azides are also readily reduced with high chemoselectivity under our standard conditions (Figure 1.14). Benzylic (**4a**), allylic (**4d**), tertiary (**4e**), secondary (**4f**), and primary azides (**4g-4l**), including simple alkyl azides are all rapidly reduced to the corresponding amine with high chemoselectivity. The reduction reaction tolerates alkenes,

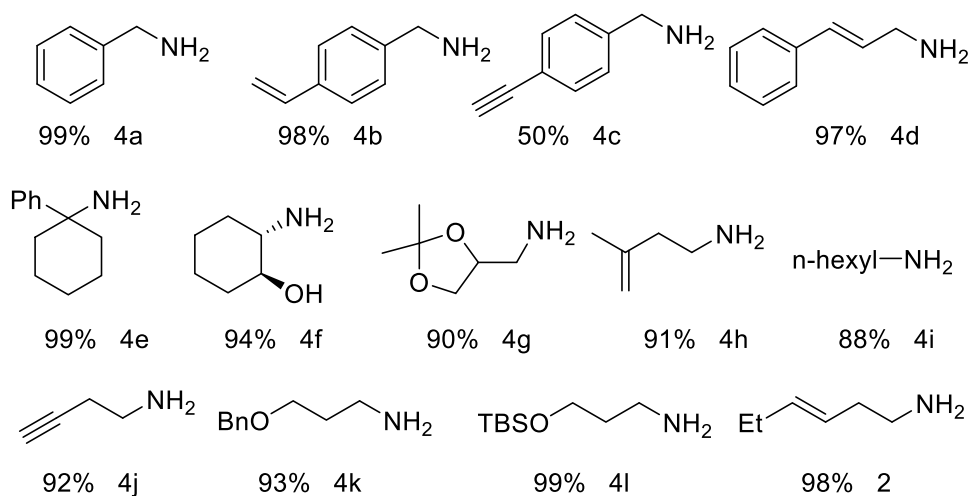


Figure 1.13 Chemoselective reduction of aromatic azides

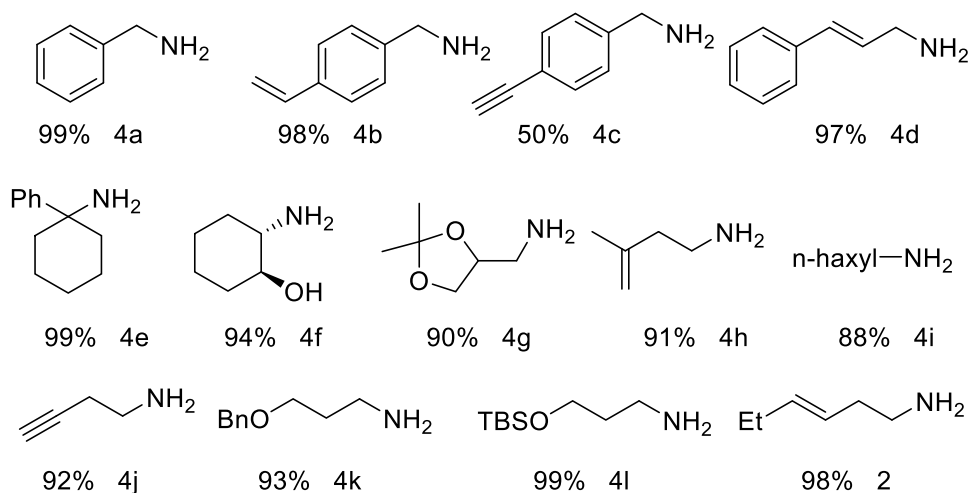


Figure 1.14 Chemoselective reduction of aliphatic azides

alkynes, benzyl and TBS ethers, acetals, and alcohols. In all cases, products were obtained with >96% selectivity toward azide reduction. One significant feature of our catalyst is its potential to be used in the context of complex molecule manipulation.

The reaction conditions were tested on different natural molecules including amino acids, steroids, saccharides, and nucleotide bases (Figure 1.15). In each case, the reaction worked with perfect yield and selectivity. After confirming the chemoselectivity of our catalyst for a variety of alkyl and aryl azides, we next sought to establish conditions for site-selective azide reductions. Using proline bis azide **5** containing primary and secondary azides, we performed several reactions to find the best conditions (Table 1.2). Under conventional conditions with trimethylphosphine as reductant, only a slight preference for the primary azide reduction was observed (entry 1). When our ruthenium nanoparticle catalyst was employed, the reaction proceeded with 3:1 selectivity in 60% yield (entry 2). By starting the reaction at 0 °C and continuing at room temperature for 5 hours, the yield (70%) and selectivity

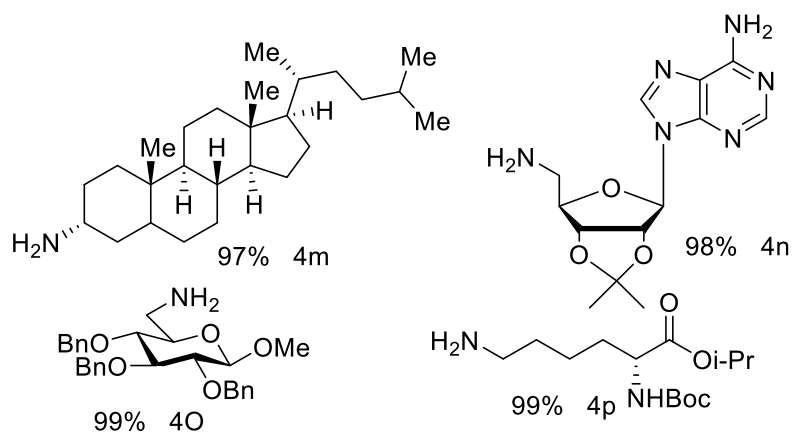
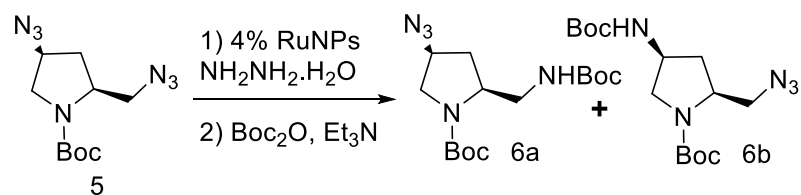


Figure 1.15 Chemoselective azide reduction in biomolecule synthesis

Table 1.2 Regioselective Azide Reduction

entry ^a	time	polystyrene	temperature	6a:6b ^b	Yield of 6a ^c
1 ^d	12h	4-H	-78 ⁰ C	1.9:1	54
2	4 h	4-H	r.t	3:1	60
3	5 h	4-H	0 ⁰ C to r.t	3.3:1	75
4	5 h	4-CF ₃	0 ⁰ C to r.t	1:2.4	28
5	5 h	4-OMe	0 ⁰ C to r.t	1:1.7	22
6	5 h	4- ^t Bu	0 ⁰ C to r.t	1:20	5
7 ^e	30 h	4-H	0 ⁰ C to r.t	3.3:1	70
8 ^{e,f}	40 h	4-H	0 ⁰ C to r.t	5.1:1	62
9 ^{g,h}	40 h	4-H	0 ⁰ C to r.t	7.9:1	79
10 ⁱ	40 h	4-H	0 ⁰ C to r.t	4.5:1	80

^aReactions run with 0.2 mmol 7, 4eq $\text{NH}_2\text{NH}_2 \cdot \text{H}_2\text{O}$, and 4mol% of RuNPs catalyst in EtOH (0.06M); ^bRatios determined by isolated yields of 8a and 8b. ^cIsolated yield. ^dRun with PMe_3 (1.2eq)for 4hrs; ^eSlow addition of NH_2NH_2 over 1hr. ^fWith 3mol% of RuNPs catalyst and 4eq $\text{NH}_2\text{NH}_2 \cdot \text{H}_2\text{O}$; ^gWith 2mol% of RuNPs catalyst and 3eq $\text{NH}_2\text{NH}_2 \cdot \text{H}_2\text{O}$.; Addition of 1eq of NH_2NH_2 after 24 h. ⁱ8% recovered 6 ; ^jRun with 5% RU on Carbon(2mol% Ru).

(3.3:1) improved (entry 3). When the electronic (entries 4 and 5) and steric (entry 6) properties of the supporting polymer were modified, lower product selectivity was observed. Optimizing the catalyst loading (entries 7-8) allowed us to obtain the mono reduction product in up to 5:1 selectivity. If an additional 1.0 equiv of hydrazine was added halfway through the reaction, conversion approached 100% and the desired product was obtained in high yield (79%) and very good selectivity (entry 9). This result is in contrast to commercially available ruthenium

on carbon, which provided very low conversion and only moderate selectivity under the same conditions (entry 10).

The applicability of our catalyst was tested on a variety of bisazide containing substrates (Figure 1.16). Primary azides were reduced with moderate yields and selectivities over electronically more activated benzylic azides (**7a-7e**). Additionally, primary azides were reduced with slight preference over secondary aliphatic azides (**7f**). Also, aromatic azides reduced preferably over primary azides (**7g**). This method proved efficient for manipulation of natural amino acids. An isopropyl ester of bis lysine azide containing an electronically activated secondary azide and a primary azide was exposed to the reaction and the primary azide reduced with relatively high selectivity (**9a:9b**, 2:1).

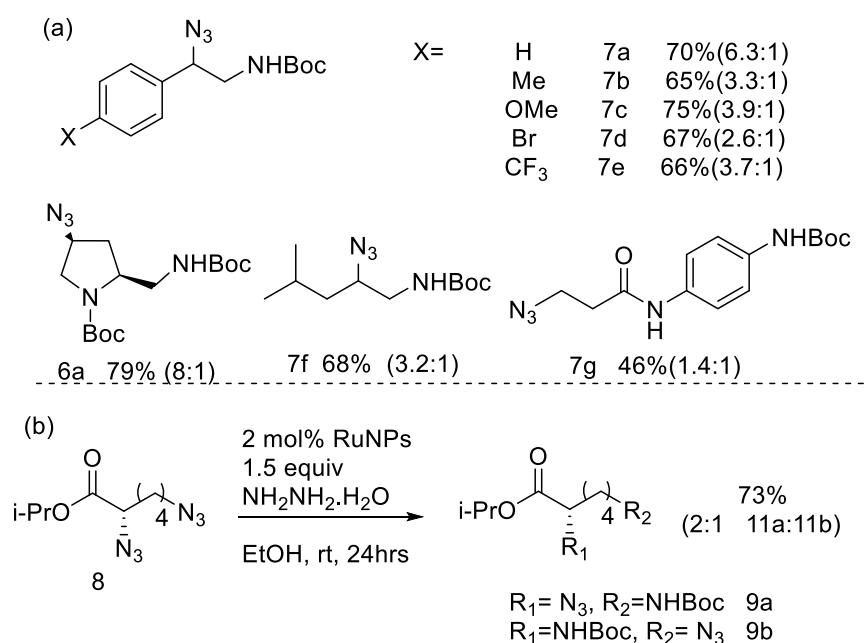


Figure 1.16 Regioselective monoazide reduction. (a) Conditions: 2mol% RuNPs Catalyst, 4eq NH₂NH₂·H₂O in EtOH (0.13M), 0 °C to r.t., 16h. Regioselectivity determined by HNMR analysis of the crude reaction mixture (b) Ratio of 11a:11b determined by isolated yield of each isomer.

Aminosugars have a rich history in sugar chemistry and vaccine discovery⁶⁹. The high selectivity we observed with various substrates led us to try our catalyst for site-selective azide reductions in multiazide-containing sugars. Previous studies by other groups reported the most electronically activated azide reduced preferentially under Staudinger reaction conditions⁶⁶. We were surprised to see excellent yields and selectivity for the sterically most available azide under our ruthenium nanoparticle catalyst (Figure 1.17). For this study, we made two bisazide sugars including the secondary azide located at anomeric or non-anomeric positions. To our surprise, even the sugar containing activated anomeric azide gave preference for the primary

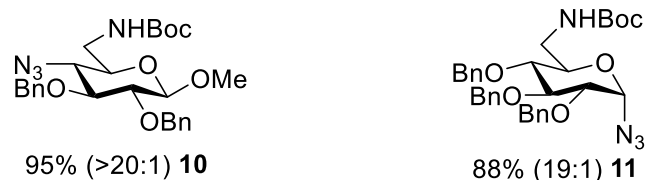


Figure 1.17 Regioselective azide reduction of polysaccharides. Conditions: 4-7mol% RuNPs Catalyst, 4-5eq $\text{NH}_2\text{NH}_2\cdot\text{H}_2\text{O}$ in EtOH (0.13M), 0 $^\circ\text{C}$ to r.t., 7-10h. Regioselectivity determined by HNMR analysis of the crude reaction mixture.

azide reduction (19:1, 88%). This amazing discovery encouraged us to test the selectivity of our catalyst in more complex systems. Kanamycin and neamine are derivatives of aminoglycosides and contain three and two saccharide rings in their structure respectively. The tetra azide versions of kanamycin and neamine were synthesized and exposed to our nanoparticle catalyst (Figure 1.18). Kanamycin-tetraazide underwent reduction at the primary position in moderate yield to give monoamine **13**. This result was remarkable as it showed a selectivity complementary to traditional Staudinger reductions, which targets the most electronically activated secondary azide (in blue).

Under similar conditions, neamine tetraazide did not reduce at the primary azide. Instead, the least electronically activated secondary azide reduced to form **15**, indicating the preference of our catalyst for binding to the most accessible azide. This result was presumably due to a particular conformation of the sugar where the primary azide is shielded and requires a high activation energy for adsorption on the surface of the nanoparticles.

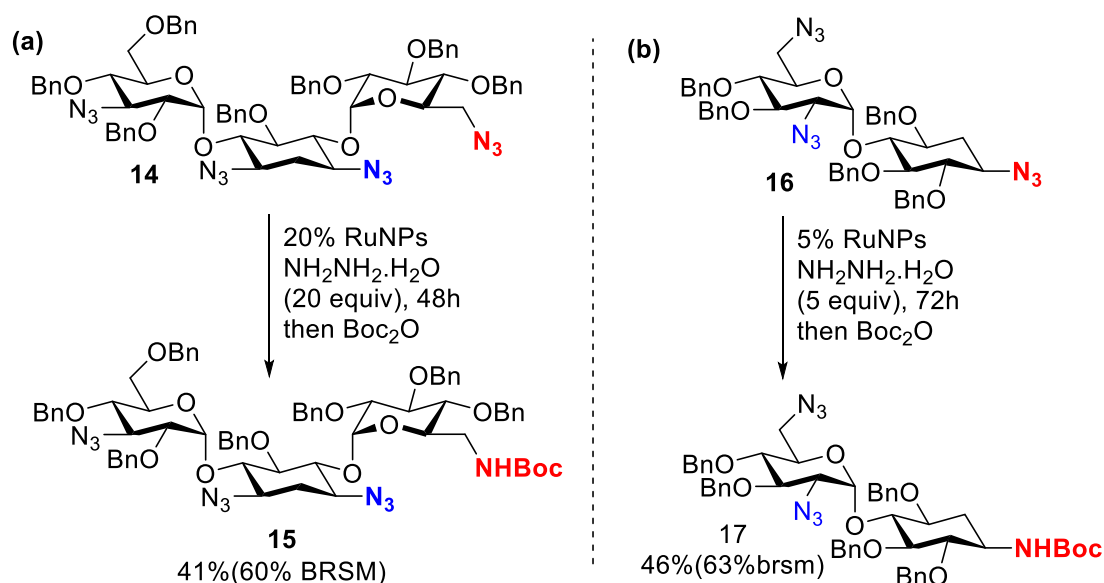


Figure 1.18 Site-selective azide reduction in aminoglycoside antibiotic derivatives including (a) Kanamycin tetraazide and (b) neamine tetraazide.

1.8 Synthesis of Aryl-Hydroxylamines via Partial Reduction of Nitroaryls with Soluble Nanoparticles

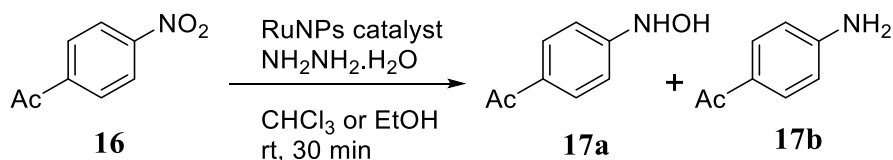
Arylhydroxylamines are important intermediates en route to heterocycle synthesis⁷⁰. Traditional methods for their synthesis include reduction of nitroarenes with stoichiometric amounts of transition metals⁷¹ (Fe, Sn). In an extension of our studies on the application of the nanoparticles to selective synthesis, we discovered that the reactivity of the nanoparticles changes when they dissolve in organic solvents. This feature can be used for optimization and control of the reaction dynamics. In our laboratory, we demonstrated that the selectivity of our ruthenium nanoparticles is affected by the solubility of our polymer-supported catalyst and it highly depends on the solvent used in the reaction⁷². During our studies on the reactivity of the polymer supported ruthenium nanoparticles in nitro arene reduction, we observed that hydroxylamine intermediate is first formed quantitatively in the reaction, which then continues to be reduced to the aniline product. We also noticed that the rate of reduction of the hydroxylamine to the aniline was highly solvent-dependent, and that by changing the solvent we could selectively favor formation of the hydroxylamine over the aniline product. This section will describe the optimization of our ruthenium nanoparticle catalysts for selective hydroxylamine formation.

1.8.1 Results and discussion

We began our optimization studies by chemoselective reduction of 4-nitroacetophenone using our ruthenium nanoparticle catalysts (Table 1.3). Using conditions previously developed for nitroarene reduction to anilines, we observed formation of a ratio of aniline to hydroxylamine (1:1) using our bimetallic Ru:Co nanoparticle catalyst and ethanol as solvent (entry 1). Using monometallic ruthenium nanoparticles did not improve the selectivity (entry 2). The selectivity did improve with our bimetallic Ru:Co nanoparticles when less polar solvents such as chloroform were employed (entry 4). However, our monometallic ruthenium nanoparticles provided a higher ratio of hydroxylamine product over aniline (entry 5). The commercially available ruthenium on carbon black showed very poor reactivity and selectivity (entry 3 and 6). Optimizing the reaction for catalyst loading and concentration dramatically improved the selectivity in favor of the hydroxylamine product (entry 7-11). By lowering the catalyst loading and equivalents of the reductant, the reduction slows down. The selective hydroxylamine formation was next investigated on substrates containing sensitive functional groups using our optimized conditions (Figure 1.19). The reactions performed with 1.1 mol%

of the catalyst and 2.5 equivalents of hydrazine gave the best selectivity over a variety of substrates.

Table 1.3 Optimization studies of nitro arene reduction to hydroxylamine



entry ^a	Mol% RuNPs	NH ₂ NH ₂ (eq)	Solvent	% Conv ^b .	Ratio(17a:17b) ^b
1 ^c	5	3	EtOH	93	1:1
2	5	3	EtOH	100	1:1
3 ^d	5	3	EtOH	33	N/A ^e
4 ^c	5	3	HCCl ₃	100	1:10
5	5	3	HCCl ₃	100	2:1
6 ^d	5	3	HCCl ₃	45	1:1
7	5	1.5	HCCl ₃	100	3:1
8	3	1.5	HCCl ₃	100	5:1
9	0.8	1.5	HCCl ₃	100	12:1
10 ^f	0.5	1.5	HCCl ₃	100	13:1
11 ^g	0.5	1.5	HCCl ₃	100(88) ^h	40:1

a Reaction run using 0.33 mmol 1a, hydrazine hydrate (as indicated), and polystyrene-supported Ru nanoparticles (0.47 mmol/g Ru) in the indicated solvent (0.167 M); *b* Determined using ¹H NMR. *c* Ru–Co nanoparticle catalyst (0.47 mmol/g Ru) was employed; *d* Ruthenium on carbon (5 wt%, 5 mol% loading) was employed as catalyst. *e* No aniline or hydroxylamine product observed; *f* NH₂NH₂ □ H₂O was added at 0 °C and the reaction warmed to rt for 45 min; *g* Run at 0.084 M in CHCl₃ for 45 min; *h* Isolated yield. PS = polystyrene.

The hydroxylamine product was obtained in high yield and purity (>95%) in the presence of other functional groups such as ketones, alkynes, esters, amides, halides, sulfonamides, and cyano groups (**20a-20o**). The reduction was also conducted on large scale (25 mmol) and gave the product in high yield (85%) and selectivity (14:1).

We also explored the viability of heteroaromatic nitro compounds to undergo selective reduction to the hydroxylamine due to the importance of heteroaromatic structures in pharmaceutical research (Figure 1.20).

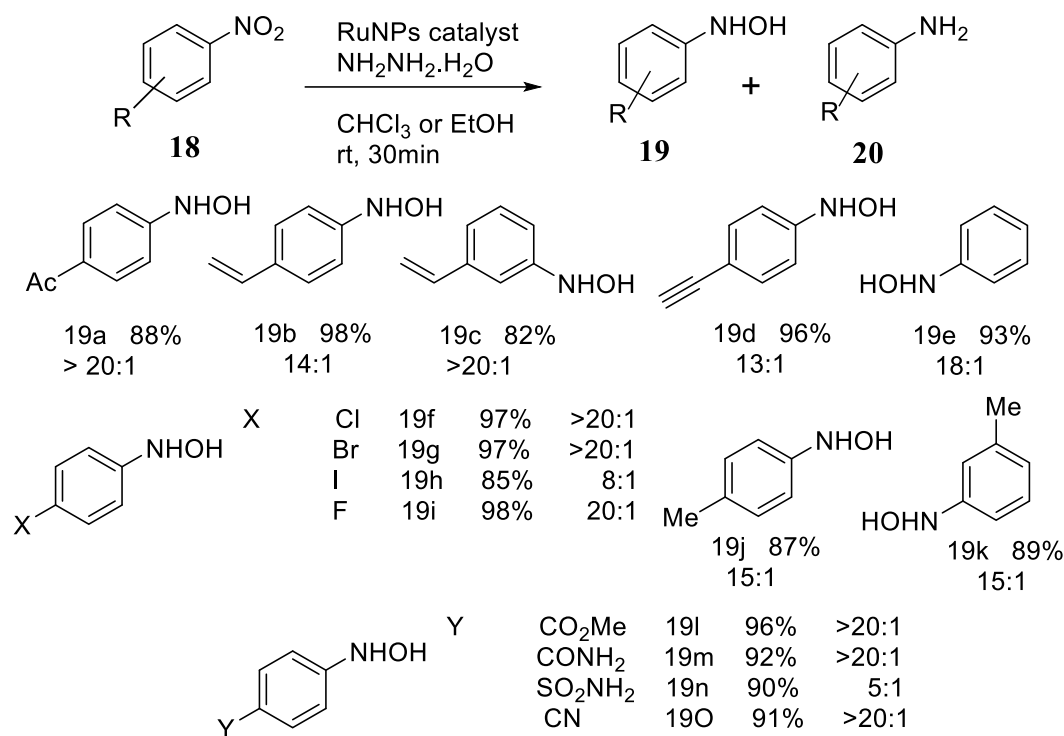


Figure 1.19 Substrate scope of hydroxylamine formation

Interestingly, we found that nitro-substituted pyridines and quinolines provided the hydroxylamines in excellent yield, including quinolines with acidic hydroxyl groups (21a-21c). For other heterocycles, the hydroxylamine was selectively generated in high yield with

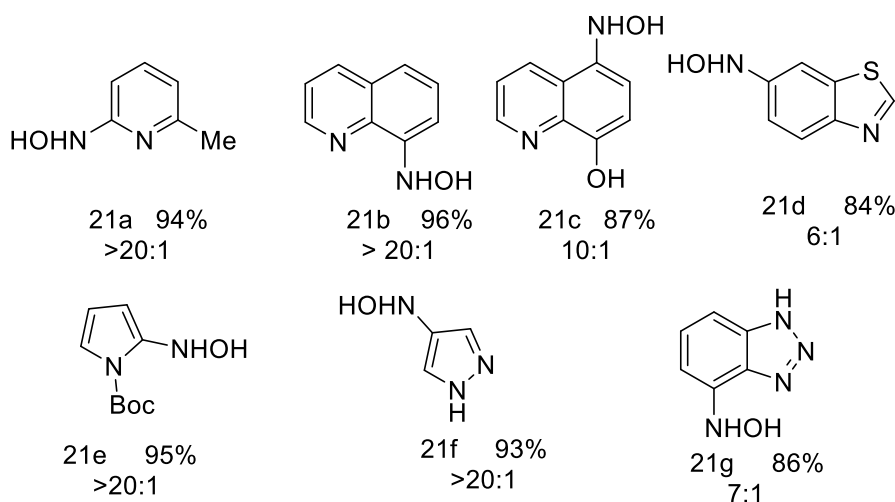


Figure 1.20 Substrate scope for heteroaryl hydroxylamine formation

substrates containing benzothiazoles, pyrroles, pyrazoles, and benzotriazoles (21d-21g). These studies confirmed that a wide variety of medicinally important N-heteroaryl hydroxylamines can be selectively generated using our reduction protocol.

1.9 Experimental Procedures and Supporting Data for Chemo and Site Selective Azide Reduction with Heterogeneous Nanoparticle Catalysts.

1.9.1 General information

All reactions were carried out in oven-dried glassware with magnetic stirring, unless otherwise indicated. All the reagents were used as obtained from commercial sources unless otherwise noted. Analytical thin-layer chromatography was performed with 0.25 mm coated commercial silica gel plates (E. Merck, DC-Plastikfolien, silicagel 60 F₂₅₄). Flash Chromatography was performed with EM Science silica gel (0.040-0.063 μ m grade). Proton nuclear magnetic resonance (¹H-NMR) data were acquired on an Inova 300 MHz, an Inova 500 MHz, or an NMR-S 500 MHz spectrometer. Chemical shifts are reported in delta (δ) units relative to the signal of the CDCl₃ solvent. Signals are reported as follows: s (singlet), d (doublet), t (triplet), q (quartet), dd (doublet of doublets), qd (quartet of doublets), brs (broad singlet), m (multiplet). Coupling constants are reported in hertz (Hz). Carbon-13 nuclear magnetic resonance (¹³C-NMR) data were acquired on an Inova or NMR-S spectrometer at 125 MHz. Chemical shifts are reported in ppm. All NMR spectra were collected at 298 K. Mass spectral data were obtained using ESI techniques (Agilent, 6210 TOF). The metal loading in the polystyrene-supported nanoparticle catalysts were obtained via ICP analysis using a Shimadzu ICPS- 7510 instrument. STEM images and EDS analyses were obtained using a JEOL JEM-2100F instrument operated at 5.0 kV. All STEM specimens were prepared by placing a drop of a homogeneous chloroform solution of the respective polymer-nanoparticle composite on a carbon coated copper grid and allowing the grid to dry in air without staining. Polystyrene (MW 35,000, Aldrich), and Ruthenium (III) chloride hydrate (STREM chemicals) were used as obtained.

1.9.2 Synthesis and characterization of Ru NP's@polystyrene

Polystyrene (1g) was added to 25 mL of THF and 8 mL of ethanol and the mixture was stirred using a Teflon-coated magnetic stir bar until polystyrene was completely dissolved. Ruthenium (III) chloride hydrate (100 mg, 0.482 mmol) anhydrous basis was added and the mixture was stirred until the solution became homogenous. Sodium borohydride (182.5 mg, 4.82 mmol) was then added portion wise. The reaction was stirred under argon atmosphere for 10 h giving a black homogeneous solution, indicating the formation of nanoparticles. The

solvent was then evaporated and Millipore water was added to the resulting solid and the mixture was stirred for 15 minutes then filtered. The solid was then washed with Millipore water (20 mL × 5) and dried under vacuum to give a black solid, which was finely ground with a mortar and pestle before use. The ruthenium loading in each batch of Ru/PS was determined by ICP analysis by comparison with standard solutions, and was determined to be ~0.47 mmol/g on average. The nanoparticle catalysts were stored under argon. When stored under argon, and used regularly, the catalysts remain active for several weeks up to a few months. Catalytic activity of the nanoparticles slowly decreases with exposure to air.

1.9.3 Preparation of the sample for ICP-analysis

To 10 mg of polymer-nanoparticle catalyst was added 1 ml conc. H₂SO₄ and the mixture heated at 140 °C. HNO₃ (1 ml) was then slowly added and the solution was heated for 10 min. 1 ml of aqua regia was then added and the mixture cooled to room temperature and diluted to 500 mL in a volumetric flask. Metal concentrations were then determined by ICP analysis by comparison to standard solutions. Typical catalysts obtained with 0.47 mmol/g loading of Ru nanoparticles in polystyrene.

1.9.4 Characterization of Ru/polystyrene nanoparticles

Size distribution of nanoparticles was obtained based on the area of each nanoparticle calculated by Image J software. The data was then transferred to Excel and used to calculate the diameters (nm). All the diameter values were rounded up to the bigger natural number and plotted against frequency.

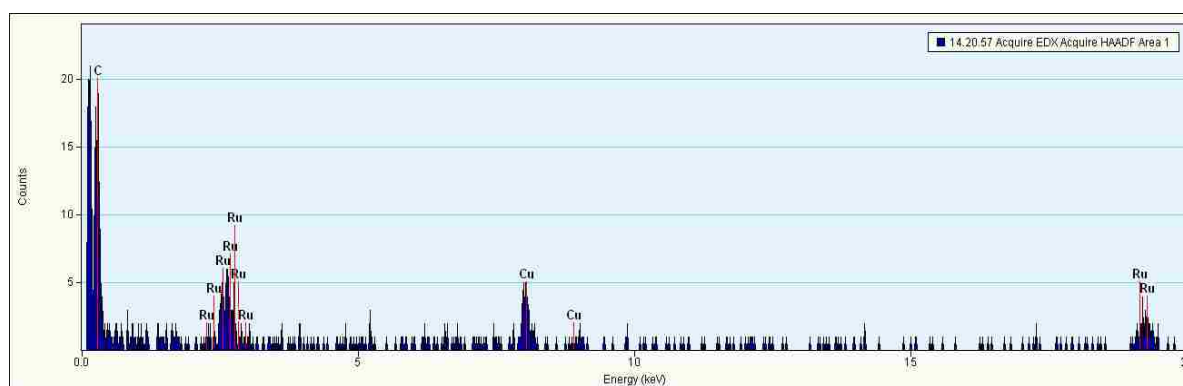


Figure 1.21 EDS spectrum of the Ru nanoparticles showing the presence of the main components Ru. Cu and C peak are background from the TEM support grid

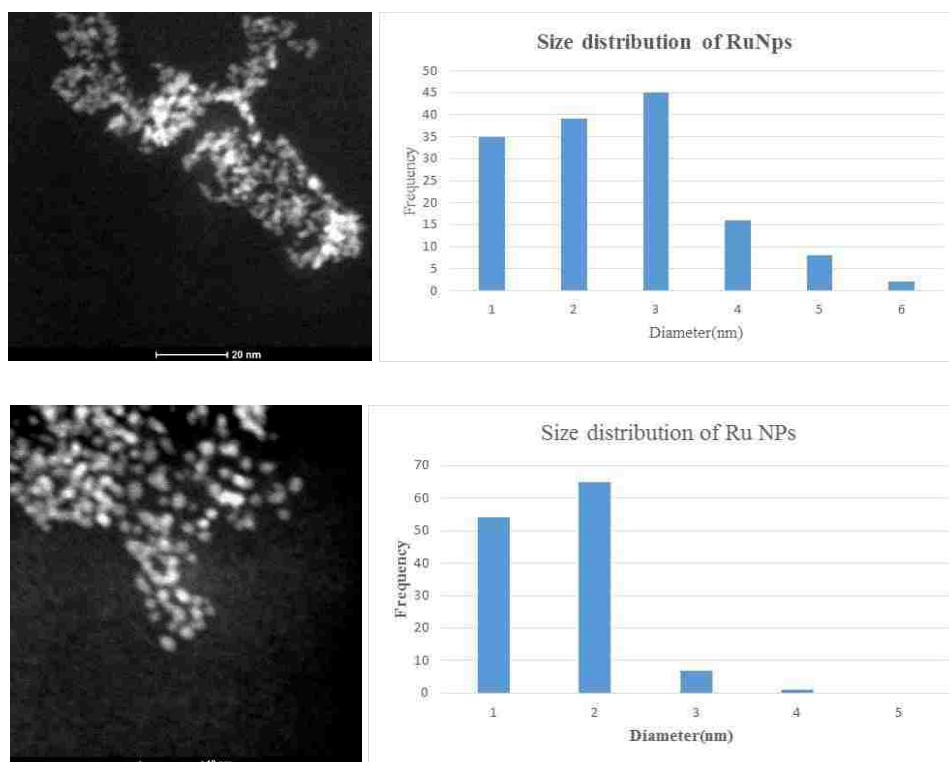


Figure 1.22 STEM image of Ru NPs on polystyrene catalyst. (a) STEM Image and statistical analysis of original polymer-encapsulated nanoparticles. (b) STEM Image and statistical analysis of nanoparticle size of the same catalyst after recycling

1.9.5 Experimental procedures

1.9.5.1 General procedure: reduction of (*E*)-1-azidohex-3-ene

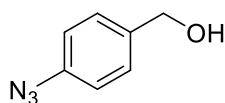
A typical procedure for the reduction of azido compounds by ruthenium nanoparticles on polystyrene is as follows: Ru/Polystyrene (17 mg, 0.47 mmol/g Ru in polystyrene, 2 mol% wrt ruthenium) was placed in a 10 mL test tube containing a Teflon-coated magnetic stir bar, followed by the addition of ethanol (1 mL), (*E*)-1-azidohex-3-ene (50 mg, 0.399 mmol), and dropwise addition of hydrazine monohydrate (1.19 mmol, 58 μ L, 3 equiv) at room temperature. The reaction vessel was then sealed with a glass stopper and stirred for 2 h. After the reaction, Ru/Polystyrene was removed by filtration through a small plug of silica gel in a pipet, and the solids washed several times with ethanol. The filtrate was collected, and the solvent removed under reduced pressure on a rotary evaporator to provide the product (39.6 mg, 0.332 mmol, 98% yield, and 100% selectivity) in excellent purity, which did not require further purification. The selectivity of the reaction was determined by ^1H NMR analysis of the pure product obtained as described

1.9.5.2 Reuse experiments of Ru NP's@polystyrene

The reduction of (*E*)-1-azidohept-3-ene (50 mg, 0.399 mmol) was performed under the typical reaction conditions (17 mg Ru/PS, (0.47 mmol/g) 2 mol%; 58 μ L, 3 equiv $\text{NH}_2\text{NH}_2\cdot\text{H}_2\text{O}$; 1 ml EtOH) in a flask containing a frit of medium porosity and a bottom stopcock. After completion of the reaction, the solution was removed via filtration through the frit. The flask was then rinsed with EtOH (3 ml) and the filtrate evaporated and the isolated yield and selectivity were determined. To the remaining nanoparticle catalyst was added a new set of reagents and solvents and the reaction was allowed to proceed for the same time. This procedure was repeated 5 times, and the results yields obtained were 97, 98, 96, 97, 95% yield on runs 1–5 respectively.

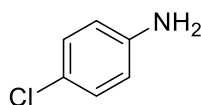
Reuse experiment to partial conversion: Substrate **6f** (2-azidocyclohexan-1-ol) was run to partial conversion according to the procedure described above (40 min reaction time) followed by filtration and removal of solvent, the following conversions were observed as determined by ^1H NMR analysis: Run 1: 56%, Run 2: 56%, Run 3: 53%, Run 4: 53%, Run 5: 47%.

1.9.5.3 Experimental procedures and spectral data

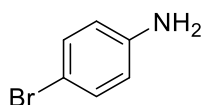


Aromatic azides were prepared from the corresponding aniline starting materials via oxidation with sodium nitrite as follows: 4-Aminobenzyl alcohol (1000 mg, 8.12 mmol) was dissolved in hydrochloric acid (5 mL, 5 M). To this solution, sodium nitrite (840 mg, 12.18 mmol) dissolved in 20 mL of water was dropwise added within 30 min. The solution was vigorously stirred in ice-cold water. Sodium azide (2100 mg, 32.3 mmol) was then added in small portions. The resulting solution was stirred at room temperature overnight. The reaction was monitored by TLC. After the completion of reaction, the reaction solution was poured into saturated aqueous NaHCO_3 and extracted with ethyl acetate. The combined organic layers were washed with brine, dried over anhydrous Na_2SO_4 , filtered and concentrated. The crude product was purified by silica gel chromatography (ethyl acetate: petroleum ether = 1:3) to obtain the pure 4-azidobenzyl alcohol as yellow oil (1450 mg, 99% yield). ^1H NMR (400 MHz, CDCl_3)

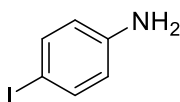
$\delta = 7.25$ (d, $J = 8.3$ Hz, 2H), 6.92 (dd, $J = 8.7$ Hz, 2.1 Hz, 2H), 4.55 (s, 2H), 2.02 ppm (s, 1H).
 ^{13}C NMR (101 MHz, CDCl_3) $\delta = 139.37, 137.61, 128.53, 119.12, 64.63$ ppm.



4-chloroaniline (3a): Ru NPs supported on polystyrene (13.8 mg, 0.47 mmol/g, 2 mol% wrt ruthenium) was placed in a 10 mL vial containing a Teflon-coated magnetic stir bar, followed by the addition of ethanol (2.0 mL), 1-azido-4-chlorobenzene (50 mg, 0.325 mmol), Hydrazine monohydrate (0.975 mmol, 47.5 μL was added dropwise, the vial was closed with a Teflon cap, and the reaction mixture was stirred for 5 h. After the reaction, the heterogeneous catalyst was removed by filtration through a small plug of silica gel in a pipet, and the solids washed several times with ethanol. The filtrate was collected, solvent was removed under reduced pressure on a rotary evaporator to give the product as a pale yellow solid (40.5 mg, 98%). Spectral data of starting material and product matched with reported values⁷³⁻⁷⁴.

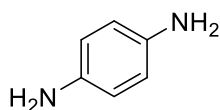


4-bromoaniline (3b): Ru NPs supported on polystyrene (10.7 mg, 0.47 mmol/g, 2 mol% wrt ruthenium) was placed in a 10 mL vial containing a Teflon-coated magnetic stir bar, followed by the addition of ethanol (2.0 mL), 1-azido-4-bromobenzene (50 mg, 0.252 mmol), Hydrazine monohydrate (0.757 mmol, 37 μL was added dropwise, the vial was closed with a Teflon cap, and the reaction mixture was stirred for 5 h. After the reaction, the heterogeneous catalyst was removed by filtration through a small plug of silica gel in a pipet, and the solids washed several times with ethanol. The filtrate was collected, solvent was removed under reduced pressure on a rotary evaporator to give the product as pale yellow solid (41.5 mg, 96%). Spectral data of starting material and product matched with reported values⁷³⁻⁷⁴.

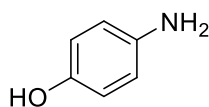


4-iodoaniline (3c): Ru NPs supported on polystyrene (8.8 mg, 0.47 mmol/g, 2 mol% wrt ruthenium) was placed in a 10 mL vial containing a Teflon-coated magnetic stir bar, followed

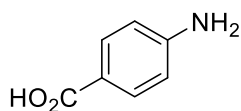
by the addition of ethanol (2.0 mL), 1-azido-4-iodobenzene (50 mg, 0.204 mmol), Hydrazine monohydrate (0.612 mmol, 30 μ L) was added dropwise, the vial was closed with a Teflon cap, and the reaction mixture was stirred for 5 h. After the reaction, the heterogeneous catalyst was removed by filtration through a small plug of silica gel in a pipet, and the solids washed several times with ethanol. The filtrate was collected, solvent was removed under reduced pressure on a rotary evaporator to give the product as pale yellow solid (43 mg, 96%). Spectral data of starting material and product matched with reported values⁷³⁻⁷⁴.



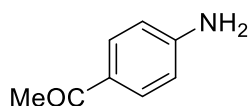
p-phenylenediamine (3d): Ru NPs supported on polystyrene (15.8 mg, 0.47 mmol/g, 2 mol% wrt ruthenium) was placed in a 10 mL vial containing a Teflon-coated magnetic stir bar, followed by the addition of ethanol (2.0 mL), 4-azidoaniline (50 mg, 0.372 mmol), Hydrazine monohydrate (1.12 mmol, 54 μ L) was added dropwise, the vial was closed with a Teflon cap, and the reaction mixture was stirred for 5 h. After the reaction, the heterogeneous catalyst was removed by filtration through a small plug of silica gel in a pipet, and the solids washed several times with ethanol. The filtrate was collected, solvent was removed under reduced pressure on a rotary evaporator to give the product as pale yellow solid (36.3 mg, 96%). Spectral data of starting material and product matched with reported values⁷³⁻⁷⁴.



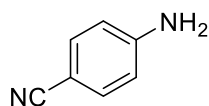
p-aminophenol (3e): Ru NPs supported on polystyrene (15.7 mg, 0.47 mmol/g, 2 mol% wrt ruthenium) was placed in a 10 mL vial containing a Teflon-coated magnetic stir bar, followed by the addition of ethanol (2.0 mL), 4-azidophenol (50 mg, 0.370 mmol), Hydrazine monohydrate (1.11 mmol, 54 μ L) was added dropwise, the vial was closed with a Teflon cap, and the reaction mixture was stirred for 5 h. After the reaction, the heterogeneous catalyst was removed by filtration through a small plug of silica gel in a pipet, and the solids washed several times with ethanol. The filtrate was collected, solvent was removed under reduced pressure on a rotary evaporator to give the product as pale yellow solid (39.5 mg, 98%). Spectral data of starting material and product matched with reported values⁷³⁻⁷⁴.



4-aminobenzoic acid (3f): Ru NPs supported on polystyrene (26.0 mg, 0.47 mmol/g, 4 mol% wrt ruthenium) was placed in a 10 mL vial containing a Teflon-coated magnetic stir bar, followed by the addition of ethanol (2.0 mL), 4-azidobenzoic acid (50 mg, 0.306 mmol), Hydrazine monohydrate (1.22 mmol, 59.5 μ L was added dropwise, the vial was closed with a Teflon cap, and the reaction mixture was stirred for 5 h. After the reaction, the heterogeneous catalyst was removed by filtration through a small plug of silica gel in a pipet, and the solids washed several times with ethanol. The filtrate was collected, solvent was removed under reduced pressure on a rotary evaporator to give the product as pale yellow solid (41.6 mg, 99%). Spectral data of starting material and product matched with reported values⁷³⁻⁷⁴.

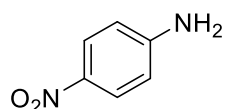


4-aminoacetophenone (3g): Ru NPs supported on polystyrene (13.2 mg, 0.47 mmol/g, 2 mol% wrt ruthenium) was placed in a 10 mL vial containing a Teflon-coated magnetic stir bar, followed by the addition of ethanol (2.0 mL), 4-azidoacetophenone (50 mg, 0.310 mmol), Hydrazine monohydrate (0.930 mmol, 45 μ L was added dropwise, the vial was closed with a Teflon cap, and the reaction mixture was stirred for 5 h. After the reaction, the heterogeneous catalyst was removed by filtration through a small plug of silica gel in a pipet, and the solids washed several times with ethanol. The filtrate was collected, solvent was removed under reduced pressure on a rotary evaporator to give the product as pale yellow solid (41.5 mg, 99%). Spectral data of starting material and product matched with reported values⁷³⁻⁷⁴.

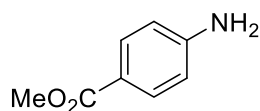


4-aminobenzonitrile (3h): Ru NPs supported on polystyrene (29 mg, 0.47 mmol/g, 4 mol% wrt ruthenium) was placed in a 10 mL vial containing a Teflon-coated magnetic stir bar, followed by the addition of ethanol (2.0 mL), 4-azidobenzonitrile (50 mg, 0.346 mmol), Hydrazine monohydrate (1.04 mmol, 50.5 μ L was added dropwise, the vial was closed with a

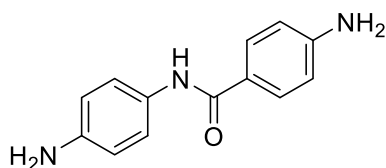
Teflon cap, and the reaction mixture was stirred for 5 h. After the reaction, the heterogeneous catalyst was removed by filtration through a small plug of silica gel in a pipet, and the solids washed several times with ethanol. The filtrate was collected, solvent was removed under reduced pressure on a rotary evaporator to give the product as pale yellow solid (38.5 mg, 94%). Spectral data of starting material and product matched with reported values⁷³⁻⁷⁴.



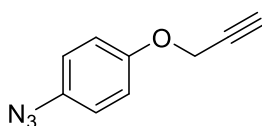
4-nitroaniline (3i): Ru NPs supported on polystyrene (9.7 mg, 0.47 mmol/g, 1.5 mol% wrt ruthenium) was placed in a 10 mL vial containing a Teflon-coated magnetic stir bar, followed by the addition of ethanol (2.0 mL), 1-azido-4-nitroaniline (50 mg, 0.304 mmol), Hydrazine monohydrate (0.913 mmol, 44 μ L was added dropwise, the vial was closed with a Teflon cap, and the reaction mixture was stirred for 6 h. After the reaction, the heterogeneous catalyst was removed by filtration through a small plug of silica gel in a pipet, and the solids washed several times with ethanol. The filtrate was collected, solvent was removed under reduced pressure on a rotary evaporator to give the product as pale yellow solid, 90% yield (calculated yield from NMR) with 10% 1,4-diaminobenzene. Spectral data of starting material and product matched with reported values⁷³⁻⁷⁴.



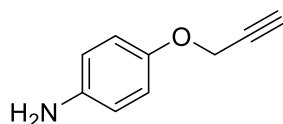
Methyl-4-aminobenzoate (3j): Ru NPs supported on polystyrene (9.0 mg, 0.47 mmol/g, 1.5 mol% wrt ruthenium) was placed in a 10 mL vial containing a Teflon-coated magnetic stir bar, followed by the addition of ethanol (2.0 mL), methyl-4-azidobenzoate (50 mg, 0.282 mmol), Hydrazine monohydrate (0.846 mmol, 41 μ L was added dropwise, closed the vial with teflon cap and stirred the reaction mixture for 6 h. After the reaction, the heterogeneous catalyst was removed by filtration through a small plug of silica gel in a pipet, and the solids washed several times with ethanol. The filtrate was collected, solvent was removed under reduced pressure on a rotary evaporator to give the product as white solid (42.2 mg, 99%). Spectral data of starting material and product matched with reported values⁷³⁻⁷⁴.



4-amino-N-(4-aminophenyl)benzamide (3m): Ru NPs supported on polystyrene (15.2 mg, 0.47 mmol/g, 4 mol% wrt ruthenium) was placed in a 10 mL vial containing a Teflon-coated magnetic stir bar, followed by the addition of toluene (2.0 mL), 4-azido-N-(4-azidophenyl)benzamide⁷ (50 mg, 0.179 mmol), Hydrazine monohydrate (0.716 mmol, 35 μ L) was added dropwise, the vial was closed with a Teflon cap, and the reaction mixture was stirred for 4 h. After the reaction, solvent was evaporated added ethanol and the heterogeneous catalyst was removed by filtration through a small plug of silica gel in a pipet, and the solids washed several times with ethanol. The filtrate was collected, solvent was removed under reduced pressure on a rotary evaporator to give the product (bis-reduction product) as yellow solid (40 mg, 98%). Spectral data of starting material and product matched with reported values⁷⁵⁻⁷⁷.

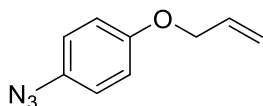


((3-1-azido-4-(prop-2-yn-1-yloxy)benzene: Synthesized according to a known procedure: ¹H NMR (500 MHz, CDCl₃) δ 6.97 (s, 4H), 4.67 (d, J = 2.5 Hz, 2H), 2.55 (t, J = 2.5 Hz, 1H); ¹³C NMR (125 MHz, CDCl₃): 154.8, 133.3, 120.0, 116.3, 78.4, 75.8, 56.2; IR (film) ν_{max} 3294, 2416, 2106, 1503, 1286, 1028, 825 cm^{-1} .

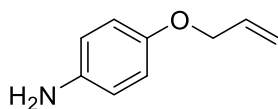


4-(prop-2-yn-1-yloxy)aniline (3k): Ru NPs supported on polystyrene (12.2 mg, 0.47 mmol/g, 2 mol% wrt ruthenium) was placed in a 10 mL vial containing a Teflon-coated magnetic stir bar, followed by the addition of ethanol (2.0 mL), ((3-1-azido-4-(prop-2-yn-1-yloxy)benzene (50 mg, 0.288 mmol), Hydrazine monohydrate (1.152 mmol, 56 μ L) was added dropwise, the vial was closed with a Teflon cap, and the reaction mixture was stirred for 12 h. After the reaction, the heterogeneous catalyst was removed by filtration through a small plug of silica

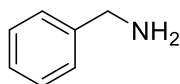
gel in a pipet, and the solids washed several times with ethanol. After filtration the solvent was removed. The yield of the product was analyzed by NMR, (81% yield). ^1H NMR (500 MHz, CDCl_3) δ 6.82 (d, $J = 8.7$ Hz, 2H), 6.64 (d, $J = 8.7$ Hz, 2H), 4.61 (d, $J = 2.4$ Hz, 2H), 2.5 (t, $J = 2.4$ Hz, 1H); ^{13}C NMR (125 MHz, CDCl_3): 151.7, 133.8, 120.0, 117.1, 78.9, 75.5, 55.9; IR (film) ν_{max} 3320, 3295, 2418, 2109, 1504, 1284, 1223, 825 cm^{-1} ; HRMS (EI) calcd. for $\text{C}_9\text{H}_9\text{NO}$, 147.0684; found, $[\text{M}+\text{H}]^+$, 148.0845



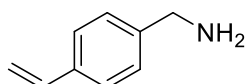
1-(allyloxy)-4-azidobenzene: Synthesized according to a known procedure: ^1H NMR (500 MHz, CDCl_3) δ 6.95 (d, $J = 9$ Hz, 2H), 6.92 (d, $J = 9$ Hz, 2H), 6.12-5.94 (m, 1H), 5.4 (dd, $J = 1.5$ Hz, 1H), 5.3 (dd, $J = 1.5$ Hz, 1H), 4.54-4.47 (m, 2H); ^{13}C NMR (125 MHz, CDCl_3): 156.0, 133.5, 133.0, 120.0, 117.8, 116.0, 69.2; IR (film) ν_{max} 2918, 2415, 2115.55, 1503, 1283, 1243, 1022, 824 cm^{-1} .



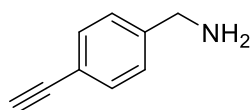
4-(allyloxy) aniline (3I): Ru NPs supported on polystyrene (12.1 mg, 0.47 mmol/g, 2 mol% wrt ruthenium) was placed in a 10 mL vial containing a Teflon-coated magnetic stir bar, followed by the addition of ethanol (2.0 mL), 1-(allyloxy)-4-azidobenzene (50 mg, 0.285 mmol), Hydrazine monohydrate (1.14 mmol, 55.5 μL was added dropwise, closed the vial with teflon cap and stirred the reaction mixture for 8 h. After the reaction, the heterogeneous catalyst was removed by filtration through a small plug of silica gel in a pipet, and the solids washed several times with ethanol, the solvent was removed. The product was obtained as a pale yellow solid (41 mg, 98% yield). ^1H NMR (500 MHz, CDCl_3) δ 6.78 (d, $J = 8.8$ Hz, 2H), 6.64 (d, $J = 8.8$ Hz, 2H), 6.07-6.02 (m, 1H), 5.41-4.37 (m, 1H), 5.27-5.25 (m, 2H), 4.47-4.45 (m, 2H), 3.41 (brs, 2H); ^{13}C NMR (125 MHz, CDCl_3): 151.8, 140.2, 133.9, 117.3, 116.4, 116.0, 69.7; IR (film) ν_{max} 3302, 3027, 2858, 1573, 1493, 1453, 1100; HRMS (EI) calcd. for $\text{C}_9\text{H}_{11}\text{NO}$, 149.0841; found, $[\text{M}+\text{H}]^+$, 150.0914.



Benzylamine (4a): Ru NPs supported on polystyrene (15.9 mg, 0.47 mmol/g, 2 mol% wrt ruthenium) were placed in a 10 mL vial containing a Teflon-coated magnetic stir bar, followed by the addition of ethanol (2.0 mL), (azidomethyl)benzene (50 mg, 0.375 mmol), Hydrazine monohydrate (1.12 mmol, 56.4 μ L was added dropwise, the vial was closed with a Teflon cap, and the reaction mixture was stirred for 4 h. After the reaction, the heterogeneous catalyst was removed by filtration through a small plug of silica gel in a pipet, and the solids washed several times with ethanol. The filtrate was collected, solvent was removed under reduced pressure on a rotary evaporator to give the product as clear oil (40 mg, 99%). Spectral data of starting material and product matched with reported values⁷⁵⁻⁷⁷.

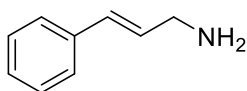


(4-vinylphenyl)methanamine (4b): Ru NPs supported on polystyrene (13.3 mg, 0.47 mmol/g, 2 mol% wrt ruthenium) was placed in a 10 mL vial containing a Teflon-coated magnetic stir bar, followed by the addition of ethanol (2.0 mL), 1-(azidomethyl)-4-vinylbenzene⁸ (50 mg, 0.314 mmol), Hydrazine monohydrate (0.942 mmol, 45.7 μ L was added dropwise, the vial was closed with a Teflon cap, and the reaction mixture was stirred for 5 h. After the reaction, the heterogeneous catalyst was removed by filtration through a small plug of silica gel in a pipet, and the solids washed several times with ethanol. The filtrate was collected, solvent was removed under reduced pressure on a rotary evaporator to give the product as clear oil (41 mg, 98%). Spectral data of starting material and product matched with reported values⁷⁵⁻⁷⁷.

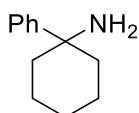


(4-ethynylphenyl)methanamine (4c): Ru NPs supported on polystyrene (13.5 mg, 0.47 mmol/g, 4 mol% wrt ruthenium) was placed in a 10mL vial containing a Teflon-coated magnetic stir bar, followed by the addition of ethanol (2.0 mL), 1-(azidomethyl)-4-ethynylbenzene (50 mg, 0.318 mmol), Hydrazine monohydrate (1.27 mmol, 62 μ L was added

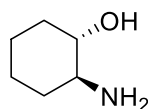
dropwise, the vial was closed with a Teflon cap, and the reaction mixture was stirred for 15 h. After the reaction, the heterogeneous catalyst was removed by filtration through a small plug of silica gel in a pipet, and the solids washed several times with ethanol. The filtrate was collected, solvent was removed under reduced pressure on a rotary evaporator to give the product as clear oil (50% based on nmr). Spectral data of starting material and product matched with reported values⁷⁸⁻⁸¹.



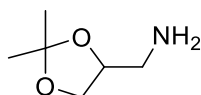
Cinnamyl amine (4d): Ru NPs supported on polystyrene (13.4 mg, 0.47 mmol/g, 2 mol% wrt ruthenium) was placed in a 10 mL vial containing a Teflon-coated magnetic stir bar, followed by the addition of ethanol (2.0 mL), (E)-(3-azidoprop-1-en-1-yl)benzene (50 mg, 0.314 mmol), Hydrazine monohydrate (0.942 mmol, 45.7 μ L) was added dropwise, the vial was closed with a Teflon cap, and the reaction mixture was stirred for 5 h. After the reaction, the heterogeneous catalyst was removed by filtration through a small plug of silica gel in a pipet, and the solids washed several times with ethanol. The filtrate was collected, solvent was removed under reduced pressure on a rotary evaporator to give the product as clear oil (40.5 mg, 97%). Spectral data of starting material and product matched with reported values⁷⁸⁻⁸¹.



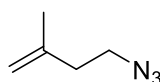
1-phenylcyclohexan-1-amine (4e): Ru NPs supported on polystyrene (10.6 mg, 0.47 mmol/g, 2 mol% wrt ruthenium) was placed in a 10 mL vial containing a Teflon-coated magnetic stir bar, followed by the addition of ethanol (2.0 mL), (1-azidocyclohexyl)benzene⁹ (50 mg, 0.248 mmol), Hydrazine monohydrate (0.993 mmol, 48.2 μ L) was added dropwise, the vial was closed with a Teflon cap, and the reaction mixture was stirred for 5 h. After the reaction, the heterogeneous catalyst was removed by filtration through a small plug of silica gel in a pipet, and the solids washed several times with ethanol. The filtrate was collected, solvent was removed under reduced pressure on a rotary evaporator to give the product as clear oil (43 mg, 99%). Spectral data of starting material and product matched with reported values⁷⁸⁻⁸¹.



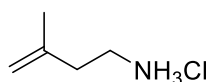
2-aminocyclohexan-1-ol (4f): Ru NPs supported on polystyrene (15.0 mg, 0.47 mmol/g, 2 mol% wrt ruthenium) was placed in a 10 mL vial containing a Teflon-coated magnetic stir bar, followed by the addition of ethanol (2.0 mL), 2-azidocyclohexan-1-ol¹⁰ (50 mg, 0.354 mmol), Hydrazine monohydrate (0.1.06 mmol, 51.5 μ L was added dropwise, the vial was closed with a Teflon cap, and the reaction mixture was stirred for 5 h. After the reaction, the heterogeneous catalyst was removed by filtration through a small plug of silica gel in a pipet, and the solids washed several times with ethanol. The filtrate was collected, solvent was removed under reduced pressure on a rotary evaporator to give the product as clear oil (38 mg, 94%). Spectral data of starting material and product matched with reported values⁷⁸⁻⁸¹.



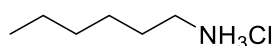
(2,2-dimethyl-1,3-dioxolan-4-yl)methanamine (4g): Ru NPs supported on polystyrene (13.5 mg, 0.47 mmol/g, 2 mol% wrt ruthenium) was placed in a 10 mL vial containing a Teflon-coated magnetic stir bar, followed by the addition of ethanol (2.0 mL), 4-(azidomethyl)-2,2-dimethyl-1,3-dioxolane¹¹ (50 mg, 0.318 mmol), Hydrazine monohydrate (0.954 mmol, 46.3 μ L was added dropwise, the vial was closed with a Teflon cap, and the reaction mixture was stirred for 5 h. After the reaction, the heterogeneous catalyst was removed by filtration through a small plug of silica gel in a pipet, and the solids washed several times with ethanol. The filtrate was collected, solvent was removed under reduced pressure on a rotary evaporator to give the product as clear oil (37.5 mg, 90%). Spectral data of starting material and product matched with reported values⁷⁸⁻⁸¹.



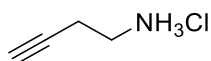
4-azido-2-methylbut-1-ene: Synthesized according to a known procedure: ¹H NMR (500 MHz, CDCl₃) δ 4.85–4.79 (d, 2H), 3.38 (t, J = 7.2 Hz, 2H), 2.31 (t, J = 7.2 Hz, 2H), 1.76 (s, 3H); ¹³C NMR (125 MHz, CDCl₃): 141.7, 112.6, 49.4, 36.7, 22.25; IR (film) ν_{max} 2937, 2098, 1650, 1259 cm^{-1} ; HRMS (EI) calcd. for C₅H₉N₃, 111.0796; found, [M+H]⁺, 112.8026.



3-methylbut-3-en-1-amine (4h): Prepared according to the general procedure using 4-azido-2-methylbut-1-ene¹² (50 mg, 0.45 mmol), Ru/Polystyrene catalyst (19.5 mg, 0.47 mmol/g Ru in polystyrene, 2 mol% wrt ruthenium), and 65.5 μ L, 3 equiv $\text{NH}_2\text{NH}_2\cdot\text{H}_2\text{O}$. After filtration 1.5 equiv Conc. HCl was added to generate the HCl salt and the solvent was removed. The product was obtained as a clear oil (50 mg, 91% yield). ^1H NMR (500 MHz, CDCl_3) δ 4.88 (d, 2H), 3.14 (t, $J = 7.2$ Hz, 2H), 2.49 (t, $J = 7.2$ Hz, 2H), 1.77 (s, 3H); ^{13}C NMR (125 MHz, CDCl_3) δ 140, 113.7, 37.9, 35.2, 22.2; IR (film) ν_{max} 3365, 3290, 1647, 885 Cm^{-1} ; HRMS (EI) calcd. for $\text{C}_5\text{H}_{12}\text{ClN}$, 121.0658; found, $[\text{M}+\text{H}]^+$, 122.1012.

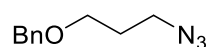


hexan-1-amine (4i): Ru NPs supported on polystyrene (0.47 mmol/g, 2 mol% wrt ruthenium) was placed in a 10 mL vial containing a Teflon-coated magnetic stir bar, followed by the addition of ethanol (2.0 mL), 1-azidohexane (50 mg, 0.393 mmol), Hydrazine monohydrate (1.18 mmol, 57.2 μ L was added dropwise, the vial was closed with a Teflon cap, and the reaction mixture was stirred for 5 h. After the reaction, the heterogeneous catalyst was removed by filtration through a small plug of silica gel in a pipet, and the solids washed several times with ethanol. The filtrate was collected, methanolic HCl was added and isolated the product as hydrochloride salt giving white solid (48 mg, 88%). Spectral data of starting material and product matched with reported values⁷⁵

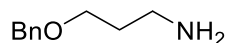


but-3-yn-1-amine (4j): Ru NPs supported on polystyrene (22.3 mg, 0.47 mmol/g, 4 mol% wrt ruthenium) was placed in a 10 mL vial containing a Teflon-coated magnetic stir bar, followed by the addition of ethanol (2.0 mL), 4-azidobut-1-yne¹³ (50 mg, 0.525 mmol), Hydrazine monohydrate (2.1 mmol, 102 μ L was added dropwise, the vial was closed with a Teflon cap, and the reaction mixture was stirred for 12 h. After the reaction, the heterogeneous catalyst was removed by filtration through a small plug of silica gel in a pipet, and the solids washed several times with ethanol. The filtrate was collected, after filtration 1.5 equiv methanolic HCl was added to generate the HCl salt and the solvent was removed. The product was obtained as white

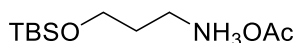
solid (51 mg, 92%). Spectral data of starting material and product matched with reported values⁷⁸⁻⁸¹.



((3-azidopropoxy)methyl)benzene: Synthesized according to a known procedure: ¹H NMR (500 MHz, CDCl₃) δ 7.32 (s, 5H), 4.48 (s, 2H), 3.52 (t, *J* = 9.5 Hz, 2H), 3.38 (t, *J* = 11 Hz, 2H), 1.75-1.85 (m, 2H); ¹³C NMR (125 MHz, CDCl₃): 138.3, 128.4, 127.7, 66.9, 48.5, 29.3; IR (film) ν_{\max} 2862, 2096, 1453, 1100, 737 cm⁻¹; HRMS (EI) calcd. for C₁₀H₁₃N₃O, 191.1059; found, [M+H]⁺, 192.1068.

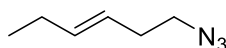


3-(benzyloxy)propan-1-amine (4k): Ru NPs supported on polystyrene (11.1 mg, 0.47 mmol/g, 2 mol% wrt ruthenium) was placed in a 10 mL vial containing a Teflon-coated magnetic stir bar, followed by the addition of ethanol (2.0 mL), ((3-azidopropoxy)methyl)benzene (50 mg, 0.261 mmol), Hydrazine monohydrate (0.784 mmol, 38 μ L) was added dropwise, the vial was closed with a Teflon cap, and the reaction mixture was stirred for 6 h. After the reaction, the heterogeneous catalyst was removed by filtration through a small plug of silica gel in a pipet, and the solids washed several times with ethanol. The filtrate was collected, solvent was removed under reduced pressure on a rotary evaporator to give the product as clear oil (40 mg, 93%). Spectral data of starting material and product matched with reported values³. ¹H NMR (500 MHz, CDCl₃) δ 7.34 (s, 5H), 4.51 (s, 2H), 3.56 (t, *J* = 6 Hz, 2H), 2.82 (t, *J* = 7 Hz, 2H), 1.76 (m, 2H); ¹³C NMR (125 MHz, CDCl₃): 138.5, 128.4, 127.6, 127.5, 72.9, 68.3, 39.6, 33.5; IR (film) ν_{\max} 3340, 2866, 1464, 1102, 736; HRMS (EI) calcd. for C₁₀H₁₅NO, 165.1154; found, [M+H]⁺, 166.1246.

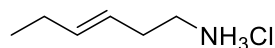


3-((tert-butyldimethylsilyloxy)propan-1-amine (4l): Ru NPs supported on polystyrene (0.401 mmol/g, 4 mol% wrt ruthenium) was placed in a 10mL vial containing a Teflon-coated magnetic stir bar, followed by the addition of ethanol (2.0 mL), (3-azidopropoxy)(tert-butyl)dimethylsilane (50 mg, 0.232 mmol), Hydrazine monohydrate (0.696 mmol, 34 μ L) was added dropwise, the vial was closed with a Teflon cap, and the reaction mixture was stirred for

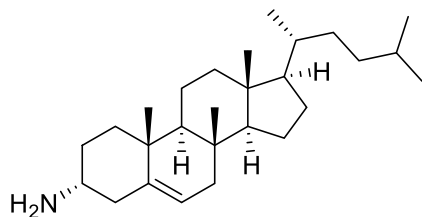
6 h. After the reaction, the heterogeneous catalyst was removed by filtration through a small plug of silica gel in a pipet, and the solids washed several times with ethanol. To the filtrate was added 1 mL acetic acid 0.24 M in water which produced a white precipitate. The precipitate was collected by filtration and dried on the high vacuum (56.5 mg, 99%). ^1H NMR(500 MHz, CDCl_3): δ 8.73(s, 3H), 3.66(t, $J = 5.14$ Hz, 2H), 2.93(t, $J = 7.34$ Hz, 2H), 1.89(s, 3H), 1.8(pent, $J = 6.56$ Hz, 2H), 0.83(s, 9H), 0.0(s, 6H); ^{13}C NMR(500 MHz, CDCl_3): 177, 61, 38, 29, 25, 21, 18, -5; IR (film) ν_{max} 2928, 1572, 1407, 1256, 1099 cm^{-1} ; HRMS (EI) calcd. for $\text{C}_9\text{H}_{24}\text{NOSi}$, 190.1622; found, $[\text{M}+\text{H}]^+$, 191.1621.



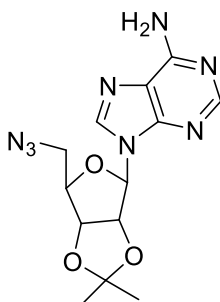
(E)-1-azidohex-3-ene: Synthesized according to the general procedure: ^1H NMR (500 MHz, CDCl_3): 5.64-5.559 (m, 1H), 5.42-5.36 (m, 1H), 3.27 (t, $J = 4.5$ Hz, 2H), 2.33-2.29 (m, 2H), 2.07-2.01 (m, 2H), 1.0-0.97 (t, 3H, $J = 4.5$ Hz); ^{13}C NMR (125 MHz, CDCl_3): 135.4, 124.4, 51.2, 32.2, 25.6, 13.5; IR (film) ν_{max} 2340, 2100, 1652, 1263; HRMS (EI) calcd. for $\text{C}_6\text{H}_{11}\text{N}_3$, 125.0953; found, $[\text{M}+\text{H}]^+$, 126.1028.



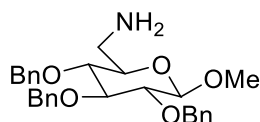
(E)-hex-3-en-1-amine (2): Prepared according to the general procedure using (50 mg 0.399 mmol) (E)-1-azidohex-3-ene, Ru/Polystyrene catalyst (17 mg, 0.47 mmol/g Ru in polystyrene, 2 mol% wrt ruthenium), and 58 μL , 3 equiv $\text{NH}_2\text{NH}_2 \cdot \text{H}_2\text{O}$. After filtration, 1.5 equiv Conc. HCl was added to generate the HCl salt and the solvent was removed. The product was obtained as white solid (53 mg, 98% yield). ^1H NMR (500 MHz, CDCl_3): 8.2 (brs, 3H), 5.7-5.6 (m, 1H), 5.38-5.33 (m, 1H), 3.13-2.91 (m, 2H), 2.58-2.35 (m, 2H), 2.0 (t, 2H, $J = 6.9$ Hz), 0.98 (t, 3H, $J = 7.2$ Hz); ^{13}C NMR (125 MHz, CDCl_3): 137.2, 122.5, 39.7, 30.5, 25.5, 13.4; IR (film) ν_{max} 3340, 3292, 1650, 889 cm^{-1} ; HRMS (EI) calcd. for $\text{C}_6\text{H}_{14}\text{N}$, 135.0815; found, $[\text{M}-\text{Cl}]^+$, 100.1032.



3 α -Cholesteryl amine (4m): Ru NPs supported on polystyrene (10.0 mg, 0.47 mmol/g, 4 mol% wrt ruthenium) was placed in a 10 mL vial containing a Teflon-coated magnetic stir bar, followed by the addition of ethanol (2.0 mL), 3 α -Cholesteryl azide¹⁴ (50 mg, 0.117 mmol), Hydrazine monohydrate (0.467 mmol, 22.7 μ L) was added dropwise at room temperature, the vial was closed with a Teflon cap, and the reaction mixture was stirred for 6 h. After the reaction, the heterogeneous catalyst was removed by filtration through a small plug of silica gel in a pipet, and the solids washed several times with ethanol, the solvent was removed. The product was obtained as a white solid (45.5 mg, 97% yield). Spectral data of both starting material and product matched with reported values⁸²⁻⁸³.

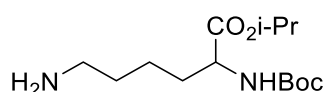


9-((3aR,4R,6R,6aR)-6-(aminomethyl)-2,2-dimethyltetrahydrofuro[3,4-d][1,3]dioxol-4-yl)-9H-purin-6-amine (4n): Ru NPs supported on polystyrene (12.7 mg, 0.47 mmol/g, 4 mol% wrt ruthenium) was placed in a 10 mL vial containing a Teflon-coated magnetic stir bar, followed by the addition of ethanol (2.0 mL), 9-((3aR,4R,6R,6aR)-6-(azidomethyl)-2,2-dimethyltetrahydrofuro[3,4-d][1,3]dioxol-4-yl)-9H-purin-6-amine¹⁵ (50 mg, 0.150 mmol), Hydrazine monohydrate (0.601 mmol, 23 μ L) was added dropwise at room temperature, the vial was closed with a Teflon cap, and the reaction mixture was stirred for 6 h. After the reaction, the heterogeneous catalyst was removed by filtration through a small plug of silica gel in a pipet, and the solids washed several times with ethanol, the solvent was removed. The product was obtained as a pale yellow solid (45 mg, 98% yield). Spectral data of both starting material and product matched with reported values⁸²⁻⁸³.

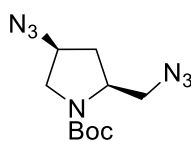


((2R,3S,4S,5R,6S)-3,4,5-tris(benzyloxy)-6-methoxytetrahydro-2H-pyran-2

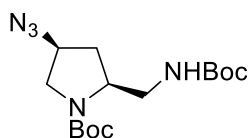
yl)methanamine (4o): Ru NPs supported on polystyrene (0.401 mmol/g, 4 mol% wrt ruthenium) was placed in a 10 mL vial containing a Teflon-coated magnetic stir bar, followed by the addition of ethanol (2.0 mL), (2R,3S,4S,5R,6S)-2-(azidomethyl)-3,4,5-tris(benzyloxy)-6-methoxytetrahydro-2H-pyran¹⁶ (50 mg, 0.102 mmol) and the glass vial was sealed with septum and wrapped the septum with parafilm. Hydrazine monohydrate (0.408 mmol, 20 μ L) was added and the reaction mixture was stirred at room temperature for 7 h. After the reaction, the heterogeneous catalyst was removed by filtration through a small plug of silica gel in a pipet and the solids washed several times with ethanol. The filtrate was collected, and the solvent removed under reduced pressure on a rotary evaporator to provide the product as yellow oil (46.7 mg, 99%). Spectral data of starting material and product matched with reported values⁸⁴.



isopropyl (tert-butoxycarbonyl)lysinate(4p): Ru NPs supported on polystyrene (0.401 mmol/g, 5 mol% wrt ruthenium) was placed in a 10mL vial containing a Teflon-coated magnetic stir bar, followed by the addition of ethanol (2.0 mL), isopropyl N²-(tert-butoxycarbonyl)-N⁶-diazolysinate¹⁷ (26.7 mg, 0.085 mmol) and the glass vial was sealed with septum and wrapped the septum with parafilm. Hydrazine monohydrate (0.424 mmol, 20.5 μ L) was added and the reaction mixture was stirred at room temperature for 14h. After the reaction, the heterogeneous catalyst was removed by filtration through a small plug of silica gel in a pipet and the solids washed several times with ethanol. The filtrate was collected, and the solvent removed under reduced pressure on a rotary evaporator to provide the product as yellow oil (24 mgr, 98%)¹H NMR(500 MHz, CDCl₃): δ 4.93-5.1(m, 2H), 4.1-4.26(m, 1H), 2.62(t, $j=6.62$ Hz, 2H), 1.68-1.77(m, 1H), 1.48-1.6(m, 3H), 1.37(s, 9H), 1.19(d, $J = 6.5$ Hz, 3H), 1.17(d, $J = 6.5$ Hz, 3H);¹³CNMR(500MHZ, CDCl₃): δ 172.3, 155.4, 79.6, 68.8, 53.54, 41.9, 33.1, 32.6, 29.7, 28.3, 22.5, 21.76 ; IR (film) ν_{\max} 3368, 2928, 1718, 1508 Cm⁻¹; HRMS(EI) calcd. For C₁₄H₂₈N₂O₄, 288.2049; found, [M+H]⁺, 289.2138.



tert-Butyl (2S,4S)-4-azido-2-(azidomethyl)pyrrolidine-1-carboxylate: Synthesized according to a known procedure¹⁸: ¹H NMR (500 MHz, CDCl₃) δ 4.2-3.86 (m, 2H), 3.8-3.25 (m, 4H), 2.31-2.20 (m, 1H), 2.1-1.99 (m, 1H), 1.47 (s, 9H); ¹³C NMR (125 MHz, CDCl₃) δ 154.1, 80.5, 59.4, 58.8, 55.8, 52.4, 51.8, 51.6, 34.4, 29.7, 28.3; IR (film) ν_{max} 2359, 2341, 2101, 1697, 1392; HRMS (EI) calcd. for C₁₀H₁₇N₇O₂, 267.1444 Cm⁻¹; found, [M+H]⁺, 268.1517.



Procedure: 1

tert-butyl 4-azido-2-(((tert-butoxycarbonyl)amino)methyl)pyrrolidine-1-carboxylate

(6a): Ru NPs supported on polystyrene (0.401 mmol/g, 4 mol% wrt ruthenium) was placed in a 10 mL vial containing a Teflon-coated magnetic stir bar, followed by the addition of ethanol (2.0 mL), tert-butyl 4-azido-2-(azidomethyl)pyrrolidine-1-carboxylate (50 mg, 0.187 mmol), Hydrazine monohydrate (0.748 mmol, 36.3 μL) was added dropwise at 0 °C, closed the vial with teflon cap and stirred the reaction mixture at room temperature for 5 h. After the reaction, the heterogeneous catalyst was removed by filtration through a small plug of silica gel in a pipet, and the solids washed several times with ethanol. The filtrate was collected, and the solvent removed under reduced pressure on a rotary evaporator to provide the crude product which was purified by column chromatography to yield mono amine as colorless liquid. To the crude product methanol (4mL), trimethylamine (131 μL, 0.935 mmol) and Boc anhydride (122.5 mg, 0.561 mmol) were added and stirred the reaction mixture at room temperature for 12h. Solvent was removed and the reaction mixture was purified by flash chromatography to yield mono amine as clear oil (48 mg, 76%).

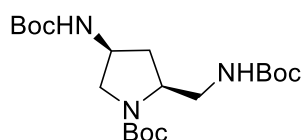
Procedure: 2

Ru NPs supported on polystyrene (0.401 mmol/g, 4 mol% wrt ruthenium) was placed in a 10 mL vial containing a Teflon-coated magnetic stir bar, followed by the addition of ethanol (2.0 mL), tert-butyl 4-azido-2-(azidomethyl)pyrrolidine-1-carboxylate (50 mg, 0.187 mmol) and the glass vial was sealed with septum and wrapped the septum with parafilm.

Hydrazine monohydrate (0.748 mmol, 36.3 μ L dissolved in 1 mL ethanol) was added dropwise at 0 $^{\circ}$ C over a period of 1 h. After completion of the addition the reaction mixture was stirred at room temperature for 30 hours. After the reaction, the heterogeneous catalyst was removed by filtration through a small plug of silica gel in a pipet, and the solids washed several times with ethanol. The filtrate was collected, and the solvent removed under reduced pressure on a rotary evaporator to provide the crude product. To the crude product methanol (4 mL), trimethylamine (131 μ L, 0.935 mmol) and boc anhydride (122.5 mg, 0.561 mmol) were added and stirred the reaction mixture at room temperature for 12 h. Solvent was removed and the reaction mixture was purified by flash chromatography to yield mono amine as clear oil (45mg, 70%, 3.3:1 **6a:6b**). ^1H NMR (500 MHz, CDCl_3) δ 5.1 (brs, 1H), 4.2–3.8 (m, 3H), 3.3–3.28 (m, 1H), 3.15–3.05 (m, 1H), 2.43–2.3 (m, 1H), 1.8–1.72 (m, 1H), 1.46 (s, 18 H); ^{13}C NMR (125 MHz, CDCl_3) δ 155.3, 154.4, 80.2, 79.7, 55.7, 53.3, 52.7, 48.5, 34.7, 28.4, 28.3, 28.2; IR (film) ν_{max} 3329, 2977, 2102, 1693, 1523, 1394, 1164 cm^{-1} ; HRMS (EI) calcd. for $\text{C}_{15}\text{H}_{27}\text{N}_5\text{O}_4$, 341.2063; found, $[\text{M}+\text{H}]^+$, 342.2137.

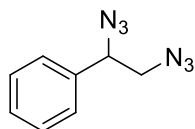
Procedure: 3

Ru NPs supported on polystyrene (0.401 mmol/g, 3 mol% wrt ruthenium) was placed in a 10 mL vial containing a Teflon-coated magnetic stir bar, followed by the addition of ethanol (2.0 mL), tert-butyl 4-azido-2-(azidomethyl)pyrrolidine-1-carboxylate (50 mg, 0.187 mmol) and the glass vial was sealed with septum and wrapped the septum with parafilm. Hydrazine monohydrate (0.748 mmol, 36.3 μ L dissolved in 1 mL ethanol) was added dropwise at 0 $^{\circ}$ C over a period of 1 h. After completion of the addition the reaction mixture was stirred at room temperature for 24 h. Again reaction mixture was cooled to 0 $^{\circ}$ C and added another 1 equivalent of hydrazine hydrate (9 μ L) dropwise over 30 min and stirred the reaction at room temperature for another 15 h. After the reaction, the heterogeneous catalyst was removed by filtration through a small plug of silica gel in a pipet, and the solids washed several times with ethanol. The filtrate was collected, and the solvent removed under reduced pressure on a rotary evaporator to provide the crude product. To the crude product methanol (4 mL), trimethylamine (131 μ L, 0.935 mmol) and boc anhydride (122.5 mg, 0.561 mmol) were added and stirred the reaction mixture at room temperature for 12 h. Solvent was removed and the reaction mixture was purified by flash chromatography to yield mono amine as clear oil (50 mg, 79%, 7.9:1 **6a:6b**).

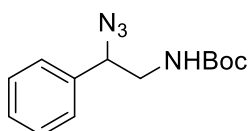


tert-butyl 4-((tert-butoxycarbonyl)amino)-2-(((tert-butoxycarbonyl)amino)methyl)pyrrolidine-1-carboxylate: Yield 21% (16.3mg). ^1H NMR (500 MHz, CDCl_3) δ 5.4 (brs, 1H), 5.2 (brs, 1H), 4.0 (brs, 1H), 3.82–3.68 (m, 2H), 3.4–3.0 (m, 3H), 2.32–2.08 (m, 1H), 1.7–1.57 (m, 1H), 1.38 (s, 27 H); ^{13}C NMR (125 MHz, CDCl_3) δ 156.7, 155.6, 154.2, 80.1, 79.5, 56.8, 53.4, 49.4, 43.9, 34.2, 30.9, 28.4, 28.3; IR (film) ν_{max} 3340, 1696, 1524, 1392, 1165 cm^{-1} ; HRMS (EI) calcd. for $\text{C}_{20}\text{H}_{37}\text{N}_3\text{O}_6$, 415.2682; found, $[\text{M}+\text{H}]^+$, 416.2740.

General procedure for the synthesis of styrenyl bis-azides: To a suspension of NaN_3 (15 mmol) and NaIO_4 (5 mmol) in 20 ml of DMSO–glacial AcOH (4:1) was added styrene (5 mmol) and the reaction mixture was stirred at 75 °C for 2 h. The reaction was monitored by TLC and then poured into water (100 ml) and extracted with EtOAc (3 X 50 ml). The combined organic layers were washed with saturated solution of aqueous NaHCO_3 (50 ml) followed by aqueous $\text{Na}_2\text{S}_2\text{O}_3$ (5%, 50 ml), dried over anhyd. Na_2SO_4 . Concentration of the organic layer gave crude diazide, which was purified by silica gel chromatography using hexane/ethyl acetate (19:1) as eluent to obtain pure 1,2-diazoethylbenzene (291% yield)

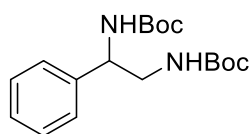


(1,2-diazoethyl)benzene: Prepared according to the general procedure (Yield 58%): ^1H NMR (500 MHz, CDCl_3) δ 7.46-7.35 (m, 5H), 4.69 (dd, $J = 5\text{Hz}$, 1H), 3.49 (qd, $J = 5, 8.5\text{Hz}$, 2H); ^{13}C NMR (125 MHz, CDCl_3): 136.3, 129.1, 129.0, 126.9, 65.5, 55.9; IR (film) ν_{max} 3032, 2926, 2103, 1454, 1258, 700 cm^{-1} .

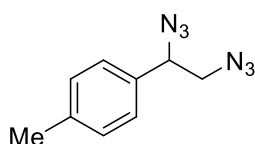


tert-butyl (2-azido-2-phenylethyl)carbamate (7a): Ru NPs supported on polystyrene (0.401 mmol/g, 2 mol% wrt ruthenium) was placed in a 10 mL vial containing a Teflon-coated magnetic stir bar, followed by the addition of ethanol (2.0 mL), (1,2-diazoethyl)benzene

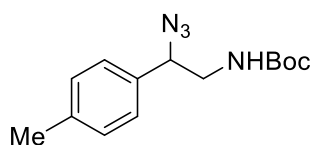
diazide (50 mg, 0.265 mmol) and the glass vial was sealed with septum and wrapped the septum with paraflim. Hydrazine monohydrate (1.06 mmol, 51 μ L) was added dropwise at 0 $^{\circ}$ C and the reaction mixture was warmed to room temperature and stirred for 6 h. After the reaction, the heterogeneous catalyst was removed by filtration through a small plug of silica gel in a pipet and the solids washed several times with ethanol. The filtrate was collected, and the solvent removed under reduced pressure on a rotary evaporator to provide the crude product. To the crude product methanol (4 mL), trimethylamine (185 μ L, 1.33 mmol) and boc anhydride (174 mg, 0.8 mmol) were added and stirred the reaction mixture at room temperature for 12 h. solvent was removed and the reaction mixture was purified by flash chromatography to yield mono amine as clear oil (48.5mg, 70%). ^1H NMR (500 MHz, CDCl_3) δ 7.44–7.30 (m, 5H), 4.86 (brs, 1H), 4.75–4.67 (m, 1H), 3.33–3.19 (m, 1H), 1.46 (s, 9H); ^{13}C NMR (125 MHz, CDCl_3) δ 155.7, 137.1, 128.9, 128.8, 128.6, 128, 126.5, 79.8, 65.6, 55.6, 46.11, 28.35; IR (film) ν_{max} 2103, 1700, 1513, 1249, 1168 cm^{-1} ; HRMS (EI) calcd. for $\text{C}_{13}\text{H}_{18}\text{N}_4\text{O}_2$, 262.1430; found, $[\text{M}+\text{Na}]^+$, 285.1312.



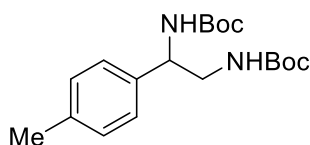
di-tert-butyl (1-phenylethane-1,2-diyl)dicarbamate: Prepared according to the general procedure (Yield 21 %, 18.7 mg). ^1H NMR (500 MHz, CDCl_3) δ 7.41–7.25 (m, 5H), 5.55 (brs, 1H), 4.94–4.67 (m, 2H), 3.59–3.32 (m, 2H), 1.47 (s, 9H), 1.44 (s, 9H); ^{13}C NMR (125 MHz, CDCl_3) δ 128.7, 127.6, 126.3, 80.5, 55.9, 45.8, 28.36; IR (film) ν_{max} 3353, 2977, 1696, 1514, 1171 cm^{-1} ; HRMS (EI) calcd. for $\text{C}_{18}\text{H}_{28}\text{N}_2\text{O}_4$, 336.2049; found, $[\text{M}+\text{H}]^+$, 337.2128.



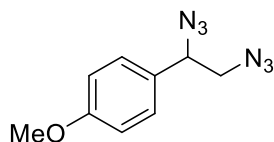
1-(1,2-diazidoethyl)-4-methylbenzene: Synthesized according to the general procedure with 2.0 g (16.9 mmol) of 4-methylstyrene. (2.2 gr, 64% yield). ^1H NMR (500 MHz, CDCl_3) δ 7.21 (s, 4H), 4.63 (dd, $J = 5\text{Hz}$, 1H), 3.46 (qd, $J = 5\text{Hz}$, 8.5, 5 Hz, 2H); ^{13}C NMR (125 MHz, CDCl_3): 139.0, 133.2, 129.7, 126.9, 65.3, 55.9, 21.2; IR (film) ν_{max} 2926, 2101, 1454, 1254, 765, 701 cm^{-1} .



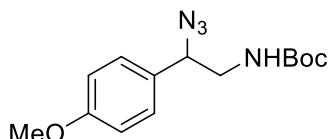
tert-butyl (2-azido-2-(p-tolyl)ethyl)carbamate (7b): Ru NPs supported on polystyrene (0.401 mmol/g, 2 mol% wrt ruthenium) was placed in a 10 mL vial containing a Teflon-coated magnetic stir bar, followed by the addition of ethanol (2.0 mL), 1-(1,2-diazidoethyl)-4-methylbenzenediazide (50 mg, 0.247 mmol) and the glass vial was sealed with septum and wrapped the septum with parafilm. Hydrazine monohydrate (0.988 mmol, 48 μ L) was added dropwise at 0 $^{\circ}$ C and the reaction mixture was stirred at room temperature for 6h. After the reaction, the heterogeneous catalyst was removed by filtration through a small plug of silica gel in a pipet and the solids washed several times with ethanol. The filtrate was collected, and the solvent removed under reduced pressure on a rotary evaporator to provide the crude product. To the crude product methanol (4 mL), trimethylamine (172.5 μ L, 1.23 mmol) and boc anhydride (162 mg, 0.742 mmol) were added and stirred the reaction mixture at room temperature for 12 h. solvent was removed and the reaction mixture was purified by flash chromatography to yield mono amine as clear oil (44.5 mg, 65%). ^1H NMR (500 MHz, CDCl_3) δ 7.13 (s, 4H), 4.81–4.71 (m, 1H), 4.63–4.54 (m, 1H), 3.44–3.30 (m, 1H), 3.20–3.10 (M, 1H), 2.28 (s, 3H), 1.37 (s, 9H); ^{13}C NMR (125 MHz, CDCl_3) δ 155.7, 138.5, 134, 129.6, 126.9, 65.4, 46.0, 28.3, 21.1; IR (film) ν_{max} 3349, 2777, 1697, 1366, 1168 Cm^{-1} ; HRMS (EI) calcd. for $\text{C}_{14}\text{H}_{20}\text{N}_4\text{O}_2$, 276.1586; found, $[\text{M}+\text{H}]^+$, 277.2026.



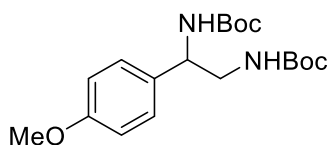
di-tert-butyl (1-(p-tolyl)ethane-1,2-diyl)dicarbamate: Synthesized according to the general procedure, Yield 18% (15.5 mg). ^1H NMR (500 MHz, CDCl_3) δ 7.15 (s, 4H), 5.47 (brs, 1H), 4.89 (brs, 1H), 4.71 (brs, 1H), 3.56–3.20 (m, 2H), 2.33 (s, 3H), 1.44 (s, 9H), 1.42 (s, 9H); ^{13}C NMR (125 MHz, CDCl_3) δ 156.8, 155.7, 137.2, 129.4, 126.2, 79.6, 55.6, 45.9, 28.3, 21.1; IR (film) ν_{max} 3338, 2977, 1697, 1366, 1168 Cm^{-1} ; HRMS (EI) calcd. for $\text{C}_{19}\text{H}_{30}\text{N}_2\text{O}_4$, 350.2206; found, $[\text{M}+\text{H}]^+$, 351. 2280.



^1H NMR (500 MHz, CDCl_3) δ 7.25 (d, $J = 8.5\text{Hz}$, 2H), 6.93 (d, $J = 8.5\text{Hz}$, 2H), 4.62 (dd, $J = 5\text{Hz}$, 1H), 3.42 (qd, $J = 5\text{Hz}$, 8.5, 5 Hz, 2H); ^{13}C NMR (125 MHz, CDCl_3): 160.0, 128.3, 128.2, 114.4, 65.0, 55.8, 55.3; IR (film) ν_{max} 2939, 2100, 1600, 1439, 1267, 1154, 782 Cm^{-1} .

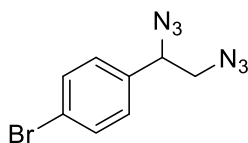


tert-butyl (2-azido-2-(4-methoxyphenyl)ethyl)carbamate (7c): Ru NPs supported on polystyrene (0.401 mmol/g, 4 mol% wrt ruthenium) was placed in a 10 mL vial containing a Teflon-coated magnetic stir bar, followed by the addition of ethanol (2.0 mL), 1-(1,2-diazoethyl)-4-methoxybenzene (50 mg, 0.229 mmol) and the glass vial was sealed with septum and wrapped the septum with parafilm. Hydrazine monohydrate (0.916 mmol, 44 μL) was added dropwise at 0 $^\circ\text{C}$ and the reaction mixture was stirred at room temperature for 32h. After the reaction, the heterogeneous catalyst was removed by filtration through a small plug of silica gel in a pipet and the solids washed several times with ethanol. The filtrate was collected, and the solvent removed under reduced pressure on a rotary evaporator to provide the crude product. To the crude product methanol (4 mL), trimethylamine (160 μL , 1.14 mmol) and boc anhydride (150 mg, 0.688 mmol) were added and stirred the reaction mixture at room temperature for 12 h. solvent was removed and the reaction mixture was purified by flash chromatography to yield mono amine as clear oil (53 mg, 79%). ^1H NMR (500 MHz, CDCl_3) δ 7.27 (d, $J = 9$ Hz, 2H), 6.95 (d, $J = 8.8$ Hz, 2H), 4.84 (brs, 1H), 4.71–4.58 (m, 1H), 3.84 (s, 3H), 3.53–3.39 (m, 1H), 3.32–3.18 (m, 1H), 1.47 (s, 9H); ^{13}C NMR (125 MHz, CDCl_3) δ 159.8, 129, 128.2, 127.7, 114.3, 114.2, 65.2, 55.3, 46.0, 28.2; IR (film) ν_{max} 2926. 2102, 1456, 1254, 763 Cm^{-1} ; HRMS (EI) calcd. for $\text{C}_{14}\text{H}_{20}\text{N}_4\text{O}_3$, 292.1535; found, $[\text{M}+\text{Na}]^+$, 315. 2292.

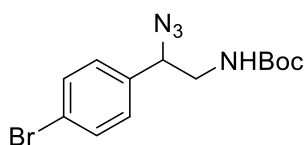


di-tert-butyl (1-(4-methoxyphenyl)ethane-1,2-diyl)dicarbamate: Yield 10% (8.3mg). ^1H NMR (500 MHz, CDCl_3) δ 7.20 (d, $J = 8$ Hz, 2H), 6.88 (d, $J = 9$ Hz, 2H), 5.39 (brs, 1H), 4.82

(brs, 1H), 4.74–4.64 (m, 1H), 3.8 (s, 3H), 3.55–3.25 (m, 2H), 1.45 (s, 9H); ^{13}C NMR (125 MHz, CDCl_3) δ 159, 127.5, 114.11, 113.8, 55.29, 45.8, 29.7, 28.3, 28.2; IR (film) ν_{max} 3350, 2924, 1454, 1252, 762 cm^{-1} ; HRMS (EI) calcd. for $\text{C}_{19}\text{H}_{30}\text{N}_2\text{O}_5$, 366.2155; found, $[\text{M}+\text{H}]^+$, 367.2208.

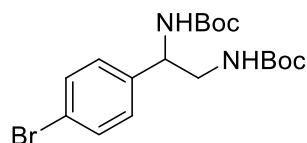


1-bromo-4-(1,2-diazidoethyl)benzene: Synthesized according to the general procedure with 2.8 g (15.3 mmol) of 4-bromostyrene. 2.1 grams product obtained, 28% yield. ^1H NMR (500 MHz, CDCl_3) δ 7.55 (d, $J = 8.5\text{Hz}$, 2H), 7.22 (d, $J = 8.5\text{Hz}$, 2H), 4.64 (dd, $J = 5\text{Hz}$, 1H), 3.45 (qd, $J = 5\text{Hz}$, 8.5, 5 Hz, 2H); ^{13}C NMR (125 MHz, CDCl_3): 135.4, 132.2, 128.6, 123.1, 64.8, 55.8; IR (film) ν_{max} 2925, 2100, 1489, 1256, 1073, 1010, 822 cm^{-1} .



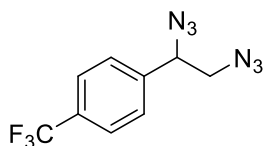
tert-butyl (2-azido-2-(4-bromophenyl)ethyl)carbamate (7d): Ru NPs supported on polystyrene (0.401 mmol/g, 2 mol% wrt ruthenium) was placed in a 10 mL vial containing a Teflon-coated magnetic stir bar, followed by the addition of ethanol (2.0 mL) and 1-bromo-4-(1,2-diazidoethyl)benzene (50 mg, 0.187 mmol). The glass vial was sealed with a septum and wrapped with parafilm. Hydrazine monohydrate (0.748 mmol, 36 μL) was added dropwise at 0 $^\circ\text{C}$ and the reaction mixture was stirred at room temperature for 7h. After the reaction, the heterogeneous catalyst was removed by filtration through a small plug of silica gel in a pipet and the solids washed several times with ethanol. The filtrate was collected, and the solvent removed under reduced pressure on a rotary evaporator to provide the crude product. To the crude product methanol (4 mL), trimethylamine (131 μL , 0.936 mmol) and boc anhydride (122.5 mg, 0.561 mmol) were added and stirred the reaction mixture at room temperature for 12 h. solvent was removed and the reaction mixture was purified by flash chromatography to yield mono amine as clear oil (42.8 mg, 67%). ^1H NMR (500 MHz, CDCl_3) δ 7.53 (d, $J = 8.5\text{Hz}$, 2H), 7.21 (d, $J = 8\text{Hz}$, 2H), 4.85 (brs, 1H), 4.72–4.65 (m, 1H), 3.49–3.39 (m, 1H), 3.25–3.14 (m, 1H), 1.45 (s, 9H); ^{13}C NMR (125 MHz, CDCl_3) δ 155.6, 136.2, 132.1, 128.6,

122.6, 80.0, 65.0, 55.4, 46.1, 28.3; IR (film) ν_{\max} 3340, 2101, 1490, 1254, 1010, 820 cm^{-1} ; HRMS (EI) calcd. for $\text{C}_{13}\text{H}_{17}\text{BrN}_4\text{O}_2$, 340.0535; found, $[\text{M}+\text{H}]^+$, 341.2090.

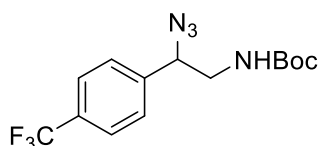


di-tert-butyl (1-(4-bromophenyl)ethane-1,2-diyl)dicarbamate: Yield 24%, (18.6 mg).

^1H NMR (500 MHz, CDCl_3) δ 7.49 (d, $J = 8.4$ Hz, 2H), 7.20 (d, $J = 8.4$ Hz, 2H), 5.6 (brs, 1H), 4.8 (brs, 1H), 4.76–4.60 (m, 1H), 3.53–3.27 (m, 2H), 1.47 (s, 9H), 1.43 (s, 9H); ^{13}C NMR (125 MHz, CDCl_3) δ 157.0, 155.6, 131.8, 128.1, 121.4, 80.0, 55.8, 45.6, 28.3, 28.1; IR (film) ν_{\max} 3330, 2100, 1696, 822 cm^{-1} ; HRMS (EI) calcd. for $\text{C}_{18}\text{H}_{27}\text{BrN}_2\text{O}_4$, 414.1154; found, $[\text{M}+\text{H}]^+$, 415.2319.

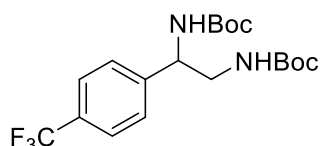


1-(1,2-diazidoethyl)-4-(trifluoromethyl)benzene: Synthesized according to the general procedure (Yield 55%). ^1H NMR (500 MHz, CDCl_3) δ 7.7 (d, $J = 8$ Hz, 2H), 7.48 (d, $J = 8$ Hz, 2H), 4.75 (dd, $J = 5$ Hz, 1H), 3.51 (qd, $J = 5$ Hz, 8.5, 5 Hz, 2H); ^{13}C NMR (125 MHz, CDCl_3): 140.4, 140.3, 131.3, 131.0, 127.4, 127.3, 126.1, 126.0, 124.8, 122.7, 64.9, 55.9; IR (film) ν_{\max} 2929, 2102, 1621, 1325, 1258, 1127, 840 cm^{-1} .

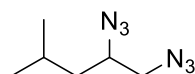


tert-butyl (2-azido-2-(4-(trifluoromethyl)phenyl)ethyl)carbamate (7e): Ru NPs supported on polystyrene (0.401 mmol/g, 2 mol% wrt ruthenium) was placed in a 10 mL vial containing a Teflon-coated magnetic stir bar, followed by the addition of ethanol (2.0 mL) and 1-(1,2-diazidoethyl)-4-(trifluoromethyl)benzene (50 mg, 0.195 mmol). The glass vial was sealed with a septum and wrapped with parafilm. Hydrazine monohydrate (0.780 mmol, 37.8 μL) was

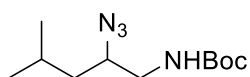
added dropwise at 0 °C and the reaction mixture was stirred at room temperature for 7 h. After the reaction, the heterogeneous catalyst was removed by filtration through a small plug of silica gel in a pipet and the solids washed several times with ethanol. The filtrate was collected, and the solvent removed under reduced pressure on a rotary evaporator to provide the crude product. To the crude product methanol (4 mL), trimethylamine (136 μ L, 0.975 mmol) and boc anhydride (128 mg, 0.585 mmol) were added and stirred the reaction mixture at room temperature for 12 h. Solvent was removed and the reaction mixture was purified by flash chromatography to yield mono amine as clear oil (42.5 mg, 66%). ^1H NMR (500 MHz, CDCl_3) δ 7.7–7.2 (m, 2H), 7.51–7.43 (m, 2H), 4.89 (brs, 1H), 4.81 (brs, 1H), 3.54–3.45 (m, 1H), 3.28–3.19 (m, 1H), 1.44 (s, 9H); ^{13}C NMR (125 MHz, CDCl_3) δ 155.6, 154.9, 141.2, 130.9, 130.6, 130.3, 127.3, 126.9, 125.9–15.77 (m), 80.0, 65.0, 55.4, 46.2, 28.3; IR (film) ν_{max} 2105, 1704, 1326, 1166 cm^{-1} ; HRMS (EI) calcd. for $\text{C}_{14}\text{H}_{17}\text{F}_3\text{N}_4\text{O}_2$, 330.1304; found, $[\text{M}+\text{H}]^+$, 331.1360.



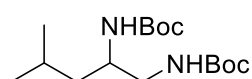
di-tert-butyl (1-(4-(trifluoromethyl)phenyl)ethane-1,2-diyl)dicarbamate: Yield 14% (11 mg). ^1H NMR (500 MHz, CDCl_3) δ 7.63 (d, $J = 8.1$ Hz, 2H), 7.43 (d, $J = 8.1$ Hz, 2H), 5.78 (brs, 1H), 4.82 (brs, 2H), 3.42 (brs, 2H), 1.47 (s, 9H), 1.44 (s, 9H); IR (film) ν_{max} 2980, 2359, 1682, 1524, 1327, 1163 cm^{-1} ; HRMS (EI) calcd. for $\text{C}_{19}\text{H}_{27}\text{F}_3\text{N}_2\text{O}_4$, 404.1923; found, $[\text{M}+\text{Na}]^+$, 427.2020



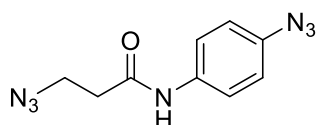
1,2-diazido-4-methylpentane : Synthesized from N-boc-L-leucinol via mesylation (MsCl , Et_3N , CH_2Cl_2 , 98%); Azide displacement (NaN_3 , DMF, 60 °C, 81%); N-Boc deprotection (TFA 4 equiv, CH_2Cl_2 , 88%); and finally azide formation with 1-imidazolesulfonyl azide HCl ,²⁰ CuSO_4 , and K_2CO_3 , 75%. ^1H NMR (500 MHz, CDCl_3) δ 3.55–3.49 (m, 1H), 3.42–3.27 (m, 2H), 1.84–1.74 (m, 1H), 1.53–1.45 (m, 1H), 1.34–1.26 (m, 1H) (dd, $J = 2$ Hz, 6H); ^{13}C NMR (125 MHz, CDCl_3) δ 60.1, 55.2, 40.5, 24.9, 22.9, 21.8; IR (film) ν_{max} 2960, 2102, 1468, 1276 cm^{-1} .



tert-butyl (2-azido-4-methylpentyl)carbamate (7f): Ru NPs supported on polystyrene (0.401 mmol/g, 2 mol% wrt ruthenium) was placed in a 10 mL vial containing a Teflon-coated magnetic stir bar, followed by the addition of ethanol (2.0 mL), 1,2-diazido-4-methylpentane (50 mg, 0.297 mmol) and the glass vial was sealed with septum and wrapped the septum with parafilm. Hydrazine monohydrate (1.19 mmol, 57 μ L) added dropwise at 0 °C and the reaction mixture stirred at room temperature for 7 h. After the reaction, the heterogeneous catalyst removed by filtration through a small plug of silica gel in a pipet and the solids washed several times with ethanol. The filtrate collected, and the solvent removed under reduced pressure on a rotary evaporator to provide the crude product. To the crude product, methanol (4 mL), trimethylamine (207 μ L, 1.48 mmol), and boc anhydride (195 mg, 0.891 mmol) were added and the reaction mixture stirred at room temperature for 7 h. The solvent was removed and the reaction mixture was purified by flash chromatography to yield mono amine as a clear oil (49mg, 68%) ^1H NMR (500 MHz, CDCl_3) δ 4.86 (brs, 1H), 3.58–3.51 (m, 1H), 3.42–3.34 (m, 1H), 3.0–2.93 (m, 1H), 1.84–1.75 (m, 1H), 1.44 (s, 9H), 1.43–1.38 (m, 1H), 1.32–1.24 (m, 1H), 0.97–0.93 (m, 6H); ^{13}C NMR (125 MHz, CDCl_3) δ 155.8, 60.8, 44.7, 40.7, 28.3, 24.9, 22.9, 22.0; IR (film) ν_{max} 3345, 2101, 1692, 1523, 1366, 1172 Cm^{-1} ; HRMS (EI) calcd. for $\text{C}_{11}\text{H}_{22}\text{N}_4\text{O}_2$, 242.1743; found, $[\text{M}+\text{H}]^+$, 243.1206.

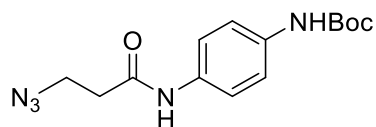


di-tert-butyl (4-methylpentane-1,2-diyl)dicarbamate: Yield 15%, (14 mg) ^1H NMR (500 MHz, CDCl_3) δ 4.88 (brs, 1H), 4.49 (brs, 1H), 3.72 (brs, 1H), 3.27–3.07 (m, 2H), 1.74–1.64 (m, 1H), 1.35–1.18 (m, 2H), 0.97–0.83 (m, 6H); ^{13}C NMR (125 MHz, CDCl_3) δ 156.5, 156.18, 79.2, 49.3, 45.4, 42.1, 28.4, 28.3, 24.8, 23.0, 22.2; IR (film) ν_{max} 3350, 2976, 1693, 1524, 1366 Cm^{-1} , 1173 Cm^{-1} ; HRMS (EI) calcd. for $\text{C}_{16}\text{H}_{32}\text{N}_4\text{O}_4$, 316.2362; found, $[\text{M}+\text{H}]^+$, 317.2441.



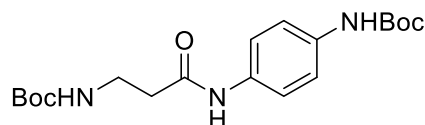
3-azido-N-(4-azidophenyl)propanamide: 4-azidoaniline (596 mg, 4.44 mmol) and triethylamine (0.57 mL, 4.04 mmol) were placed in DCM in a round bottom flask. 3-

chloroacetyl chloride (prepared freshly by refluxing 6 mmol of 3-chloro acetic acid in 10 mL sulfonyl chloride for an hour and removing the excess of sulfonyl chloride on a rotovap) was dissolved in DCM and added slowly to aniline solution at 0°C. The mixture stirred at 0°C for 2 hours. The mixture warmed up to room temperature, was diluted with DCM, and washed with 2M HCl. Organics were dried and the solvent was removed to give N-(4-azidophenyl)-3-chloropropanamide as a brown solid which was used in the next step without further purification. The mixture of N-(4-azidophenyl)-3-chloropropanamide (680 mg, 3.03 mmol) and NaN₃ (395 mg, 6.07 mmol) in DMF was heated to 80°C for 14 hours. The solvent was removed and the residue was taken in DCM, and washed with water. The organic was collected, dried over sodium sulfate and concentrated on rotovap. The crude was purified by column chromatography(ETOAC: HEX) to give 200 mgr(30% yield) of product as a brown solid. ¹H NMR(500 MHz, CDCl₃): δ 7.43(d, j=8.9,2H), 7.4(brs, 1H), 6.9(d, j=8.9 Hz, 2H), 3.64(t, j=6.5 Hz, 2H), 2.52(t, j= 6.3 Hz, 2H) ; ¹³CNMR(500MHZ, CDCl₃): δ 168.2, 136.2, 134.4, 121.6, 119.5, 47.3, 36.8; IR (film) ν_{max} 3311, 2917, 2119, 1664, 1602, 1540, 739 Cm⁻¹; HRMS(EI)calcd. For C₉H₉N₇O, 231.0869; found, [M]⁺, 231.1001



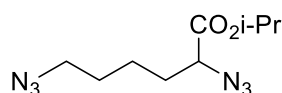
tert-butyl (4-(3-azidopropanamido)phenyl)carbamate(7i): Ru NPs supported on polystyrene (0.401 mmol/g, 2 mol% wrt ruthenium) was placed in a 10 mL vial containing a Teflon-coated magnetic stir bar, followed by the addition of ethanol (1.0 mL), 3-azido-N-(4-azidophenyl)propanamide (25 mg, 0.108 mmol) and the glass vial was sealed with septum and wrapped the septum with parafilm. Hydrazine monohydrate (0.216 mmol, 10.5 μL) added dropwise at 0 °C and the reaction mixture stirred at room temperature for 12 h. After the reaction, the heterogeneous catalyst removed by filtration through a small plug of silica gel in a pipet and the solids washed several times with ethanol. The filtrate collected, and the solvent removed under reduced pressure on a rotary evaporator to provide the crude product. To the crude product methanol (4 mL), trimethylamine (61 μL, 0.432 mmol) and boc anhydride (94 mg, 0.432 mmol) were added and stirred the reaction mixture at room temperature for 10 h. The solvent was removed and the reaction mixture was purified by flash chromatography to yield mono amine as white solid(15 mgr, 46%). ¹H NMR(500 MHz, CDCl₃) δ 7.43(S, 1H), 7.33(d, j=9.02 Hz, 2H), 7.22(d, j=9.02 Hz, 2H), 6.45(brs, 1H), 3.61(t, j=6.44 Hz, 2H), 2.49(t,

$j=6.6$ Hz, 2H), 1.44(s,9H); ^{13}C NMR(500MHZ, CDCl_3): δ 168, 153, 135, 132.8, 121, 119.4, 47.3, 36.7, 28.3; IR (film) ν_{max} 3386, 2360, 1701, 1655, 1541; HRMS(EI) calcd. For $\text{C}_{14}\text{H}_{19}\text{N}_5\text{O}_3$, 305.1488; found, $[\text{M}+18]^+$, 323.18

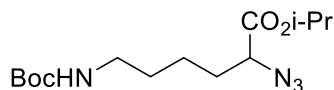


tert-butyl(3-((4-((tert-butoxycarbonyl)amino)phenyl)amino)-3-oxopropyl)carbamate:

yield 34%(14 mgr). ^1H NMR(500 MHz, CDCl_3) δ 7.57(brs, 1H), 7.37(d, $j=8.87\text{Hz}$, 2H), 7.23(d, $j=8.87$ Hz, 2H), 6.43(brs, 1H), 5.11(brs, 1H), 3.41(dt, $j=6$, 6 Hz, 2H), 2.5(t, $j=4.78\text{Hz}$, 2H), 1.44(s,9H), 1.36(s, 9H); ^{13}C NMR(500MHZ, CDCl_3) δ :169.5, 152.8, 134.79, 133, 120.7, 119.16, 37.53, 36.52, 28.39, 28.34; IR (film) ν_{max} 3348, 2364, 1695, 1654, 1541; HRMS(EI)calcd. For $\text{C}_{19}\text{H}_{29}\text{N}_3\text{O}_5$, 379.2107; found, $[\text{M}+\text{H}]^+$, 380.2201

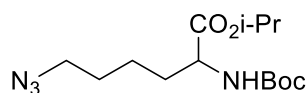


isopropyl 2,6-diazidohexanoate: Synthesized from L-lysine according to a known procedure²¹: ^1H NMR (500 MHz, CDCl_3) δ 5.1 (septet, $J = 6.5$ Hz, 1H), 3.79 (dd, $J = 5.5$ Hz, 1H), 3.3 (t, $J = 7$ Hz, 2H), 1.84-1.74 (m, 2H), 1.66-1.59 (m, 2H), 1.52-1.48 (m, 2H), 1.28 (dd, $J = 4$ Hz, 6H); ^{13}C NMR (125 MHz, CDCl_3): 169.8, 69.7, 61.8, 51.0, 30.8, 28.3, 22.9, 21.7; IR (film) ν_{max} 2101, 1736, 1200, 1105 Cm^{-1} ; HRMS (EI) calcd. for $\text{C}_9\text{H}_{16}\text{N}_6\text{O}_2$, 240.1335; found, $[\text{M}+\text{H}]^+$, 241.1402.

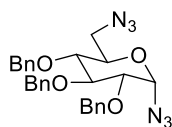


isopropyl 2-azido-6-((tert-butoxycarbonyl)amino)hexanoate (9a): Ru NPs supported on polystyrene (0.401 mmol/g, 2 mol% wrt ruthenium) were placed in a 10 mL vial containing a Teflon-coated magnetic stir bar, followed by the addition of ethanol (2.0 mL), isopropyl 2,6-diazidohexanoate (52.9 mg, 0.220 mmol) and the glass vial was sealed with septum and wrapped the septum with paraflim. Hydrazine monohydrate (0.330 mmol, 16 μL) was added and the reaction mixture was stirred at room temperature for 24 h. After the reaction, the heterogeneous catalyst removed by filtration through a small plug of silica gel in a pipet and

the solids washed several times with ethanol. The filtrate collected, and the solvent removed under reduced pressure on a rotary evaporator to provide the crude product. To the crude product methanol (4 mL), trimethylamine (150 μ L, 1.1 mmol) and boc anhydride (240 mg, 1.1 mmol) added and stirred the reaction mixture at room temperature for 10h. The solvent was removed and the reaction mixture was purified by flash chromatography to yield mono amine as clear oil (34 mgr, 49%). ^1H NMR (500 MHz, CDCl_3): δ 5.02(sep, $J = 6.61$ Hz, 1H), 4.48(brs, 1H), 3.69(dd, $J = 8.03, 5.14$ Hz, 1H), 3.05(dt, $J = 6.05, 6.05$ Hz, 2H), 1.63-1.81(m, 2H), 1.41-1.52(m, 4H), 1.37(s, 9H), 1.22(d, $J = 2.4$ Hz, 3H), 1.21(d, $J = 2.13$ Hz, 3 H); ^{13}C NMR (500 MHz, CDCl_3): δ 170, 156, 69.8, 62.1, 40.2, 30.9, 29.6, 29.5, 28.4, 22.99, 21.7; IR (film) ν_{max} 3357, 2979, 2930, 2106, 1701 cm^{-1} ; HRMS(EI) calcd. For $\text{C}_{14}\text{H}_{26}\text{N}_4\text{O}_4$, 314.1954; found, $[\text{M}+18]^+$, 332.2317.



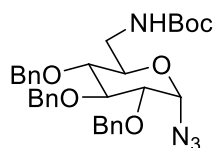
isopropyl N2-(tert-butoxycarbonyl)-N6-diazolysinate(9b): yield 17 mg(24%) ^1H NMR (500 MHz, CDCl_3): δ 4.97-5.15(m, 2H), 4.25(dt, $J = 7.28, 7.28$ Hz, 1H), 3.27(t, $J = 6.747$ Hz, 2H), 1.77-1.89(m, 1H), 1.56-1.71(m, 3H), 1.46(s, 1H), 1.23-1.28(m, 8H), 2.5(t, $J = 4.78$ Hz, 2H), 1.44(s, 9H), 1.36(s, 9H); ^{13}C NMR (500 MHz, CDCl_3): δ 172.1, 155.8, 79.8, 69, 53.4, 51.1, 32.4, 29.7, 28.4, 28.3, 22.4, 21.7; IR (film) ν_{max} 3374, 2923, 2096, 1717, 1507 cm^{-1} ; HRMS(EI) calcd. For $\text{C}_{14}\text{H}_{26}\text{N}_4\text{O}_4$, 314.1954; found, $[\text{M}+18]^+$, 332.2317.



(2S,3R,4S,5R,6R)-2-azido-6-(azidomethyl)-3,4,5-tris(benzyloxy)tetrahydro-2H-pyran:

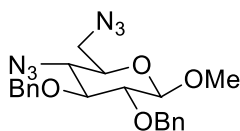
Synthesized from methyl 6-azido-2,3,4-tri-O-benzyl-6-deoxy- α -D-glycopyranoside²² (500 mg) via a reported procedure.²³ Product isolated after chromatographic separation of the α -anomer (90 mg, 19% yield) and β -anomer (40 mg, 8%). α -anomer: ^1H NMR (500 MHz, CDCl_3) δ 7.46-7.26 (m, 15H), 5.26 (d, $J = 4.2$ Hz, 1H), 5.0 (d, $J = 10.8$ Hz, 1H), 4.96 (d, $J = 11$ Hz, 1H), 4.85 (dd, $J = 3.6$ Hz, 2H), 4.7 (d, $J = 11.7$ Hz, 1H), 4.65 (d, $J = 11$ Hz, 1H), 4.0-3.86 (m, 2H), 3.68 (dd, $J = 4.2$ Hz, 1H), 3.6-3.48 (m, 2H), 3.4 (dd, $J = 4.5$ Hz, 1H); ^{13}C NMR (125 MHz, CDCl_3) δ 138.3, 137.7, 137.5, 128.7, 128.5, 128.3, 128.1, 128, 127.9, 127.8, 87.7, 81.5, 79.6, 77.5,

75.8, 75.2, 73.8, 72.1, 51.0; IR (film) ν_{\max} 3030, 2108, 1091, 697 cm^{-1} ; HRMS (EI) calcd. for $\text{C}_{27}\text{H}_{28}\text{N}_6\text{O}_4$, 500.2172; found, $[\text{M}+\text{H}]^+$, 501.2236.



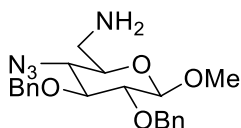
tert-butyl(((2R,3R,4S,5R,6S)-6-azido-3,4,5-tris(benzyloxy)tetrahydro-2H-pyran-2-yl)methyl)carbamate(10)

: Ru NPs supported on polystyrene (0.401 mmol/g, 7 mol% wrt ruthenium) was placed in a 10 mL vial containing a Teflon-coated magnetic stir bar, followed by the addition of ethanol (2.0 mL) and (2S,3R,4S,5R,6R)-2-azido-6-(azidomethyl)-3,4,5-tris(benzyloxy)tetrahydro-2H-pyran (11 mg, 0.0219 mmol). Hydrazine monohydrate (0.175 mmol, 8 μL) was added dropwise. The vial closed with a Teflon cap and the reaction mixture stirred for 7 h. After the reaction, the heterogeneous catalyst removed by filtration through a small plug of silica gel in a pipet, and the solids washed several times with ethanol, the solvent removed to give the crude product. To the crude product methanol (4 mL), triethylamine (30 μL , 0.432 mmol) and Boc anhydride (50 mg, 0.131 mmol) added and stirred the reaction mixture at room temperature for 10 h. Solvent removed and the reaction mixture purified by flash chromatography to yield the product as yellow oil. (11 mg, 88% yield). ^1H NMR(500 MHz, CDCl_3) δ 7.12-7.36(m, 16H), 5.06(d, $J = 3.44$ Hz, 1H), 4.86(d, $J = 10.7$ Hz, 1H), 4.74(t, $J = 10.7$ Hz, 3H), 4.50-4.64(m, 3H), 3.8(t, $J = 9.9$ Hz, 1H), 3.68-3.76(m, 1H), 3.49(dd, $J = 9.5$, 4.01 Hz, 1H), 3.37-3.46(m, 1H), 3.28-3.37(m, 2H), 3.25(t, $J = 9.3$ Hz, 1H), 1.35(s, 9H); ^{13}C NMR(500 MHz, CDCl_3): δ 138.3, 137.8, 137.5, 128.6, 128.4, 128.3, 128.2, 128.08, 128, 127.9, 127.8, 87.6, 81.5, 79.5, 77.8, 75.8, 75.2, 73.8, 71.9, 40.7, 29.7, 28.3 ; IR (film) ν_{\max} 3364, 2923, 2112, 1714, 1497, 739 cm^{-1} ; HRMS(EI)calcd. For $\text{C}_{32}\text{H}_{38}\text{N}_4\text{O}_6$, 574.3891; found, $[\text{M}+18]^+$, 592.3181.

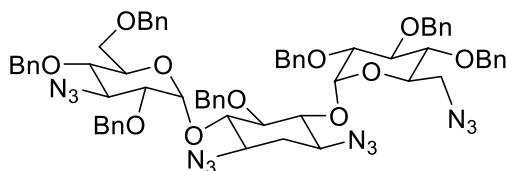


(2R,3R,4S,5R,6R)-3-azido-2-(azidomethyl)-4,5-bis(benzyloxy)-6-methoxytetrahydro-2H-pyran.²⁴ ^1H NMR (500 MHz, CDCl_3) δ 7.41-7.26 (m, 10H), 4.85 (d, $J = 3.5$ Hz, 1H), 4.83 (d, $J = 4$ Hz, 1H), 4.75 (d, $J = 11.5$ Hz, 1H), 4.65 (d, 12.5 Hz, 1H), 4.6 (d, $J = 3.5$ Hz, 1H), 4.0 (dd, $J = 4$ Hz, 1H), 3.87-3.82 (m, 3H), 3.52 (dd $J = 8$ Hz, 1H), 3.38 (s, 3H), 3.2 (dd, $J = 5$ Hz, 1H);

^{13}C NMR (125 MHz, CDCl_3) δ 138.1, 137.9, 128.5, 128.4, 128.1, 127.9, 127.7, 98.7, 77.7, 75.8, 73.8, 73.4, 67.5, 61.5, 55.6, 51.6; IR (film) ν_{max} 2911, 2100, 1277, 1117, 1044, 739, 698 cm^{-1} ; HRMS (EI) calcd. for $\text{C}_{21}\text{H}_{24}\text{N}_6\text{O}_4$, 424.1859; found, $[\text{M}+\text{H}]^+$, 425.1268.

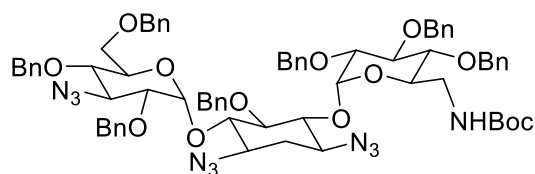


((2R,3R,4S,5R,6R)-3-azido-4,5-bis(benzyloxy)-6-methoxytetrahydro-2H-pyran-2-yl)methanamine (11): Ru NPs supported on polystyrene (0.401 mmol/g, 4 mol% wrt ruthenium) was placed in a 10 mL vial containing a Teflon-coated magnetic stir bar, followed by the addition of ethanol (2.0 mL) and (2R,3R,4S,5R,6R)-3-azido-2-(azidomethyl)-4,5-bis(benzyloxy)-6-methoxytetrahydro-2H-pyran (50 mg, 0.117 mmol). The glass vial was sealed with a septum and wrapped with parafilm. Hydrazine monohydrate (0.471 mmol, 23 μL) was added dropwise at room temperature and the reaction mixture was stirred at room temperature for 7 h. After the reaction, the heterogeneous catalyst was removed by filtration through a small plug of silica gel in a pipet and the solids washed several times with ethanol, solvent was evaporated to give the product as clear oil (44.5 mg, 95%) ^1H NMR (500 MHz, CDCl_3) δ 7.42–7.2 (m, 10H), 4.87–4.70 (m, 3H), 4.68–4.52 (m, 2H), 4.0–3.96 (m, 1H), 3.92–3.77 (m, 2H), 3.69–3.58 (m, 1H), 3.36 (s, 3H), 3.0–2.87 (m, 1H), 2.78–2.65 (m, 1H); ^{13}C NMR (125 MHz, CDCl_3) δ 128.5, 128.4, 128.1, 128.0, 127.9, 127.8, 127.7, 127.0, 98.6, 78.1, 76.6, 73.8, 73.2, 70.0, 62.0, 55.4, 43.1; IR (film) ν_{max} 3386, 2910, 2100, 1276, 1116, 1044, 739 cm^{-1} ; HRMS (EI) calcd. for $\text{C}_{22}\text{H}_{28}\text{BrN}_4\text{O}_3$, 396.2161; found, $[\text{M}+\text{H}]^+$, 397.2240.



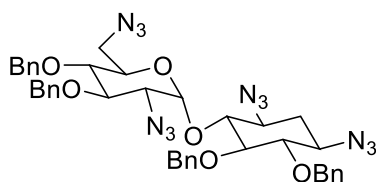
((2R,3S,4S,5R,6S)-4-azido-3,5-bis(benzyloxy)-2-((benzyloxy)methyl)-6(((1S,2R,3R,4S,6R)-4,6-diazido-3-(((2R,3R,4S,5R,6R)-6-(azidomethyl)-3,4,5-tris(benzyloxy)tetrahydro-2H-pyran-2-yl)oxy)-2-(benzyloxy)cyclohexyl)oxy)tetrahydro-2H-pyran (12): this compound was made according to previous procedures²⁵ from tetraazido derivative of kanamycin (251 mg, 0.42 mmol), NaH(170 mg, 4.25mmol), and benzyl bromide(1 mL, 8 mmol) to give perbenzylated tetraazido kanamycin as white foamy solid (328 mg, 63%). ^1H NMR (CDCl_3 ,

400 MHz) δ 7.45-6.81 (m, 35H), 5.56 (d, $J = 3.7$ Hz, 2H), 5.04 (d, $J = 12$ Hz, 1H), 4.89-4.47 (m, 9H), 4.42 (d, $J = 12.0$ Hz, 1H), 4.30 (ddd, $J = 2.4, 4.6, 9.9$ Hz, 1H), 4.21-4.09 (m, 3H), 4.16 (t, $J = 18.8$ Hz, 1H), 3.77-3.22 (m, 14H), 3.11 (dd, $J = 1.8, 11.0$ Hz, 1H), 2.84 (dd, $J = 2.4, 11.0$ Hz, 1H), 2.39 (td, $J = 4.4, 13.1$ Hz, 1H), 1.65 (dd, $J = 12.4, 25$ Hz, 1H). ^{13}C NMR (CDCl_3 , 300 MHz): 138.0, 137.6, 137.5, 137.2, 137.1, 136.9, 128.1, 128.0, 127.9, 127.8, 127.6, 127.5, 127.4, 127.3, 127.1, 127.0, 126.8, 126.5, 125.2, 96.8, 95.5, 82.1, 81.3, 78.8, 77.9, 76.3, 75.5, 75.1, 74.5, 74.0, 73.5, 72.6, 70.4, 69.5, 67.1, 65.0, 59.9, 58.9, 50.9, 31.7. HRMS (EI) calcd for $\text{C}_{67}\text{H}_{70}\text{N}_{12}\text{O}_{11}$, 1241.531, found: 1241.5231.

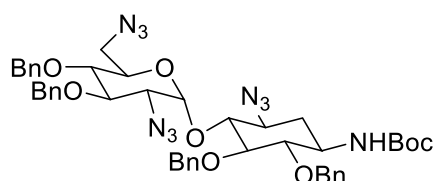


tert-butyl (((2R,3R,4S,5R,6S)-6-(((1R,2S,3R,4R,6S)-2-azido-3-(((2R,3R,4R,5R,6R)-3-azido-6-(azidomethyl)-4,5-bis(benzyloxy)tetrahydro-2H-pyran-2-yl)oxy)-4-(benzyloxy)-6-((tert-butoxycarbonyl)amino)cyclohexyl)oxy)-3,4,5-tris(benzyloxy)tetrahydro-2H-pyran-2-yl)methyl)carbamate (13): Ru NPs supported on polystyrene (0.401 mmol/g, 10 mol% wrt ruthenium) was placed in a 10 mL vial containing a Teflon-coated magnetic stir bar, followed by the addition of ethanol (2.0 mL) and (2R,3S,4S,5R,6S)-4-azido-3,5-bis(benzyloxy)-2-((benzyloxy)methyl)-6-(((1S,2R,3R,4S,6R)-4,6-diazido-3-(((2R,3R,4S,5R,6R)-6-(azidomethyl)-3,4,5-tris(benzyloxy)tetrahydro-2H-pyran-2-yl)oxy)-2-(benzyloxy)cyclohexyl)oxy)tetrahydro-2H-pyran (12) (42.3 mg, 0.0347 mmol). The glass vial was sealed with a septum and wrapped with parafilm. Hydrazine monohydrate (0.694 mmol, 33.5 μL) was added and the reaction mixture was stirred at room temperature for 48h. After the reaction, the heterogeneous catalyst was removed by filtration through a small plug of silica gel in a pipet and the solids washed several times with ethanol. The filtrate was collected, and the solvent removed under reduced pressure on a rotary evaporator to provide the crude product. To the crude product DCM (4 mL), triethylamine (47 μL , 0.347 mmol) and boc anhydride (75 mg, 0.347 mmol) were added and stirred the reaction mixture at room temperature for 10 h. Solvent was removed and the reaction mixture was purified by flash chromatography to yield product as clear oil (18 mg, 41%). ^1H (CDCl_3 , 500 MHz) δ 7.28 (m, 25H), 7.01 (m, 10H), 5.59 (d, $J = 3.5$, 1H), 5.49 (d, $J = 2.9$, 1H), 5.08 (d, $J = 11.9$, 1H), 4.85 (d, $J = 11.9$, 1H), 4.84 (m, 1H), 4.82 (d, $J = 11.9$, 1H), 4.77 (s, 2H), 4.72 (d, $J = 11.9$, 1H), 4.65 (d, $J = 11.1$, 2H), 4.56 (d, $J = 11.4$, 2H), 4.45 (d, $J = 11.8$, 1H), 4.22 (d, $J = 12.4$, 1H), 4.20 (d,

$J = 11.6$, 1H), 4.19 (m, 1H), 4.16 (d, $J = 11.2$, 1H), 4.01 (dd, $J = 9.5$, 9.5, 1H), 3.71 (dd, $J = 10.0$, 10.0, 1H), 3.69 (m, 2H), 3.61 (m, 3H), 3.54 (dd, $J = 9.1$, 9.1, 1H), 3.52 (m, 1H), 3.40 (m, 1H), 3.36 (m, 3H), 3.30 (dd, $J = 9.7$, 9.7, 1H), 3.14 (d, $J = 11.1$, 1H), 2.88 (dd, $J = 11.1$, 2.4, 1H), 2.41 (ddd, $J = 13.2$, 4.2, 4.2, 1H), 1.64 (d, $J = 13.2$, 1H), 1.48 (s, 9H); ^{13}C (CDCl₃, 125 MHz) δ 155.90, 138.40, 138.08, 137.95, 137.74, 137.64, 137.58, 137.34, 128.52, 128.42, 128.34, 128.26, 128.21, 128.19, 128.17, 128.13, 128.11, 128.07, 128.06, 127.87, 127.78, 127.75, 127.74, 127.56, 127.49, 127.47, 127.25, 126.94, 125.76, 97.36, 96.01, 82.47, 81.80, 79.30, 79.25, 78.59, 78.22, 77.91, 77.33, 75.92, 75.52, 75.01, 74.53, 74.41, 73.94, 73.49, 73.03, 70.42, 69.89, 67.57, 65.37, 60.28, 59.47, 40.93, 32.23, 28.47; IR (film) ν_{max} 3447, 2924, 2106, 1710, 1554; HRMS(EI) calcd. For C₄₀H₄₂N₁₂O₆, 1292.24; found, [M+18]⁺, 1310.6248.



(2R,3R,4R,5R,6R)-3-azido-6-((azidomethyl)-4,5-bis(benzyloxy)-2-(((1R,3S,4R,6S)-4,6-diazido-2,3-bis(benzyloxy)cyclohexyl)oxy)tetrahydro-2H-pyran (14): Prepared according to known procedures.²⁵ ^1H NMR(500 MHz, CDCl₃) δ 7.14-7.31(m, 20 H), 5.5(d, $J = 3.9$ Hz, 1.0 H), 4.9(d, $J = 10.83$ Hz, 1H), 4.85(d, $J = 10.8$ Hz, 1H), 4.71-4.82(m, 5H), 4.54(d, $J = 11.3$ Hz, 1H), 4.17-4.22(m, 1H), 3.92(t, $J = 9.6$ Hz, 1H), 3.27-3.56(m, 8H), 3.23(dd, $J = 10.3$, 3.9 Hz, 1H), 2.24(dt, $J = 13.3$, 4.4 Hz, 1H), 1.34-1.51(m, 2H); ^{13}C NMR(500MHz, CDCl₃): δ 137.9, 137.6, 137.3, 128.5, 128.4, 128.1, 128.04, 128, 127.9, 127.8, 127.6, 126.9, 97.65, 84.6, 84.3, 80.1, 78.6, 77.6, 76, 75.5, 75.2, 75.1, 71.0, 63.2, 60.2, 59.25, 51.07, 32.34; IR (film) ν_{max} 3031, 2915, 2102, 1606, 1497 cm^{-1} ; HRMS(EI) calcd. For C₄₀H₄₂N₁₂O₆, 786.3350; found, [M+18]⁺, 804.3609.



tert-butyl ((1R,2S,3R,4R,5S)-5-azido-4-(((2R,3R,4R,5R,6R)-3-azido-6-(azidomethyl)-4,5-bis(benzyloxy)tetrahydro-2H-pyran-2-yl)oxy)-2,3-bis(benzyloxy)cyclohexyl)carbamate (15): Ru NPs supported on polystyrene (0.401 mmol/g, 5 mol% wrt ruthenium) was placed in

a 10 mL vial containing a Teflon-coated magnetic stir bar, followed by the addition of ethanol (2.0 mL) and (2R,3R,4R,5R,6R)-3-azido-6-(azidomethyl)-4,5-bis(benzyloxy)-2-(((1R,3S,4R,6S)-4,6-diazido-2,3-bis(benzyloxy)cyclohexyl)oxy)tetrahydro-2H-pyran (28.3 mg, 0.0407 mmol). The glass vial was sealed with a septum and wrapped with parafilm. Hydrazine monohydrate (0.203 mmol, 10 μ L) was added and the reaction mixture was stirred at room temperature for 72 h. After the reaction, the heterogeneous catalyst was removed by filtration through a small plug of silica gel in a pipet and the solids washed several times with ethanol. The filtrate was collected, and the solvent removed under reduced pressure on a rotary evaporator to provide the crude product. To the crude product methanol (4 mL), triethylamine (57 μ L, 0.407 mmol) and boc anhydride (88 mg, 0.407 mmol) were added and stirred the reaction mixture at room temperature for 10h. Solvent was removed and the reaction mixture was purified by flash chromatography to yield product as white solid. (16 mgr, 46%). ^1H (CDCl_3 , 500 MHz) δ 7.32 (m, 20H), 5.59 (d, $J = 11.00$ Hz, 1H), 5.03 (d, $J = 11.00$ Hz, 1H), 4.97 (s, 1H), 4.90 (d, $J = 11.20$ Hz, 3H), 4.84 (d, $J = 11.20$ Hz, 1H), 4.67 (d, $J = 11.20$ Hz, 1H), 4.63 (d, $J = 11.20$ Hz, 1H), 4.33 (ddd, $J = 9.5, 4.2, 2.3$ Hz, 1H), 4.28 (d, $J = 7.40$ Hz, 1H), 4.03 (dd, $J = 10.0, 8.7$ Hz, 1H), 3.64 (m, 1H), 3.61 (m, 1H), 3.59 (m, 1H), 3.54 (m, 1H), 3.52 (m, 1H), 3.44 (m, 1H), 3.40 (dd, $J = 13.4, 4.2$ Hz, 1H), 3.36 (m, 1H), 3.34 (m, 1H), 2.41 (ddd, $J = 12.9, 4.3, 2.3$ Hz, 1H), 1.45 (s & m, 10H); ^{13}C (CDCl_3 , 125 MHz) δ 155.32, 138.13, 137.72, 137.69, 137.65, 128.64, 128.51, 128.50, 128.48, 128.35, 128.14, 128.06, 127.96, 127.92, 127.78, 127.61, 127.10, 97.60, 84.98, 82.43, 80.18, 79.87, 78.70, 77.96, 75.54, 75.13, 75.09, 75.09, 70.87, 63.35, 59.57, 51.03, 49.87, 33.21, 28.37; IR (film) ν_{max} 2103, 1647, 1522, 1454 Cm^{-1} ; HRMS(EI)calcd. For $\text{C}_{40}\text{H}_{42}\text{N}_{12}\text{O}_6$, 860.39; found, $[\text{M}+18]^+$, 878.43.

1.10 Experimental Procedures and Supporting Data for the Synthesis of Arylhydroxylamines via Partial Reduction of Nitroarenes with Nanoparticle Catalysts

1.10.1 General information

All reactions were carried out in oven-dried glassware with magnetic stirring, unless otherwise indicated. All the reagents were used as obtained from commercial sources unless otherwise noted. Analytical thin-layer chromatography was performed with 0.25 mm coated commercial silica gel plates (E. Merck, DC-Plastikfolien, silica gel 60 F₂₅₄). Flash Chromatography was performed with EM Science silica gel (0.040-0.063 μm grade). Proton

nuclear magnetic resonance ($^1\text{H-NMR}$) data were acquired on an Inova 300 MHz, an Inova 500 MHz, or an NMR-S 500 MHz spectrometer. Chemical shifts are reported in delta (δ) units relative to the 2H signal of the CDCl_3 solvent. Signals are reported as follows: s (singlet), d (doublet), t (triplet), q (quartet), dd (doublet of doublets), qd (quartet of doublets), bs (broad singlet), m (multiplet), rot (rotamers). Coupling constants are reported in hertz (Hz). Carbon-13 nuclear magnetic resonance ($^{13}\text{C-NMR}$) data were acquired on an Inova at 75 MHz or Inova or NMR-S spectrometer at 125 MHz. Chemical shifts are reported in ppm. All NMR spectra were collected at 298 K. Mass spectral data were obtained using ESI techniques (Agilent, 6210 TOF). The content of all metals in the final material was determined by ICP analysis using a Shimadzu ICPS- 7510 instrument. STEM images and EDS analyses were obtained using a JEOL JEM-2100F instrument operated at 5.0 kV. All STEM specimens were prepared by placing a drop of a homogeneous chloroform solution of the respective polymer-nanoparticle composite on a carbon coated copper grid and allowed to dry in air without staining. Polystyrene (MW 35,000, Aldrich), and Ruthenium (III) chloride hydrate (STREM chemicals) were used as obtained.

1.10.2 Synthesis and characterization of Ru NP's in polystyrene

Polystyrene (1g) was added to 25 mL of THF and 8 mL of ethanol and the mixture was stirred using a Teflon-coated magnetic stir bar until polystyrene was completely dissolved. Ruthenium (III) chloride hydrate (100 mg, 0.482 mmol) anhydrous basis was added and the mixture was stirred until the solution became homogenous. Sodium borohydride (182.5 mg, 4.82 mmol) was then added portion wise. The reaction was stirred under argon atmosphere for 10 h giving a black homogeneous solution, indicating the formation of nanoparticles. The solvent was then evaporated and Millipore water was added to the resulting solid and the mixture was stirred for 15 minutes then filtered. The solid was then washed with Millipore water ($20\text{ mL} \times 5$) and dried under vacuum to give a black solid ($\sim 1.0\text{ g}$), which was finely ground with a mortar and pestle before use. The ruthenium loading in each batch of Ru/PS was determined by ICP analysis by comparison with standard solutions, and was determined to be $\sim 0.47\text{ mmol/g}$ on average. The nanoparticle catalysts were stored under argon. When stored under argon and in the freezer, and used regularly, the catalysts remain active for several weeks up to a few months. Catalytic activity of the nanoparticles slowly decreases with exposure to air.

1.10.3 Preparation of the sample for ICP-analysis

To 10 mg of polymer-nanoparticle catalyst was added 1 ml conc. H_2SO_4 and the mixture was heated at 140 °C. HNO_3 (1 ml) was then slowly added and the solution was heated for 10 min. 1 ml of aqua regia was then added and the mixture cooled to room temperature and diluted to 500 mL in a volumetric flask. Metal concentrations were then determined by ICP analysis by comparison to standard solutions. Typical catalysts obtained with 0.47 mmol/g loading of Ru nanoparticles in polystyrene.

1.10.4 Characterization of Ru/polystyrene nanoparticles

We further characterized our nanoparticles with different state of the art techniques in order to explore the size and constituents of the nanoparticles. STEM imaging and statistical analysis revealed the size distribution of nanoparticles to be in the range of 1- 2.5 nanometers with the average size of 1.5 being the most populated one. Also EDS spectrum showed that ruthenium is the main component presented in the structure.

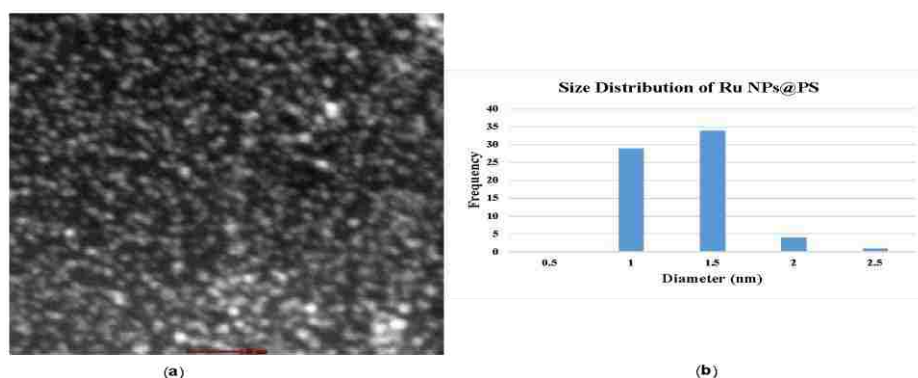


Figure 1.23 STEM image of Ru NPs in polystyrene catalyst. (a) STEM Image of polymer-encapsulated nanoparticles. (b) Statistical analysis of nanoparticle size (average size: 1.33 nm). STEM Scale bar = 10nm.

1.10.5 Experimental procedures

1.10.5.1 General procedure for the synthesis of *N*-aryl hydroxylamines:

Into a 2 dram vial was placed 4-nitroacetophenone (55 mg, 0.33 mmol), Ru/PS nanoparticle catalyst (8.0 mg, 0.477 mmol Ru/gram catalyst, 1 mol%), and hydrazine monohydrate (42 μL , 2.5 equiv) in 4 ml of chloroform. The reaction mixture was stirred for 1.25 h, at which point the solvent was removed under reduced pressure. The product was extracted from the solid mixture with 3x 2 ml EtOH. The combined ethanol extracts were then passed through a short silica plug in a pipet and the silica plug was washed 2 times with 1 ml

ethanol. The EtOH was then removed on a rotary evaporator under reduced pressure. The product 4-(hydroxyamino)acetophenone was isolated as a pale yellow solid (44.3 mg, 0.29 mmol, 88% yield) as a >20:1 mixture of hydroxylamine to aniline. ¹H NMR (300 MHz, CDCl₃): 7.93-7.90 (d, J = 8.7 Hz, 2H), 7.02-6.99 (d, J = 8.7 Hz, 2H), 5.28 (bs, 1H), 2.56 (s, 3H). Spectra match literature values. After extraction of the product with ethanol from the reaction mixture, the resulting polymer-catalyst matrix is obtained as an oily substance. Due to the difficulty of handling this substance, reusability studies were not performed.

1.10.5.2 Large scale reaction

Into a 500 ml RB flask was placed 4-nitroacetophenone (4.13 g, 25 mmol), Ru/PS nanoparticle catalyst (524 mg, 0.477 mmol Ru/gram catalyst, 1 mol%) in 300 ml CHCl₃. The reaction was placed into a room temperature water bath and then hydrazine monohydrate (3.0 ml, 2.5 equiv) was added dropwise over ~3 minutes. The reaction mixture was stirred for 1.25 h, at which point the solvent was removed under reduced pressure. The product was extracted from the solid mixture with 3 x 20 ml EtOH. The combined ethanol extracts were then passed through a silica gel plug and the silica plug was washed 2 times with 20 ml ethanol. The EtOH was then removed on a rotary evaporator under reduced pressure. The product 4-(hydroxyamino)acetophenone was isolated as a pale yellow solid (3.25 g, 21.5 mmol, 86% yield) as a 14:1 mixture of hydroxylamine to aniline. When conducted in THF (Table 2, entry 2) the reaction of substrate **2a** was complete in under 10 minutes.

1.10.5.3 Reaction time course study

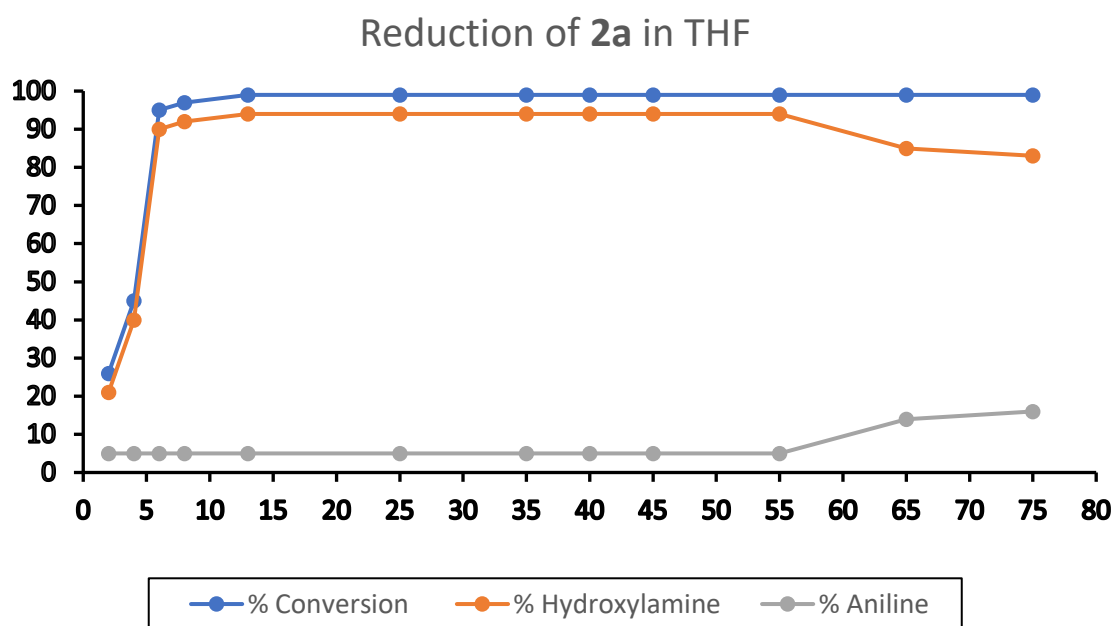
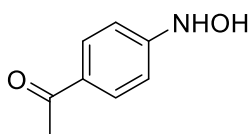


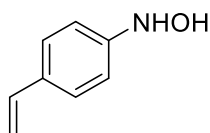
Figure 1.24 Time dependent conversion of nitrobenzene to hydroxyl amine product or aniline

In order to track the progress of the reduction reaction, we conducted a time course study with substrate **2a** in THF where aliquots of the reaction were removed over the course of 1.5 hrs (See graph below). We previously observed that reactions in THF proceed in essentially 10 minutes with THF as solvent. As seen in the graph, the reaction proceeds to completion in under 10 minutes with very high selectivity. As the reaction proceeds, and especially after ~1 hr, formation of aniline product begins to occur. In general, reactions were performed for 1.25 hrs in CHCl₃ as the reaction proceeds more slowly and to ensure all substrates achieved 100% conversion to product.

Note: Hydroxylamine products readily decompose in the presence of air. Isolated yields in Table 2, Figure 1, and Figure 2 represent crude yields of a mixture of products 2:3 after filtration through a plug of silica and removal of solvent. Chromatography on silica gel or alumina leads to decomposition of the hydroxylamine product. Products can be further purified via recrystallization from degassed EtOH.

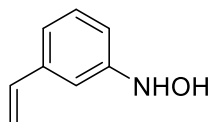


N-(4-Acetylphenyl) hydroxylamine (19a): The General Procedure was used with 55 mg of 4-nitroacetophenone (0.33 mmol) and 3 eq. Hydrazine monohydrate (42 μ L) and 2.5 mol % Ru/PS catalyst (3.5 mg). 44.3 mg (88% isolated yield) of product were obtained. Previously Characterized¹. ¹H NMR (300 MHz, CDCl₃): δ 7.93-7.90 (d, J = 8.7 Hz, 2H), 7.02-6.99 (d, J = 8.7 Hz, 2H), 5.28 (bs, 1H), 2.56 (s, 3H) ¹³C NMR (125 MHz, CDCl₃): δ 154.3, 131.2, 130.3, 113.1, 31.2.

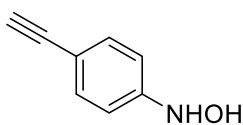


N-(4-Vinylphenyl) hydroxylamine (19b): The General Procedure was used with 49 mg of 4-nitrostyrene (0.33 mmol) and 3 eq. Hydrazine monohydrate (42 μ L) and 2.5 mol % Ru/PS catalyst (8 mg). 43.7 mg (98% isolated yield) of product were obtained. Previously Characterized¹. ¹H NMR (500 MHz, CDCl₃): δ 7.35-7.34 (d, J = 8.5 Hz, 2H), 6.96-6.95 (d, J = 8.5 Hz, 2H), 6.69-6.63 (dd, J_1 = 17.5 Hz, J_2 = 11 Hz, 1H), 5.66-5.62 (d, J = 17.5 Hz, 1H),

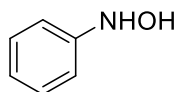
5.15-5.13 (d, $J = 11$ Hz, 1H) ; ^{13}C NMR (75 MHz, CDCl_3): δ 149.9, 136.99, 132.6, 127.6, 115.3, 112.5.



N-(3-vinylphenyl) hydroxylamine (19c): The General Procedure was used with 49 mg of 3-nitrostyrene (0.33 mmol) and 3 eq. Hydrazine monohydrate (42 μL) and 1.1 mol % Ru/PS catalyst (8 mg). 36.6 mg (82% isolated yield, ~90% purity) of N-(3-vinylphenyl) hydroxylamine was obtained as a pale yellow solid. ^1H NMR (500 MHz, CDCl_3): δ 7.24-7.21 (t, $J = 6.5$ Hz, 1H), 7.04-7.03 (m, 1H) 6.88-6.87 (d, $J = 7.5$ Hz), 6.70-6.64 (dd, $J_1 = 17.5$, $J_2 = 11$ Hz, 1H), 5.74-5.71 (d, $J = 17.5$ Hz, 1H), 5.25-5.23 (d, $J = 11$ Hz, 1H). ^{13}C NMR (125 MHz, CDCl_3): δ 150.1, 138.6, 136.9, 129.3, 120.7, 114.4, 114.3, 112.4 .

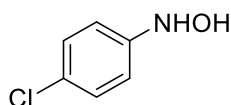


N-(4-ethynylphenyl)hydroxylamine (19d): The General Procedure was used with 49 mg of 1-ethynyl-4-nitrobenzene (0.33 mmol) and 3 eq. Hydrazine monohydrate (42 μL) and 1.1 mol % Ru/PS catalyst (8 mg). 43.9 mg (96% isolated yield) of N-(3-vinylphenyl) hydroxylamine was obtained as a yellow solid. ^1H NMR (500 MHz, CDCl_3): 7.41-7.39 (d, $J = 8.5$ Hz, 2H), 6.91-6.90 (d, $J = 8.5$ Hz, 2H), 3.00 (s, 1H); ^{13}C NMR (125 MHz, CDCl_3): δ 150.6, 133.2, 115.3, 114.0.

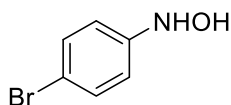


N-phenylhydroxylamine: (19e): The General Procedure was used with 41 mg of nitrobenzene (0.33 mmol) and 2.5 eq. Hydrazine monohydrate (42 μL) and 1.1 mol % Ru/PS catalyst (8 mg). 33.5 mg (93% isolated yield) of N-phenylhydroxylamine were obtained as long transparent crystals. Previously Characterized¹. ^1H NMR (500 MHz, CDCl_3): δ 7.31-7.28 (t, $J = 7.5$ Hz, 2H), 7.02-6.97 (m, 3H); ^{13}C NMR (125 MHz, CDCl_3): δ 149.8, 129.2, 122.5, 114.8. Single Crystals were grown using a vapor deposition method with

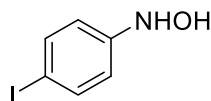
Dichloromethane and Pentane. XRD analysis was used to confirm this structure. The Calculated Structure is Shown Below.



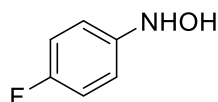
N-(4-Chlorophenyl) hydroxylamine (19f): The General Procedure was used with 52 mg of 1-chloro-4-nitrobenzene (0.33 mmol) and 2.5 eq. Hydrazine monohydrate (42 μ L) and 1.1 mol % Ru/PS catalyst (8 mg). 46.0 mg (97 % isolated yield) of product were obtained. Previously Characterized¹. ¹H NMR (500 MHz, CDCl₃): δ 7.25-7.23 (d, J = 9 Hz, 2H), 6.94-6.92 (d, J = 9 Hz, 2H); ¹³C NMR (125 MHz, CDCl₃): δ 148.4, 129.1, 127.3, 116.0.



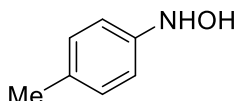
N-(4-bromophenyl) hydroxylamine (19g): The General Procedure was used with 67 mg of 1-bromo-4-nitrobenzene (0.33 mmol) and 2.5 eq. Hydrazine monohydrate (42 μ L) and 1.1 mol % Ru/PS catalyst (8 mg). 60.2 mg (97 % isolated yield) of N-(4-bromophenyl) hydroxylamine was obtained as white, slightly opaque crystals. Previously Characterized¹. ¹H NMR (300 MHz, CDCl₃): δ 7.39-7.36 (d, J = 9 Hz, 2H), 6.90-6.87 (d, J = 9 Hz, 2H) ¹³C NMR (125 MHz, CDCl₃): δ 148.9, 132.8, 132.0, 116.4 Single Crystals were grown using a vapor deposition method with Chloroform and Pentane. XRD analysis was used to confirm this structure.



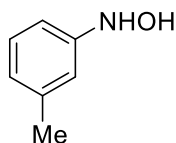
N-(4-Iodophenyl) hydroxylamine (19h): The General Procedure was used with 82 mg of 1-iodo-4-nitrobenzene (0.33 mmol) and 2.5 eq. Hydrazine monohydrate (42 μ L) and 1.1 mol % Ru/PS catalyst (8 mg). 69.9 mg (85 % isolated yield) of product was obtained. Previously Characterized¹. ¹H NMR (300 MHz, CDCl₃) δ : 7.57-7.54 (d, J = 8.7 Hz, 2H), 7.15 (bs, 1H), 6.79-6.76 (d, J = 8.7 Hz, 2H), 5.39 (bs, 1H). ¹³C NMR (125 MHz, CDCl₃) δ : 149.7, 137.9, 116.7, 84.6.



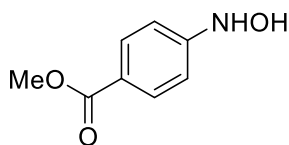
N-(4-fluorophenyl) hydroxylamine (19i): The General Procedure was used with 47 mg of 1-fluoro-4-nitrobenzene (0.33 mmol) and 2.5 eq. Hydrazine monohydrate (42 μ L) and 1.1 mol % Ru/PS catalyst (8 mg). 41.1 mg (98 % isolated yield) of N-(4-fluorophenyl) hydroxylamine was obtained as a pale yellow solid. Previously Characterized². ¹H NMR (500 MHz, CDCl₃): δ 6.99-6.67 (m, 4H). ¹³C NMR (125 MHz, CDCl₃): δ 159.9-158.0 (d, J = 239 Hz), 145.6 (d, J = 3 Hz), 116.6 (d, J = 8 Hz), 115.9-115.7 (d, J = 23 Hz). ¹⁹F NMR (470 MHz, CDCl₃): δ -121.6 (m, 1F). Spectra match literature values⁸⁵.



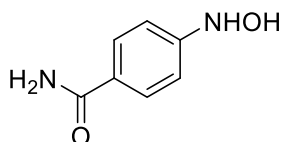
N-(p-tolyl) hydroxylamine (19j): The General Procedure was used with 45 mg of 4-nitrotoluene (0.33 mmol) and 2.5 eq. Hydrazine monohydrate (42 μ L) and 1.1 mol % Ru/PS catalyst (8 mg). 35.4 mg (87 % isolated yield) of N-(p-tolyl) hydroxylamine was obtained as a pale yellow solid. ¹H NMR (500 MHz, CDCl₃): δ 7.09-7.08 (d, J = 8 Hz, 2H), 6.92-6.90 (d, J = 8 Hz, 2H), 2.30 (s, 3H). ¹³C NMR (125 MHz, CDCl₃): δ 147.3, 132.1, 129.6, 115.3, 18.5.



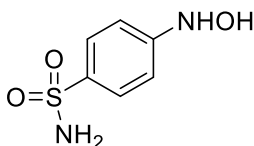
N-(m-tolyl) hydroxylamine (19k): The General Procedure was used with 45 mg of 3-nitrotoluene (0.33 mmol) and 2.5 eq. Hydrazine monohydrate (42 μ L) and 1.1 mol % Ru/PS catalyst (8 mg). 36.2 mg (89 % isolated yield) of N (m-tolyl) hydroxylamine was obtained as a pale yellow solid. ¹H NMR (300 MHz, CDCl₃) δ 7.17-7.16 (1H, t, J = 7.8), 6.85-6.82 (3H, m), 6.80 (1H, bs), 5.77 (1H, bs), 2.35 (3H, s).



Methyl-4-(hydroxyamino) benzoate (19l): The General Procedure was used with 60 mg of methyl-4-nitrobenzene (0.33 mmol) and 2.5 eq. Hydrazine monohydrate (42 μ L) and 1.1 mol % Ru/PS catalyst (8 mg). 53.7 mg (96 % isolated yield) of Methyl-4-(hydroxyamino) benzoate was obtained as a yellow solid. Previously Characterized². ¹H NMR (500 MHz, DMSO-*d*₆): δ 8.98 (s, 1H), 8.67 (s, 1H), 7.78-7.76 (d, *J* = 9 Hz, 2H), 6.84-6.82 (d, *J* = 9 Hz, 2H), 3.76 (s, 3H). ¹³C NMR (125 MHz, DMSO-*d*₆): δ 116.2, 156.0, 130.5, 119.1, 111.2, 51.4. Spectra match literature values⁸⁶.

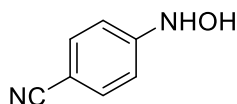


4-(hydroxyamino) benzamide (19m): The General Procedure was used with 55.2 mg of 4-nitrobenzamide (0.33 mmol) and 2.5 eq. Hydrazine monohydrate (42 μ L) and 1.1 mol % Ru/PS catalyst (8 mg). 45.2 mg (90 % isolated yield) of 4-(hydroxyamino) benzamide were obtained as a yellow solid. Previously Characterized². ¹H NMR (500 MHz, DMSO-*d*₆): δ 8.67 (s, 1H), 8.51 (s, 1H), 7.72-7.70 (d, *J* = 9 Hz, 2H), 7.69 (s, 1H), 7.00 (s, 1H), 6.80-6.78 (d, *J* = 9 Hz, 2H). ¹³C NMR (125 MHz, DMSO-*d*₆): 167.8, 154.5, 128.5, 124.5, 111.3. Spectra match literature values⁸⁶.

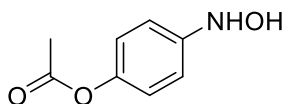


4-(hydroxyamino) benzene sulfonamide (19n): The General Procedure was used with 67.2 mg of 4-nitrobenzene sulfonamide (0.33 mmol) and 2.5 eq. Hydrazine monohydrate (42 μ L) and 1.1 mol % Ru/PS catalyst (8 mg). 56.1 mg (90 % isolated yield) of product were obtained. ¹H NMR (300 MHz, DMSO-*d*₆): δ 8.83 (bs, 1H), 8.62 (bs, 1H), 7.62-7.65 (d, *J* = 9 Hz, 2H), 7.03 (bs, 2H), 6.88-6.91 (d, *J* = 9 Hz, 2H). ¹³C NMR (125 MHz, CD₃CN): δ 154.7, 134.2,

127.3, 112.3; IR (film): ν_{max} 3700, 3400, 3250, 1600, 1450, 1200 Cm^{-1} ; HRMS (ESI) calcd. for $\text{C}_6\text{H}_9\text{N}_2\text{O}_3\text{S}$, 189.0334; found, $[\text{M}+\text{H}]^+$, 189.0418.



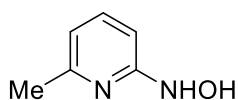
4-(hydroxyamino)benzonitrile (19o): The General Procedure was used with 49 mg of 4-nitrobenzenonitrile (0.33 mmol) and 2.5 eq. Hydrazine monohydrate (42 μL) and 1.1 mol % Ru/PS catalyst (8 mg). 40.3 mg (91 % isolated yield) of 4-(hydroxyamino)benzonitrile were obtained as product. ^1H NMR (500 MHz, CDCl_3): δ 7.54-7.53 (d, $J = 7$ Hz, 2H), 7.01-7.00 (d, $J = 7$ Hz, 2H), 5.67 (bs, 2H); ^{13}C NMR (125 MHz, CDCl_3): δ 153.9, 133.6, 119.7, 113.8, 104.2.



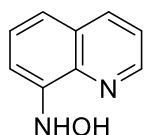
4-(hydroxyamino)phenyl acetate (19): The General Procedure was used with 60 mg of 4-nitrophenyl acetate (0.33 mmol) and 2.5 eq. Hydrazine monohydrate (42 μL) and 1.1 mol % Ru/PS catalyst (8 mg). 50 mg (94 % isolated yield) of 4-(hydroxyamino)phenyl acetate were obtained as product. ^1H NMR (500 MHz, CDCl_3): δ 8.13-8.11(d, $J = 9$ Hz, 2H), 7.12 (bs, 2H), 6.91-6.89 (d, $J = 9$ Hz, 2H), 1.99 (s, 3H); ^{13}C NMR (125 MHz, CDCl_3): δ 171.6, 163.5, 126.4, 116.4, 115.9, 21.1; IR(film): ν_{max} 3400, 1800 Cm^{-1} ; HRMS (ESI) calcd. for $\text{C}_8\text{H}_{10}\text{NO}_3$, 168.0661; found, $[\text{M}+\text{H}]^+$, 168.0702.

General Procedure for the Synthesis of N-Heteroaryl Hydroxylamines: Into a 2 dram vial was placed 5-nitro-8-hydroxyquinoline (63 mg, 0.33 mmol), Ru/PS nanoparticle catalyst (8.0 mg, 0.477 mmol Ru/gram catalyst, 1.2 mol%), and hydrazine monohydrate (42 μL , 2.5 equiv) in 4 ml of THF. The reaction mixture was stirred for 2 hr, at which point the solvent was removed under reduced pressure. The product was extracted from the solid mixture with 3x 2 ml EtOH. The combined ethanol extracts were then passed through a short silica plug in a pipet and the silica plug was washed 2 times with 1 ml ethanol. The EtOH was then removed on a rotary evaporator under reduced pressure. The product 5-(hydroxyamino)quinolin-8-ol was isolated as an orange solid (51 mg, 0.29 mmol, 87% yield). For some of the more complex

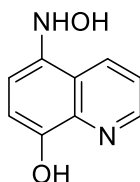
substrates, the reaction results are highly temperature sensitive, the reactions can be forced to completion by adding extra equivalents of hydrazine, and by raising the temperature to 27 °C.



N-(6-methylpyridin-2-yl) hydroxylamine (20a): The General Procedure was used with 46 mg of 2-methyl-6-nitropyridine (0.33 mmol) and 2.5 eq. Hydrazine monohydrate (42 μ L) and 1.1 mol % Ru/PS catalyst (8 mg). 39 mg (94 % isolated yield) of N-(6-methylpyridin-2-yl) hydroxylamine were obtained as product; ^1H NMR (300 MHz, CDCl_3) δ : 7.51 (t, $J = 7.5$ Hz, 1H), 6.89-6.86 (d, $J = 7.5$ Hz, 1H), 6.70-6.67 (d, $J = 7.5$ Hz, 1H), 2.44 (s, 3H). ^{13}C NMR (75 MHz, CDCl_3): δ 161.9, 156.1, 139.0, 116.5, 106.0, 23.8; IR (film): ν_{max} 3400, 2900, 1500 Cm^{-1} ; HRMS (ESI) calcd. for $\text{C}_6\text{H}_9\text{N}_2\text{O}$, 125.0715; found, $[\text{M}+\text{H}]^+$, 125.0800.

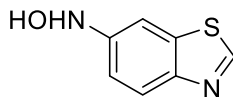


N-(quinolin-8-yl)hydroxylamine (20b): The General Procedure was used with 57 mg of 8-nitroquinoline (0.33 mmol) and 2.5 eq. Hydrazine monohydrate (42 μ L) and 1.1 mol % Ru/PS catalyst (8 mg) in Chloroform. 51 mg (96% isolated yield) of N-(quinolin-8-yl)hydroxylamine were obtained as product. Spectra match literature values. ^1H NMR (300 MHz, CDCl_3) δ : 8.77 (m, 1H), 8.07 (m, 1H), 7.38-7.26, (m, 2H), 7.17 (m, 1H), 6.93 (m, 1H); ^{13}C NMR (75 MHz, CDCl_3): δ 148.1, 147.6, 139.1, 136.3, 128.2, 127.6, 121.5, 116.3, 110.4.

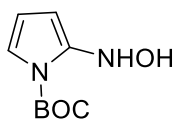


5-(hydroxyamino)quinolin-8-ol (20c): The General Procedure was used with 63 mg of 5-nitro-8-hydroxyquinonine (0.33 mmol) and 2.5 eq. Hydrazine monohydrate (42 μ L) and 1.1 mol % Ru/PS catalyst (8 mg) in Chloroform. 51 mg (87% isolated yield) of 5-(hydroxyamino)quinolin-8-ol were obtained as product; IR (film): ν_{max} 3400, 1800 Cm^{-1} ; HRMS (ESI) calcd. for $\text{C}_9\text{H}_9\text{N}_2\text{O}_2$, 177.0664; found, $[\text{M}+\text{H}]^+$, 177.0741. ^1H NMR (300 MHz,

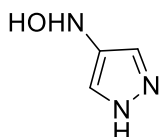
CDCl₃) δ : 8.78 (m, 1H), 8.22 (d, J = 9 Hz, 1H), 7.43-7.40 (m, 1H), 7.02 (d, J = 9 Hz, 1H), 6.78 (d, J = 9 Hz, 1H); ¹³C NMR (75 MHz, CDCl₃): δ 147.8, 145.6, 138.5, 133.6, 130.5, 120.4, 199.6, 111.6, 109.9.



N-(benzo[d]thiazol-6-yl)hydroxylamine (20d): The General Procedure was used with 59 mg of 6-nitrobenzothiazole (0.33 mmol) and 5 eq. Hydrazine monohydrate (84 μ L) and 1.1 mol % Ru/PS catalyst (8 mg) for 4 hours. 46.1 mg (84 % isolated yield) of N-(benzo[d]thiazol-6-yl)hydroxylamine were obtained as product; IR (film): ν_{max} 3450, 1900 cm^{-1} ; HRMS (ESI) calcd. for C₇H₇N₂OS, 167.0279; found, [M+H]⁺, 167.0301. ¹H NMR (300 MHz, CDCl₃) δ : 8.28-8.26 (d, J = 9 Hz, 1H), 8.20 (s, 1H), 7.61 (d, 1H), 7.09-7.07 (dd, 1H);

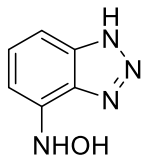


tert-butyl 2-(hydroxyamino)-1H-pyrrole-1-carboxylate (20e): The General Procedure was used with 70 mg of *tert*-butyl 2-nitro-1H-pyrrole-1-carboxylate (0.33 mmol) and 5 eq. Hydrazine monohydrate (84 μ L) and 1.1 mol % Ru/PS catalyst (8 mg) for 4 hours. 62 mg (95 % isolated yield) of *tert*-butyl 2-(hydroxyamino)-1H-pyrrole-1-carboxylate were obtained as product; ¹H NMR (500 MHz, CDCl₃) δ : 7.36 (bs, 1H), 7.13-7.12 (dd, J_1 = 4 Hz, J_2 = 1.5 Hz, 1H), 6.98-6.97 (dd, J_1 = 3 Hz, J_2 = 2 Hz, 1H), 6.32-6.31 (dd, J_1 = 4Hz, J_2 = 3Hz, 1H), 1.51-1.46 (d rot, J = 23.5 Hz, 9H); ¹³C NMR (125 MHz, CDCl₃): δ 160.1, 123.7, 111.8, 111.7, 77.2, 28.3; IR(film): ν_{max} 3400, 3250, 1800, 1750, 1400 cm^{-1} ; HRMS (ESI) calcd. for C₉H₁₅N₂O₃, 199.1083; found, [M+H]⁺, 199.1088.



N-(1H-pyrazol-4-yl)hydroxylamine (20f): The General Procedure was used with 37 mg of 4-nitropyrazole (0.33 mmol) and 5 eq. Hydrazine monohydrate (84 μ L) and 1.1 mol % Ru/PS catalyst (8 mg) for 4 hours. 30 mg (93 % isolated yield) of N-(1H-pyrazol-4-yl)hydroxylamine

were obtained as product; ^1H NMR (500 MHz, CDCl_3) δ : 7.23 (s, 2H); ^{13}C NMR (125 MHz, CDCl_3): δ 128.8, 124.9 (2C); IR(film): ν_{max} 3200, 2900, 1750 Cm^{-1} ; HRMS (ESI) calcd. for $\text{C}_3\text{H}_6\text{N}_3\text{O}$, 100.0511; found, $[\text{M}+\text{H}]^+$, 100.0507.



N-(1H-benzo[d][1,2,3]triazol-4-yl)hydroxylamine (20g): The General Procedure was used with 54 mg of 4-nitro-1H-benzo[d][1,2,3]triazole (0.33 mmol) and 2.5 eq. Hydrazine monohydrate (42 μL) and 1.1 mol % Ru/PS catalyst (8 mg). 43 mg (86 % isolated yield) of N-(1H-benzo[d][1,2,3]triazol-4-yl)hydroxylamine were obtained as product; ^1H NMR (500 MHz, CDCl_3) δ : 7.25-7.22 (t, $J = 7.5$ Hz, 1H), 6.98-6.95 (d, $J = 7.5$ Hz, 1H), 6.53-6.51 (d, $J = 7.5$ Hz, 1H), 5.04 (bs, 2H); ^{13}C NMR (125 MHz, CD_3CN): δ 127.5, 127.1, 106.0, 104.8, 104.1, 98.6; IR(film): ν_{max} 3400, 1800, 1200 Cm^{-1} ; HRMS (ESI) calcd. for $\text{C}_6\text{H}_7\text{N}_4\text{O}$, 151.0620; found, $[\text{M}+\text{H}]^+$, 151.0603.

1.11 References

1. Chorkendorff, I.; Niemantsverdriet, J. W., *Concepts of modern catalysis and kinetics*. John Wiley & Sons: 2017.
2. Jessop, P. G.; Ikariya, T.; Noyori, R., Homogeneous catalysis in supercritical fluids. *Chemical Reviews* **1999**, *99* (2), 475-494.
3. Astruc, D.; Lu, F.; Aranzaes, J. R., Nanoparticles as recyclable catalysts: the frontier between homogeneous and heterogeneous catalysis. *Angewandte Chemie International Edition* **2005**, *44* (48), 7852-7872.
4. Somorjai, G. A.; Kliewer, C. J., Reaction selectivity in heterogeneous catalysis. *Reaction Kinetics and Catalysis Letters* **2009**, *96* (2), 191-208.
5. Shylesh, S.; Schünemann, V.; Thiel, W. R., Magnetically separable nanocatalysts: bridges between homogeneous and heterogeneous catalysis. *Angewandte Chemie International Edition* **2010**, *49* (20), 3428-3459.
6. Madhavan, N.; Jones, C. W.; Weck, M., Rational approach to polymer-supported catalysts: synergy between catalytic reaction mechanism and polymer design. *Accounts of Chemical Research* **2008**, *41* (9), 1153-1165.

7. Udumula, V.; Tyler, J. H.; Davis, D. A.; Wang, H.; Linford, M. R.; Minson, P. S.; Michaelis, D. J., Dual optimization approach to bimetallic nanoparticle catalysis: Impact of M1/M2 ratio and supporting polymer structure on reactivity. *ACS Catalysis* **2015**, *5* (6), 3457-3462.
8. Gates, B., Supported metal clusters: synthesis, structure, and catalysis. *Chemical Reviews* **1995**, *95* (3), 511-522.
9. Zhou, X.; Xu, W.; Liu, G.; Panda, D.; Chen, P., Size-dependent catalytic activity and dynamics of gold nanoparticles at the single-molecule level. *Journal of the American Chemical Society* **2009**, *132* (1), 138-146.
10. Blaser, H. U.; Steiner, H.; Studer, M., Selective catalytic hydrogenation of functionalized nitroarenes: an update. *ChemCatChem* **2009**, *1* (2), 210-221.
11. Petkar, D. R.; Kadu, B. S.; Chikate, R. C., Highly efficient and chemoselective transfer hydrogenation of nitroarenes at room temperature over magnetically separable Fe–Ni bimetallic nanoparticles. *RSC Advances* **2014**, *4* (16), 8004-8010.
12. Park, J.-Y.; Lee, Y.-J.; Khanna, P. K.; Jun, K.-W.; Bae, J. W.; Kim, Y. H., Alumina-supported iron oxide nanoparticles as Fischer–Tropsch catalysts: Effect of particle size of iron oxide. *Journal of Molecular Catalysis A: Chemical* **2010**, *323* (1-2), 84-90.
13. Costa, N. J.; Rossi, L. M., Synthesis of supported metal nanoparticle catalysts using ligand assisted methods. *Nanoscale* **2012**, *4* (19), 5826-5834.
14. Zhou, X.; Huang, X.; Qi, X.; Wu, S.; Xue, C.; Boey, F. Y.; Yan, Q.; Chen, P.; Zhang, H., In situ synthesis of metal nanoparticles on single-layer graphene oxide and reduced graphene oxide surfaces. *The Journal of Physical Chemistry C* **2009**, *113* (25), 10842-10846.
15. Altin, O.; Özbelge, H. Ö.; Dogu, T., Effect of pH in an aqueous medium on the surface area, pore size distribution, density, and porosity of montmorillonite. *Journal of Colloid and Interface Science* **1999**, *217* (1), 19-27.
16. Wang, Y.; Xiao, Z.; Wu, L., Metal-nanoparticles supported on solid as heterogeneous catalysts. *Current Organic Chemistry* **2013**, *17* (12), 1325-1333.
17. Zheng, N.; Stucky, G. D., A general synthetic strategy for oxide-supported metal nanoparticle catalysts. *Journal of the American Chemical Society* **2006**, *128* (44), 14278-14280.
18. Zheng, N.; Fan, J.; Stucky, G. D., One-step one-phase synthesis of monodisperse noble-metallic nanoparticles and their colloidal crystals. *Journal of the American Chemical Society* **2006**, *128* (20), 6550-6551.

19. Kralik, M.; Biffis, A., Catalysis by metal nanoparticles supported on functional organic polymers. *Journal of Molecular Catalysis A: Chemical* **2001**, *177* (1), 113-138.
20. Hao, E.; Kelly, K. L.; Hupp, J. T.; Schatz, G. C., Synthesis of silver nanodisks using polystyrene mesospheres as templates. *Journal of the American Chemical Society* **2002**, *124* (51), 15182-15183.
21. Zhang, S.; Zhang, X.; Jiang, G.; Zhu, H.; Guo, S.; Su, D.; Lu, G.; Sun, S., Tuning nanoparticle structure and surface strain for catalysis optimization. *Journal of the American Chemical Society* **2014**, *136* (21), 7734-7739.
22. Almora-Barrios, N.; Cano, I.; van Leeuwen, P. W.; Lopez, N. r., Concerted chemoselective hydrogenation of acrolein on secondary phosphine oxide decorated gold nanoparticles. *ACS Catalysis* **2017**, *7* (6), 3949-3954.
23. Yasukawa, T.; Miyamura, H.; Kobayashi, S., Polymer-incarcerated chiral Rh/Ag nanoparticles for asymmetric 1, 4-addition reactions of arylboronic acids to enones: remarkable effects of bimetallic structure on activity and metal leaching. *Journal of the American Chemical Society* **2012**, *134* (41), 16963-16966.
24. Mostafa, S.; Behafarid, F.; Croy, J. R.; Ono, L. K.; Li, L.; Yang, J. C.; Frenkel, A. I.; Cuenya, B. R., Shape-dependent catalytic properties of Pt nanoparticles. *Journal of the American Chemical Society* **2010**, *132* (44), 15714-15719.
25. Jin, R., The impacts of nanotechnology on catalysis by precious metal nanoparticles. *Nanotechnology Reviews* **2012**, *1* (1), 31-56.
26. Xiong, Y.; Wiley, B. J.; Xia, Y., Nanocrystals with unconventional shapes—a class of promising catalysts. *Angewandte Chemie International Edition* **2007**, *46* (38), 7157-7159.
27. Li, Y.; Liu, Q.; Shen, W., Morphology-dependent nanocatalysis: metal particles. *Dalton Transactions* **2011**, *40* (22), 5811-5826.
28. Collins, G.; Schmidt, M.; O'Dwyer, C.; Holmes, J. D.; McGlacken, G. P., The Origin of Shape Sensitivity in Palladium-Catalyzed Suzuki–Miyaura Cross Coupling Reactions. *Angewandte Chemie* **2014**, *126* (16), 4226-4229.
29. Narayanan, R.; El-Sayed, M. A., Catalysis with transition metal nanoparticles in colloidal solution: nanoparticle shape dependence and stability. ACS Publications: 2005.
30. Thathagar, M. B.; Beckers, J.; Rothenberg, G., Copper-catalyzed Suzuki cross-coupling using mixed nanocluster catalysts. *Journal of the American Chemical Society* **2002**, *124* (40), 11858-11859.

31. Isaifan, R. J.; Ntais, S.; Baranova, E. A., Particle size effect on catalytic activity of carbon-supported Pt nanoparticles for complete ethylene oxidation. *Applied Catalysis A: General* **2013**, *464*, 87-94.
32. Valden, M.; Pak, S.; Lai, X.; Goodman, D., Structure sensitivity of CO oxidation over model Au/TiO₂ catalysts. *Catalysis Letters* **1998**, *56* (1), 7-10.
33. Ketchie, W. C.; Fang, Y.-L.; Wong, M. S.; Murayama, M.; Davis, R. J., Influence of gold particle size on the aqueous-phase oxidation of carbon monoxide and glycerol. *Journal of Catalysis* **2007**, *250* (1), 94-101.
34. Tsung, C.-K.; Kuhn, J. N.; Huang, W.; Aliaga, C.; Hung, L.-I.; Somorjai, G. A.; Yang, P., Sub-10 nm platinum nanocrystals with size and shape control: catalytic study for ethylene and pyrrole hydrogenation. *Journal of the American Chemical Society* **2009**, *131* (16), 5816-5822.
35. Zaera, F., Nanostructured materials for applications in heterogeneous catalysis. *Chemical Society Reviews* **2013**, *42* (7), 2746-2762.
36. Kaizuka, K.; Miyamura, H.; Kobayashi, S., Aerobic Oxidation of Alcohols and Direct Oxidative Ester Formation Catalyzed by Polymer-Immobilized Bimetallic Nanocluster Catalysts. *Kobunshi Ronbunshu* **2011**, *68* (7).
37. Groppo, E.; Agostini, G.; Borfecchia, E.; Wei, L.; Giannici, F.; Portale, G.; Longo, A.; Lamberti, C., Formation and growth of Pd nanoparticles inside a highly cross-linked polystyrene support: Role of the reducing agent. *The Journal of Physical Chemistry C* **2014**, *118* (16), 8406-8415.
38. Nakazawa, M.; Somorjai, G. A., Adsorption of substituted benzenes on polycrystalline gold and on zinc oxide and iron oxide overlayers. *Applied surface science* **1993**, *68* (4), 517-537.
39. Miyamura, H.; Matsubara, R.; Miyazaki, Y.; Kobayashi, S., Aerobic oxidation of alcohols at room temperature and atmospheric conditions catalyzed by reusable gold nanoclusters stabilized by the benzene rings of polystyrene derivatives. *Angewandte Chemie International Edition* **2007**, *46* (22), 4151-4154.
40. Okamoto, K.; Akiyama, R.; Kobayashi, S., Suzuki–Miyaura Coupling Catalyzed by Polymer-Incarcerated Palladium, a Highly Active, Recoverable, and Reusable Pd Catalyst. *Organic Letters* **2004**, *6* (12), 1987-1990.
41. Soul, J.-F. o.; Miyamura, H.; Kobayashi, S., Copolymer-incarcerated nickel nanoparticles with N-heterocyclic carbene precursors as active cross-linking agents for Corriu–

Kumada–Tamao reaction. *Journal of the American Chemical Society* **2013**, *135* (29), 10602-10605.

42. Soul, J.-F. o.; Miyamura, H.; Kobayashi, S., Powerful amide synthesis from alcohols and amines under aerobic conditions catalyzed by gold or gold/iron,-nickel or-cobalt nanoparticles. *Journal of the American Chemical Society* **2011**, *133* (46), 18550-18553.

43. Kaizuka, K.; Miyamura, H.; Kobayashi, S., Remarkable effect of bimetallic nanocluster catalysts for aerobic oxidation of alcohols: combining metals changes the activities and the reaction pathways to aldehydes/carboxylic acids or esters. *Journal of the American Chemical Society* **2010**, *132* (43), 15096-15098.

44. Yasukawa, T.; Miyamura, H.; Kobayashi, S., Chiral ligand-modified metal nanoparticles as unique catalysts for asymmetric C–C bond-forming reactions: how are active species generated? *ACS Catalysis* **2016**, *6* (11), 7979-7988.

45. Jansat, S.; Gómez, M.; Philippot, K.; Muller, G.; Guiu, E.; Claver, C.; Castellón, S.; Chaudret, B., A case for enantioselective allylic alkylation catalyzed by palladium nanoparticles. *Journal of the American Chemical Society* **2004**, *126* (6), 1592-1593.

46. Akiyama, R.; Kobayashi, S., Microencapsulated palladium catalysts: Allylic substitution and Suzuki coupling using a recoverable and reusable polymer-supported palladium catalyst. *Angewandte Chemie International Edition* **2001**, *40* (18), 3469-3471.

47. Mori, K.; Kondo, Y.; Yamashita, H., Synthesis and characterization of FePd magnetic nanoparticles modified with chiral BINAP ligand as a recoverable catalyst vehicle for the asymmetric coupling reaction. *Physical Chemistry Chemical Physics* **2009**, *11* (39), 8949-8954.

48. Han, D.; Li, X.; Zhang, H.; Liu, Z.; Hu, G.; Li, C., Asymmetric hydroformylation of olefins catalyzed by rhodium nanoparticles chirally stabilized with (R)-BINAP ligand. *Journal of Molecular Catalysis A: Chemical* **2008**, *283* (1-2), 15-22.

49. Park, K. H.; Chung, Y. K., Immobilized Co/Rh Heterobimetallic Nanoparticle-Catalyzed Pauson–Khand-Type Reaction. *Advanced Synthesis & Catalysis* **2005**, *347* (6), 854-866.

50. Goubert, G.; McBreen, P. H., In-Situ Spectroscopic Detection of Active Surface Species in Asymmetric Heterogeneous Catalysis. *ChemCatChem* **2013**, *5* (3), 683-685.

51. Crabtree, R. H., Resolving heterogeneity problems and impurity artifacts in operationally homogeneous transition metal catalysts. *Chemical Reviews* **2011**, *112* (3), 1536-1554.

52. Meemken, F.; Maeda, N.; Hungerbühler, K.; Baiker, A., Platinum-Catalyzed Asymmetric Hydrogenation: Spectroscopic Evidence for an O-H-O Hydrogen-Bond Interaction between Substrate and Modifier. *Angewandte Chemie International Edition* **2012**, *51* (33), 8212-8216.
53. Maeda, N.; Hungerbühler, K.; Baiker, A., Asymmetric hydrogenation on chirally modified Pt: Origin of hydrogen in the N-H-O interaction between cinchonidine and ketone. *Journal of the American Chemical Society* **2011**, *133* (49), 19567-19569.
54. Yasukawa, T.; Kuremoto, T.; Miyamura, H.; Kobayashi, S., Asymmetric Arylation of Imines Catalyzed by Heterogeneous Chiral Rhodium Nanoparticles. *Organic Letters* **2016**, *18* (11), 2716-2718.
55. Yasukawa, T.; Suzuki, A.; Miyamura, H.; Nishino, K.; Kobayashi, S., Chiral metal nanoparticle systems as heterogeneous catalysts beyond homogeneous metal complex catalysts for asymmetric addition of arylboronic acids to α , β -unsaturated carbonyl compounds. *Journal of the American Chemical Society* **2015**, *137* (20), 6616-6623.
56. Yasukawa, T.; Saito, Y.; Miyamura, H.; Kobayashi, S., Chiral Nanoparticles/Lewis Acids as Cooperative Catalysts for Asymmetric 1, 4-Addition of Arylboronic Acids to α , β -Unsaturated Amides. *Angewandte Chemie* **2016**, *128* (28), 8190-8193.
57. Ranganath, K. V.; Schäfer, A. H.; Glorius, F., Comparison of Superparamagnetic Fe₃O₄-Supported N-Heterocyclic Carbene-Based Catalysts for Enantioselective Allylation. *ChemCatChem* **2011**, *3* (12), 1889-1891.
58. Parella, R.; Babu, S. A., Magnetic nano Fe₃O₄ and CuFe₂O₄ as heterogeneous catalysts: a green method for the stereo- and regioselective reactions of epoxides with indoles/pyrroles. *Catalysis Communications* **2012**, *29*, 118-121.
59. Shih, H.-H.; Williams, D.; Mack, N. H.; Wang, H.-L., Conducting polymer-based electrodeless deposition of Pt nanoparticles and its catalytic properties for regioselective hydrosilylation reactions. *Macromolecules* **2008**, *42* (1), 14-16.
60. Udumula, V.; Nazari, S. H.; Burt, S. R.; Alfindie, M. N.; Michaelis, D. J., Chemo- and Site-Selective Alkyl and Aryl Azide Reductions with Heterogeneous Nanoparticle Catalysts. *ACS Catalysis* **2016**, *6* (7), 4423-4427.
61. Mahatthananchai, J.; Dumas, A. M.; Bode, J. W., Catalytic selective synthesis. *Angewandte Chemie International Edition* **2012**, *51* (44), 10954-10990.
62. Lewis, C. A.; Miller, S. J., Site-selective derivatization and remodeling of erythromycin A by using simple peptide-based chiral catalysts. *Angewandte Chemie International Edition* **2006**, *45* (34), 5616-5619.

63. Han, S.; Miller, S. J., Asymmetric catalysis at a distance: catalytic, site-selective phosphorylation of teicoplanin. *Journal of the American Chemical Society* **2013**, *135* (33), 12414-12421.
64. Pathak, T. P.; Miller, S. J., Site-selective bromination of vancomycin. *Journal of the American Chemical Society* **2012**, *134* (14), 6120-6123.
65. Fowler, B. S.; Laemmerhold, K. M.; Miller, S. J., Catalytic site-selective thiocarbonylations and deoxygenations of vancomycin reveal hydroxyl-dependent conformational effects. *Journal of the American Chemical Society* **2012**, *134* (23), 9755-9761.
66. Nyffeler, P. T.; Liang, C.-H.; Koeller, K. M.; Wong, C.-H., The chemistry of amine-azide interconversion: catalytic diazotransfer and regioselective azide reduction. *Journal of the American Chemical Society* **2002**, *124* (36), 10773-10778.
67. Liang, F. S.; Wang, S. K.; Nakatani, T.; Wong, C. H., Targeting RNAs with tobramycin analogues. *Angewandte Chemie International Edition* **2004**, *43* (47), 6496-6500.
68. Li, J.; Wang, J.; Czyryca, P. G.; Chang, H.; Orsak, T. W.; Evanson, R.; Chang, C.-W. T., Application of glycodiversification: expedient synthesis and antibacterial evaluation of a library of kanamycin B analogues. *Organic Letters* **2004**, *6* (9), 1381-1384.
69. Seeberger, P. H.; Werz, D. B., Automated synthesis of oligosaccharides as a basis for drug discovery. *Nature Reviews Drug Discovery* **2005**, *4* (9), 751.
70. Vyas, P. M.; Roychowdhury, S.; Woster, P. M.; Svensson, C. K., Reactive oxygen species generation and its role in the differential cytotoxicity of the arylhydroxylamine metabolites of sulfamethoxazole and dapsone in normal human epidermal keratinocytes. *Biochemical Pharmacology* **2005**, *70* (2), 275-286.
71. Shi, Q. X.; Lu, R. W.; Jin, K.; Zhang, Z. X.; Zhao, D. F., Ultrasound-promoted highly chemoselective reduction of aromatic nitro compounds to the corresponding N-arylhydroxylamines using zinc and HCOONH₄ in CH₃CN. *Chemistry Letters* **2006**, *35* (2), 226-227.
72. Tyler, J. H.; Nazari, S. H.; Patterson, R. H.; Udumula, V.; Smith, S. J.; Michaelis, D. J., Synthesis of N-aryl and N-heteroaryl hydroxylamines via partial reduction of nitroarenes with soluble nanoparticle catalysts. *Tetrahedron Letters* **2017**, *58* (1), 82-86.
73. Kitamura, M.; Kato, S.; Yano, M.; Tashiro, N.; Shiratake, Y.; Sando, M.; Okauchi, T., A reagent for safe and efficient diazo-transfer to primary amines: 2-azido-1, 3-dimethylimidazolium hexafluorophosphate. *Organic & Biomolecular Chemistry* **2014**, *12* (25), 4397-4406.

74. Ahammed, S.; Saha, A.; Ranu, B. C., Hydrogenation of azides over copper nanoparticle surface using ammonium formate in water. *The Journal of Organic Chemistry* **2011**, *76* (17), 7235-7239.
75. Thomas, J. R.; Liu, X.; Hergenrother, P. J., Size-specific ligands for RNA hairpin loops. *Journal of the American Chemical Society* **2005**, *127* (36), 12434-12435.
76. Bidal, Y. D.; Lesieur, M.; Melaimi, M.; Cordes, D. B.; Slawin, A. M.; Bertrand, G.; Cazin, C. S., A simple access to transition metal cyclopropenyliene complexes. *Chemical Communications* **2015**, *51* (23), 4778-4781.
77. Williamson, K. S.; Yoon, T. P., Iron-catalyzed aminohydroxylation of olefins. *Journal of the American Chemical Society* **2010**, *132* (13), 4570-4571.
78. Li, Z.; Fowler, F. W.; Lauher, J. W., Weak interactions dominating the supramolecular self-assembly in a salt: a designed single-crystal-to-single-crystal topochemical polymerization of a terminal aryldiacetylene. *Journal of the American Chemical Society* **2008**, *131* (2), 634-643.
79. Chen, H.; Yang, W.; Wu, W.; Jiang, H., Palladium-catalyzed regioselective azidation of allylic C–H bonds under atmospheric pressure of dioxygen. *Organic & Biomolecular Chemistry* **2014**, *12* (21), 3340-3343.
80. Hanessian, S.; Simard, D.; Deschênes-Simard, B.; Chenel, C.; Haak, E., Proximity-Assisted Cycloaddition Reactions Facile Lewis Acid-Mediated Synthesis of Diversely Functionalized Bicyclic Tetrazoles. *Organic Letters* **2008**, *10* (7), 1381-1384.
81. Kapat, A.; K nig, A.; Montermini, F.; Renaud, P., A radical procedure for the anti-markovnikov hydroazidation of alkenes. *Journal of the American Chemical Society* **2011**, *133* (35), 13890-13893.
82. Sun, Q.; Cai, S.; Peterson, B. R., Practical synthesis of 3 β -amino-5-cholestene and related 3 β -halides involving i-steroid and retro-i-steroid rearrangements. *Organic Letters* **2008**, *11* (3), 567-570.
83. Xu, S.; Giuseppone, N., Self-duplicating amplification in a dynamic combinatorial library. *Journal of the American Chemical Society* **2008**, *130* (6), 1826-1827.
84. Goddard-Borger, E. D.; Stick, R. V., An efficient, inexpensive, and shelf-stable diazotransfer reagent: imidazole-1-sulfonyl azide hydrochloride. *Organic Letters* **2007**, *9* (19), 3797-3800.
85. Richmond, E.; Duguet, N.; Slawin, A. M.; Lebl, T.; Smith, A. D., Asymmetric pericyclic cascade approach to spirocyclic oxindoles. *Organic Letters* **2012**, *14* (11), 2762-2765.

86. Shil, A. K.; Das, P., Solid supported platinum (0) nanoparticles catalyzed chemo-selective reduction of nitroarenes to N-arylhydroxylamines. *Green Chemistry* **2013**, *15* (12), 3421-3428.

Chapter 2 Nickel-Catalyzed Suzuki Cross-Couplings with Unprotected Allylic Alcohols Enabled by Bidentate N-Heterocyclic Carbene (NHC)/Phosphine Ligands

2.1 Introduction

Carbon-Carbon bond formation is the backbone of organic chemistry and a fundamental reaction for drug discovery in the pharmaceutical industry¹. Classical methods for C–C bond formation includes addition of main-group metal reagents (RLi, RMgX) to electrophiles that are limited in substrate scop². Transition metals have emerged as a promising alternative to traditional methods and offer a straightforward route for C-C bond formation³. The past two decades have witnessed a remarkable improvement in reaction design using noble transition metals like palladium as catalysts⁴. A variety of methods were introduced that facilitate formation of bigger molecules from small subunits. However, a revolution happened when a new class of transformations named cross-coupling reactions were introduced to the science³. In these reactions, two metals including a catalyst and stoichiometric amount of the second metal work in concert to form a carbon-carbon bond. Depending on the second metal used in the reaction, there are different categories of the cross-coupling reactions including Kumada⁵ (Mg), Stille⁶ (Sn), and Suzuki⁷ reactions. In the Kumada and Stille cross-coupling reactions, collaboration between palladium as catalyst and an aryl/alkyl magnesium halide or an aryl/alkyl stannane as the coupling partner (nucleophile) with an alkyl/aryl halide (electrophile) are used in the formation of product. The Suzuki cross-coupling reaction, which employs an aryl or alkyl boron reagent as nucleophile, is one of the most important methods for new carbon-carbon bond formation reactions and drug development in the pharmaceutical industries. Since its discovery, it has been the subject of extensive research in search of better reaction conditions and a broader substrate scope. Traditional Suzuki cross-coupling methods employ expensive noble metals such as rhodium⁸, iridium⁹, and palladium¹⁰ as the catalyst. The cost, toxicity, and poor reactivity of palladium toward inactive substrates (such as allylic alcohols) requires development of new strategies that preclude the need for activation of electrophilic substrate¹¹. Nickel is the younger sibling of palladium and it is the catalyst of choice in pharmaceutical synthesis due to its abundance (low cost) and nontoxicity¹². However, due to the lack of appropriate ligands to support nickel in the solution, methods that employ nickel as a catalyst in Suzuki cross-coupling reactions are still underdeveloped. In this chapter, the classical Suzuki cross-coupling reactions will be discussed first. Our most recent discoveries in the Suzuki reaction will be presented at the end.

Keywords: Nickel catalyst, Suzuki cross coupling, Allylic arylation, Phenyl boronic ester.

2.2 Transition Metal Catalyzed Suzuki Cross-Coupling Reactions.

2.2.1 Palladium catalyzed Suzuki cross-coupling reactions

For the past decade, palladium-catalyzed Suzuki reactions have emerged as a reliable method for construction of biaryl structures that form the core of many natural products. There are a myriad of benefits of using the Suzuki reaction, including functional group tolerance, mild reaction conditions, and the stability/low reactivity of the reagents³. Conventional Suzuki coupling reactions employ triaryl phosphine ligands to support and stabilize palladium in the solution. While the system is compatible with a wide range of substrates, there is a high demand from pharmaceutical companies for new catalytic systems that enable synthesis of bulky biaryl products¹³. Buchwald, who is a pioneer in new ligand design for cross-coupling reactions, has designed numerous ligands for cross-coupling reactions⁴. Most recently, he has designed

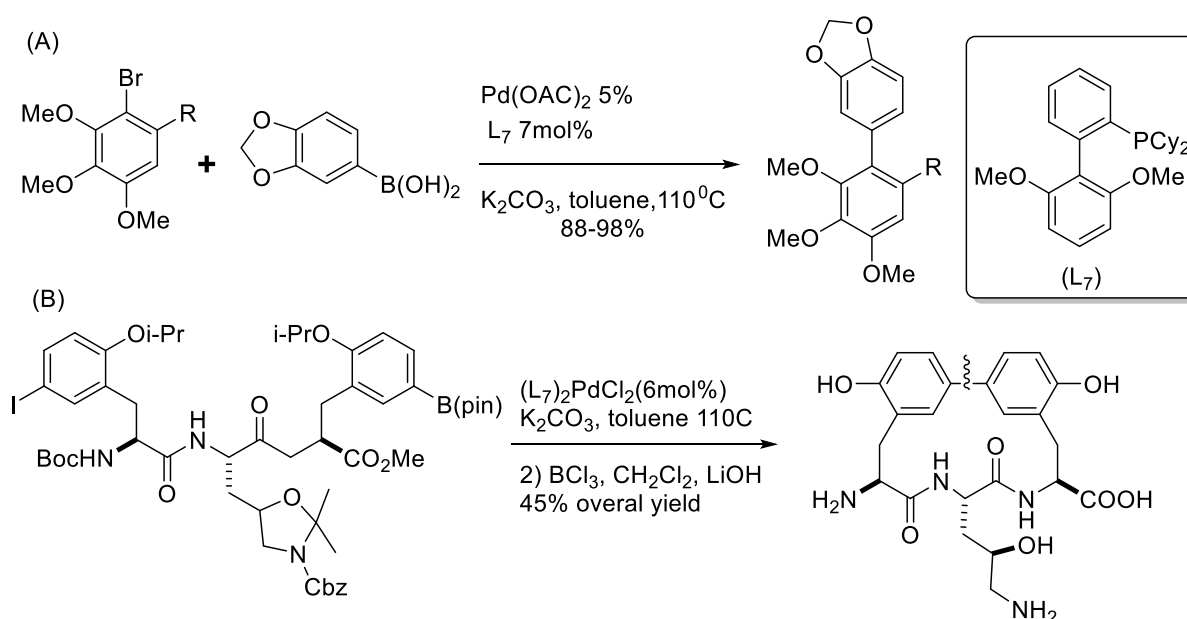


Figure 2.1 Application of Buchwald's ligand in Synthesis

several dialkyl biaryl ligands for palladium-catalyzed Suzuki cross-coupling of highly substituted aryl and heteroaryl couplings¹⁴ (Figure 2.1). Mechanistic studies revealed that the to a higher catalyst lifetime. The ligands are pretty stable to oxygen and heat, providing the electron-rich nature of the ligands boosts the thermodynamic stability of the complex leading

possibility for bench-top reactions that do not require rigorously dry and air free setups. One great aspect of Buchwald's ligands is their widespread utility in the synthesis of polyfunctionalized arenes. The conditions are applicable to inter (Figure 2.1a) and intramolecular (Figure 2.1b) cross-coupling reactions. Although the palladium catalysts developed by Buchwald and others show great reactivity against active electrophiles, they are not the catalyst of choice when it comes to less reactive electrophiles¹⁵ (such as aryl chlorides or ether/alcohol electrophiles). The electrophilic partner in Suzuki reactions catalyzed by palladium is usually an aryl bromide or aryl iodide. Recent advances in the Suzuki reaction has focused on the development of new strategies that reduce the cost and minimize the waste accumulation during the reaction.

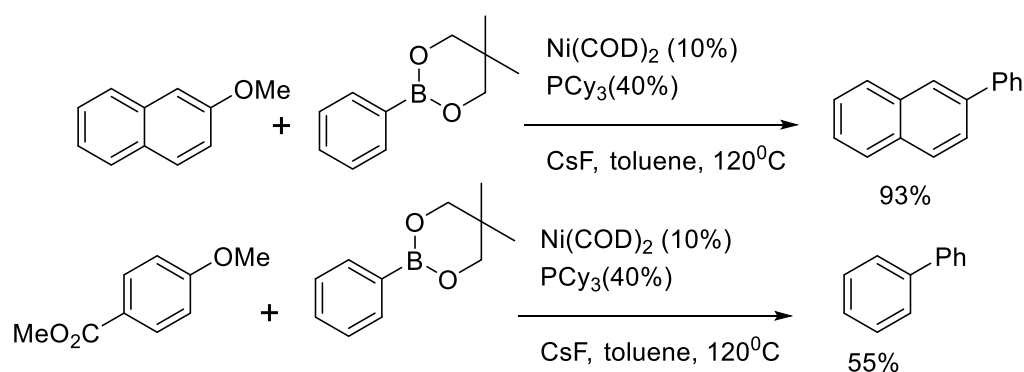


Figure 2.2 Nickel-catalyzed cross coupling of aryl ethers

Nickel has some features that makes it suitable for cross coupling of inactive electrophiles. As a group ten metal it has ten d-electrons, making it relatively electron rich. Thus, it has a smaller atomic radius and higher electron density compared to palladium. This high electron density lowers barrier of oxidative addition and facilitates utilization of weaker electrophiles containing C-Cl, C-F or even C-O bonds in the Suzuki cross-coupling reaction¹². In 2008, Chatani and coworkers reported the first cross coupling of aryl ethers with arylboronic acids with nickel (0) as a catalyst and PCy₃ as a ligand¹⁶. Electron deficient aryl ether substrates worked best for this system, as the fused aromatic rings or ester-containing substrates were demonstrated to be the best in the reaction (Figure 2.2).

Aryl fluorides are the weakest electrophiles among aryl halides. However, their potential use as a leaving group in cross couplings is starting to gain attention to chemists as this strategy would enable late stage functionalization of highly functionalized fluorinated substrates¹⁷. Efforts towards palladium catalyzed cross coupling of aryl fluorides have proven

difficult unless the fluoride is adjacent to an electron withdrawing group like nitro group, leading to a nucleophilic aromatic substitution mechanism¹⁷.

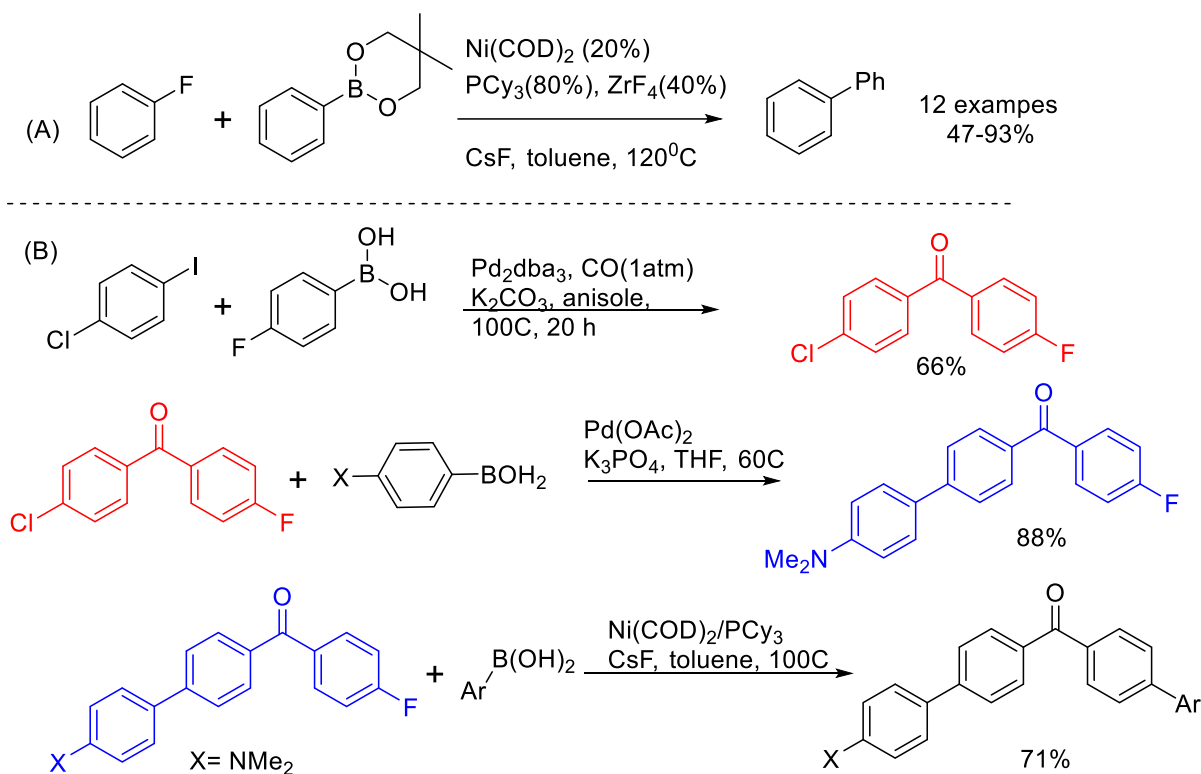


Figure 2.3 Nickel catalyzed cross coupling of aryl fluorides (A) late state synthesis of poly aryl ketones (B)

The first nickel-catalyzed cross-coupling of aryl fluorides with aryl boronic acids was reported by Radius and coworkers in 2006¹⁸. Using an N-heterocyclic carbene (NHC) ligand, they were able to couple pentafluoro trifluoromethyl benzene with phenyl boronic acid with only 2 mol% of $\text{Ni}(\text{COD})_2$ as catalyst. In their study, they were also able to identify the Ni-F species as an intermediate in catalysis. Chatani and coworkers later reported improved conditions for cross-coupling of aryl fluorides using $\text{Ni}(\text{COD})_2/\text{PCy}_3$ and zirconium fluoride as an additive¹⁹ (Figure 2.3a). In their study, they confirmed the pivotal role of a fluorine salt as a co-catalyst for the success of the reaction. By incorporating a directing group in the structure of the aryl fluoride, they enhanced the yield to almost quantitative. The significance of this discovery was demonstrated in their work by multistep discriminative synthesis of polyaryl ketones (Figure 2.3b). The prevalence of the allyl moiety in natural products and the versatility of alkenes in chemical synthesis and drug development prompted synthetic chemists to capitalize on allylic substrates as coupling partners in the Suzuki reaction²⁰. Allylic alcohols represent a highly useful class of substrates for this purpose as they provide chemists with a

step and atom economic process for C-C bond formation²¹. In addition, cross couplings with simple alcohols obviate the need for activation of the electrophile substrate as a halide or sulfonate leaving group. Factors including the acidic nature of the O–H bond, the stability of undesired M-alkoxide complexes, the poor leaving group ability of OH, and the basicity of the alcohol electrophile have made cross couplings with unprotected alcohols challenging to achieve²². Thus, allylic carbonates, sulfonates, acetates, phosphonates, or halogens are typically employed in allylic functionalization reactions, which adds undesirable synthetic steps²³.

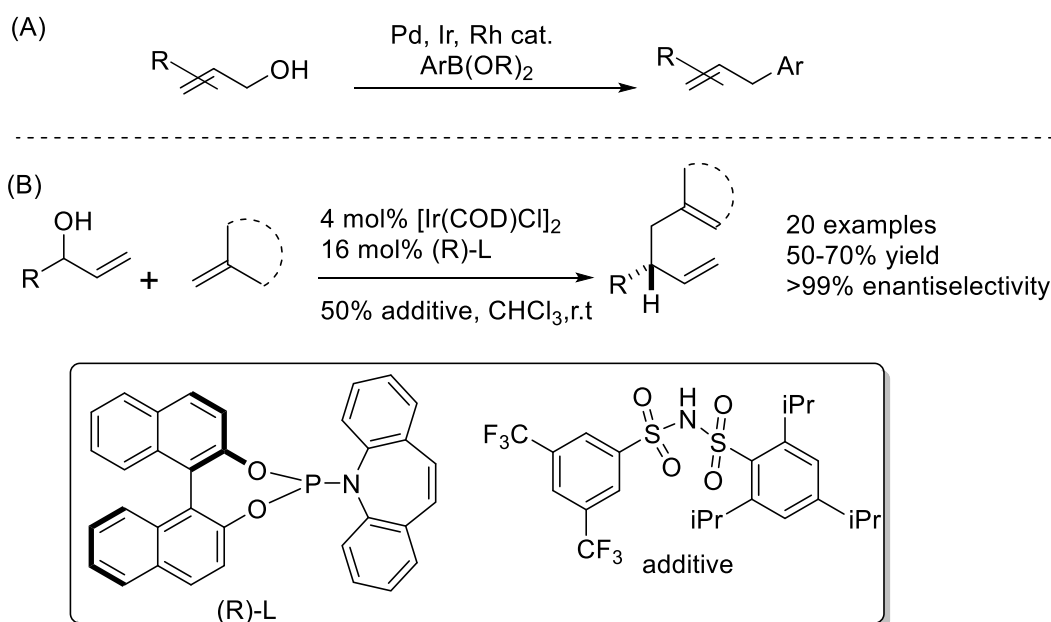


Figure 2.4 Allylic arylation with noble metals (A) enantioselective synthesis of 1,5 diene

Recent advances in cross couplings with unprotected allylic alcohols have generally required the use of expensive noble-metal catalysts, such as iridium²⁴, ruthenium²⁵, rhodium²⁶, or palladium²⁷ (Figure 2.4 A). A quintessential example of allylic substitution with unprotected allylic alcohols was presented by Carreira where he cross-coupled two allyl moieties enantioselectively using iridium as catalyst and a chiral ligand²⁸. While the results of allylic substitution with noble transition metals are impressive, many efforts have focused on developing catalytic systems that employ more abundant and less toxic first row transition metals. Nickel represents an ideal catalyst for these transformations because of its low cost and high abundance. Nickel-catalyzed allylic substitutions, including allylic aminations²⁹, alkylations³⁰, and Negishi cross-couplings with unprotected allyl alcohols³¹ have been reported to date. However, the nickel-catalyzed C-C bond-forming Suzuki-Miyaura reaction with unprotected allyl alcohols has remained unexplored³.

In the Michaelis laboratory, we are interested in developing new classes of ligands for nickel catalysts that enable new reactivity. In particular, we have developed new classes of bidentate NHC-phosphine ligands that enable an efficient nickel-catalyzed Suzuki–Miyaura cross-coupling methodology that employs simple, unprotected allylic alcohols as the electrophilic coupling partners³². These results expand the current repertoire of nickel-catalyzed transformations and provide a convenient method for generating allylic arene and heteroarene products. In addition, our catalytic method rivals similar methods developed with more expensive noble metal catalysts, in terms of product yield and catalyst loading¹⁰. Key to obtaining high yields in these transformations is the use of bidentate NHC/phosphine ligands that extend catalyst lifetime and allow reactions to proceed with as little as 1.25 mol % nickel catalyst. The results of this study will be the subject of discussion in the next section of this chapter.

2.3 Nickel-Catalyzed Suzuki Cross-Couplings with Unprotected Allylic Alcohols Enabled by Bidentate N-Heterocyclic Carbene (NHC)/Phosphine Ligands

Nickel catalysis is rapidly becoming a staple of modern organic chemistry. A significant challenge with nickel catalysts is that nickel (0) complexes are generally unstable and readily decompose during catalysis, leading to short catalyst lifetimes. Nickel N-heterocyclic carbene (NHC) complexes have found widespread application in nickel catalysis, because of their relatively high stability¹³. In the Michaelis laboratory, we designed and synthesized numerous bidentate NHC/Phosphine ligands and demonstrated that they are suitable catalysts for the Suzuki reaction with unprotected allylic alcohols. The power of our catalyst relies on its ability to stabilize nickel (0) in the solution and extend the catalyst lifetime. Our results showed that our bidentate NHC/phosphine ligands increase catalyst stability and lifetime leading to higher yields in Suzuki cross-couplings with simple allylic alcohols (Figure 2.5).

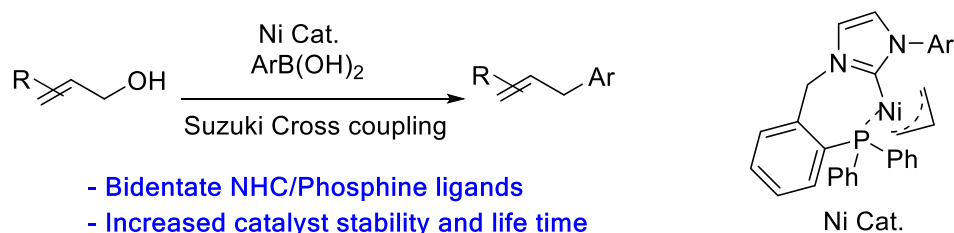


Figure 2.5 New NHC/Phosphine ligands for Suzuki cross coupling reactions

2.3.1 Results and discussion

We began our study by designing various bidentate ligands. The basic structure includes an NHC core structure with several different pendant coordinating groups, including pyridine and diphenylphosphine groups, with diverse bite angles between the two binding groups. The

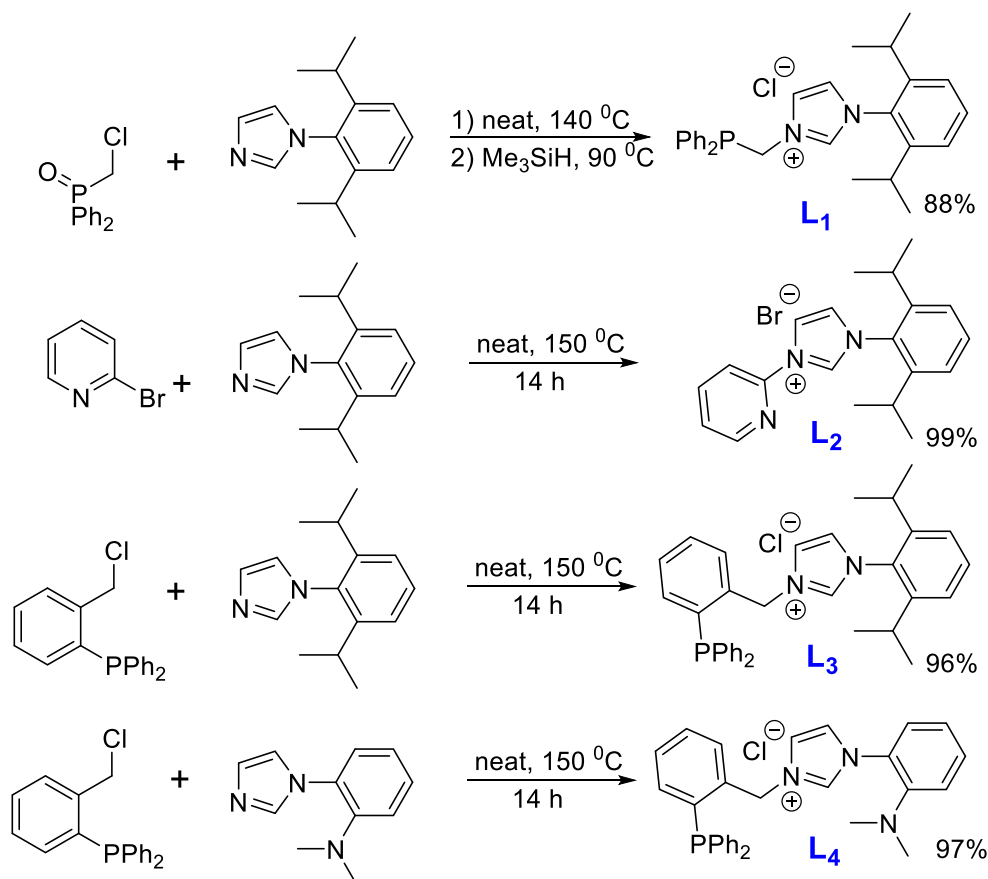
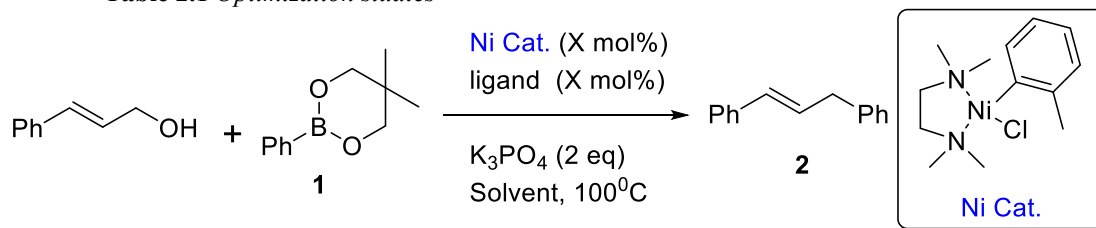


Figure 2.6 Synthetic route and the structures of bidentate NHC ligands

synthetic route and the structures of the ligands are shown in Figure 2.6. The synthesis of the ligands is straightforward and occurs with nearly quantitative yield without any need for purification. We next compared the activity of our ligand with traditional NHC and phosphine ligands (Table 2.1). For example, in the Suzuki coupling of cinnamyl alcohol with phenyl boronic ester (**1**), IPrHCl (1,3-bis(2,6-diisopropylphenyl)imidazolium chloride) or dppf (1,1'-bis-(diphenylphosphino)ferrocene) provided only 23% and 46% conversion to product **2**, respectively (Table 2.1, entries 1 and 2). Our mechanistic studies revealed that for IPrHCl and dppf , the reaction proceeds to the observed level over about 1 hour and then stops, indicating catalyst decomposition or deactivation. When bidentate ligands L1-L4 were utilized, conversion enhanced dramatically in all cases, with ligands L3 and L4 giving the highest conversion (Table 2.1, entries 3-6). Importantly, we made a significant observation with our

Table 2.1 Optimization studies

entry ^a	ligand	catalyst (mol%)	solvent	yield (%)
1 ^b	dppf	10	MeCN	46
2 ^c	IPrHCl	10	MeCN	23
3	L ₁	10	MeCN	68
4	L ₂	10	MeCN	70
5	L ₃	10	MeCN	72
6	L ₄	10	MeCN	73
7 ^d	L ₃	10	toluene	51
8	L ₃	10	dioxane	31
9	L ₃	10	DMF	78
10	L ₃	10	Ethanol	51
11 ^e	L ₃	10	MeCN	89
12 ^f	L ₃	5	MeCN	92
13 ^g	L ₃	2.5	MeCN	92
14 ^h	L ₃	1.25	MeCN	91
15 ⁱ	IPrHCl	10	MeCN	20

^aReactions run using 0.02 mmol [(TMEDA)Ni(*o*-tolyl)Cl], 0.02 mmol *t*-BuOK, 0.2 mmol allylic alcohol, 1.5 equiv boronic ester, and 2.0 equiv K₃PO₄ at 100 °C for 1.5 h unless otherwise noted. All reaction proceeded with >100:1 selectivity for the linear product, unless otherwise noted. ^bdppf = 1,1'-bis(diphenylphosphino)-ferrocene. ^cIPrHCl = 1,3-bis(2,6-diisopropylphenyl)imidazolium chloride. ^dBranched:linear ratio = 20:1. ^eRun for 3 h. ^fRun at 1 M in allylic alcohol for 10 h. ^gRun at 2.0 M for 10 h. ^hRun at 4.0 M for 10 h. ⁱPPh₃ (10 mol %) was added to the reaction.

bidentate ligands in comparison to traditional NHC and phosphine ligands. While the reaction decelerated with our ligands, it smoothly proceeded and went to completion over the indicated times. In continuing optimization studies, acetonitrile was found as the best solvent for the reaction (Table 2.1, entries 7–10). We also discovered that catalyst loading could be lowered

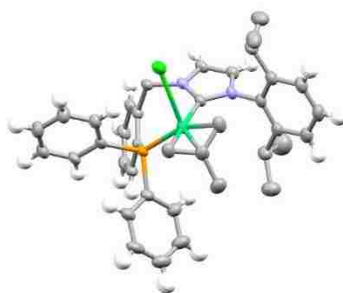


Figure 2.7 Crystal structure of allyl nickel complex

while maintaining high reaction yields. For example, with 1.25 mol % catalyst, 91% yield was obtained within just 10 h (Table 2.1, entries 11–14). Importantly, no progress in the reaction conversion was observed when IPrHCl and PPh₃ were used together in the reaction, indicating that the bidentate nature of the NHC phosphine ligand was necessary in order to observe enhanced catalyst stability in this case (Table 2.1, entry 15). In order to gain a better understanding of the structure of our nickel catalyst species, we grew X-ray-quality single crystals of a nickel (II) allyl species with ligand L₃. The crystal structure confirmed that the proposed nickel (II) allyl intermediate is cationic in nature with the phosphine bound to the nickel in a pseudo-square planar arrangement (Figure 2.7). This nickel(II) allyl intermediate presumably undergoes transmetalation with the phenylboronic ester, then reductive elimination to give the cross-coupled product. This structure clearly confirmed our previous assumption that the pendant phosphine stabilizes the nickel catalyst during the reaction. We believe that

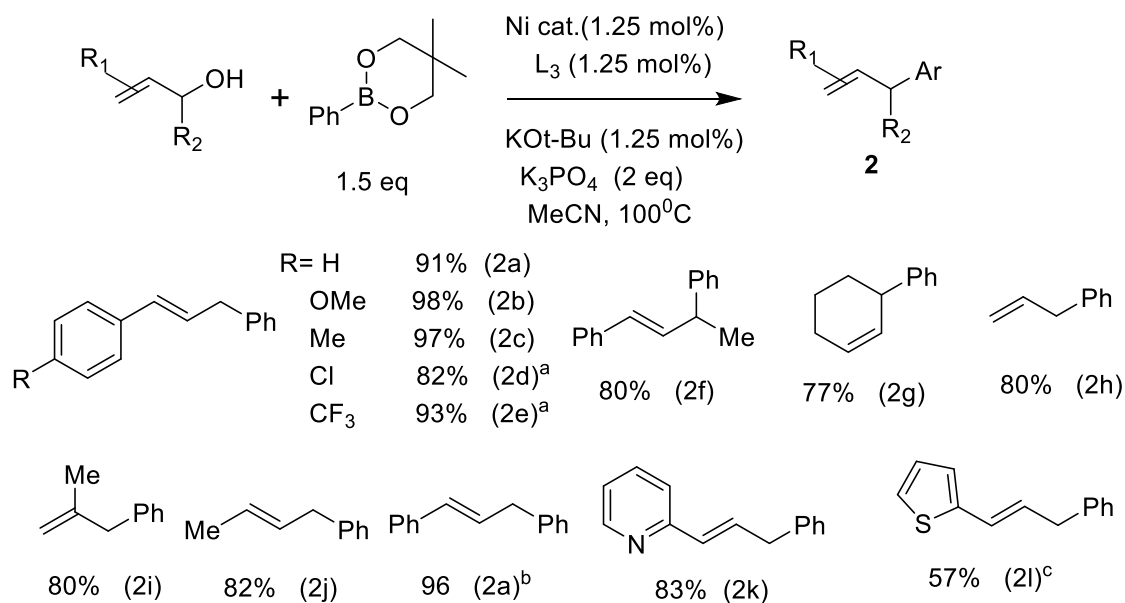


Figure 2.8 Substrate scope for allylic alcohol partner: (a) reaction run with 2.5 mol% Ni and 2.5 mol% L₃, (b) 1-propyl-2-propen-1-ol was used as starting material, and (c) reaction run with 5 mol% Ni and 5 mol% L₃.

the phosphine moiety prevents aggregation of the Ni (0) catalyst during the reaction, providing more Ni (0) for the oxidative addition step. Using our optimized reaction conditions, we next explored the substrate scope of the reaction employing different allylic alcohols (Figure 2.8).

A library of allylic alcohols including electron-deficient and electron-rich alcohols were tested under optimized conditions, providing products **2a-2e**. In each case, excellent yield was observed. Sterically more hindered secondary allylic alcohols reacted very well and gave good yields (**2f-2g**). Moreover, the regioselectivity was also high (>100:1) for addition of the phenyl at the terminal, less hindered end of the allyl moiety, providing the linear reaction product. The linear cross-coupling product **2a** was isolated as the only observed product (96% yield). Heterocycles such as pyridines (**2k**) and thiophenes (**2l**) are also tolerated in this reaction. These heterocyclic substrates are not tolerated under traditional palladium catalysis and the reported yield is very poor for the thiophene substrate¹⁰. Linear aliphatic allyl alcohols reacted perfectly and produced product with relatively high yields (**2h-2j**). When isomeric 1-phenyl-2-propen-1-ol was used instead of cinnamyl alcohol, the utility of our system was also tested for various boronic ester coupling partners (Figure 2.9). All substituents including electron-donating and

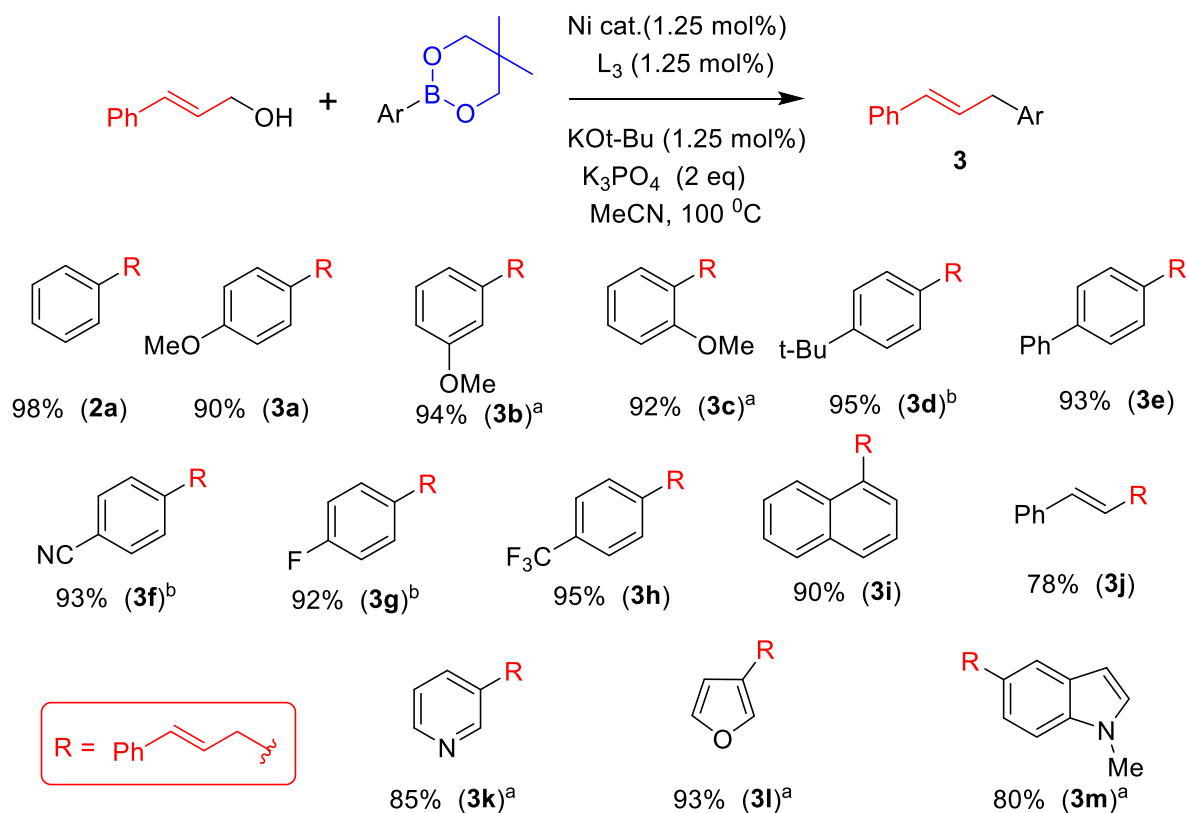


Figure 2.9 Substrate scope for boronic ester coupling partner: (a) reaction run with 2.5 mol% Ni and 2.5 mol% L_3 , (b) reaction run with 5mol% Ni and 5mol% L_3 .

electron-withdrawing groups at different positions on the phenyl ring were compatible with the reaction conditions (**3a-3h**). Aryl and alkenyl boronic acids were also acceptable of the reaction conditions (**3i-3j**). Importantly, a variety of heterocyclic boronic esters including pyridine (**3k**), furan (**3l**), and indole (**3m**) substrates performed very well and gave the cross coupling product in high yield and regioselectivity.

As a synthetic application of our new nickel catalyst system, we performed a tandem cyclization/arylation reaction using allylic alcohol substrates containing a pendant alkyne group (Figure 2.10). To our surprise, with our bidentate ligands the catalysis was slow and led to only modest yield. However, with the traditional IPrHCl ligand, the yield and the reaction rate increased dramatically. We assume that the pendant alkyne stabilizes the nickel (0) specie in the solution in the same manner as the pendant phosphine in the ligand does. However, using a bidentate ligand would prevent coordination of the alkyne to the nickel and hampers the insertion of alkyne into the allyl intermediate. We found that a variety of substrates including N-tosyl amine (**4a** and **4b**), malonate (**4c**), and ether (**4d**) tethered substrates worked efficiently and gave the product in high yield.

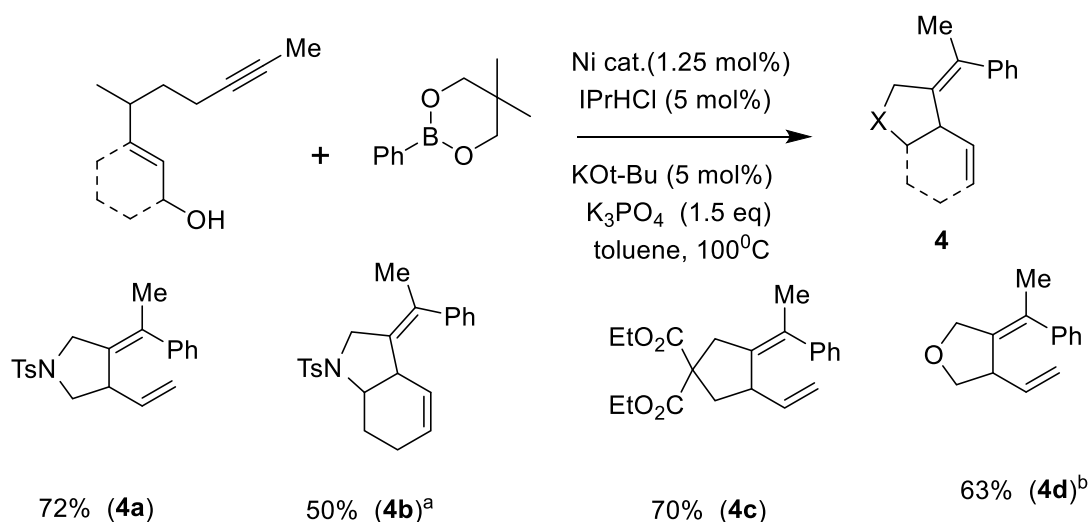


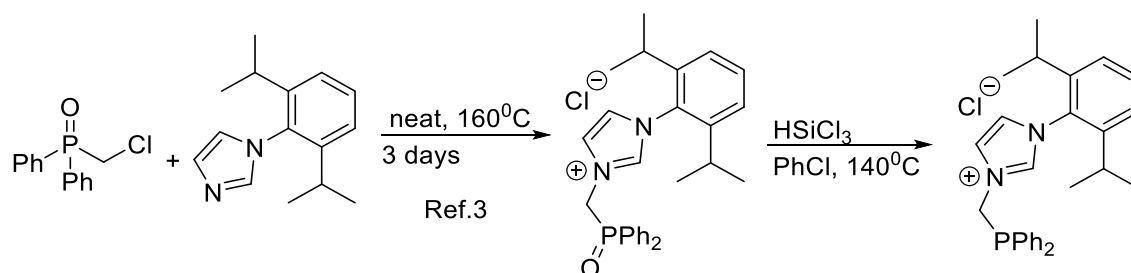
Figure 2.10 Tandem cyclization/cross coupling reaction: (a) run with Ni(COD)₂ and (b) ligand L₂ was employed in MeCN

2.3.2 Experimental data and supporting information for Nickel-catalyzed Suzuki cross-couplings with unprotected allylic alcohols enabled by bidentate N-heterocyclic carbene (NHC)/phosphine ligands

2.3.2.1 General information

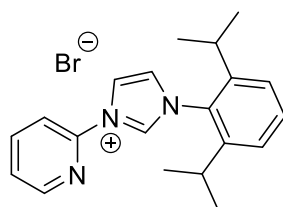
All reactions were carried out under an atmosphere of nitrogen or argon in oven-dried glassware with magnetic stirring, unless otherwise indicated. Solvents were dried by J. C. Meyer's Solvent Purification System. The nickel pre catalyst and the ligands were prepared by literature procedures¹⁻⁶ or as described below. All other reagents were used as obtained unless otherwise noted. Flash Chromatography was performed with EM Science silica gel (0.040-0.063 μm grade). Analytical thin-layer chromatography was performed with 0.25 mm coated commercial silica gel plates (E. Merck, DC-Plastikfolien, kieselgel 60 F254). Proton nuclear magnetic resonance (¹H-NMR) data were acquired on a Mercury 400 (400 MHz) or on a Varian Unity Inova-500 (500 MHz) spectrometer. Chemical shifts are reported in delta (δ) units, in parts per million (ppm) downfield from tetramethylsilane or from DMSO (2.54 ppm). Splitting patterns are designated as s, singlet; d, doublet; t, triplet; q, quartet; p, pentet; m, multiplet, br, broad. Carbon-13 nuclear magnetic resonance (¹³C-NMR) data were acquired at 100 MHz on a Mercury 400 or at 125 MHz on a Varian Unity Inova 500 spectrometer. Chemical shifts are reported in ppm relative to the center line of a triplet at 77.23 ppm for chloroform-*d* or from the center line of DMSO-*d* 40.45 ppm. Infrared (IR) data were recorded as films on sodium chloride plates on a Thermo Scientific Nicolet IR100 FT-IR spectrometer. Absorbance frequencies are reported in reciprocal centimeters (cm^{-1}). Chiral HPLC analyses were performed on a Thermo Separation Products Spectra Series P-100 or 200 and UV100 (254 nm) using Chiralcel[®] columns (OD-H, OB-H, OJ, AD, AS, OC, IA, IB or IC) eluting with heptane / *iso*-propanol mixtures indicated. Optical rotations were measured on a Jasco P-2000 digital polarimeter using 5 cm cells and the sodium D line (589 nm) at ambient temperature in the solvent and concentration indicated. Gas Chromatograms were obtained on a Hewitt Packard 6890 series GC system.

2.4 Synthesis of Ligands



1-(2,6-diisopropylphenyl)-3-((diphenylphosphaneyl)methyl)-1H-imidazol-3-ium chloride

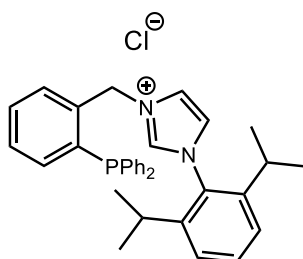
(L₁): Into a 20 mL dram vial were placed (chloromethyl)diphenylphosphine oxide (2.5 g, 10 mmol, 1 eq), 1-(2,6-diisopropylphenyl)-1H-imidazole² (2.75 g, 12 mmol, 1.2 eq), and a stir bar. The vial was sealed with a Teflon cap and heated to 160°C for 48 hrs in an oil bath. Trituration with ether and filtration gave the pure product (4.1 g, 86%). 1-(2,6-diisopropylphenyl)-3-((diphenylphosphoryl)methyl)-1H-imidazol-3-ium chloride (2.4 g, 5.01 mmol, 1 eq) and trichlorosilane (3.05 ml, 30.06 mmol, 6 eq) were added into a sealed reactor tube containing chlorobenzene (80 ml). The tube was sealed and heated to 120 °C for 3 hours. Degassed water was added and the aqueous was extracted with degassed DCM three times. Evaporation of the solvent and trituration with pentane gave the pure product as a white solid (1.8 g, 78%). ¹H NMR (500 MHz, CDCl₃) δ 10.73 (s, 1H), 7.74-7.86 (m, 3H), 7.39-7.57 (m, 8H), 7.23-7.32 (m, 4H), 7.00 (m, 1H), 5.84 (d, *J* = 6.33 Hz, 2H), 2.05 (sep, *J* = 6.95 Hz, 2H), 1.14 (d, *J* = 6.79 Hz, 6H), 1.07 (d, *J* = 6.79 Hz, 6H); ¹³C NMR (75 MHz, CDCl₃) δ 148.7, 145.17, 141.20, 135.58, 132.30, 130.04, 125.71, 125.15, 124.91, 121.0, 116.79, 4, 24.44, 24.13; ³¹P NMR (300 MHz, CDCl₃) δ -11.19; IR (film) ν_{max} 2911, 3402, 2964, 2361, 1189 cm⁻¹; HRMS(EI) calcd. for C₂₈H₃₂N₂P, [M+H]⁺; 428.2376, found 428.2371.



1-(2,6-diisopropylphenyl)-3-(pyridin-2-yl)-1H-imidazol-3-ium bromide (L₂):

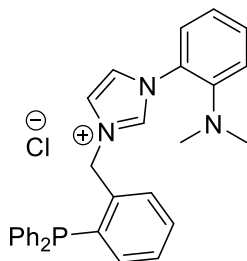
Into a 20 mL dram vial were placed 2-bromo pyridine (1.58 g, 10 mmol, 1 eq), 1-(2,6-diisopropylphenyl)-1H-imidazole² (2.75 g, 12 mmol, 1.2 eq), and a stir bar. The vial was sealed with a Teflon cap and heated to 150 °C for 12 hrs in an oil bath. Trituration with ether and filtration gave the pure product (3.65 g, 95%). ¹H NMR (500 MHz, CDCl₃) δ 11.05 (s, 1H), 9.32-9.4 (m, 2H),

8.53 (dd, $J = 1.36, 4.75$ Hz, 1H), 8.15 (dt, $J = 2.18, 7.81$ Hz, 1H), 7.59 (t, $J = 7.93$ Hz, 1H), 7.52 (dd, $J = 4.8, 7.46$ Hz, 1H), 7.33-7.4 (m, 3H), 2.43 (sep, $J = 7.14$ Hz, 2H), 1.3 (d, $J = 6.82$ Hz, 6H), 1.19 (d, $J = 6.82$ Hz, 6H); ^{13}C NMR (75 MHz, CDCl_3) δ 148.7, 145.17, 141.20, 135.58, 132.30, 130.04, 125.71, 125.15, 124.91, 121.0, 116.79, 49.3, 28.94, 24.44 ; IR (film) ν_{max} 2911, 3413, 2964, 2927, 2869, 1599, 1475 Cm^{-1} ; HRMS(EI) calcd. for $\text{C}_{20}\text{H}_{24}\text{N}_3$, $[\text{M}+\text{H}]^+$, 307.2043; found, 307.2046.



1-(2,6-diisopropylphenyl)-3-(2-(diphenylphosphaneyl)benzyl)-1H-imidazol-3-ium (L₃):

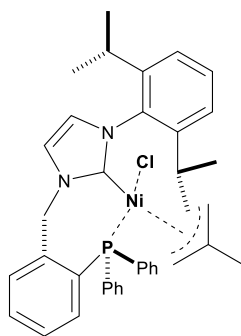
Inside a glove box and in a 10 ml dram vial were placed (2-(chloromethyl)phenyl)diphenylphosphane (310 mg, 1 mmol, 1 eq) and 1-(2,6-diisopropylphenyl)-1H-imidazole (300 mg, 1.3 mmol, 1.3 eq). The mixture was stirred at 120 $^{\circ}\text{C}$ for 3 hrs. Cooled down to room temperature and triturated with ether 5 times. The white solid was filtered and dried on the high vacuum to get the pure product (500 mg, 92%). ^1H NMR (500 MHz, CDCl_3) δ 10.91 (s, 1H), 8.11-8.19 (m, 1H), 7.74 (s, 1H), 7.16-7.59 (m, 16H), 6.98 (m, 2H), 6.27 (s, 2H), 2.26 (sep, $J = 6.86$ Hz, 2H), 1.23 (d, $J = 6.77$ Hz, 6H), 1.10 (d, $J = 6.77$ Hz, 6H); ^{13}C NMR (75 MHz, CDCl_3) δ 148.7, 145.44, 139.28, 133.97, 131.84, 130.69, 130.28, 129.87, 129.51, 129.00, 124.65, 123.52, 122.51, 69.87, 28.73, 24.38, 24.14 ; ^{31}P NMR (300 MHz, CDCl_3) δ -15.41; IR (film) ν_{max} 2911, 3416, 2964, 2359, 1652, 1558, 1456 Cm^{-1} ; HRMS(EI) calcd. for $\text{C}_{34}\text{H}_{36}\text{N}_2\text{P}$, $[\text{M}+\text{H}]^+$, 504.2689; found, 504.2682.



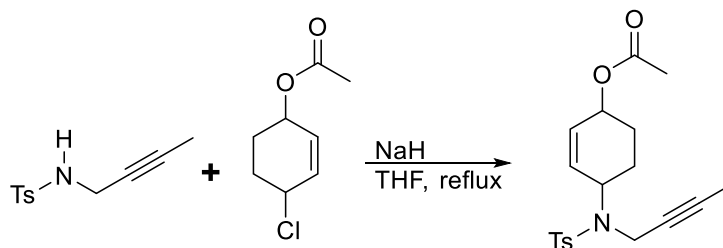
1-(2-(dimethylamino)phenyl)-3-(2-(diphenylphosphaneyl)benzyl)-1H-imidazol-3-ium (L₄):

inside a glove box and Into a 20 ml dram vial were placed (2-(chloromethyl)phenyl)diphenylphosphane⁴ (547 mg, 1.76 mmol, 1 eq), 2-(1H-imidazol-1-yl)-N,N-dimethylaniline⁵ (380 mg, 2 mmol, 1.15 eq), and a stir bar. The vial was sealed with a

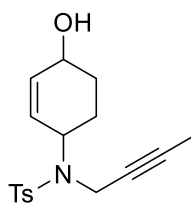
Teflon cap and heated to 120⁰C for 4 hrs. Trituration with ether and filtration gave the pure product (750 mg, 92%). ¹H NMR (500 MHz, CDCl₃) δ 10.85 (s, 1H), 8.12-8.17 (m, 1H), 7.55-7.6 (m, 1H), 7.45-7.49 (m, 2H), 7.40 (d, *J* = 7.85 Hz, 2H), 7.28-7.38 (m, 8H), 7.19-7.25 (m, 5H), 7.14 (dd, *J* = 8.22, 15.61 Hz, 2H), 6.95-7.0 (m, 1H), 6.15 (s, 2H), 2.49 (s, 6H); ¹³C NMR (75 MHz, CDCl₃) δ 138.10, 137.88, 137.71, 134.93, 134.32, 133.86, 133.69, 132.26, 131.28, 130.67, 129.89, 129.41, 128.97, 128.91, 127.25, 126.53, 123.56, 122.05, 121.88, 120.36, 69.92, 43.06; ³¹P NMR (300 MHz, CDCl₃) δ -15.97; IR (film) ν_{max} 2911, 3402, 3053, 1453, 1187 Cm⁻¹; HRMS(EI) calcd. for C₃₀H₂₉N₃P, [M+H]⁺, 463.2172; found, 463.2175.



Synthesis of nickel methallyl complex: to a solution of 1-(2,6-diisopropylphenyl)-3-(2-(diphenylphosphaneyl)benzyl)-1H-imidazol-3-ium (270 mg, 0.5 mmol) in THF (5 ml) was added sodium t-butoxide (61 mg, 0.65 mmol) at room temperature. After stirring for 6 hours at room temperature, the solvent was distilled off, and the crude solid was dissolved in benzene and passed through celite. Evaporation of the solvent gave the pure product as a puffy white solid (226 mg, 90%). A solution of 3-(2,6-diisopropylphenyl)-1-(2-(diphenylphosphaneyl)benzyl)-1H-imidazol-3-ium-2-ide (250 mg, 0.5 mmol) in toluene (2 ml) was added drop wise to a solution of methallylnickel chloride dimer (75 mg, 0.25 mmol of dimer) in toluene (3 ml). The reaction mixture stirred for 2 hours at room temperature and the solvent evaporated off. The solid was dissolved in benzene/Hexane (V:V, 2:11) and passed through celite. Evaporation of the solvent gave the product as red solid (260 mg, 80%). Crystals suitable for crystallography was prepared by dissolving the solid in benzene/Hexane (V:V, 2:11) and cooling the liquid to -40 ⁰C. the hexane layer on top was separated from the bottom layer of the frozen benzene. Slow evaporation of the hexane at room temperature gave needle type crystals.

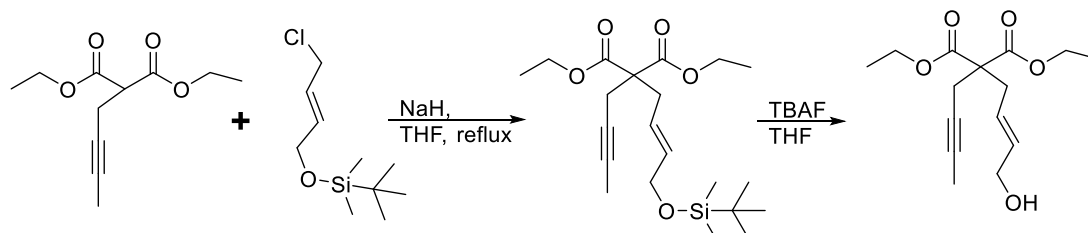


4-((N-(but-2-yn-1-yl)-4-methylphenyl)sulfonamido)cyclohex-2-en-1-yl acetate : In a flame dried round bottom flask equipped with stir bar were added THF (80 ml), N-(but-2-yn-1-yl)-4-methylbenzenesulfonamide (2 g, 8.95 mmol, 1 eq) at room temperature. The reaction mixture stirred for 1 hour. A solution of 4-chlorocyclohex-2-en-1-yl acetate (1.56 g, 8.95 mmol, 1 eq) in DMF (30 ml) was added and the reaction was heated to 90 °C for 14 hours under argon. After cooling down to room temperature, Water (80 ml) was added and the mixture was extracted with DCM three times. The combined organics were dried, concentrated, and purified on column using EtOAc/Hex (10%) giving the pure product as colorless liquid (2.5 g, 77%). ¹H NMR (500 MHz, CDCl₃) δ 7.79 (d, *J* = 4.26 Hz, 2H), 7.26-7.31 (m, 2H), 5.76(d, *J* = 5.09 Hz, 1H), 5.50 (d, *J* = 5.50 Hz, 2H), 5.30 (s, 2H), 4.54-4.61 (m, 1H), 4.04 (dd, *J* = 8.05, 1.19 Hz, 1H), 3.83 (dd, *J* = 9.66, 1.14 Hz, 1H), 2.43 (s, 3H), 2.10-2.19 (m, 1H), 2.04 (s, 3H), 1.87-1.93 (m, 2H), 1.67-1.70 (m, 3H), 1.65-1.54 (m, 2H) ; ¹³C NMR (75 MHz, CDCl₃) δ 170.82, 143.41, 138.12, 132.19, 131.22, 129.46, 127.54, 80.57, 75.28, 68.87, 54.76, 33.44, 28.31, 26.55, 21.74, 21.26, 3.63; IR (film)vmax 2911, 3582, 1730, 1240, 1160 Cm⁻¹; HRMS(EI) calcd. for C₁₉H₂₃NO₄S, [M+NH₄]⁺, 379.1692; found, 379.1696.



N-(but-2-yn-1-yl)-N-(4-hydroxycyclohex-2-en-1-yl)-4-methylbenzenesulfonamide : In a flame dried round bottom flask equipped with stir bar were placed dry THF (10 ml), 4-((N-(but-2-yn-1-yl)-4-methylphenyl)sulfonamido)cyclohex-2-en-1-yl acetate (1.2 g, 3.32 mmol, 1 eq), potassium carbonate (1.4 g, 10 mmol, 3 eq), and methanol (10 ml). The reaction stirred for 24 hours and the solid was filtered off. Concentration of the liquid and purification on column (EtOAc/Hex: 10% to 45%) gave the product as a thick liquid (950 mg, 90%). ¹H NMR (500 MHz, CDCl₃) δ 7.8 (d, *J* = 3.94 Hz, 2H), 7.26-7.32 (m, 2H), 5.84 (d, *J* = 5.04 Hz, 1H), 5.38-

5.45 (m, 1H), 4.54 (s, 1H), 4.27 (s, 1H), 3.98-4.08 (m, 1H), 3.8-3.88 (m, 1H), 2.43 (s, 3H), 2.10-2.19 (m, 1H), 1.77-1.94 (m, 2H), 1.68 (s, 3H), 1.37-1.64 (m, 3H); ^{13}C NMR (125 MHz, CDCl_3) δ 143.20, 136.26, 129.53, 127.58, 80.27, 75.28, 66.60, 54.88, 33.40, 32.53, 26.89, 21.68, 3.67; IR (film) ν_{max} 2911, 3744, 3503, 2919, 1995, 1332, 1158 cm^{-1} ; HRMS(EI) calcd. for $\text{C}_{17}\text{H}_{21}\text{NO}_3\text{S}$, $[\text{M}+\text{H}]^+$, 320.1320; found, 320.1326.

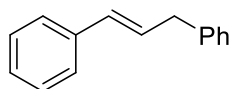


diethyl (E)-2-(but-2-yn-1-yl)-2-(4-hydroxybut-2-en-1-yl)malonate : in a round bottom flask were placed dry THF (80 ml) and diethyl 2-(but-2-yn-1-yl)malonate (1.27 g, 6 mmol, 1 eq). NaH (405 mg, 10.13 mmol, 60% dispersion in mineral oil) was added at room temperature and the reaction mixture stirred for 40 minute. (E)-tert-butyl((4-chlorobut-2-en-1-yl)oxy)dimethylsilane (1.32 g, 6 mmol, 1 eq) and tetrabutyl ammonium iodide (220 mg, 0.6 mmol, 0.1 eq) were added and reaction was refluxed for 10 hours. After cooling to room temperature, EtOAc and water (50 ml) were added and the aqueous was extracted with EtOAc, dried on sodium sulfate and concentrated. Purification on silica gel column with EtOAc/Hex gave the product which was taken to the next step (1.95 g, 81%).

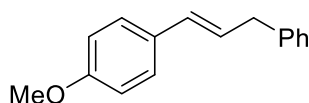
To a solution of the product (1.7 g, 4.3 mmol, 1 eq) in THF (30ml) was added tetra butyl ammonium fluoride hydrate (2.3 g, 8.6 mmol, 3 eq) at 0 $^{\circ}\text{C}$. The reaction mixture was stirred at room temperature overnight and diluted with EtOAc (50 ml) and water (30 ml). The aqueous was extracted with EtOAc three times, and the combined organics were dried on sodium sulfate and concentrated on vacuum. Purification on silica gel column using EtOAc/Hex (10%to 20%) as eluent gave the pure product as a yellowish liquid (650 mg, 60%). ^1H NMR (300 MHz, CDCl_3) δ 5.75-5.87 (m, 1H), 5.29-5.42 (m, 1H), 4.11-4.29 (m, 6H), 2.84 (d, J = 8.31 Hz, 2H), 2.67-2.77 (m, 2H), 1.77 (t, J = 2.49 Hz, 3H), 1.53-1.65 (m, 1H), 1.25 (t, J = 7.15 Hz, 6H); ^{13}C NMR (75 MHz, CDCl_3) δ 170.06, 133, 125.86, 79.4, 73.5, 61.84, 58.21, 57, 30.06, 22.95, 14.92, 3.47; IR (film) ν_{max} 2911, 3453, 2983, 1995, 1765 cm^{-1} ; HRMS(EI) calcd. for $\text{C}_{15}\text{H}_{22}\text{O}_5$, $[\text{M}+\text{H}]^+$, 283.1545; found, 283.1549.

General experimental procedure for nickel-catalyzed cross-coupling of allylic alcohols: Into a 3 mL dram vial containing stir bar were placed nickel pre catalyst (0.0125 eq), Ligand (0.0125 eq), and KOtBu (0.015 eq). Solvent (300 μL) was added and the mixture was stirred

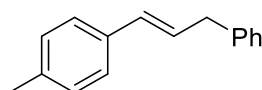
at room temperature for 15 min. Allyl alcohol (1 eq), phenyl boronic ester (1.5 eq), and K_3PO_4 (1.5 eq) were added and the vial was sealed by a Teflon cap. The reaction mixture was heated to 100 °C for 10 hours. The solvent was evaporated and the crude mixture was purified on column using pure hexane to 1% EtOAc/Hex as eluent.



(E)-prop-1-ene-1,3-diylidibenzene(2a): prepared following the general procedure using cinnamyl alcohol (54 mg, 0.4 mmol, 1 eq), 5,5-dimethyl-2-phenyl-1,3,2-dioxaborinane (108 mg, 0.6 mmol, 1.5 eq), potassium phosphate (128 mg, 0.6 mmol, 1.5 eq), nickel catalyst (1.5 mg, 0.005 mmol, 0.0125 eq), Ligand L_3 (3 mg, 0.005 mmol, 0.0125 eq), and potassium t-butoxide (1 mg, 0.008 mmol, 0.02 eq) in 200 μ l of acetonitrile. Product was purified on column using pure hexane to 1% EtOAc/Hex as eluent (72 mg, 93%). Spectral data are in accordance with the reported values³³.

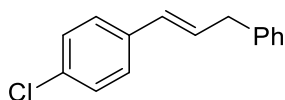


(E)-1-methoxy-4-(3-phenylprop-1-en-1-yl)benzene (2b): prepared following the general procedure using 4-methoxy cinnamyl alcohol (66 mg, 0.4 mmol, 1 eq), 5,5-dimethyl-2-phenyl-1,3,2-dioxaborinane (108 mg, 0.6 mmol, 1.5 eq), potassium phosphate (128 mg, 0.6 mmol, 1.5 eq), nickel catalyst (1.5 mg, 0.005 mmol, 0.0125 eq), Ligand L_3 (3 mg, 0.005 mmol, 0.0125 eq), and potassium t-butoxide (1 mg, 0.008 mmol, 0.02 eq) in 200 μ l of acetonitrile. Product was purified on column using pure hexane to 1% EtOAc/Hex as eluent (88 mg, 98%). Spectral data are in accordance with the reported values³⁴.

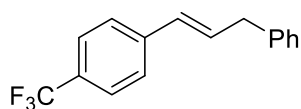


(E)-1-methyl-4-(3-phenylprop-1-en-1-yl)benzene (2c): prepared following the general procedure using 4-methyl cinnamyl alcohol (60 mg, 0.4 mmol, 1 eq), 5,5-dimethyl-2-phenyl-1,3,2-dioxaborinane (108 mg, 0.6 mmol, 1.5 eq), potassium phosphate (128 mg, 0.6 mmol, 1.5

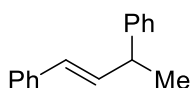
eq), nickel catalyst(1.5 mg, 0.005 mmol, 0.0125 eq), Ligand L₃ (3 mg, 0.005 mmol, 0.0125 eq), and potassium t-butoxide (1 mg, 0.008 mmol, 0.02 eq) in 200 μ l of acetonitrile. Product was purified on column using pure hexane to 1% EtOAc/Hex as eluent (81 mg, 97%). Spectral data are in accordance with the reported values³⁴.



(E)-1-chloro-4-(3-phenylprop-1-en-1-yl)benzene (2d): prepared following the general procedure using (E)-3-(4-chlorophenyl)prop-2-en-1-ol (67.5 mg, 0.4 mmol, 1 eq), 5,5-dimethyl-2-phenyl-1,3,2-dioxaborinane (108 mg, 0.6 mmol, 1.5 eq), potassium phosphate(128 mg, 0.6 mmol, 1.5 eq), nickel catalyst (3 mg, 0.01 mmol, 0.025 eq), Ligand L₃ (6 mg, 0.01 mmol, 0.025 eq), and potassium t-butoxide (2 mg, 0.016 mmol, 0.03 eq) in 200 μ l of acetonitrile. Product was purified on column using pure hexane to 1% EtOAc/Hex as eluent (73 mg, 82%). Spectral data are in accordance with the reported values³⁵.

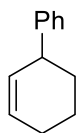


(E)-1-(3-phenylprop-1-en-1-yl)-4-(trifluoromethyl)benzene (2e): prepared following the general procedure using (E)-3-(4-(trifluoromethyl)phenyl)prop-2-en-1-ol (81 mg, 0.4 mmol, 1 eq), 5,5-dimethyl-2-phenyl-1,3,2-dioxaborinane (108 mg, 0.6 mmol, 1.5 eq), potassium phosphate (128 mg, 0.6 mmol, 1.5 eq), nickel catalyst (3 mg, 0.01 mmol, 0.025 eq), ligand L₃ (6 mg, 0.01 mmol, 0.025 eq), and potassium t-butoxide (2 mg, 0.016 mmol, 0.03 eq) in 200 μ l of acetonitrile. Product was purified on column using pure hexane to 1% EtOAc/Hex as eluent (97.5mg, 93%). Spectral data are in accordance with the reported values³⁵.

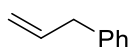


(E)-but-1-ene-1,3-diyl dibenzene (2f): prepared following the general procedure using (E)-4-phenylbut-3-en-2-ol (59.5 mg, 0.4 mmol, 1 eq), 5,5-dimethyl-2-phenyl-1,3,2-dioxaborinane (108 mg, 0.6 mmol, 1.5 eq), potassium phosphate (128 mg, 0.6 mmol, 1.5 eq), nickel catalyst

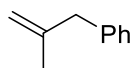
(1.5 mg, 0.005 mmol, 0.0125 eq), ligand L₃ (3 mg, 0.005 mmol, 0.0125 eq), and potassium t-butoxide (1 mg, 0.008 mmol, 0.02 eq) in 200 μ l of acetonitrile. Product was purified on column using pure hexane to 1% EtOAc/Hex as eluent (66 mg, 80%). Spectral data are in accordance with the reported values³⁴.



1,2,3,4-tetrahydro-1,1'-biphenyl (2g): prepared following the general procedure using cyclohex-2-en-1-ol (39.5 mg, 0.4 mmol, 1 eq), 5,5-dimethyl-2-phenyl-1,3,2-dioxaborinane (108 mg, 0.6 mmol, 1.5 eq), potassium phosphate (128 mg, 0.6 mmol, 1.5 eq), nickel catalyst (1.5 mg, 0.005 mmol, 0.0125 eq), Ligand L₃ (3 mg, 0.005 mmol, 0.0125 eq), and potassium t-butoxide (1 mg, 0.008 mmol, 0.02 eq) in 200 μ l of acetonitrile. Product was purified on column using pure Hexane to 1% EtOAc/Hex as eluent (47 mg, 74%). Spectral data are in accordance with the reported values³⁴.

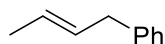


Allylbenzene (2h): prepared following the general procedure using allyl alcohol (23.5 mg, 0.4 mmol, 1 eq), 5,5-dimethyl-2-phenyl-1,3,2-dioxaborinane (108 mg, 0.6 mmol, 1.5 eq), potassium phosphate (128 mg, 0.6 mmol, 1.5 eq), nickel catalyst (1.5 mg, 0.005 mmol, 0.0125 eq), Ligand L₃ (3 mg, 0.005 mmol, 0.0125 eq), and potassium t-butoxide (1 mg, 0.008 mmol, 0.02 eq) in 200 μ l of acetonitrile. Product was purified on column using pure pentane to 1% EtOAc/pent as eluent (38 mg, 80%). Spectral data are in accordance with the reported values³⁶.

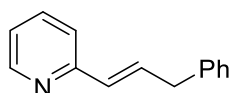


(2-methylallyl)benzene (2i): prepared following the general procedure using methallyl alcohol (29 mg, 0.4 mmol, 1 eq), 5,5-dimethyl-2-phenyl-1,3,2-dioxaborinane (108 mg, 0.6 mmol, 1.5 eq), potassium phosphate (128 mg, 0.6 mmol, 1.5 eq), nickel catalyst (1.5 mg, 0.005 mmol, 0.0125 eq), Ligand L₃ (3 mg, 0.005 mmol, 0.0125 eq), and potassium t-butoxide (1 mg, 0.008 mmol, 0.02 eq) in 200 μ l of acetonitrile. Product was purified on column using pure

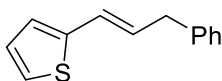
pentane to 1% EtOAc/pent as eluent (42 mg, 80%). Spectral data are in accordance with the reported values³⁶.



(E)-but-2-en-1-ylbenzene (2j): prepared following the general procedure using (E)-but-2-en-1-ol (29 mg, 0.4 mmol, 1 eq), 5,5-dimethyl-2-phenyl-1,3,2-dioxaborinane (108 mg, 0.6 mmol, 1.5 eq), potassium phosphate (128 mg, 0.6 mmol, 1.5 eq), nickel catalyst (1.5 mg, 0.005 mmol, 0.0125 eq), Ligand L₃ (3 mg, 0.005 mmol, 0.0125 eq), and potassium t-butoxide (1 mg, 0.008 mmol, 0.02 eq) in 200 μ l of acetonitrile. Product was purified on column using pure pentane to 1% EtOAc/pent as eluent (43 mg, 82%). Spectral data are in accordance with the reported values³⁷.

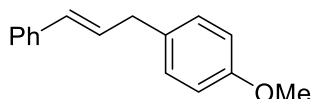


(E)-2-(3-phenylprop-1-en-1-yl)pyridine (2k): prepared following the general procedure using (E)-3-(pyridin-2-yl)prop-2-en-1-ol (54 mg, 0.4 mmol, 1 eq), 5,5-dimethyl-2-phenyl-1,3,2-dioxaborinane (108 mg, 0.6 mmol, 1.5 eq), potassium phosphate (128 mg, 0.6 mmol, 1.5 eq), nickel catalyst (3 mg, 0.01 mmol, 0.025 eq), Ligand L₃ (6 mg, 0.01 mmol, 0.025 eq), and potassium t-butoxide (2 mg, 0.016 mmol, 0.03 eq) in 200 μ l of acetonitrile. Product was purified on column using pure hexane to 1% EtOAc/Hex as eluent (65 mg, 83%). ¹H NMR (500 MHz, CDCl₃) δ 8.53 (d, *J* = 2.56 Hz, 1H), 7.61 (td, *J* = 0.98, 7.79 Hz 1H), 7.21-7.34 (m, 5H), 7.09-7.14 (m, 1H), 6.83-6.95 (m, 2H), 6.52-6.58 (m, 1H), 3.61 (d, *J* = 3.42 Hz, 2H), ; ¹³C NMR (125 MHz, CDCl₃) δ 149.46, 139.54, 136.57, 134.30, 131.04, 129.63, 128.92, 128.64, 126.37, 121.84, 121.13, 115.46, 39.26, 29.77; IR (film) ν_{max} 2911, 2100, 1277, 1117, 1044, 739, 698 cm^{-1} ; HRMS(EI) calcd. for C₁₄H₁₃N, [M+H]⁺, 196.1126; found, 196.1122.

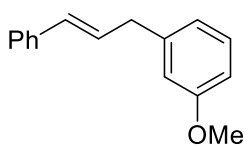


(E)-2-(3-phenylprop-1-en-1-yl)thiophene (2l): prepared following the general procedure using (E)-3-(thiophen-2-yl)prop-2-en-1-ol (56 mg, 0.4 mmol, 1 eq), 5,5-dimethyl-2-phenyl-

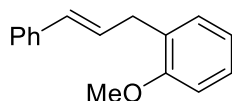
1,3,2-dioxaborinane (108 mg, 0.6 mmol, 1.5 eq), potassium phosphate (128 mg, 0.6 mmol, 1.5 eq), nickel catalyst (6 mg, 0.02 mmol, 0.05 eq), Ligand L₃ (12 mg, 0.02 mmol, 0.05 eq), and potassium t-butoxide (4 mg, 0.032 mmol, 0.06 eq) in 200 μ l of acetonitrile. Product was purified on column using pure hexane to 1% EtOAc/Hex as eluent (45 mg, 56%). Spectral data are in accordance with the reported values³⁴.



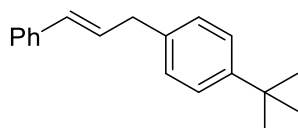
1-cinnamyl-4-methoxybenzene (3a): prepared following the general procedure using cinnamyl alcohol (54 mg, 0.4 mmol, 1 eq), 2-(4-methoxyphenyl)-5,5-dimethyl-1,3,2-dioxaborinane (132 mg, 0.6 mmol, 1.5 eq), potassium phosphate (128 mg, 0.6 mmol, 1.5 eq), nickel catalyst (1.5 mg, 0.005 mmol, 0.0125 eq), Ligand L₃ (3 mg, 0.005 mmol, 0.0125 eq), and potassium t-butoxide (1 mg, 0.008 mmol, 0.02 eq) in 200 μ l of acetonitrile. Product was purified on column using pure hexane to 2% EtOAc/Hex as eluent (80 mg, 90%). ¹H NMR (500 MHz, CDCl₃) δ 7.36-7.41 (m, 2H) 7.32 (t, *J* = 7.54 Hz, 2H), 7.17-7.27 (m, 3H), 6.89 (d, *J* = 4.25 Hz, 2H), 6.44-6.49 (m, 1H), 6.34-6.42 (m, 1H), 3.82 (s, 3H), 3.52 (d, *J* = 3.32 Hz, 2H); ¹³C NMR (75 MHz, CDCl₃) δ 158.17, 137.57, 132.29, 130.86, 129.72, 128.58, 127.15, 126.15, 114.02, 55.53, 38.49; IR (film) ν_{max} 2911, 3025, 2927, 2833, 1511, 1245, 1036 Cm^{-1} ; HRMS(EI) calcd. for C₁₆H₁₆O, [M+H]⁺, 225.1279; found, 225.1273.



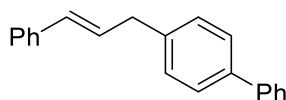
1-cinnamyl-3-methoxybenzene (3b): prepared following the general procedure using cinnamyl alcohol (54 mg, 0.4 mmol, 1 eq), 2-(3-methoxyphenyl)-5,5-dimethyl-1,3,2-dioxaborinane (132 mg, 0.6mmol, 1.5eq), potassium phosphate (128 mg, 0.6mmol, 1.5eq), nickel catalyst (3 mg, 0.01 mmol, 0.025eq), Ligand L₃ (3mg, 0.01 mmol, 0.025 eq), and potassium t-butoxide (2mg, 0.016 mmol, 0.03 eq) in 200 μ l of acetonitrile. Product was purified on column using pure hexane to 2% EtOAc/Hex as eluent (84mg, 94%). Spectral data are in accordance with the reported values³⁸.



1-cinnamyl-2-methoxybenzene (3c): prepared following the general procedure using cinnamyl alcohol (54 mg, 0.4 mmol, 1 eq), 2-(2-methoxyphenyl)-5,5-dimethyl-1,3,2-dioxaborinane (132 mg, 0.6 mmol, 1.5 eq), potassium phosphate (128 mg, 0.6 mmol, 1.5 eq), nickel catalyst (3 mg, 0.01 mmol, 0.025 eq), Ligand L₃ (3 mg, 0.01 mmol, 0.025 eq), and potassium t-butoxide (2 mg, 0.016 mmol, 0.03 eq) in 200 μ l of acetonitrile. Product was purified on column using pure hexane to 2% EtOAc/Hex as eluent (81 mg, 92%). ¹H NMR (500 MHz, CDCl₃) δ 7.34-7.4 (m, 2H), 7.26-7.33 (m, 2H), 7.18-7.26 (m, 3H), 6.87-6.97 (m, 2H), 6.36-6.50 (m, 2H), 3.87 (s, 3H), 3.56 (d, J = 3.01 Hz, 2H); ¹³C NMR (75 MHz, CDCl₃) δ 157.42, 137.80, 130.79, 129.93, 128.94, 128.70, 128.47, 127.45, 127.07, 126.92, 126.21, 120.62, 110.46, 55.49, 33.44; IR (film) ν_{max} 2911, 2918, 2348, 1995, 1598, 1498, 1240 Cm^{-1} ; HRMS(EI) calcd. for C₁₆H₁₆O, [M+H]⁺, 225.1279; found, 225.1276.

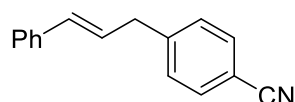


1-(tert-butyl)-4-cinnamylbenzene(3d): prepared following the general procedure using cinnamyl alcohol (54 mg, 0.4 mmol, 1 eq), 2-(4-(tert-butyl)phenyl)-5,5-dimethyl-1,3,2-dioxaborinane (147 mg, 0.6 mmol, 1.5 eq), potassium phosphate (128 mg, 0.6 mmol, 1.5 eq), nickel catalyst (6 mg, 0.02 mmol, 0.05eq), Ligand L₃ (12 mg, 0.02 mmol, 0.05 eq), and potassium t-butoxide (4 mg, 0.032 mmol, 0.06 eq) in 200 μ l of acetonitrile. Product was purified on column using pure hexane to 1% EtOAc/Hex as eluent (95 mg, 95%). Spectral data are in accordance with the reported values³⁹.

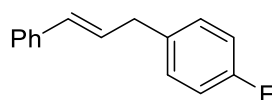


4-cinnamyl-1,1'-biphenyl(3e): prepared following the general procedure using cinnamyl alcohol (54 mg, 0.4 mmol, 1 eq), 2-([1,1'-biphenyl]-4-yl)-5,5-dimethyl-1,3,2-dioxaborinane (160 mg, 0.6mmol, 1.5eq), potassium phosphate (128 mg, 0.6 mmol, 1.5 eq), nickel catalyst (3 mg, 0.01 mmol, 0.025 eq), Ligand L₃ (3 mg, 0.01 mmol, 0.025 eq), and potassium t-butoxide

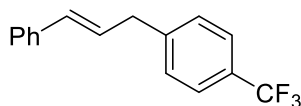
(2 mg, 0.016 mmol, 0.03 eq) in 200 μ l of acetonitrile. Product was purified on column using pure hexane to 2% EtOAc/Hex as eluent (100 mg, 93%). Spectral data are in accordance with the reported values³⁹.



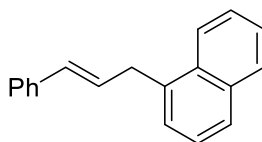
4-cinnamylbenzonitrile(3f): prepared following the general procedure using cinnamyl alcohol (54 mg, 0.4 mmol, 1 eq), 4-(5,5-dimethyl-1,3,2-dioxaborinan-2-yl)benzonitrile (130 mg, 0.6 mmol, 1.5 eq), potassium phosphate (128 mg, 0.6 mmol, 1.5 eq), nickel catalyst (3 mg, 0.01 mmol, 0.025 eq), Ligand L₃ (3 mg, 0.01 mmol, 0.025 eq), and potassium t-butoxide (2 mg, 0.016 mmol, 0.03 eq) in 200 μ l of acetonitrile. Product was purified on column using pure hexane to 2% EtOAc/Hex as eluent (81 mg, 93%). ¹H NMR (500 MHz, CDCl₃) δ 7.58-7.66 (m, 2H), 7.22-7.49 (m, 7H), 6.25-6.61 (m, 2H), 3.63 (t, *J* = 5.57 Hz, 2H); ¹³C NMR (125 MHz, CDCl₃) δ 145.87, 142.02, 139.31, 137.04, 133.76, 132.48, 129.49, 128.78, 127.64, 127.21, 126.64, 126.36, 119.09, 110.41, 39.49; IR (film) ν_{max} 2911, 3026, 2919, 2359, 1889, 1508, 1223 cm^{-1} ; HRMS(EI) calcd. for C₁₆H₁₃N, [M+H]⁺, 220.1126; found, 220.1122.



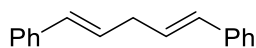
1-cinnamyl-4-fluorobenzene(3g): prepared following the general procedure using cinnamyl alcohol (54 mg, 0.4 mmol, 1 eq), 2-(4-fluorophenyl)-5,5-dimethyl-1,3,2-dioxaborinane (125 mg, 0.6 mmol, 1.5 eq), potassium phosphate (128 mg, 0.6 mmol, 1.5 eq), nickel catalyst (6 mg, 0.02 mmol, 0.05 eq), Ligand L₃ (12 mg, 0.02 mmol, 0.05 eq), and potassium t-butoxide (4 mg, 0.032 mmol, 0.06 eq) in 200 μ l of acetonitrile. Product was purified on column using pure hexane to 1% EtOAc/Hex as eluent (77 mg, 92%). ¹H NMR (500 MHz, CDCl₃) δ 7.32-7.45 (m, 4H), 7.20-7.32 (m, 3H), 6.98-7.10 (m, 2H), 6.26-6.54 (m, 2H), 3.58 (t, *J* = 6.75 Hz, 2H); ¹³C NMR (125 MHz, CDCl₃) δ 131.27, 130.14, 128.63, 127.63, 127.38, 126.24, 115.31, 39.42, 38.54; IR (film) ν_{max} 2911, 3026, 2918, 2361, 2225, 1603, 1506, 976 cm^{-1} ; HRMS(EI) calcd. for C₁₅H₁₃F, [M+H]⁺, 213.1080; found, 213.1084.



1-cinnamyl-4-(trifluoromethyl)benzene(3h): prepared following the general procedure using cinnamyl alcohol (54 mg, 0.4 mmol, 1 eq), 5,5-dimethyl-2-(4-(trifluoromethyl)phenyl)-1,3,2-dioxaborinane (155 mg, 0.6 mmol, 1.5 eq), potassium phosphate (128 mg, 0.6 mmol, 1.5 eq), nickel catalyst (6 mg, 0.02 mmol, 0.05 eq), Ligand L₃ (12 mg, 0.02 mmol, 0.05 eq), and potassium t-butoxide (4 mg, 0.032 mmol, 0.06 eq) in 200 μ l of acetonitrile. Product was purified on column using pure hexane to 2% EtOAc/Hex as eluent (99.5 mg, 95%). Spectral data are in accordance with the reported values⁴⁰.

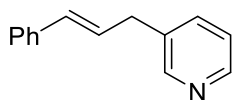


1-cinnamyl-naphthalene(3i): prepared following the general procedure using cinnamyl alcohol (54 mg, 0.4 mmol, 1 eq), 5,5-dimethyl-2-(naphthalen-1-yl)-1,3,2-dioxaborinane (145 mg, 0.6 mmol, 1.5 eq), potassium phosphate (128 mg, 0.6 mmol, 1.5 eq), nickel catalyst (1.5 mg, 0.005 mmol, 0.0125 eq), Ligand L₃ (3 mg, 0.005 mmol, 0.0125 eq), and potassium t-butoxide (1 mg, 0.008 mmol, 0.02 eq) in 200 μ l of acetonitrile. Product was purified on column using pure hexane to 2% EtOAc/Hex as eluent (88 mg, 90%). ¹H NMR (500 MHz, CDCl₃) δ 8.10-8.19 (m, 1H), 7.89-7.98 (m, 1H), 7.77-7.85 (m, 1H), 7.43-7.61 (m, 4H), 7.20-7.42 (m, 5H), 6.47-6.63 (m, 2H), 4.05 (d, J = 2.45 Hz, 2H); ¹³C NMR (125 MHz, CDCl₃) δ 137.55, 136.31, 133.94, 132.07, 131.45, 128.96, 128.59, 127.22, 126.47, 126.22, 125.72, 124.11, 36.58; IR (film) ν_{max} 2911, 3025, 2920, 2359, 1596, 1496, 1447 cm^{-1} ; HRMS(EI) calcd. for C₁₉H₁₆, [M+H]⁺, 245.1330; found, 245.1337.

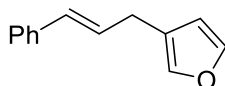


(1E,4E)-1,5-diphenylpenta-1,4-diene(3j): prepared following the general procedure using cinnamyl alcohol (54 mg, 0.4 mmol, 1 eq), (E)-5,5-dimethyl-2-styryl-1,3,2-dioxaborinane (130mg, 0.6 mmol, 1.5 eq), potassium phosphate (128 mg, 0.6 mmol, 1.5 eq), nickel catalyst (3 mg, 0.01 mmol, 0.025 eq), Ligand L₃ (3 mg, 0.01 mmol, 0.025 eq), and potassium t-butoxide (2 mg, 0.016 mmol, 0.03 eq) in 200 μ l of acetonitrile. Product was purified on column using

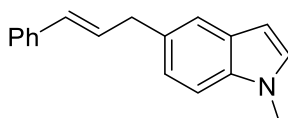
pure hexane to 2% EtOAc/Hex as eluent (68 mg, 78%). Spectral data are in accordance with the reported values⁴⁰.



3-cinnamylpyridine(3k): prepared following the general procedure using cinnamyl alcohol (54 mg, 0.4 mmol, 1 eq), 3-(5,5-dimethyl-1,3,2-dioxaborinan-2-yl)pyridine (115mg, 0.6mmol, 1.5eq), potassium phosphate (128 mg, 0.6mmol, 1.5eq), nickel catalyst (3 mg, 0.01 mmol, 0.025 eq), Ligand L₃ (3 mg, 0.01 mmol, 0.025 eq), and potassium t-butoxide (2 mg, 0.016 mmol, 0.03 eq) in 200 μ l of acetonitrile. Product was purified on column using pure hexane to 5% EtOAc/Hex as eluent (63 mg, 85%). ¹H NMR (500 MHz, CDCl₃) δ 8.44-8.55 (m, 2H), 7.56 (d, *J*=3.74 Hz, 1H), 7.33-7.38 (m, 2H), 7.26-7.33 (m, 2H), 7.19-7.26 (m, 2H), 6.47 (d, *J*= 8.59 Hz, 1H), 6.27-6.36 (m, 1H), 3.55 (d, *J* = 3.36 Hz, 2H) ; ¹³C NMR (500 MHz, CDCl₃) δ 137.13, 132.14, 128.66, 127.58, 126.28, 36.65; IR (film) ν_{max} 2911, 3431.04, 2358.93, 1643.30, 1422.07, 966.40 Cm^{-1} ; HRMS(EI) calcd. for C₁₄H₁₃N, [M+H]⁺, 196.1126; found, 196.1123.

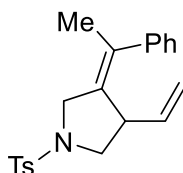


3-cinnamylfuran(3l): prepared following the general procedure using cinnamyl alcohol (54 mg, 0.4 mmol, 1 eq), 2-(furan-3-yl)-5,5-dimethyl-1,3,2-dioxaborinane (108 mg, 0.6 mmol, 1.5 eq), potassium phosphate (128 mg, 0.6 mmol, 1.5 eq), nickel catalyst (3 mg, 0.01 mmol, 0.025 eq), Ligand L₃ (3 mg, 0.01 mmol, 0.025 eq), and potassium t-butoxide (2 mg, 0.016 mmol, 0.03 eq) in 200 μ l of acetonitrile. Product was purified on column using pure hexane to 5% EtOAc/Hex as eluent (68.5 mg, 93%). Spectral data are in accordance with the reported values⁴¹.

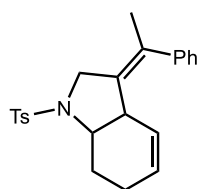


5-cinnamyl-1-methyl-1H-indole (3m): prepared following the general procedure using cinnamyl alcohol (54 mg, 0.4 mmol, 1 eq), 5-(5,5-dimethyl-1,3,2-dioxaborinan-2-yl)-1-

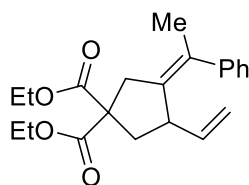
methyl-1H-indole (145 mg, 0.6 mmol, 1.5 eq), potassium phosphate (128 mg, 0.6 mmol, 1.5 eq), nickel catalyst (3 mg, 0.01 mmol, 0.025 eq), Ligand L₃ (3 mg, 0.01 mmol, 0.025 eq), and potassium t-butoxide (2 mg, 0.016 mmol, 0.03 eq) in 200 μ l of acetonitrile. Product was purified on column using pure hexane to 5% EtOAc/Hex as eluent (80 mg, 80%). ¹H NMR (500 MHz, CDCl₃) δ 7.53 (s, 1H), 7.38-7.44 (m, 2H), 7.26-7.37 (m, 3H), 7.20-7.26 (m, 1H), 7.12-7.20 (m, 1H), 7.06 (d, *J* = 1.5 Hz, 1H), 6.44-6.57 (m, 2H), 3.8 (t, *J* = 9.8 Hz, 3H), 3.69 (d, *J* = 2.78, 2H); ¹³C NMR (500 MHz, CDCl₃) δ 138.00, 135.61, 130.83, 130.40, 129.10, 128.66, 126.93, 126.28, 122.81, 120.64, 109.35, 100.67, 39.69, 32.96; IR (film) ν_{max} 2911, 3438.86, 2920.50, 1597.99, 1345.34, 1161.75, 765.13 cm^{-1} ; HRMS(EI) calcd. for C₁₈H₁₇N; [M+H]⁺, 248.1439; found, 248.1433.



3-benzyl-3-methyl-1-tosyl-4-vinylpyrrolidine (4a): prepared following the general procedure using (E)-N-(but-2-yn-1-yl)-N-(4-hydroxybut-2-en-1-yl)-4-methylbenzenesulfonamide (59 mg, 0.2 mmol, 1 eq), 5,5-dimethyl-2-phenyl-1,3,2-dioxaborinane (54 mg, 0.6 mmol, 1.5eq), potassium phosphate (64 mg, 0.3 mmol, 1.5 eq), nickel catalyst (3 mg, 0.01 mmol, 0.05 eq), Ligand L₂ (4 mg, 0.01 mmol, 0.05 eq), and potassium t-butoxide (2 mg, 0.016 mmol, 0.06 eq) in 300 μ l of toluene. Product was purified on column using pure hexane to 6% EtOAc/Hex as eluent (51 mg, 72%). ¹H NMR (500 MHz, CDCl₃) δ 7.75 (d, *J* = 4.31 Hz, 2H), 7.37 (d, *J* = 3.88 Hz, 2H), 7.18-7.33 (m, 3H), 7.07-7.11(m, 2H), 5.47-5.56 (m, 1H), 4.77 (d, *J* = 5.17 Hz, 1H), 4.64 (d, *J* = 8.84 Hz, 1H), 4.02 (d, *J* = 7.33 Hz, 1H), 3.86 (d, *J* = 7.33 Hz, 1H), 3.25-3.33 (m, 2H), 3.16-3.22 (m, 1H), 2.46 (s, 4H), 1.92 (s, 3H); ¹³C NMR (75 MHz, CDCl₃) δ 143.75, 142.42, 137.65, 132.88, 131.82, 129.83, 128.18, 127.92, 127.52, 126.85, 115.17, 53.85, 50.53, 45.22, 21.72; IR (film) ν_{max} 2911, 3054, 2922, 2852, 2359, 1598, 1347, 1163 cm^{-1} ; HRMS(EI) calcd. for C₂₁H₂₃NO₂S, [M+H]⁺, 354.1528; found, 354.1529.

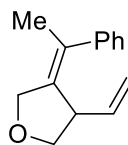


(E)-3-(1-phenylethylidene)-1-(phenylsulfonyl)-2,3,3a,6,7,7a-hexahydro-1H-indole (4b): prepared following the general procedure using N-(but-2-yn-1-yl)-N-(4-hydroxycyclohex-2-en-1-yl)benzenesulfonamide (64 mg, 0.2 mmol, 1 eq), 5,5-dimethyl-2-phenyl-1,3,2-dioxaborinane (54 mg, 0.6 mmol, 1.5 eq), potassium phosphate (64 mg, 0.3 mmol, 1.5 eq), nickel catalyst (3 mg, 0.01 mmol, 0.05 eq), Ligand L₂ (4 mg, 0.01 mmol, 0.05 eq), and potassium t-butoxide (2 mg, 0.016 mmol, 0.06 eq) in 300 μ l of toluene. Product was purified on column using pure hexane to 2% EtOAc/Hex as eluent. ¹H NMR (500 MHz, CDCl₃) δ 7.77 (d, *J* = 3.98 Hz, 2H), 7.37 (d, *J* = 4.20 Hz, 2H), 7.2-7.3 (m, 3H), 6.96 (d, *J* = 3.53 Hz, 2H), 5.64-5.70 (m, 1H), 5.04 (d, *J* = 5.38 Hz, 1H), 4.07 (q, *J* = 14.96 Hz, 2H), 3.59-3.68 (m, 1H), 3.125 (s, 1H), 2.48 (s, 3H), 2.21-2.33 (m, 2H), 1.82-1.930 (m, 4H), 1.55-1.67 (m, 2H); ¹³C (75 MHz, CDCl₃) δ 143.62, 142.85, 134.10, 132.81, 129.98, 129.73, 128.44, 127.67, 127.61, 126.90, 125.48, 59.09, 51.37, 42.37, 25.26, 21.91, 21.65, 20.24; IR (film) ν_{max} 2911, 3438, 2920, 2597, 1345, 1161 cm^{-1} ; HRMS(EI) calcd. for C₂₃H₂₅NO₂S, [M+H]⁺, 380.1684; found, 380.1688.



diethyl (Z)-3-(1-phenylethylidene)-4-vinylcyclopentane-1,1-dicarboxylate (4c): prepared following the general procedure using diethyl (E)-2-(but-2-yn-1-yl)-2-(4-hydroxybut-2-en-1-yl)malonate (57 mg, 0.2 mmol, 1 eq), 5,5-dimethyl-2-phenyl-1,3,2-dioxaborinane (54 mg, 0.6 mmol, 1.5 eq), potassium phosphate (64 mg, 0.3 mmol, 1.5 eq), nickel catalyst (3 mg, 0.01 mmol, 0.05 eq), Ligand L₂ (4 mg, 0.01 mmol, 0.05 eq), and potassium t-butoxide (2 mg, 0.016 mmol, 0.06 eq) in 300 μ l of toluene. Product was purified on column using pure hexane to 6% EtOAc/Hex as eluent (46 mg, 70%). ¹H NMR (500 MHz, CDCl₃) δ 7.22-7.28 (m, 2H), 7.11-7.2 (m, 3H), 5.34-5.44 (m, 1H), 4.53-4.64 (m, 2H), 4.16-4.27 (m, 4H), 3.09 (q, *J* = 16.69 Hz, 2H), 2.53 (q, *J* = 7.9 Hz, 1H), 2.11 (q, *J* = 6.22 Hz, 1H), 2.01 (s, 3H), 1.25-1.31 (m, 6H); ¹³C NMR (75 MHz, CDCl₃) δ 172.12, 143.72, 139.94, 136.59, 131.33, 127.99, 126.23, 113.96,

61.54, 58.99, 45.44, 40.50, 38.91, 22.33, 14.53; IR (film) ν_{max} 2911, 3465, 3078, 2980, 1732, 1443, 1250 cm^{-1} ; HRMS(EI) calcd. for $\text{C}_{21}\text{H}_{26}\text{O}_4$, $[\text{M}+\text{NH}_4]^+$, 343.1909; found, 343.1907.



(E)-3-(1-phenylethylidene)-4-vinyltetrahydrofuran (4d) : prepared following the general procedure using (E)-4-(but-2-yn-1-yloxy)but-2-en-1-ol (31 mg, 0.2 mmol, 1 eq), 5,5-dimethyl-2-phenyl-1,3,2-dioxaborinane (54 mg, 0.6 mmol, 1.5 eq), potassium phosphate (64 mg, 0.3 mmol, 1.5 eq), nickel catalyst (3 mg, 0.01 mmol, 0.05 eq), Ligand L₁ (4 mg, 0.01 mmol, 0.05 eq), and potassium t-butoxide (2 mg, 0.016 mmol, 0.06 eq) in 300 μl of acetonitrile. Product was purified on column using pure hexane to 2% EtOAc/Hex as eluent (25 mg, 63%). Spectral data are in accordance with the reported values⁴¹.

2.5 References

1. Li, C. J., Organic reactions in aqueous media-with a focus on carbon-carbon bond formation. *Chemical Reviews* **1993**, 93 (6), 2023-2035.
2. Brahmachari, G., Design for carbon-carbon bond forming reactions under ambient conditions. *RSC Advances* **2016**, 6 (69), 64676-64725.
3. Han, F.-S., Transition-metal-catalyzed Suzuki-Miyaura cross-coupling reactions: a remarkable advance from palladium to nickel catalysts. *Chemical Society Reviews* **2013**, 42 (12), 5270-5298.
4. Martin, R.; Buchwald, S. L., Palladium-catalyzed Suzuki-Miyaura cross-coupling reactions employing dialkylbiaryl phosphine ligands. *Accounts of Chemical Research* **2008**, 41 (11), 1461-1473.
5. Breitenfeld, J.; Ruiz, J.; Wodrich, M. D.; Hu, X., Bimetallic oxidative addition involving radical intermediates in nickel-catalyzed alkyl-alkyl Kumada coupling reactions. *Journal of the American Chemical Society* **2013**, 135 (32), 12004-12012.
6. Handy, S. T.; Zhang, X., Organic synthesis in ionic liquids: the Stille coupling. *Organic Letters* **2001**, 3 (2), 233-236.
7. Bellina, F.; Carpita, A.; Rossi, R., Palladium catalysts for the Suzuki cross-coupling reaction: an overview of recent advances. *Synthesis* **2004**, 2004 (15), 2419-2440.

8. Kabalka, G. W.; Dong, G.; Venkataiah, B., Rhodium-catalyzed Cross-coupling of allyl alcohols with aryl-and vinylboronic acids in ionic liquids. *Organic Letters* **2003**, *5* (6), 893-895.
9. García-Yebra, C.; Janssen, J. P.; Rominger, F.; Helmchen, G., Asymmetric iridium (I)-catalyzed allylic alkylation of monosubstituted allylic substrates with phosphinooxazolines as ligands. Isolation, characterization, and reactivity of chiral (allyl) iridium (III) complexes. *Organometallics* **2004**, *23* (23), 5459-5470.
10. Tsukamoto, H.; Sato, M.; Kondo, Y., Palladium (0)-catalyzed direct cross-coupling reaction of allyl alcohols with aryl-and vinyl-boronic acids. *Chemical Communications* **2004**, (10), 1200-1201.
11. Trost, B. M.; Van Vranken, D. L., Asymmetric transition metal-catalyzed allylic alkylations. *Chemical Reviews* **1996**, *96* (1), 395-422.
12. Tasker, S. Z.; Standley, E. A.; Jamison, T. F., Recent advances in homogeneous nickel catalysis. *Nature* **2014**, *509* (7500), 299.
13. Henrion, M.; Ritleng, V.; Chetcuti, M. J., Nickel N-heterocyclic carbene-catalyzed C–C bond formation: reactions and mechanistic aspects. *ACS Catalysis* **2015**, *5* (2), 1283-1302.
14. Ruiz-Castillo, P.; Buchwald, S. L., Applications of palladium-catalyzed C–N cross-coupling reactions. *Chemical Reviews* **2016**, *116* (19), 12564-12649.
15. Reizman, B. J.; Wang, Y.-M.; Buchwald, S. L.; Jensen, K. F., Suzuki–Miyaura cross-coupling optimization enabled by automated feedback. *Reaction Chemistry & engineering* **2016**, *1* (6), 658-666.
16. Tobisu, M.; Shimasaki, T.; Chatani, N., Nickel-Catalyzed Cross-Coupling of Aryl Methyl Ethers with Aryl Boronic Esters. *Angewandte Chemie* **2008**, *120* (26), 4944-4947.
17. Kim, Y. M.; Yu, S., Palladium (0)-catalyzed amination, Stille coupling, and Suzuki coupling of electron-deficient aryl fluorides. *Journal of the American Chemical Society* **2003**, *125* (7), 1696-1697.
18. Schaub, T.; Backes, M.; Radius, U., Catalytic C–C Bond Formation Accomplished by Selective C–F Activation of Perfluorinated Arenes. *Journal of the American Chemical Society* **2006**, *128* (50), 15964-15965.
19. Tobisu, M.; Xu, T.; Shimasaki, T.; Chatani, N., Nickel-catalyzed Suzuki–Miyaura reaction of aryl fluorides. *Journal of the American Chemical Society* **2011**, *133* (48), 19505-19511.
20. Muzart, J., Palladium-catalysed reactions of alcohols. Part B: Formation of C–C and C–N bonds from unsaturated alcohols. *Tetrahedron* **2005**, *17* (61), 4179-4212.

21. Butt, N. A.; Zhang, W., Transition metal-catalyzed allylic substitution reactions with unactivated allylic substrates. *Chemical Society Reviews* **2015**, *44* (22), 7929-7967.
22. Weaver, J. D.; Recio III, A.; Grenning, A. J.; Tunge, J. A., Transition metal-catalyzed decarboxylative allylation and benzylation reactions. *Chemical Reviews* **2011**, *111* (3), 1846-1913.
23. Madec, D.; Prestat, G.; Martini, E.; Fristrup, P.; Poli, G.; Norrby, P.-O., Surprisingly mild “enolate-counterion-free” Pd (0)-catalyzed intramolecular allylic alkylations. *Organic Letters* **2005**, *7* (6), 995-998.
24. Lafrance, M.; Roggen, M.; Carreira, E. M., Direct, Enantioselective Iridium-Catalyzed Allylic Amination of Racemic Allylic Alcohols. *Angewandte Chemie International Edition* **2012**, *51* (14), 3470-3473.
25. Miyata, K.; Kutsuna, H.; Kawakami, S.; Kitamura, M., A Chiral Bidentate sp²-N Ligand, Naph-diPIM: Application to CpRu-Catalyzed Asymmetric Dehydrative C-, N-, and O-Allylation. *Angewandte Chemie International Edition* **2011**, *50* (20), 4649-4653.
26. Han, S. H.; Choi, M.; Jeong, T.; Sharma, S.; Mishra, N. K.; Park, J.; Oh, J. S.; Kim, W. J.; Lee, J. S.; Kim, I. S., Rhodium-Catalyzed C–H Alkylation of Indolines with Allylic Alcohols: Direct Access to β -Aryl Carbonyl Compounds. *The Journal of Organic Chemistry* **2015**, *80* (21), 11092-11099.
27. Kayaki, Y.; Koda, T.; Ikariya, T., A highly effective (triphenyl phosphite) palladium catalyst for a cross-coupling reaction of allylic alcohols with organoboronic acids. *European Journal of Organic Chemistry* **2004**, *2004* (24), 4989-4993.
28. Hamilton, J. Y.; Sarlah, D.; Carreira, E. M., Iridium-catalyzed enantioselective allyl-alkene coupling. *Journal of the American Chemical Society* **2014**, *136* (8), 3006-3009.
29. Kita, Y.; Sakaguchi, H.; Hoshimoto, Y.; Nakauchi, D.; Nakahara, Y.; Carpentier, J. F.; Ogoshi, S.; Mashima, K., Pentacoordinated Carboxylate π -Allyl Nickel Complexes as Key Intermediates for the Ni-Catalyzed Direct Amination of Allylic Alcohols. *Chemistry–A European Journal* **2015**, *21* (41), 14571-14578.
30. Kita, Y.; Kavthé, R. D.; Oda, H.; Mashima, K., Asymmetric Allylic Alkylation of β -Ketoesters with Allylic Alcohols by a Nickel/Diphosphine Catalyst. *Angewandte Chemie International Edition* **2016**, *55* (3), 1098-1101.
31. Yang, B.; Wang, Z.-X., Nickel-Catalyzed Cross-Coupling of Allyl Alcohols with Aryl- or Alkenylzinc Reagents. *The Journal of Organic Chemistry* **2016**, *82* (9), 4542-4549.
32. Nazari, S. H.; Bourdeau, J. E.; Talley, M. R.; Valdivia-Berroeta, G. A.; Smith, S. J.; Michaelis, D. J., Nickel-Catalyzed Suzuki Cross Couplings with Unprotected Allylic Alcohols

Enabled by Bidentate N-Heterocyclic Carbene (NHC)/Phosphine Ligands. *ACS Catalysis* **2017**, *8* (1), 86-89.

33. Dong, Z.; Ye, Z., Reusable, Highly Active Heterogeneous Palladium Catalyst by Convenient Self-Encapsulation Cross-Linking Polymerization for Multiple Carbon-Carbon Cross-Coupling Reactions at ppm to ppb Palladium Loadings. *Advanced Synthesis & Catalysis* **2014**, *356* (16), 3401-3414.

34. Hamasaka, G.; Sakurai, F.; Uozumi, Y., A palladium NNC-pincer complex: an efficient catalyst for allylic arylation at parts per billion levels. *Chemical Communications* **2015**, *51* (18), 3886-3888.

35. Yamada, Y. M.; Sarkar, S. M.; Uozumi, Y., Self-assembled poly (imidazole-palladium): Highly active, reusable catalyst at parts per million to parts per billion levels. *Journal of the American Chemical Society* **2012**, *134* (6), 3190-3198.

36. Junquera, L. B.; Fernández, F. E.; Puerta, M. C.; Valerga, P., Nickel (II) N-Heterocyclic Carbene Complexes: Versatile Catalysts for C-C, C-S and C-N Coupling Reactions. *European Journal of Inorganic Chemistry* **2017**, *2017* (19), 2547-2556.

37. Saito, K.; Kondo, K.; Akiyama, T., B(C₆F₅)₃-Catalyzed Hydrodesulfurization Using Hydrosilanes-Metal-Free Reduction of Sulfides. *Organic Letters* **2015**, *17* (13), 3366-3369.

38. Zhang, Z.; Xu, L.; Chen, Z.; Liu, Z.; Miao, M.; Song, J.; Ren, H., Nickel-Catalyzed Regioselective Reductive Cross-Coupling of Aryl Halides with Polysubstituted Allyl Halides in the Presence of Imidazolium Salts. *Synlett* **2015**, *26* (20), 2784-2788.

39. Li, M. B.; Wang, Y.; Tian, S. K., Regioselective and Stereospecific Cross-Coupling of Primary Allylic Amines with Boronic Acids and Boronates through Palladium-Catalyzed C-N Bond Cleavage. *Angewandte Chemie* **2012**, *124* (12), 3022-3025.

40. Tsukamoto, H.; Uchiyama, T.; Suzuki, T.; Kondo, Y., Palladium (0)-catalyzed direct cross-coupling reaction of allylic alcohols with aryl- and alkenylboronic acids. *Organic & Biomolecular Chemistry* **2008**, *6* (16), 3005-3013.

41. Zhu, G.; Zhang, Z., Palladium-Catalyzed Tandem Cyclization/Suzuki Coupling of 1, 6-Enynes. *Organic Letters* **2003**, *5* (20), 3645-3648.

Chapter 3 C-N Bond Formation from Allylic Alcohols via Cooperative Nickel and Titanium Catalysis

Titanium Catalysis

3.1 Introduction

Catalysis is a critical science for modern society and improvements in catalytic processes increase the efficiency of chemical transformations. Transition metal catalysts are invaluable tools for organic synthesis and significant efforts have been dedicated to the development of new modular catalytic systems. Recent efforts in reaction design have focused on the development of cooperative catalytic processes, wherein two catalysts work in concert to create new types of coupling reactions¹ (Figure 3.1). This strategy in reaction development enables unprecedented reactivity by activating both substrates, or by catalytically generating two reactive intermediates via two separate catalytic cycles.

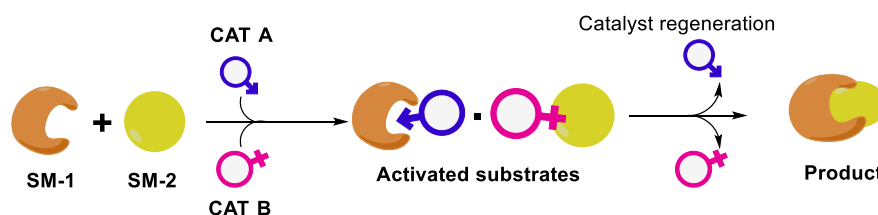


Figure 3.1 The concept of cooperative catalysis

In contrast to the many very successful examples of cooperative catalysis in biological systems, the design and utilization of cooperative systems in synthetic chemistry is still in its infancy, especially with respect to applications in transition metal catalysis. Only recently has this approach been recognized as a promising way to address synthetic problems and to discover previously unknown transformations². Metal-catalyzed allylic functionalization reactions, including allylic aminations, are widely employed in modern catalysis due to the ability of these reactions to proceed with high product selectivity under mild reaction conditions³. The use of unactivated allylic alcohols in this transformation is attractive because it precludes the need for stoichiometric activation of the alcohol. However, the acidity of the OH bond and the poor leaving group ability of alcohols makes this transformation difficult to achieve⁴. There are numerous examples of precious metals including palladium⁵, ruthenium⁶, rhodium⁷, and iridium⁸ that catalyze allylic functionalizations with allylic alcohols, including examples of enantioselective allylic aminations. Despite the high cost and toxicity of these

noble metals, reactions catalyzed with these metals have some unique features that are worth elaborating. For example, reactions catalyzed by ruthenium, rhodium or iridium are usually more efficient when an allyl carbonate is used as substrate in allylic aminations. The reaction also proceeds by retention of chirality at the branched carbon (branched to linear = b/l) and facilitates enantioselective transformation⁹⁻¹⁰ (Figure 3.2 A). On the other hand, reactions that employ palladium or nickel as a catalyst favor amination at the less-hindered carbon, which is the linear product¹¹⁻¹² (Figure 3.2 B). Although the palladium- or nickel-catalyzed aminations work with unprotected allylic alcohols, they generally require high temperatures for better

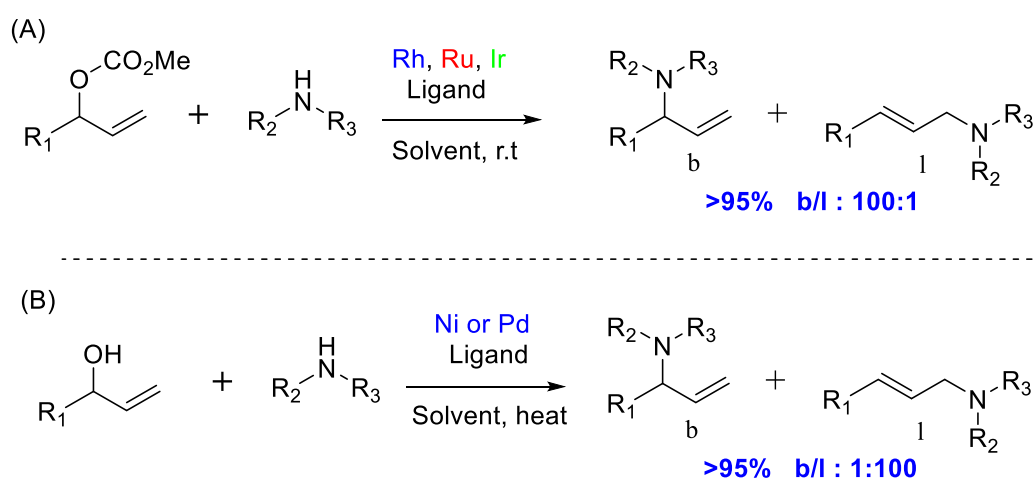


Figure 3.2 Regioselectivity of allylic amination with Rh, Ru, or Ir (A). regioselectivity with Ni or Pd(B)

conversion and yields¹¹. Recent advances in allylic amination catalyzed by nickel or palladium include the development of new ligands that incorporate a Lewis acid binding site such as boron¹ (Figure 3.3 A) or use of an additive that facilitates catalysis at lower temperatures and catalyst loading¹¹ (Figure 3.3 B, TBAA = tetrabutylammonium acetate). Our group is interested in the discovery and development of cooperative catalysis systems, including those with heterobimetallic complexes. Our results presented herein demonstrate that catalytic activation of the allylic alcohol substrate is a viable strategy for rapid organic transformations under nickel catalysis and that this approach provides unique substrate reactivity not observed in single catalyst systems. The aim of this chapter is to describe a rational design of such a system, which has worked for the development of new synthetic transformations. We discovered a new catalytic system that enables a facile transformation of allylic alcohols to the corresponding allyl amine. In this transformation, facile oxidative addition prompted by Ni/Ti catalyst system is followed by nucleophilic attack by an amine at the least hindered carbon of the allyl metal intermediate to form the product (Figure 3.4 A). A unique feature of this system is the

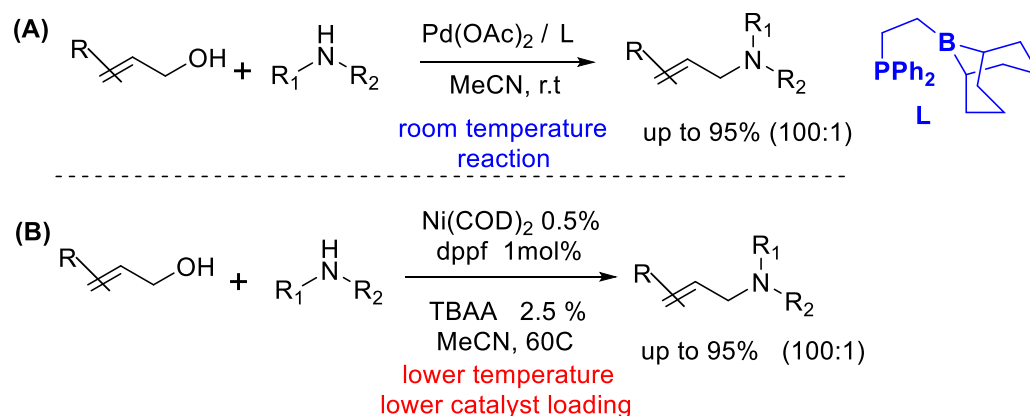


Figure 3.3 Advances in allylic amination; with Pd/new ligand (A). with Nickel at lower catalyst loading (B)

possibility to conduct tandem cyclization/amination reactions, which are not feasible under other catalytic systems (Figure 3.4 B). Overall, this cooperative catalysis system will enable the efficient coupling of allylic alcohols with amines to generate a tailored allylic amination product. This approach is an efficient method that can be used in the synthesis of complex molecules.

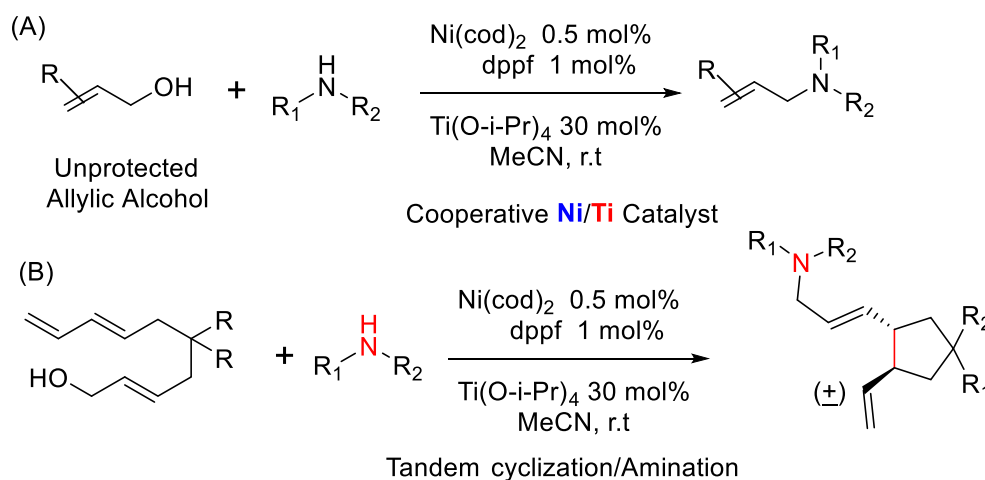


Figure 3.4 Allylic amination under mild conditions (A) Tandem cyclization/Amination (B)

Keywords: C-N bond forming reaction, cross coupling, Nickel catalyzed amination, dppf

3.2 Results and Discussions

During the course of our studies in Suzuki cross-coupling reactions with unprotected allylic alcohols¹³, we wondered if similar reaction conditions could be employed for allylic aminations under nickel catalysis. Our literature search indicated that titanium

tetraisopropoxide undergoes trans-alkoxylation with alcohols¹⁴⁻¹⁵. We hypothesized that formation of a Ti-OR complex with our allylic alcohol substrate would weaken the C-O bond and accelerate the oxidative addition step. This would lead to allylic amination reactions under very mild conditions. On these grounds, we envisioned a cooperative catalytic system in which the in situ activation of alcohol electrophiles by Lewis acids (Ti(OiPr)₄) facilitates cross-coupling reactions with amines to form allyl amine products. This approach enables the use of readily available allylic alcohols as electrophilic partners for cross couplings without the need for stoichiometric activation of the alcohol as a carbonate, halide, or ester. Moreover, this step-economic procedure will produce the corresponding product in addition to titanium oxide as a byproduct. Accordingly, the mechanism of our designed cooperative catalytic system involves activation of the allylic alcohol as the titanium ether. Formation of a π -allyl nickel intermediate ensues through oxidative addition of Ni (0) into the C-O bond. This electrophilic allyl species is attacked by an amine nucleophile to produce the allylic substitution product. (Figure 3.5). This Lewis acid activation accelerates the reaction rate by lowering the activation energy of the oxidative addition step, leading to efficient reaction rates at room temperature.

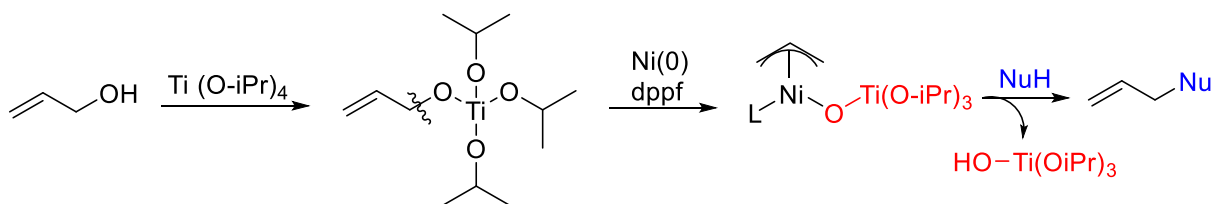
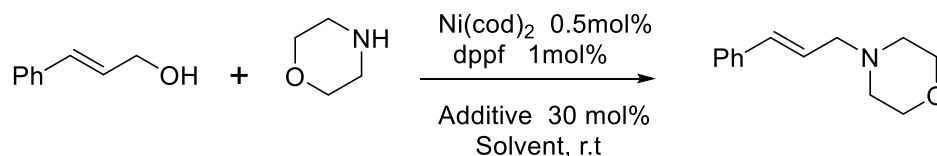


Figure 3.5 Plausible reaction mechanism for cooperative Ni/Ti catalyst

We began our optimization studies¹⁶ by adding Ni(cod)₂ and bis(diphenylphosphino)-ferrocene (dppf) to the reaction mixture containing morpholine and cinnamyl alcohol (Table 3.1). The reaction resulted in a very low yield of the amination product (Table 1, entry 1). However, when a catalytic amount of titanium isopropoxide (30%) was added to the reaction, it dramatically improved the rate of product formation via alcohol activation (entry 2). Importantly, this allylic amination occurs under very mild conditions at room temperature with inexpensive nickel catalysts. No conversion was observed in the absence of nickel and in the presence of titanium (entry 3), and lower amounts of titanium led to slower reactions (entry 4). Under conditions previously reported for nickel-catalyzed allylic aminations using tetrabutylammonium acetate (TBAA) as additive, only 12% yield was observed (entry 5). Catalytic amounts of alternative Lewis acids also accelerated the transformation (entries 6–8), but not to the same degree as with titanium isopropoxide. We also investigated the impact of

the phosphine ligand structure on the rate of catalysis and found that various phosphines could be employed, but dppf provided the highest yield in the reaction(entries 9–13). Acetonitrile as solvent was also found to be important for obtaining good conversions (entries 14–17).

Table 3.1 Optimization of the cooperative catalysis system



entry ^a	ligand	additive	solvent	Time(h)	Conv ^b .(yield)
1	dppf		MeCN	24	3
2	dppf	Ti(OiPr) ₄	MeCN	12	90 (85)
3		Ti(OiPr) ₄	MeCN	20	
4 ^c	dppf	Ti(OiPr) ₄	MeCN	20	36
5	TBAA	Ti(OiPr) ₄	MeCN	12	14
6	dppf	TiCl ₄	MeCN	12	22
7	dppf	BF ₃	MeCN	12	45
8	dppf	AlCl ₃	MeCN	12	65
9	PPh ₃	Ti(OiPr) ₄	MeCN	12	46
10	dppe	Ti(OiPr) ₄	MeCN	12	21
11	dppp	Ti(OiPr) ₄	MeCN	12	41
12	dppb	Ti(OiPr) ₄	MeCN	12	86
13	BINAP	Ti(OiPr) ₄	MeCN	12	87
14	dppf	Ti(OiPr) ₄	toluene	12	9
15	dppf	Ti(OiPr) ₄	THF	12	6
16	dppf	Ti(OiPr) ₄	dioxane	12	6
17	dppf	Ti(OiPr) ₄	DMF	12	1
18 ^d	dppf	Ti(OiPr) ₄	MeCN	4	96
19 ^e	dppf	Ti(OiPr) ₄	MeCN	2	99 (96)

^aReaction run with 1.6 mmol of alcohol, 2.4mmol of amine (1.5 eq) in solvent (4M). ^bConversion measured by ¹HNMR analysis of the crude reaction. ^cWith 10% of Ti(O-iPr)₄. ^dWith 50% of Ti(O-iPr)₄. ^eWith 100% of Ti(O-iPr)₄.

In order to further investigate the role of titanium, we also conducted the reaction with 0.5 and 1.0 equiv of the Lewis acid and found that the rate increased as the amount of titanium increased (Table 1, entry 18 and entry 19). This supports our hypothesis that titanium activates

the alcohol toward oxidative addition by the nickel catalyst, presumably via formation of the $\text{Ti}(\text{O-allyl})_4$ species. Indeed, when titanium isopropoxide is mixed with cinnamyl alcohol in the presence or absence of morpholine, shifts in the ^1H NMR spectrum indicate coordination of the alcohol with the Lewis acid. However, when titanium isopropoxide was added to the preformed nickel dppf catalyst, no change in the ^1H NMR spectrum was observed (see experimental section). This final result suggests that the titanium does not impact the structure of the nickel catalyst.

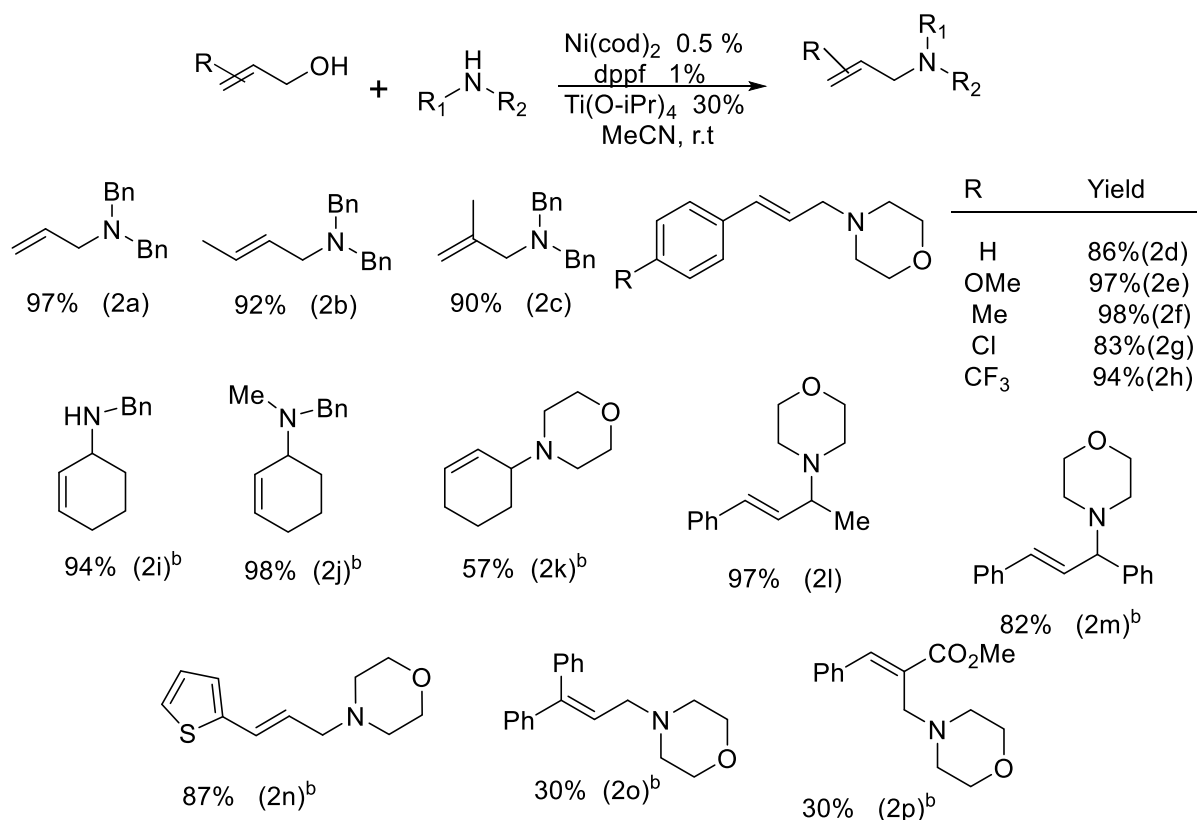


Figure 3.6 Amination of various primary and secondary alcohol substrates. (a) Reaction run with 2 mol% of Ni and 0.5 eq of $\text{Ti}(\text{O-}i\text{Pr})_4$. (b) Reaction run with 5 mol% of Ni and 1 eq of $\text{Ti}(\text{O-}i\text{Pr})_4$.

Using our optimization conditions, we demonstrated that the reaction is compatible with a variety of allyl alcohols (Figure 3.6). Simple unsubstituted or monosubstituted allyl alcohols reacted with high yield (**2a-2c**). Incorporating electron-donating or electron-withdrawing groups on the aryl ring of the cinnamyl alcohol did not affect the reaction and in each case high yields and excellent selectivities were obtained. Secondary allylic alcohols, including examples with phenyl substitution at the hydroxyl carbon, are well tolerated in the reaction provide moderate to excellent yields (**2i-2m**). Allylic alcohols containing heterocyclic thiophene rings also reacted in high yield (**2n**). Trisubstituted alkenes and Baylis-Hillman

adducts also reacted, but in lower yields (**2o-2p**). For most of the substrates, a catalytic amount of $\text{Ti}(\text{O-}i\text{Pr})_4$ (30%) was sufficient for high reactivity. However, in some cases (**2i-k**, **2m** or **2n**, **2p**) stoichiometric amounts of titanium were required to ensure complete consumption of the starting material and high yields. The scope of amine substrates were next tested (Figure 3.7). Secondary amines proved to be the best substrates for this transformation including dialkylamines (**3a**, **3b**, **3d**, **3e**, **3f**), diaryl amines (**3c**), and various heterocyclic amines (**3g-3i**). While modest yields were obtained by primary amines (**3j,k**), α -branched primary alcohols (**3k**) or amination with secondary allyl alcohols and primary amines (**3m**) gave high yields. Steric hindrance associated with the latter cases is necessary to prevent overalkylation of the amine. However, highly hindered secondary amines also ended up with reduced yields (**3n**).

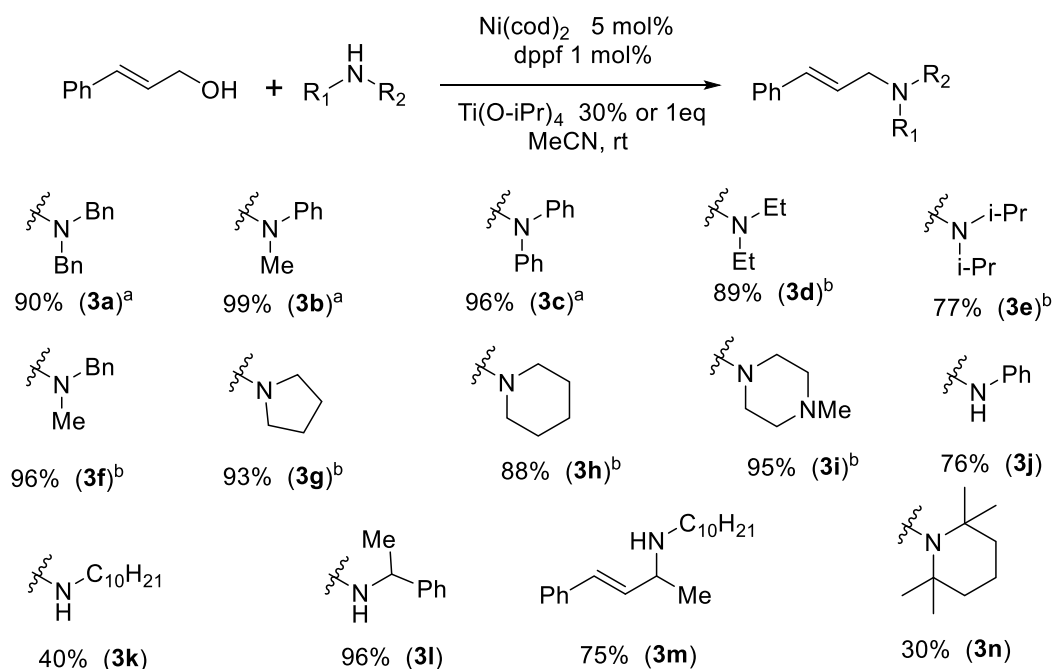


Figure 3.7 Substrate scope for the amine nucleophile. (a) Reaction run with 2 mol% of Ni and 1 eq of $\text{Ti}(\text{O-}i\text{Pr})_4$. (b) Reaction run with 1 eq of $\text{Ti}(\text{O-}i\text{Pr})_4$

A significant advantage of our cooperative system is the feasibility of tandem cyclization amination processes that enabled the synthesis of complex structures. When we incorporated a pendent diene into the structure of our allylic alcohol substrate, oxidative addition would be rapidly followed by insertion into the pendant diene (Figure 3.8). This cyclization created a five-membered ring and a second nickel-allyl intermediate, which would then go on to react with the amine nucleophile to generate the final product. In particular, when our cooperative catalysis system was applied, the cyclized products (**4**) were observed as the major product and in good yield when 5% nickel catalyst and 100% titanium isopropoxide were

used. In contrast, under the catalytic conditions developed by Mashima¹¹ using tetrabutylammonium acetate as additive, only amination was observed and no cyclization. This new transformation generates a multifunctional cyclopentane product containing two stereocenters with moderate to good diastereoselectivity. The reaction proceeds in moderate to high

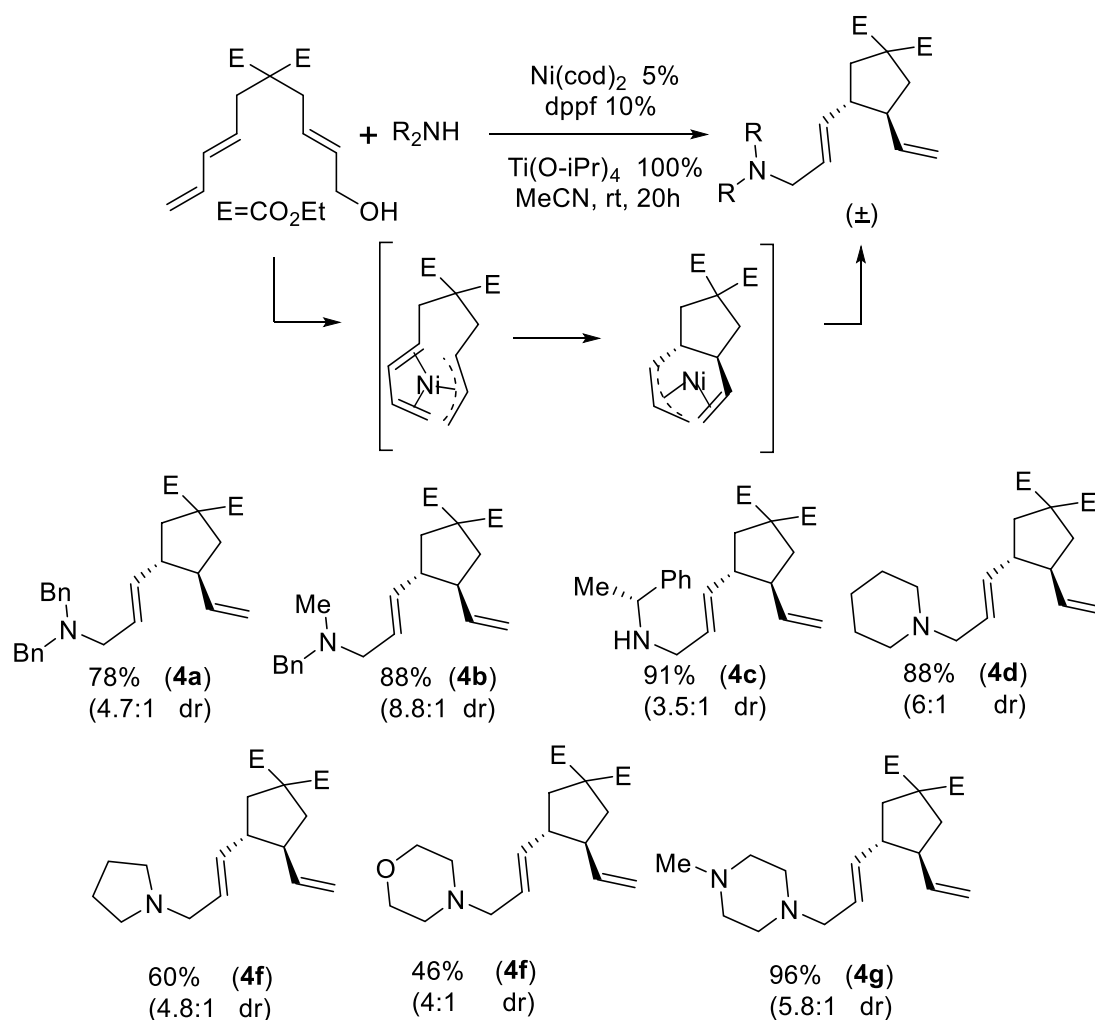


Figure 3.8 Tandem cyclization amination of diene containing substrates

yield with a variety of amine nucleophiles, including acyclic (**4a**, **4b**, **4c**), cyclic (**4d**, **4e**), and heterocyclic amines (**4f**, **4g**). These new amine products could be valuable intermediates in the synthesis of complex alkaloids due to the dense arrangement of reactive functional groups.

In conclusion, our optimization studies led to the development of a cooperative catalysis system where titanium and nickel work in concert to enable highly efficient and selective allylic aminations. Our results demonstrate the necessity of both the titanium and nickel to achieve optimal reactivity. In addition, these new cooperative catalysis conditions uniquely enable a

tandem cyclization/amination process that generates highly functionalized cyclopentane rings in good yield.

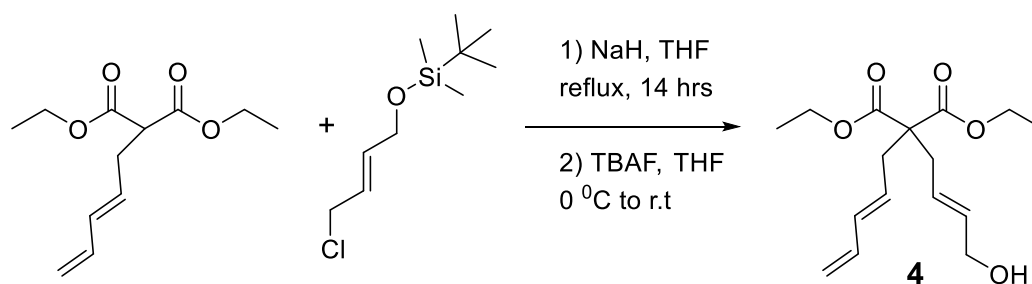
3.3 Experimental Procedures and Supporting Information for C–N Bond Formation from Allylic Alcohols via Cooperative Nickel and Titanium Catalysis

3.3.1 General information

All reactions were carried out under an atmosphere of nitrogen or argon in oven-dried glassware with magnetic stirring, unless otherwise indicated. Solvents were dried by J. C. Meyer's Solvent Purification System. The substrates were prepared by literature procedures or as described below. All other reagents were used as obtained unless otherwise noted. Flash Chromatography was performed with EM Science silica gel (0.040-0.063 μm grade). Analytical thin-layer chromatography was performed with 0.25 mm coated commercial silica gel plates (E. Merck, DC-Plastikfolien, kieselgel 60 F254). Proton nuclear magnetic resonance (^1H -NMR) data were acquired on a Mercury 400 (400 MHz) or on a Varian Unity Inova-500 (500 MHz) spectrometer. Chemical shifts are reported in delta (δ) units, in parts per million (ppm) downfield from tetramethylsilane or from DMSO (2.54 ppm). Splitting patterns are designated as s, singlet; d, doublet; t, triplet; q, quartet; p, pentet, m, multiplet, br, broad. Carbon-13 nuclear magnetic resonance (^{13}C -NMR) data were acquired at 100 MHz on a Mercury 400 or at 125 MHz on a Varian Unity Inova 500 spectrometer. Chemical shifts are reported in ppm relative to the center line of a triplet at 77.23 ppm for chloroform-*d* or from the center line of DMSO-*d* 40.45 ppm. Infrared (IR) data were recorded as films on sodium chloride plates on a Thermo Scientific Nicolet IR100 FT-IR spectrometer. Absorbance frequencies are reported in reciprocal centimeters (cm^{-1}). Chiral HPLC analyses were performed on a Thermo Separation Products Spectra Series P-100 or 200 and UV100 (254 nm) using Chiralcel[®] columns (OD-H, OB-H, OJ, AD, AS, OC, IA, IB or IC) eluting with heptane / *iso*-propanol mixtures indicated. Optical rotations were measured on a Jasco P-2000 digital polarimeter using 5 cm cells and the sodium D line (589 nm) at ambient temperature in the solvent and concentration indicated. Gas Chromatograms were obtained on a Hewitt Packard 6890 series GC system.

3.3.1.1 Synthesis of the substrates

Substrates **2i-2k** were synthesized according to previously reported procedures.



diethyl 2-((E)-4-hydroxybut-2-en-1-yl)-2-((E)-penta-2,4-dien-1-yl)malonate (4):

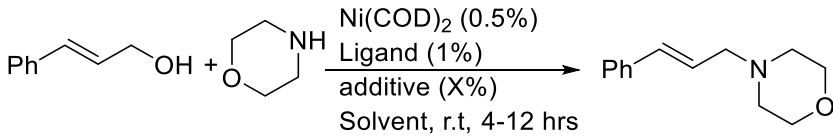
to a solution of diethyl (E)-2-(penta-2,4-dien-1-yl)malonate^{6b} (L₁, 550 mg, 2.43 mmol, 1 eq) in THF was added sodium hydride (60% dispersion in mineral oil, 146 mg, 3.64 mmol, 1.5 eq) at 0°C and stirred at room temperature for 30 minutes. A solution of (E)-tert-butyl((4-chlorobut-2-en-1-yl)oxy)dimethylsilane^{6c} (L₂, 642 mg, 2.91 mmol, 1.2 eq) in DMSO (2 ml) was added and the mixture stirred overnight. The reaction mixture diluted with ethyl acetate and washed with NaHCO₃ (aq), dried over magnesium sulfate, and concentrated in vacuum. Purification on column using EtOAc/Hex (1% to 2.5%) gave the product as a yellowish liquid (900 mgr, 76%). ¹H NMR (500 MHz, CDCl₃) δ 6.19-6.35 (m, 1H), 6.02-6.13 (m, 1H), 5.41-5.68 (m, 3H), 5.08 (d, *J* = 16.91 Hz, 1H), 5.0 (d, *J* = 10.55 Hz, 1H), 4.17 (q, *J* = 14.23 Hz, 4H), 4.10 (d, *J* = 4.66 Hz, 2H), 2.63 (t, *J* = 7.82 Hz, 4H), 1.23 (t, *J* = 7.12 Hz, 6H), 0.9 (s, 9H), 0.055 (s, 6H); ¹³C NMR (75 MHz, CDCl₃) δ 170.79, 136.68, 135.01, 134.08, 128.03, 123.90, 116.27, 63.55, 61.32, 57.66, 35.75, 35.48, 25.95, 14.18, -5.09; IR (film) ν_{max} 2929, 2856, 1736, 1462, 1256, 1133 cm⁻¹; HRMS(EI) calcd. for C₃₀H₂₉N₃P, [M+H]⁺, 463.2172; found, 463.2175.

To a solution of the product (1 g, 2.5 mmol, 1 eq) in THF was added tetra butyl ammonium fluoride (1 M in THF, 6 ml, 6 mmol, 2 eq) at 0 °C. The reaction mixture warmed up and stirred at room temperature overnight. The mixture was diluted with EtOAc and washed with water. Organics were dried on sodium sulfate, concentrated, and purified on column chromatography using Hex/EtOAc (0 to 25%) gave the product as a colorless liquid (600 mg, 82%). ¹H NMR (500 MHz, CDCl₃) δ 6.22-6.32 (m, 1H), 6.05-6.13 (m, 1H), 5.68-5.77 (m, 1H), 5.47-5.59 (m, 2H), 5.12 (d, *J* = 17.34 Hz, 1H), 5.01 (d, *J* = 10.42 Hz, 1H), 4.18 (q, *J* = 14.31 Hz, 4H), 4.08 (t, *J* = 5.39 Hz, 2H), 2.64 (dd, *J* = 7.96, 11.23 Hz, 4H), 1.24 (t, *J* = 7.18 Hz, 6H); ¹³C NMR (75 MHz, CDCl₃) δ 170.68, 136.60, 135.06, 133.80, 127.86, 126.06, 116.45, 63.35, 61.35, 57.61, 35.80, 35.40, 14.19; IR (film) ν_{max} 3465, 2980, 1732, 1456, 1202 cm⁻¹; HRMS(EI) calcd. for C₃₀H₂₉N₃P, [M+H]⁺, 463.2172; found, 463.2175.

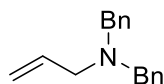
General procedure for Nickel-catalyzed cross coupling of allylic alcohols with amines: inside a glove box and in a 3 ml dram vial were placed Ni (COD)₂ (2.2 mg, 0.008 mmol, 0.005

eq) and dppf (9 mg, 0.016 mmol, 0.01 eq) in acetonitrile (300 μ l). The mixture stirred for 5 minutes, and after addition of the allylic alcohol (1.6 mmol, 1 eq), the amine (2.4 mmol, 1.5 eq), and Ti(O-*i*pr)₄ (0.1 ml, 0.3 eq, 4.879 M solution in toluene), the vial was sealed and the reaction mixture stirred for 12 hours. All the volatiles were removed on the rotovap, and the crude mixture was purified on column using EtOAc and Hexane as eluent.

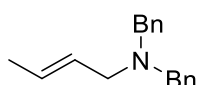
3.3.1.2 Optimization studies:



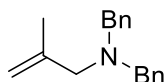
entry	ligand	Additive(mol%)	solvent	Conversion(yield)
1	-	Ti(<i>o</i> ipr) ₄ (30)	MeCN	-
2	dppf	-	MeCN	3
3	dppf	TBAA(2.5)	MeCN	14
4	dppf	TiCl ₄ (30)	MeCN	22
5	dppf	Ti(<i>o</i> ipr) ₄ (30)	MeCN	90(85)
6	dppf	Ti(<i>o</i> ipr) ₄ (30)	toluene	9
7	dppf	Ti(<i>o</i> ipr) ₄ (30)	THF	6
8	dppf	Ti(<i>o</i> ipr) ₄ (30)	dioxane	6
9	dppf	Ti(<i>o</i> ipr) ₄ (30)	DMF	1
10	PPh ₃	-	MeCN	-
11	PPh ₃	Ti(<i>o</i> ipr) ₄ (30)	MeCN	46
12	dppe	-	MeCN	-
13	dppe	Ti(<i>o</i> ipr) ₄ (30)	MeCN	21
14	dppp	-	MeCN	-
15	dppp	Ti(<i>o</i> ipr) ₄ (30)	MeCN	41
16	dppb	-	MeCN	6
17	dppb	Ti(<i>o</i> ipr) ₄ (30)	MeCN	86
18	BINAP	-	MeCN	6
19	BINAP	Ti(<i>o</i> ipr) ₄ (30)	MeCN	67
20	Ip _r .HCl	-	MeCN	-
21	Ip _r .HCl	Ti(<i>o</i> ipr) ₄ (30)	MeCN	3



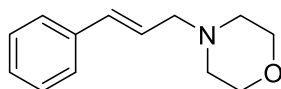
N,N-dibenzylprop-2-en-1-amine (2a): prepared following the general procedure using Ni(COD)₂ (2.2 mg, 0.008 mmol, 0.005 eq), dppf (9 mg, 0.016 mmol, 0.01eq), allyl alcohol (93 mg, 1.6 mmol, 1 eq), dibenzyl amine (473 mg, 2.4 mmol, 1.5 eq), and Ti(O-*i*-pr)₄ (0.1 ml, 0.3 eq, 4.879 M solution in toluene) in acetonitrile (300 μ l). Product was purified on column using pure hexane to 50% EtOAc/Hex as eluent (368 mg, 97%). Spectral data are in accordance with the reported values¹⁷.



(E)-N,N-dibenzylbut-2-en-1-amine (2b): prepared following the general procedure using Ni(COD)₂ (2.2 mg, 0.008 mol, 0.005 eq), dppf (9 mg, 0.016 mmol, 0.01eq), E-2-butene-1-ol (115 mg, 1.6 mmol, 1 eq), dibenzyl amine (473 mg, 2.4 mmol, 1.5 eq), and Ti(O-*i*-pr)₄ (0.1 ml, 0.3 eq, 4.879 M solution in toluene) in acetonitrile (300 μ l). Product was purified on column using pure hexane to 50% EtOAc/Hex as eluent (369 mg, 92%). Spectral data are in accordance with the reported values¹⁷.

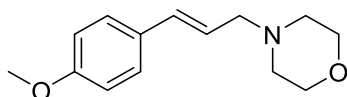


N,N-dibenzyl-2-methylprop-2-en-1-amine (2c) : prepared following the general procedure using Ni(COD)₂ (2.2 mg, 0.008 mmol, 0.005 eq), dppf (9 mg, 0.016 mmol, 0.01 eq), 2-methyl-2-propene-1-ol (115 mg, 1.6 mmol, 1 eq), dibenzyl amine (473 mg, 2.4 mmol, 1.5 eq), and Ti(O-*i*-pr)₄ (0.1 ml, 0.3 eq, 4.879 M solution in toluene) in acetonitrile (300 μ l). Product was purified on column using pure hexane to 50% EtOAc/Hex as eluent (361 mg, 90%). Spectral data are in accordance with the reported values¹².

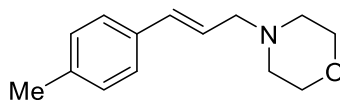


4-cinnamylmorpholine(2d): prepared following the general procedure using Ni(COD)₂ (2.2 mg, 0.008 mmol, 0.005 eq), dppf (9 mg, 0.016 mmol, 0.01 eq), cinnamyl alcohol (214 mg, 1.6

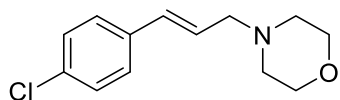
mmol, 1 eq), morpholine (236 mg, 2.4 mmol, 1.5 eq), and $\text{Ti}(\text{O-}i\text{pr})_4$ (0.1 ml, 0.3 eq, 4.879 M solution in toluene) in acetonitrile (300 μl). Product was purified on column using pure hexane to 50% EtOAc/Hex as eluent (277 mg, 86%). Spectral data are in accordance with the reported values¹².



(E)-4-(3-(4-methoxyphenyl)allyl)morpholine (2e): prepared following the general procedure using $\text{Ni}(\text{COD})_2$ (1.1 mg, 0.004 mmol, 0.005 eq), dppf (9 mg, 0.008 mmol, 0.01 eq), (E)-3-(4-methoxyphenyl)prop-2-en-1-ol (132 mg, 0.8 mmol, 1 eq), morpholine (140 mg, 1.2 mmol, 1.5 eq), and $\text{Ti}(\text{O-}i\text{pr})_4$ (0.05 ml, 0.3 eq, 4.879 M solution in toluene) in acetonitrile (100 μl). Product was purified on column using pure hexane to 50% EtOAc/Hex as eluent (90.5 mg, 97%). Spectral data are in accordance with the reported values¹².

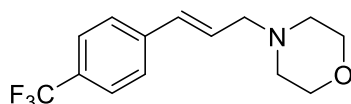


(E)-4-(3-(p-tolyl)allyl)morpholine (2f): prepared following the general procedure using $\text{Ni}(\text{COD})_2$ (1.1 mg, 0.008 mmol, 0.005 eq), dppf (9 mg, 0.008 mmol, 0.01 eq), (E)-3-(p-tolyl)prop-2-en-1-ol (120 mg, 0.8 mmol, 1 eq), morpholine (140 mg, 1.2 mmol, 1.5 eq), and $\text{Ti}(\text{O-}i\text{pr})_4$ (0.05 ml, 0.3 eq, 4.879 M solution in toluene) in acetonitrile (100 μl). Product was purified on column using pure hexane to 50% EtOAc/Hex as eluent (85 mg, 98%). Spectral data are in accordance with the reported values¹⁸.

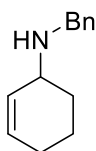


(E)-4-(3-(4-chlorophenyl)allyl)morpholine (2g): prepared following the general procedure using $\text{Ni}(\text{COD})_2$ (2.2 mg, 0.008 mmol, 0.02 eq), dppf (9 mg, 0.016 mmol, 0.04 eq), (E)-3-(4-chlorophenyl)prop-2-en-1-ol (68 mg, 0.4 mmol, 1 eq), morpholine (70 mg, 0.6 mmol, 1.5 eq), and $\text{Ti}(\text{O-}i\text{pr})_4$ (0.05 ml, 0.5 eq, 4.879 M solution in toluene) in acetonitrile (100 μl). Product was purified on column using pure hexane to 50% EtOAc/Hex as eluent (79 mg, 83%). ¹H

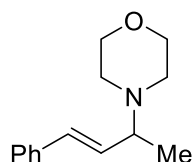
NMR (500 MHz, CDCl₃) δ 7.22-7.36 (m, 4H), 6.48 (d, J = 16.33 Hz, 1H), 6.16-6.28 (m, 1H), 3.73 (t, J = 4.62 Hz, 4H), 3.13 (dd, J = 1.38, 6.74 Hz, 2H), 2.49 (t, J = 4.64 Hz, 4H); ¹³C NMR (75 MHz, CDCl₃) δ 132.05, 128.74, 127.52, 126.92, 67.00, 61.35, 53.73; IR (film) ν_{max} 2856, 2464, 1492, 1452, 1119 cm⁻¹; HRMS(EI) calcd. for C₁₃H₁₆ClNO, [M+H]⁺, 239.0891; found, 239.0897.



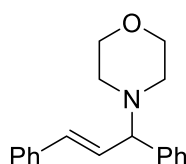
(E)-4-(3-(4-(trifluoromethyl)phenyl)allyl)morpholine(2h): prepared following the general procedure using Ni(COD)₂ (2.2 mg, 0.008 mmol, 0.02 eq), dppf (9 mg, 0.016 mmol, 0.04 eq), (E)-3-(4-(trifluoromethyl)phenyl)prop-2-en-1-ol (80 mg, 0.4 mmol, 1 eq), morpholine (70 mg, 0.6 mmol, 1.5 eq), and Ti(O-*i*-pr)₄ (0.05 ml, 0.5 eq, 4.879 M solution in toluene) in acetonitrile (100 μ l). Product was purified on column using pure hexane to 50% EtOAc/Hex as eluent (101.5 mg, 94%). ¹H NMR (500 MHz, CDCl₃) δ 7.38-7.63 (m, 4H), 6.57 (d, J = 15.68 Hz, 1H), 6.27-6.45 (m, 1H), 3.73 (t, J = 4.62 Hz, 4H), 3.13 (dd, J = 1.38, 6.74 Hz, 2H), 2.49 (t, J = 4.64 Hz, 4H); ¹³C NMR (75 MHz, CDCl₃) δ 131.88, 129.11, 126.47, 125.57, 66.97, 61.25, 53.73; IR (film) ν_{max} 2958, 2806, 1615, 1325, 1117 cm⁻¹; HRMS(EI) calcd. for C₁₄H₁₆F₃NO, [M+H]⁺, 272.1218; found, 272.1212.



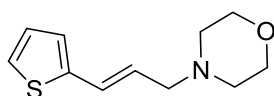
N-benzylcyclohex-2-en-1-amine (2i): prepared following the general procedure using Ni(COD)₂ (5.5 mg, 0.02 mmol, 0.05 eq), dppf (18 mg, 0.04 mmol, 0.1 eq), cyclohex-2-en-1-ol (40 mg, 0.4 mmol, 1 eq), benzylamine (64 mg, 0.6 mmol, 1.5 eq), and Ti(O-*i*-pr)₄ (0.08 ml, 1 eq, 4.879 M solution in toluene) in acetonitrile (100 μ l). Product was purified on column using pure hexane to 50% EtOAc/Hex as eluent (101.5 mg, 94%). Spectral data are in accordance with the reported values¹⁹.



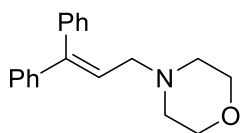
(E)-4-(4-phenylbut-3-en-2-yl)morpholine (2l): prepared following the general procedure using $\text{Ni}(\text{COD})_2$ (2.2 mg, 0.008 mmol, 0.02 eq), dppf (9 mg, 0.016 mmol, 0.04 eq), (E)-4-phenylbut-3-en-2-ol (60 mg, 0.4 mmol, 1 eq), morpholine (64 mg, 0.6 mmol, 1.5 eq), and $\text{Ti}(\text{O-}i\text{pr})_4$ (0.05 ml, 0.5 eq, 4.879 M solution in toluene) in acetonitrile (100 μl). Product was purified on column using pure hexane to 50% EtOAc/Hex as eluent (84.2 mg, 97%). Spectral data are in accordance with the reported values²⁰.



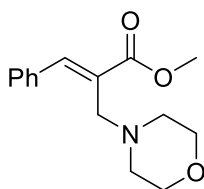
(E)-4-(1,3-diphenylallyl)morpholine (2m): prepared following the general procedure using $\text{Ni}(\text{COD})_2$ (5.5 mg, 0.02 mmol, 0.05 eq), dppf (18 mg, 0.04 mmol, 0.1 eq), (E)-1,3-diphenylprop-2-en-1-ol (84 mg, 0.4 mmol, 1 eq), morpholine (64 mg, 0.6 mmol, 1.5 eq), and $\text{Ti}(\text{O-}i\text{pr})_4$ (0.08 ml, 1 eq, 4.879 M solution in toluene) in acetonitrile (100 μl). Product was purified on column using pure hexane to 50% EtOAc/Hex as eluent (91 mg, 82%). Spectral data are in accordance with the reported values¹⁹.



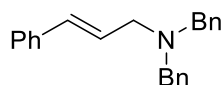
(E)-4-(3-(thiophen-2-yl)allyl)morpholine (2n): prepared following the general procedure using $\text{Ni}(\text{COD})_2$ (5.5 mg, 0.02 mmol, 0.05 eq), dppf (18 mg, 0.04 mmol, 0.1 eq), (E)-3-(thiophen-2-yl)prop-2-en-1-ol (56 mg, 0.4 mmol, 1 eq), morpholine (64 mg, 0.6 mmol, 1.5 eq), and $\text{Ti}(\text{O-}i\text{pr})_4$ (0.08 ml, 1 eq, 4.879 M solution in toluene) in acetonitrile (100 μl). Product was purified on column using pure hexane to 50% EtOAc/Hex as eluent (73 mg, 87%). Spectral data are in accordance with the reported values²¹.



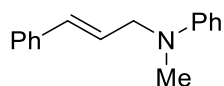
4-(3,3-diphenylallyl)morpholine(2o): prepared following the general procedure using $\text{Ni}(\text{COD})_2$ (5.5 mg, 0.02 mmol, 0.05 eq), dppf (18 mg, 0.04 mmol, 0.1 eq), 3,3-diphenylprop-2-en-1-ol (84 mg, 0.4 mmol, 1 eq), morpholine (64 mg, 0.6 mmol, 1.5 eq), and $\text{Ti}(\text{O-}i\text{pr})_4$ (0.08 ml, 1 eq, 4.879 M solution in toluene) in acetonitrile (100 μl). Product was purified on column using pure hexane to 50% EtOAc/Hex as eluent (33 mg, 30%). Spectral data are in accordance with the reported values²².



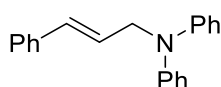
methyl (E)-2-(morpholinomethyl)-3-phenylacrylate (2p) : prepared following the general procedure using $\text{Ni}(\text{COD})_2$ (5.5 mg, 0.02 mmol, 0.05 eq), dppf (18 mg, 0.04 mmol, 0.1 eq), methyl 2-(hydroxy(phenyl)methyl)acrylate (77 mg, 0.4 mmol, 1 eq), morpholine (64 mg, 0.6 mmol, 1.5 eq), and $\text{Ti}(\text{O-}i\text{pr})_4$ (0.08 ml, 1 eq, 4.879 M solution in toluene) in acetonitrile (100 μl). Product was purified on column using pure hexane to 50% EtOAc/Hex as eluent (23mg, 30%). Spectral data are in accordance with the reported values¹².



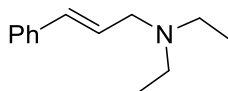
(E)-N,N-dibenzyl-3-phenylprop-2-en-1-amine (3a) : prepared following the general procedure using $\text{Ni}(\text{COD})_2$ (2.2 mg, 0.008 mmol, 0.02eq), dppf (9 mg, 0.016 mmol, 0.04 eq), cinnamyl alcohol (54 mg, 0.4 mmol, 1 eq), dibenzyl amine (118 mg, 0.6 mmol, 1.5 eq), and $\text{Ti}(\text{O-}i\text{pr})_4$ (0.08 ml, 1 eq, 4.879 M solution in toluene) in acetonitrile (100 μl). Product was purified on column using pure hexane to 50% EtOAc/Hex as eluent (112.5 mg, 90%). Spectral data are in accordance with the reported values²³.



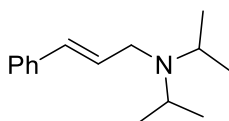
N-cinnamyl-N-methylaniline (3b): prepared following the general procedure using Ni(COD)₂ (2.2 mg, 0.008 mmol, 0.02 eq), dppf (9 mg, 0.016 mmol, 0.04 eq), cinnamyl alcohol (54 mg, 0.4 mmol, 1 eq), N-methyl aniline (64 mg, 0.6 mmol, 1.5 eq), and Ti(O-*i*-pr)₄ (0.08 ml, 1 eq, 4.879 M solution in toluene) in acetonitrile (100 μ l). Product was purified on column using pure hexane to 50% EtOAc/Hex as eluent (88.5 mg, 99%). Spectral data are in accordance with the reported values¹².



N-cinnamyl-N-phenylaniline (3c): prepared following the general procedure using Ni(COD)₂ (2.2 mg, 0.008 mmol, 0.02 eq), dppf (9 mg, 0.016 mmol, 0.04 eq), cinnamyl alcohol (54 mg, 0.4 mmol, 1 eq), diphenyl amine (100 mg, 0.6 mmol, 1.5 eq), and Ti(O-*i*-pr)₄ (0.08 ml, 1 eq, 4.879 M solution in toluene) in acetonitrile (100 μ l). Product was purified on column using pure hexane to 50% EtOAc/Hex as eluent (109 mg, 96%). Spectral data are in accordance with the reported values²⁴.

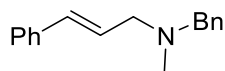


(E)-N,N-diethyl-3-phenylprop-2-en-1-amine (3d): prepared following the general procedure using Ni(COD)₂ (1.1 mg, 0.008 mmol, 0.005 eq), dppf (9 mg, 0.008 mmol, 0.01 eq), cinnamyl alcohol (54 mg, 0.4 mmol, 1 eq), diethylamine (44 mg, 0.6 mmol, 1.5 eq), and Ti(O-*i*-pr)₄ (0.05 ml, 0.5 eq, 4.879 M solution in toluene) in acetonitrile (100 μ l). Product was purified on column using pure hexane to 50% EtOAc/Hex as eluent (67 mg, 89%). Spectral data are in accordance with the reported values²⁵.

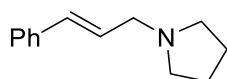


(E)-N,N-diisopropyl-3-phenylprop-2-en-1-amine (3e) : prepared following the general procedure using Ni(COD)₂ (2.2 mg, 0.008 mmol, 0.02 eq), dppf (9 mg, 0.016 mmol, 0.04 eq),

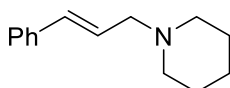
cinnamyl alcohol (54 mg, 0.4 mmol, 1 eq), diisopropyl amine (60 mg, 0.6 mmol, 1.5 eq), and $\text{Ti}(\text{O-}i\text{pr})_4$ (0.05 ml, 0.5 eq, 4.879 M solution in toluene) in acetonitrile (100 μl). Product was purified on column using pure hexane to 50% EtOAc/Hex as eluent (67 mg, 77%). Spectral data are in accordance with the reported values¹¹.



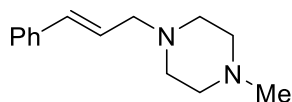
(E)-N-benzyl-N-methyl-3-phenylprop-2-en-1-amine (3f): prepared following the general procedure using $\text{Ni}(\text{COD})_2$ (2.2 mg, 0.008 mmol, 0.02 eq), dppf (9 mg, 0.016 mmol, 0.04 eq), cinnamyl alcohol (54 mg, 0.4 mmol, 1 eq), N-methyl-1-phenylmethanamine (73 mg, 0.6 mmol, 1.5 eq), and $\text{Ti}(\text{O-}i\text{pr})_4$ (0.05 ml, 0.5 eq, 4.879 M solution in toluene) in acetonitrile (100 μl). Product was purified on column using pure hexane to 50% EtOAc/Hex as eluent (91mg, 96%). Spectral data are in accordance with the reported values²⁶.



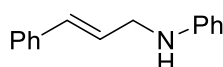
1-cinnamylpyrrolidine (3g): prepared following the general procedure using $\text{Ni}(\text{COD})_2$ (2.2 mg, 0.008 mmol, 0.02 eq), dppf (9 mg, 0.016 mmol, 0.04 eq), cinnamyl alcohol (54 mg, 0.4 mmol, 1 eq), pyrrolidine (43 mg, 0.6 mmol, 1.5 eq), and $\text{Ti}(\text{O-}i\text{pr})_4$ (0.05 ml, 0.5 eq, 4.879 M solution in toluene) in acetonitrile (100 μl). Product was purified on column using pure hexane to 50% EtOAc/Hex as eluent (69.6mg, 93%). Spectral data are in accordance with the reported values¹².



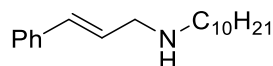
1-cinnamylpiperidine (3h): prepared following the general procedure using $\text{Ni}(\text{COD})_2$ (2.2 mg, 0.008 mmol, 0.02 eq), dppf (9 mgr, 0.016 mmol, 0.04 eq), cinnamyl alcohol (54 mg, 0.4mmol, 1 eq), piperidine (51 mg, 0.6 mmol, 1.5 eq), and $\text{Ti}(\text{O-}i\text{pr})_4$ (0.05 ml, 0.5 eq, 4.879 M solution in toluene) in acetonitrile (100 μl). Product was purified on column using pure hexane to 50% EtOAc/Hex as eluent (70.4 mg, 88%). Spectral data are in accordance with the reported values²⁷.



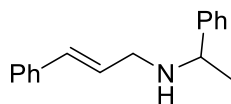
1-cinnamyl-4-methylpiperazine (3i): prepared following the general procedure using $\text{Ni}(\text{COD})_2$ (2.2 mg, 0.008 mmol, 0.02 eq), dppf (9 mgr, 0.016 mmol, 0.04 eq), cinnamyl alcohol (54 mg, 0.4 mmol, 1 eq), N-methyl piperazine (60 mgr, 0.6 mmol, 1.5 eq), and $\text{Ti}(\text{O-}i\text{pr})_4$ (0.05 ml, 0.5 eq, 4.879 M solution in toluene) in acetonitrile (100 μl). Product was purified on column using pure hexane to 50% EtOAc/Hex as eluent (82 mg, 95%). Spectral data are in accordance with the reported values²⁸.



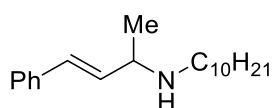
N-cinnamylaniline (3j): prepared following the general procedure using $\text{Ni}(\text{COD})_2$ (2.2 mg, 0.008 mmol, 0.02 eq), dppf (9 mg, 0.016 mmol, 0.04 eq), cinnamyl alcohol (54 mg, 0.4 mmol, 1 eq), aniline (56 mg, 0.6 mmol, 1.5 eq), and $\text{Ti}(\text{O-}i\text{pr})_4$ (0.05 ml, 0.5 eq, 4.879 M solution in toluene) in acetonitrile (100 μl). Product was purified on column using pure hexane to 50% EtOAc/Hex as eluent (63 mg, 76%). Spectral data are in accordance with the reported values²⁹.



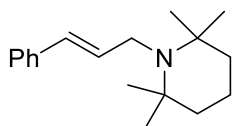
(E)-N-(4-phenylbut-3-en-2-yl)decan-1-amine (3k): prepared following the general procedure using $\text{Ni}(\text{COD})_2$ (1.1 mg, 0.008 mmol, 0.005 eq), dppf (9 mg, 0.008 mmol, 0.01 eq), cinnamyl alcohol (54 mgr, 0.4 mmol, 1 eq), decylamine (94 mg, 0.6 mmol, 1.5 eq), and $\text{Ti}(\text{O-}i\text{pr})_4$ (0.05 ml, 0.5 eq, 4.879 M solution in toluene) in acetonitrile (100 μl). Product was purified on column using pure hexane to 20% Methanol/EtOAc as eluent (46 mg, 40%). ^1H NMR (500 MHz, CDCl_3) δ 7.38 (d, $J = 4.04$ Hz, 2H), 7.31 (t, $J = 7.45$ Hz, 2H), 7.20-7.25 (m, 1H), 6.52 (d, $J = 7.45$ Hz, 1H), 6.26-6.35 (m, 1H), 3.29 (d, $J = 3.19$, 2H), 2.51 (t, $J = 7.55$ Hz, 1H), 1.48-1.57 (m, 1H), 1.19-1.33 (m, 8H), 0.85-0.95 (m, 2H); ^{13}C NMR (75 MHz, CDCl_3) δ 137.18, 134.62, 129.67, 128.52, 127.25, 136.25, 56.37, 47.74, 31.91, 30.36, 29.61, 29.58, 29.34, 27.46, 22.69, 22.12, 14.14; IR (film) ν_{max} 2924, 2359, 1733, 1456, 1273 Cm^{-1} ; HRMS(EI) calcd. for $\text{C}_{19}\text{H}_{31}\text{N}$, $[\text{M}+\text{H}]^+$, 274.2490; found, 274.2496.



(E)-3-phenyl-N-(1-phenylethyl)prop-2-en-1-amine(3l): prepared following the general procedure using Ni(COD)₂ (1.1 mg, 0.008 mmol, 0.005 eq), dppf (9 mg, 0.008 mmol, 0.01 eq), cinnamyl alcohol (54 mg, 0.4 mmol, 1 eq), 1-phenylethan-1-amine (73 mg, 0.6 mmol, 1.5 eq), and Ti(O-*i*-pr)₄ (0.05 ml, 0.5 eq, 4.879 M solution in toluene) in acetonitrile (100 μ l). Product was purified on column using pure hexane to 50% EtOAc/Hex as eluent (91 mg, 96%). Spectral data are in accordance with the reported values³⁰.

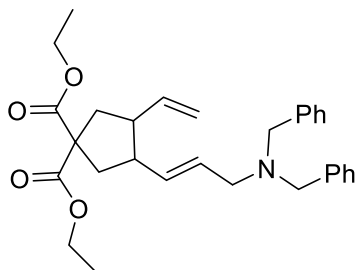


(E)-N-(4-phenylbut-3-en-2-yl)decan-1-amine (3m): prepared following the general procedure using Ni(COD)₂ (2.2 mg, 0.008 mmol, 0.02 eq), dppf (9 mg, 0.016 mmol, 0.04 eq), (E)-4-phenylbut-3-en-2-ol (60 mg, 0.4mmol, 1 eq), decylamine (94 mg, 0.6 mmol, 1.5 eq), and Ti(O-*i*-pr)₄ (0.05 ml, 0.5 eq, 4.879 M solution in toluene) in acetonitrile (100 μ l). Product was purified on column using 20% Methanol/EtOAc as eluent (86 mg, 75%). ¹H NMR (500 MHz, CDCl₃) δ 7.39 (d, *J* = 3.7 Hz, 2H), 7.31 (t, *J* = 7.64 Hz, 2H), 7.20-7.25 (m, 1H), 6.47 (d, *J* = 7.96 Hz, 1H), 6.09 (q, *J* = 7.89 Hz, 1H), 3.36 (quin, *J* = 6.68, 1H), 2.61-2.68 (m, 1H), 2.53-2.60 (m, 1H), 1.45-1.55 (m, 2H), 1.23-1.34 (m, 18H), 0.89 (t, *J* = 6.68 Hz, 3H); ¹³C NMR (75 MHz, CDCl₃) δ 137.18, 134.62, 129.67, 128.52, 127.25, 136.25, 56.37, 47.74, 31.91, 30.36, 29.61, 29.58, 29.34, 27.46, 22.69, 22.12, 14.14; IR (film) ν_{max} 2924, 2359, 1465, 1136, 964 cm^{-1} ; HRMS(EI) calcd. for C₂₀H₃₃N, [M+H]⁺, 288.2647; found, 288.2641.



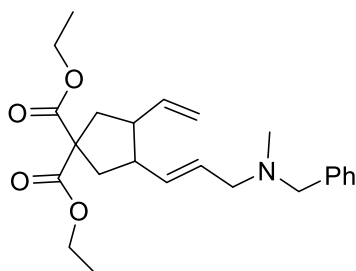
1-cinnamyl-2,2,6,6-tetramethylpiperidine (3n): prepared following the general procedure using Ni(COD)₂ (5.5 mg, 0.02 mmol, 0.05 eq), dppf (18 mg, 0.04 mmol, 0.1 eq), cinnamyl alcohol (54 mg, 0.4 mmol, 1 eq), 2,2,6,6-tetramethylpiperidine (85 mg, 0.6 mmol, 1.5 eq), and Ti(O-*i*-pr)₄ (0.08 ml, 1 eq, 4.879 M solution in toluene) in acetonitrile (100 μ l). Product was purified on column using pure hexane to 50% EtOAc/Hex as eluent (31 mg, 30%). Spectral

data are in accordance with the reported values³⁰.



diethyl(E)-3-(3-(dibenzylamino)prop-1-en-1-yl)-4-vinylcyclopentane-1,1

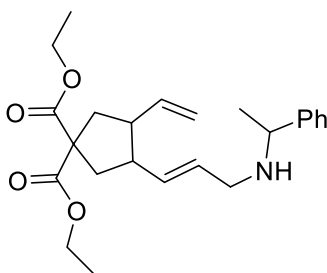
dicarboxylate(4a): prepared following the general procedure using Ni(COD)₂ (1.5 mg, 0.005 mmol, 0.05 eq), dppf (5.5 mg, 0.01 mmol, 0.1 eq), diethyl 2-((E)-4-hydroxybut-2-en-1-yl)-2-((E)-penta-2,4-dien-1-yl)malonate (30 mg, 0.1 mmol, 1 eq), dibenzylamine (24 mg, 0.12 mmol, 1.2 eq), and Ti(O-*i*-pr)₄ (0.03 ml, 1 eq, 4.879 M solution in toluene) in acetonitrile (50 μ l). The product was obtained as an unseparable mixture of two diastereomers (4.7:1) after purification on column using pure hexane to 70% EtOAc/Hex as eluent (37 mg, 78%). ¹H NMR (500 MHz, CDCl₃) δ 7.21-7.39 (m, 10H) 5.62-5.78 (m, 1H), 5.48-5.58 (m, 2H), 4.94-5.03 (m, 2H), 4.16-4.24 (m, 4H), 3.56 (s, 4H), 3.01 (2,2H), 2.74-2.84 (m, 2H), 2.44-2.58 (m, 2H), 2.14-2.26 (m, 2H), 1.20-1.31 (m, 6H); ¹³C NMR (300 MHz, CDCl₃) δ 172.74, 139.81, 138.67, 133.47, 128.84, 128.29, 128.19, 126.79, 115.24, 61.58, 61.52, 59.14, 57.63, 55.29, 50.10, 48.77, 47.31, 46.13, 39.19, 38.71, 14.09 ; IR (film) ν_{max} 2979, 2793, 1729, 1254, 1104 Cm^{-1} ; HRMS(EI) calcd. for C₃₀H₃₇NO₄, 476.2756; found, [M+H]⁺, 476.2753.



diethyl(E)-3-(3-(benzyl(methyl)amino)prop-1-en-1-yl)-4-vinylcyclopentane-1,1

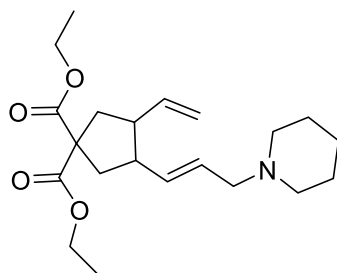
dicarboxylate(4b): prepared following the general procedure using Ni(COD)₂ (1.5 mg, 0.005 mmol, 0.05 eq), dppf (5.5 mg, 0.01 mmol, 0.1 eq), diethyl 2-((E)-4-hydroxybut-2-en-1-yl)-2-((E)-penta-2,4-dien-1-yl)malonate (30 mg, 0.1 mmol, 1 eq), N-methyl-1-phenylmethanamine (15 mg, 0.12 mmol, 1.2 eq), and Ti(O-*i*-pr)₄ (0.03 ml, 1 eq, 4.879 M solution in toluene) in acetonitrile (50 μ l). The product was obtained as an unseparable mixture of two diastereomers (8.8:1) after purification on column using pure hexane to 70% EtOAc/Hex as eluent (35 mg, 88%). ¹H NMR (500 MHz, CDCl₃) δ 5.63-5.78 (m, 1H), 5.45-5.55 (m, 2H), 4.94-5.00 (m, 2H),

4.19 (dq, $J = 7.15, 7.03$ Hz, 4H), 3.46 (d, $J = 2.85$ Hz, 2H), 2.94-2.97 (m, 2H), 2.72-2.84 (m, 2H), 2.47 (dd, $J = 13.89, 13.89$ Hz, 2H), 2.16-2.24 (m, 2H), 2.15 (s, 3H), 1.20-1.28 (m, 6H); ^{13}C NMR (75 MHz, CDCl_3) δ 172.69, 172.38, 139.06, 138.59, 133.69, 129.13, 128.19, 126.92, 115.21, 61.54, 61.47, 59.46, 59.14, 47.27, 46.06, 42.01, 39.17, 38.71, 29.72, 14.05; IR (film) ν_{max} 2925, 2359, 1730, 1453, 1254 cm^{-1} ; HRMS(EI) calcd. for $\text{C}_{24}\text{H}_{33}\text{NO}_4$, $[\text{M}+\text{H}]^+$, 400.2443; found, 400.2447



diethyl(E)-3-(3-((1-phenylethyl)amino)prop-1-en-1-yl)-4-vinylcyclopentane-1,1-

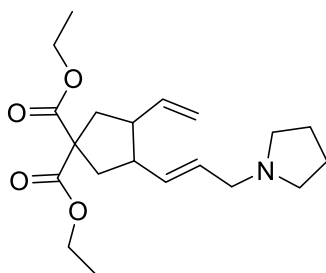
dicarboxylate (4c): prepared following the general procedure using $\text{Ni}(\text{COD})_2$ (1.5 mg, 0.005 mmol, 0.05 eq), dppf (5.5 mg, 0.01 mmol, 0.1 eq), diethyl 2-((E)-4-hydroxybut-2-en-1-yl)-2-((E)-penta-2,4-dien-1-yl)malonate (30 mg, 0.1 mmol, 1 eq), 1-phenylethan-1-amine (15 mg, 0.12 mmol, 1.2 eq), and $\text{Ti}(\text{O-}i\text{pr})_4$ (0.03 ml, 1 eq, 4.879 M solution in toluene) in acetonitrile (50 μl). The product was obtained as an unseparable mixture of two diastereomers (3.5:1) after purification on column using pure hexane to 70% EtOAc/Hex as eluent (36.3 mg, 91%). H NMR (500 MHz, CDCl_3) δ 7.20-7.36 (m, 5H), 5.59-5.75 (m, 1H), 5.29-5.55 (m, 2H), 4.92-5.08 (m, 2H), 4.12-4.23 (m, 4H), 3.78 (q, $J = 6.24$ Hz, 1H), 2.97-3.09 (m, 2H), 2.70-2.79 (m, 2H), 2.37-2.56 (m, 2H), 2.10-2.23 (m, 2H), 1.34 (d, $J = 6.44$ Hz, 3H), 1.24 (q, $J = 6.85$ Hz, 6H); ^{13}C NMR (75 MHz, CDCl_3) δ 172.68, 172.36, 145.47, 138.56, 138.51, 132.07, 129.47, 129.44, 128.41, 126.88, 126.66, 126.64, 115.33, 61.46, 59.07, 57.23, 49.80, 49.32, 48.39, 47.21, 45.89, 40.25, 39.95, 39.11, 39.04, 38.72, 24.16, 21.79, 21.48, 14.03; IR (film) ν_{max} 2924, 1728, 1254, 1178 cm^{-1} ; HRMS(EI) calcd. for $\text{C}_{24}\text{H}_{33}\text{NO}_4$, $[\text{M}+\text{H}]^+$, 400.2443; found, 400.2448.



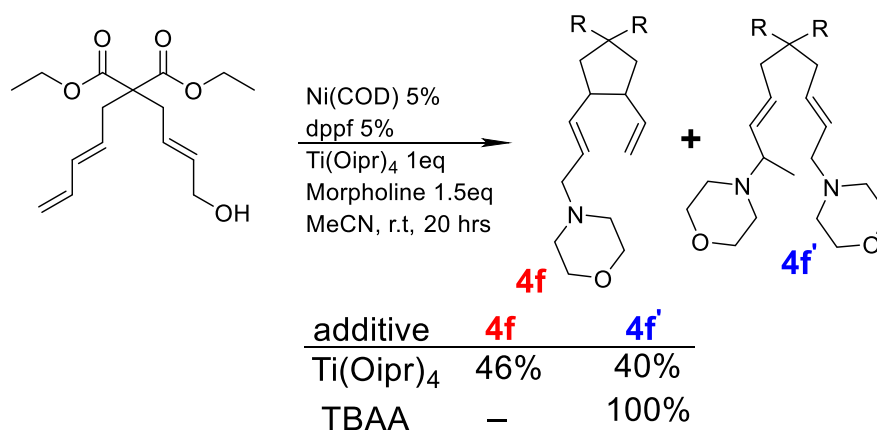
diethyl(E)-3-(3-(piperidin-1-yl)prop-1-en-1-yl)-4-vinylcyclopentane-1,1-

dicarboxylate(4d): prepared following the general procedure using $\text{Ni}(\text{COD})_2$ (1.5 mg, 0.005

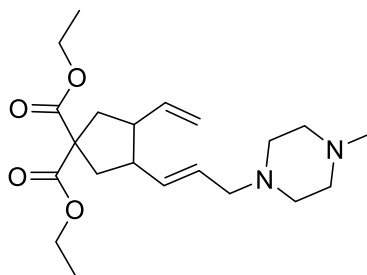
mmol, 0.05 eq), dppf (5.5 mg, 0.01 mmol, 0.1eq), diethyl 2-((E)-4-hydroxybut-2-en-1-yl)-2-((E)-penta-2,4-dien-1-yl)malonate (30 mg, 0.1 mmol, 1 eq), piperidine (11 mg, 0.12 mmol, 1.2 eq), and Ti(O-*i*pr)₄ (0.03 ml, 1 eq, 4.879 M solution in toluene) in acetonitrile (50 μl). The product was obtained as an unseparable mixture of two diastereomers (6:1) after purification on column using pure hexane to 70% EtOAc/Hex as eluent (29 mg, 88%). ¹H NMR (500 MHz, CDCl₃) δ 5.65-5.76 (m, 1H), 5.43-5.54 (m, 2H), 4.93-5.03 (m, 2H), 4.19 (q, *J* = 8.02 Hz, 4H), 2.89-2.93 (m, 2H), 2.71-2.83 (m, 2H), 2.46 (q, *J* = 7.14 Hz, 2H), 2.27-2.40 (s, 4H), 2.13-2.24 (m, 2H), 1.58 (t, *J* = 5.28 Hz, 4H), 1.42 (s, 2H), 1.24 (m, 6H); ¹³C NMR (75 MHz, CDCl₃) δ 172.66, 172.35, 138.57, 133.84, 127.60, 115.11, 114.39, 67.52, 61.51, 59.10, 54.30, 47.74, 47.20, 45.96, 48.39, 47.21, 45.89, 39.04, 38.72, 24.21, 21.48, 14.03; IR (film) ν_{max} 2933, 2795, 1730, 1443, 1254 cm⁻¹; HRMS(EI) calcd. for C₂₁H₃₃NO₄, [M+H]⁺, 364.2443; found, 364.2449.



diethyl (E)-3-(3-(pyrrolidin-1-yl)prop-1-en-1-yl)-4-vinylcyclopentane-1,1-dicarboxylate (4e): prepared following the general procedure using Ni(COD)₂ (1.5 mg, 0.005 mmol, 0.05 eq), dppf (5.5 mg, 0.01 mmol, 0.1 eq), diethyl 2-((E)-4-hydroxybut-2-en-1-yl)-2-((E)-penta-2,4-dien-1-yl)malonate (30 mg, 0.1 mmol, 1 eq), pyrrolidine (11 mg, 0.12 mmol, 1.2 eq), and Ti(O-*i*pr)₄ (0.03 ml, 1 eq, 4.879 M solution in toluene) in acetonitrile (50 μl). The product was obtained as an unseparable mixture of two diastereomers (4.8:1) after purification on column using pure hexane to 70% EtOAc/Hex as eluent (21 mg, 60%). ¹H NMR (500 MHz, CDCl₃) δ 5.63-5.76 (m, 1H), 5.47-5.60 (m, 2H), 4.94-5.07 (m, 2H), 4.19 (q, *J* = 7.19 Hz, 4H), 3.06-3.15 (m, 2H), 2.71-2.82 (m, 2H), 2.44 (s, 4H), 2.47 (q, *J* = 7.10 Hz, 2H), 2.14-2.24 (m, 2H), 1.78-1.83 (m, 4H), 1.21-1.28 (m, 6H); ¹³C NMR (300 MHz, CDCl₃) δ 172.38, 138.47, 115.24, 61.55, 59.08, 57.98, 53.72, 47.21, 45.95, 39.07, 38.66, 23.40, 14.03 ; IR (film) ν_{max} 2925, 2359, 1729, 1255, 1178 cm⁻¹; HRMS(EI) calcd. for C₂₀H₃₁NO₄, 350.2287; found, [M+H]⁺, 350.2281.



diethyl (E)-3-(3-morpholinoprop-1-en-1-yl)-4-vinylcyclopentane-1,1-dicarboxylate (4f): prepared following the general procedure using Ni(COD)₂ (3 mg, 0.01 mmol, 0.05 eq), dppf (11 mg, 0.02 mmol, 0.1 eq), diethyl 2-((E)-4-hydroxybut-2-en-1-yl)-2-((E)-penta-2,4-dien-1-yl)malonate (60 mg, 0.2 mmol, 1 eq), morpholine (30 mg, 0.3 mmol, 1.5 eq), and Ti(O-*i*-pr)₄ (0.05 ml, 1 eq, 4.879 M solution in toluene) in acetonitrile (50 μ l). The product was obtained as an unseparable mixture of two diastereomers (4:1) after purification on column using pure hexane to 70% EtOAc/Hex as eluent (33 mg, 46%). ¹H NMR (500 MHz, CDCl₃) δ 5.60-5.74 (m, 1H), 5.40-5.55 (m, 2H), 4.93-5.08 (m, 2H), 4.19 (q, J = 7.13 Hz, 4H), 3.70 (t, J = 4.64 Hz, 4H), 2.88-3.02 (m, 2H), 2.71-2.83 (m, 2H), 2.43-2.50 (m, 2H), 2.33-2.54 (m, 6H), 2.11-2.24 (m, 2H), 1.19-1.29 (m, 6H); ¹³C NMR (75 MHz, CDCl₃) δ 172.61, 172.32, 139.33, 138.48, 134.57, 126.77, 115.46, 115.24, 66.96, 61.55, 59.07, 53.66, 53.48, 49.92, 48.51, 47.21, 45.96, 40.21, 39.94, 39.05, 38.66, 29.69, 14.03; IR (film) ν_{max} 2926, 2806, 1729, 1453, 1257, 1118 cm^{-1} ; HRMS(EI) calcd. for C₂₀H₃₁NO₅, [M+H]⁺, 366.2236; found, 366.2231. **Product (4f')** was isolated as the byproduct of the reaction as a brown liquid (30 mg, 40%) using Methanol/Ethylacetate as eluent. (20%). ¹H NMR (500 MHz, CDCl₃) δ 5.52-5.65 (m, 1H), 5.41-5.52 (m, 2H), 5.29-5.41 (m, 2H), 4.16 (q, J = 7.18 Hz, 4H), 3.70 (s, 8H), 2.93 (d, J = 6.33 Hz, 2H), 2.75-2.85 (m, 2H), 2.53-2.65 (m, 4H), 2.30-2.52 (m, 8H), 1.20-1.30 (m, 6H), 1.12 (d, J = 6.47 Hz, 4H); ¹³C NMR (75 MHz, CDCl₃) δ 170.71, 170.66, 136.94, 130.97, 127.90, 125.45, 67.14, 66.94, 62.67, 61.25, 61.05, 57.58, 53.51, 50.55, 35.36, 17.93, 14.14; IR (film) ν_{max} 2958, 2807, 1731, 1453, 1265, 1200 cm^{-1} ; HRMS(EI) calcd. for C₃₀H₂₉N₃P, [M+H]⁺, 463.2172; found, 463.2175.



diethyl(E)-3-(3-(4-methylpiperazin-1-yl)prop-1-en-1-yl)-4-vinylcyclopentane-1,1

dicarboxylate (4g): prepared following the general procedure using Ni(COD)₂ (1.5 mg, 0.005 mmol, 0.05 eq), dppf (5.5 mg, 0.01 mmol, 0.1 eq), diethyl 2-((E)-4-hydroxybut-2-en-1-yl)-2-((E)-penta-2,4-dien-1-yl)malonate (30 mg, 0.1 mmol, 1 eq), N-methylpiperazine (15 mg, 0.12 mmol, 1.2 eq), and Ti(O-*i*-pr)₄ (0.03 ml, 1 eq, 4.879 M solution in toluene) in acetonitrile (50 μ l). The product was obtained as an unseparable mixture of two diastereomers (5.8:1) after purification on column using 10% MeOH/EtOAc as eluent (36.5 mg, 96%). ¹H NMR (500 MHz, CDCl₃) δ 5.60-5.78 (m, 1H), 5.46-5.55 (m, 2H), 4.90-5.06 (m, 2H), 4.19 (q, *J* = 7.10 Hz, 4H), 2.91-2.98 (m, 2H), 2.71-2.85 (m, 2H), 2.37-2.59 (m, 10H), 2.29 (s, 3H), 2.15-2.24 (m, 2H), 1.19-1.30 (m, 6H); ¹³C NMR (300 MHz, CDCl₃) δ 172.37, 138.55, 134.25, 127.25, 115.24, 61.57, 61.51, 60.07, 59.12, 55.11, 53.18, 52.93, 47.24, 46.05, 39.09, 38.71, 14.07 ; IR (film) ν_{max} 2934, 2794, 2359, 1730, 1456, 1256, 1178 cm^{-1} ; HRMS(EI) calcd. for C₂₁H₃₄N₂O₄, 379.2553; found, [M+H]⁺, 379.2557.

3.4 References

1. Allen, A. E.; MacMillan, D. W., Synergistic catalysis: a powerful synthetic strategy for new reaction development. *Chemical Science* **2012**, 3 (3), 633-658.
2. van der Vlugt, J. I., Cooperative catalysis with first-row late transition metals. *European Journal of Inorganic Chemistry* **2012**, 2012 (3), 363-375.
3. Tsuji, J., *Transition metal reagents and catalysts: innovations in organic synthesis*. John Wiley & Sons: 2002.
4. Tamaru, Y., Activation of allyl alcohols as allyl cations, allyl anions, and amphiphilic allylic species by palladium. *European Journal of Organic Chemistry* **2005**, 2005 (13), 2647-2656.
5. Sundararaju, B.; Achard, M.; Bruneau, C., Transition metal catalyzed nucleophilic allylic substitution: activation of allylic alcohols via π -allylic species. *Chemical Society Reviews* **2012**, 41 (12), 4467-4483.

6. Miyata, K.; Kutsuna, H.; Kawakami, S.; Kitamura, M., A Chiral Bidentate sp²-N Ligand, Naph-diPIM: Application to CpRu-Catalyzed Asymmetric Dehydrative C-, N-, and O-Alkylation. *Angewandte Chemie International Edition* **2011**, *50* (20), 4649-4653.
7. KumaráMishra, N.; HwanáKwak, J.; SuáKim, I., Cp* Rh (iii)-catalyzed C (sp³)-H alkylation of 8-methylquinolines in aqueous media. *Chemical Communications* **2017**, *53* (21), 3006-3009.
8. Schafroth, M. A.; Rummelt, S. M.; Sarlah, D.; Carreira, E. M., Enantioselective Iridium-Catalyzed Allylic Cyclizations. *Organic Letters* **2017**, *19* (12), 3235-3238.
9. Takeuchi, R.; Ue, N.; Tanabe, K.; Yamashita, K.; Shiga, N., Iridium complex-catalyzed allylic amination of allylic esters. *Journal of the American Chemical Society* **2001**, *123* (39), 9525-9534.
10. Evans, P. A.; Lai, K. W.; Zhang, H.-R.; Huffman, J. C., Regioselective and enantiospecific rhodium-catalyzed allylic amination with thymine: synthesis of a new conformationally rigid nucleoside. *Chemical Communications* **2006**, (8), 844-846.
11. Kita, Y.; Sakaguchi, H.; Hoshimoto, Y.; Nakauchi, D.; Nakahara, Y.; Carpentier, J. F.; Ogoshi, S.; Mashima, K., Pentacoordinated Carboxylate π -Allyl Nickel Complexes as Key Intermediates for the Ni-Catalyzed Direct Amination of Allylic Alcohols. *Chemistry—A European Journal* **2015**, *21* (41), 14571-14578.
12. Hirata, G.; Satomura, H.; Kumagae, H.; Shimizu, A.; Onodera, G.; Kimura, M., Direct Allylic Amination of Allylic Alcohol Catalyzed by Palladium Complex Bearing Phosphine–Borane Ligand. *Organic Letters* **2017**, *19* (22), 6148-6151.
13. Nazari, S. H.; Bourdeau, J. E.; Talley, M. R.; Valdivia-Berroeta, G. A.; Smith, S. J.; Michaelis, D. J., Nickel-Catalyzed Suzuki Cross Couplings with Unprotected Allylic Alcohols Enabled by Bidentate N-Heterocyclic Carbene (NHC)/Phosphine Ligands. *ACS Catalysis* **2017**, *8* (1), 86-89.
14. Zaitsev, K. V.; Bermeshev, M. V.; Karlov, S. S.; Oprunenko, Y. F.; Churakov, A. V.; Howard, J. A.; Zaitseva, G. S., Synthesis and structure of titanium alkoxides based on tetraphenyl substituted 2, 6-dimethanolpyridine moiety. *Inorganica Chimica Acta* **2007**, *360* (7), 2507-2512.
15. Suzuki, N.; Yoneyama, S.; Shiba, K.; Hasegawa, T.; Masuyama, Y., Synthesis of O, N, OP multidentate ligands and the formation of early–late heterobimetallic complexes. *Inorganica Chimica Acta* **2018**, *471*, 355-363.

16. Nazari, S. H.; Tiempos-Flores, N.; Forson, K. G.; Bourdeau, J. E.; Michaelis, D. J., C–N Bond Formation from Allylic Alcohols via Cooperative Nickel and Titanium Catalysis. *The Journal of Organic Chemistry* **2018**, *83* (17), 10646-10654.
17. Cazorla, C.; Billamboz, M.; Bricout, H.; Monflier, E.; Len, C., Green and Scalable Palladium-on-Carbon-Catalyzed Tsuji–Trost Coupling Reaction Using an Efficient and Continuous Flow System. *European Journal of Organic Chemistry* **2017**, *2017* (6), 1078-1085.
18. Woan, K.; Pyrgiotakis, G.; Sigmund, W., Photocatalytic carbon-nanotube–TiO₂ composites. *Advanced Materials* **2009**, *21* (21), 2233-2239.
19. Nishina, N.; Yamamoto, Y., Gold-catalyzed intermolecular hydroamination of allenes: First example of the use of an aliphatic amine in hydroamination. *Synlett* **2007**, *2007* (11), 1767-1770.
20. Park, K.; Lee, S., Additive-free decarboxylative coupling of cinnamic acid derivatives in water: Synthesis of allyl amines. *Organic Letters* **2015**, *17* (5), 1300-1303.
21. Xie, Y.; Hu, J.; Wang, Y.; Xia, C.; Huang, H., Palladium-catalyzed vinylation of aminals with simple alkenes: a new strategy to construct allylamines. *Journal of the American Chemical Society* **2012**, *134* (51), 20613-20616.
22. Goldfogel, M. J.; Roberts, C. C.; Meek, S. J., Intermolecular hydroamination of 1, 3-dienes catalyzed by bis (phosphine) carbodicarbene–rhodium complexes. *Journal of the American Chemical Society* **2014**, *136* (17), 6227-6230.
23. Wang, M.; Xie, Y.; Li, J.; Huang, H., letter Palladium-Catalyzed Direct Amination of Allylic Alcohols at Room Temperature. *Synlett* **2014**, *25*, 2781-2786.
24. Shimizu, Y.; Obora, Y.; Ishii, Y., Intermolecular Aerobic oxidative allylic amination of simple alkenes with diarylamines catalyzed by the Pd (OCOCF₃)₂/NPMoV/O₂ system. *Organic Letters* **2010**, *12* (6), 1372-1374.
25. Chardon, A.; Mohy El Dine, T.; Legay, R.; De Paolis, M.; Rouden, J.; Blanchet, J., Borinic Acid Catalysed Reduction of Tertiary Amides with Hydrosilanes: A Mild and Chemoselective Synthesis of Amines. *Chemistry–A European Journal* **2017**, *23* (9), 2005-2009.
26. Jing, J.; Huo, X.; Shen, J.; Fu, J.; Meng, Q.; Zhang, W., Direct use of allylic alcohols and allylic amines in palladium-catalyzed allylic amination. *Chemical Communications* **2017**, *53* (37), 5151-5154.
27. Horn, P. A.; Braun, R. K.; Isoppo, V. G.; Costa, J. S. d.; Lüdtkke, D. S.; Moro, A. V., Combining Copper-Catalyzed Hydroboration with Palladium-Catalyzed Suzuki Coupling for

the One-pot Synthesis of Arylallylamines under Micellar Conditions. *Advanced Synthesis & Catalysis* **2017**, 359 (13), 2322-2328.

28. Yu, H.; Gao, B.; Hu, B.; Huang, H., Charge-Transfer Complex Promoted C–N Bond Activation for Ni-Catalyzed Carbonylation. *Organic Letters* **2017**, 19 (13), 3520-3523.

29. Takale, B. S.; Tao, S. M.; Yu, X. Q.; Feng, X. J.; Jin, T.; Bao, M.; Yamamoto, Y., Exclusive Chemoselective Reduction of Imines in the Coexistence of Aldehydes Using AuNPore Catalyst. *Organic Letters* **2014**, 16 (9), 2558-2561.

30. Walker, W. K.; Anderson, D. L.; Stokes, R. W.; Smith, S. J.; Michaelis, D. J., Allylic Aminations with Hindered Secondary Amine Nucleophiles Catalyzed by Heterobimetallic Pd–Ti Complexes. *Organic Letters* **2015**, 17 (3), 752-755.

Chapter 4 Boron-Templated Dimerization of Allylic Alcohols Catalyzed by Strong Acid: Formal Difunctionalization Of Alkenes

4.1 Introduction

Cascade reactions constitute a powerful strategy for rapid assembly of complex structures starting from small and simple precursors. Importantly, these domino reactions are easily triggered under mild and environmentally friendly conditions using simple organocatalysts, Lewis acids, Lewis base, or even Brønsted acids¹. Economy wise, these reactions are desirable to the pharmaceutical industry as they reduce both the production cost as well as waste accumulation². However, the design and execution of efficient cascade reactions is challenging due to the requirement that several reactions proceed in concert without generating byproducts from reactive intermediates³. The application of cascade reactions in natural product synthesis has opened new doors for the synthesis of polycyclic structures. A striking example of domino reactions in natural product synthesis can be seen in the total synthesis of (±)-Progesterone using trifluoroacetic acid to promote the polyolefin cyclization⁴ (Figure 4.1).

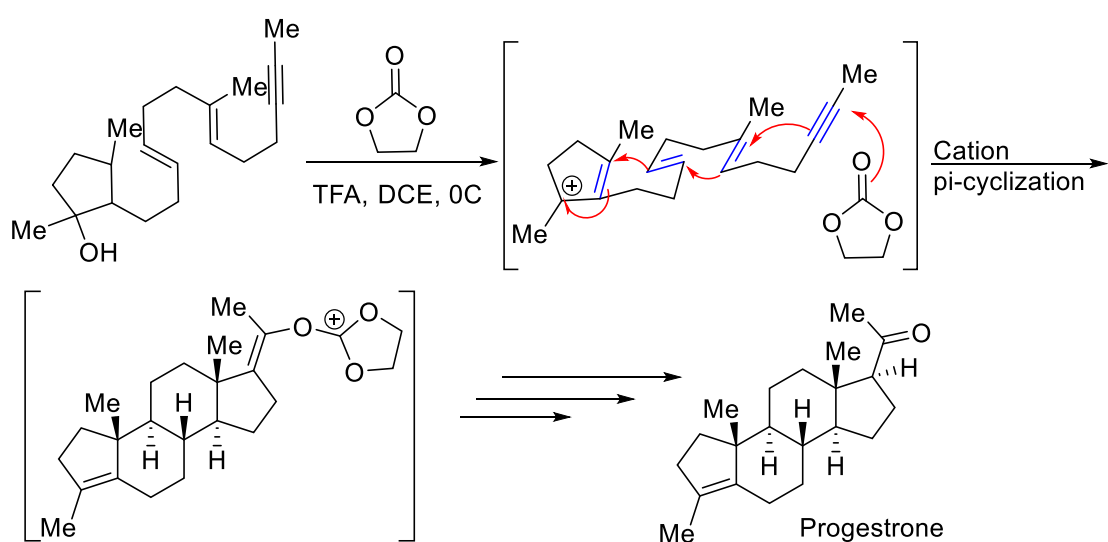


Figure 4.1 Cascade polyolefine cyclization in the total synthesis of progesterone.

Since the discovery of the Friedel-Crafts reaction, efforts have focused on development of new methods that extend applications of Lewis acid catalyzed reactions for the synthesis of more challenging structures⁵. Importantly, efforts have been directed towards enantioselective

transformations where an easily available chiral Lewis acid induces chirality. A quintessential example of Lewis acid catalyzed enantioselective cascade reactions was reported by Rueping⁶ and coworkers in 2008 (Figure 4.2). Using chiral phosphoric acid, they were able to obtain a variety of tailored tetrahydropyridines with high yields and excellent enantiomeric excess. The key to high enantioselectivity in this reaction is the involvement of

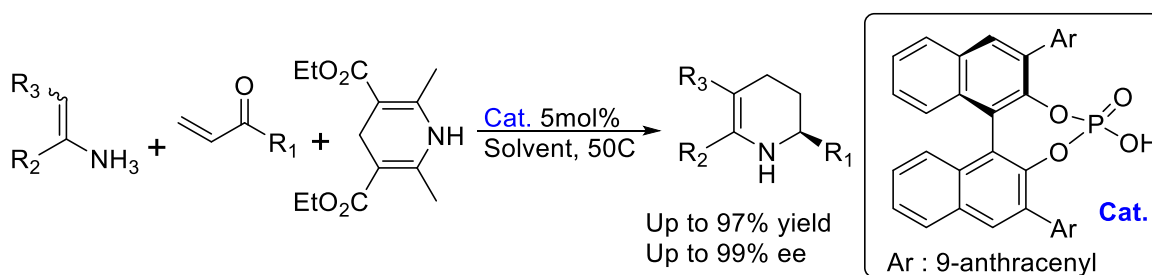


Figure 4.2 Brønsted acid catalyzed cascade reaction for the synthesis of tetrahydropyridine

the catalyst in every step of the reaction. Carbon-carbon bond formation is the bedrock reaction in organic chemistry for construction of complex structures⁷. Although there are numerous transition-metal-catalyzed transformations that facilitate these reactions, the desired transition-metal-free methods are limited. As an extension of Friedel-Crafts reactions, a variety of transformations including annulations⁸⁻⁹, ring openings¹⁰, arylations¹¹, cycloadditions¹², ene reactions¹³ and many C-hetero ester formation¹⁴ reactions have been reported. A significant advance in this area was made when trifluoromethanesulfonic acid was employed as a Brønsted acid catalyst. The preference of triflic-acid-catalyzed reactions over other methods under otherwise identical conditions is rooted on its chemoselectivity, broader substrate scope,

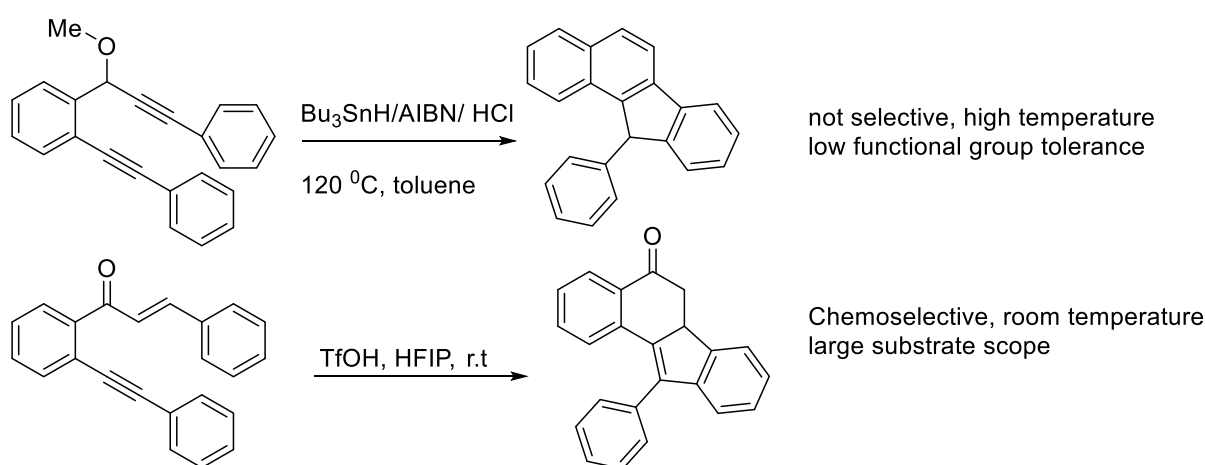


Figure 4.3 Comparison of two different strategies in cyclizations; Radical Cascade (A) Brønsted acid catalyzed (B)

and higher yields under milder reaction conditions¹⁵ (Figure 4.3). Highly substituted 2-cyanoamides are an important class of drug candidates and their synthesis requires harsh reaction conditions under expensive transition metal catalysts¹⁶. Reported procedures for their synthesis employ gold¹⁷, ruthenium¹⁸, and silver¹⁹ as the catalyst at elevated temperatures to hydrate bis-nitriles to 2-cyano amides. The Dong group also reported a copper catalyzed strategy for this transformation²⁰ (Figure 4.4 A). Despite the competitive cost of copper to Brønsted acids, the reaction still suffers from over-hydration of the amide to the acid by product. Also, the copper-catalyzed conditions and other transition metal-catalyzed reaction conditions suffer from low functional group tolerance, the necessity of air free conditions, and harsh reaction conditions. The first triflic-acid-catalyzed synthesis of these compounds was reported by Suryavanashi and coworkers where they were able to perform economical tandem reactions that show great substrate scope and excellent diastereoselectivity¹⁶ (Figure 4.4 B).

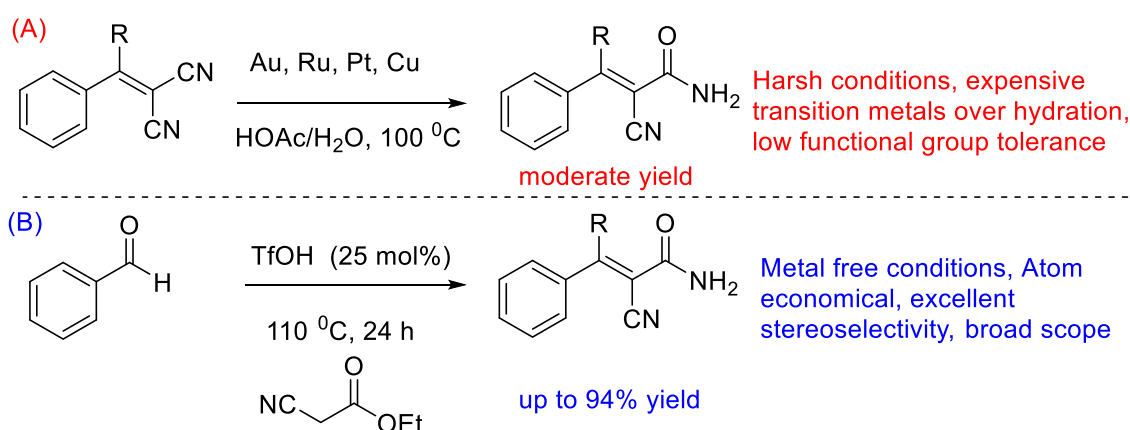


Figure 4.4 Comparison of the strategies towards the synthesis of 2-cyanoacrylamide; (A) Transition meta catalyzed hydration reaction. (B) Brønsted acid catalyzed tandem coupling hydrolysis

Recent advances in Brønsted acid-catalyzed transformations include C(sp³)-H functionalization. A striking example is shown in the work of Akyiama who reported a highly diastereoselective double C(sp³)-H functionalization strategy for the synthesis of polycyclic pyrans²¹ (Figure 4.5). In this process, a [1,5]-[1,5]-hydride shift occurred successively to afford tricyclic fused pyran derivatives in excellent chemical yields with excellent diastereoselectivities (up to >20 : 1). The key to this reaction was the introduction of two methyl groups at the benzylic position, which was effective in both hydride shift processes: (1) the Thorpe–Ingold effect for the first hydride shift and (2) conformational control in the second hydride shift. In the Michaelis laboratory, we are developing a new class of Brønsted acid-catalyzed dimerizations of allyl alcohols in the context of natural product synthesis

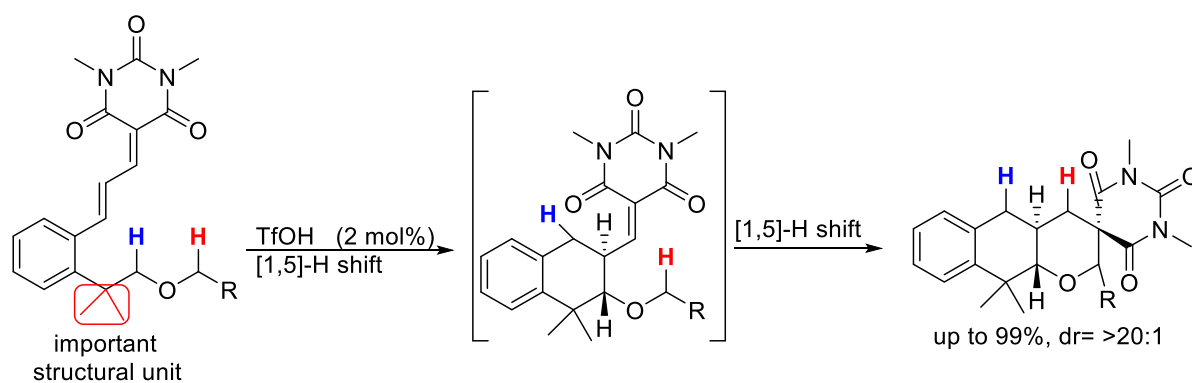


Figure 4.5 Double C(SP³)-H bond functionalization in alkyl phenylether derivatives

(Figure 4.6a). This transformation represents an efficient tandem strategy for allyl alkoxylation of a double bond where C-C and C-O bonds are forged in a single step (Figure 4.6 B). In this process, we believe the phenyl boronic acid serves to template two olefins and enable selective dimerization. The boronic acid also serves as the source of hydroxyl group for C-O bond forming step. This chapter will describe the discovery and optimization of this new acid-catalyzed tandem reaction and explore the substrate scope of this new transformation. Importantly, this dimerization of allylic alcohols provides a new route to the core structure of (+)-Wutaienin²² and other polyol natural products^{23, 24} (Figure 4.6b).

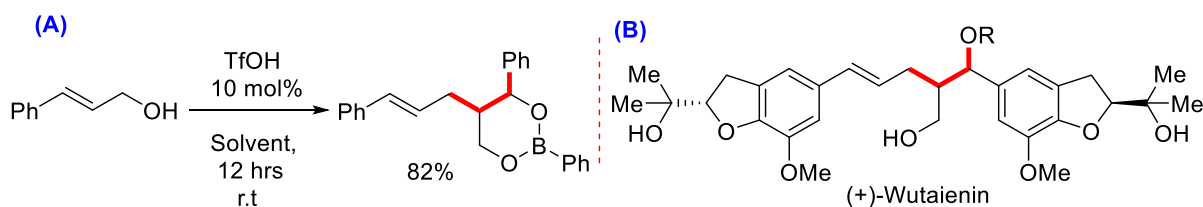


Figure 4.6 Bronsted acid catalyzed dimerization of allyl alcohol (A) Application in natural product synthesis (B)

Keywords: Cascade reaction, Acid catalyzed cyclization, dimerization, Cinnamyl alcohol

4.2 Results and Discussion

During the course of our studies on copper catalyzed allylic arylation, we noticed the formation of a new compound in the crude mixture. A mixture of cinnamyl alcohol (1eq) and phenyl boronic acid (1.5 eq) were exposed to Cu(OTf)₂ (10 mol%) and dppf (dppf = 1,1'-bis(diphenylphosphino)ferrocene, 10 mol%) in toluene as a solvent and a mixture of two products were obtained in total yield of 35%. Identification techniques including NMR, Mass,

and IR confirmed the presence of three phenyl rings and a boron atom in the structure. Further studies also confirmed the presence of two chiral centers and a cyclic chain in the structure. X-ray analysis of a single crystal of the product confirmed our analysis and the proposed structure (Figure 4.7). Importantly, this transformation proceeds with high diastereoselectivity (8:1), giving preferentially the diastereomer shown. Having established the structure of our product, we next sought to optimize the reaction for yield and diastereoselectivity.

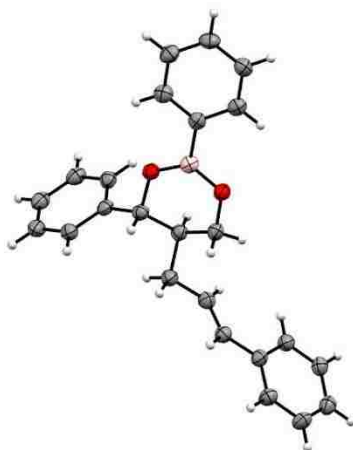
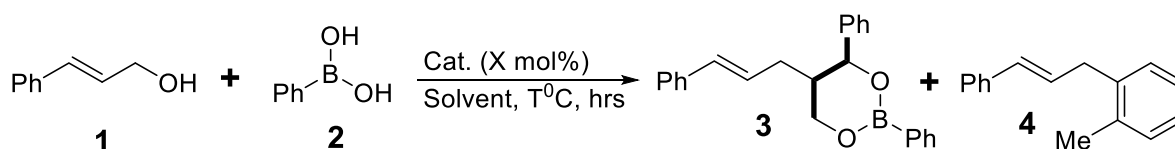


Figure 4.7 *Crystal structure of the dimerization product*

Our optimization studies are presented in Table 4.1. Using 2 equiv of the cinnamyl alcohol and 1 equiv of the phenyl boronic acid improved the yield to 42% (Table 4.1 entry 1). Increasing the amount of the cinnamyl alcohol to 2.5 or 3 equivalents did not improve the yield (entries 2 and 3). Also, various ligand structures including bidentate and monodentate phosphines were explored. While other bidentate ligands with different bite angles totally shut down the reaction, triphenyl phosphine gave the same results (entry 4-8). We also investigated other copper sources and found that the reaction only proceeded in the presence of copper triflate (entries 9-13). Based on these results, we wondered if $\text{Cu}(\text{OTf})_2$ was acting as a source of triflic acid and if triflic acid was indeed the catalyst for the reaction. Indeed, when trifluoromethanesulfonic acid was used as a catalyst, the same product was obtained even at room temperature with dramatic increase in yield (entry 14). By switching the solvent to dichloroethane and increasing the concentration of the solution, the yield increased even more (entry 15). Heteroatom-containing solvents including acetonitrile, THF, dioxane, and DMF were found to suppress formation of product **3** due to the acid-leveling effect of these solvents. (entries 16–19). Also, our studies revealed that the reaction is not as efficient when the catalyst loading of triflic acid is decreased (entry 20).

Our mechanistic hypothesis for this transformation is depicted in Figure 4.8. We believe that the reaction starts by double esterification of the phenyl boronic acid with cinnamyl alcohol. Protonation of one of the boron ester oxygens is then followed by attack of the other

Table 4.1 Optimization studies of dimerization of allylic alcohols



Entry ^a	Cat (mol%)	Ligand	Solvent	T (°C)	Time (h)	Yield (3)	Yield (4)
1	Cu(OTf) ₂ (10)	Dppf (10)	Toluene	60	16	42	20
2 ^b	Cu(OTf) ₂ (10)	Dppf (10)	Toluene	60	16	40	20
3 ^c	Cu(OTf) ₂ (10)	Dppf (10)	Toluene	60	16	43	20
4	Cu(OTf) ₂ (10)	BINAP	Toluene	60	16	-	20
5	Cu(OTf) ₂ (10)	dppb	Toluene	60	16	-	32
6	Cu(OTf) ₂ (10)	dppe	Toluene	60	16	-	20
7	Cu(OTf) ₂ (10)	PPh ₃	Toluene	60	16	42	20
8	CuCl ₂ (10)	dppf	Toluene	60	16	-	20
9	Cu(OAc) ₂ (10)	dppf	Toluene	60	16	-	25
10	CuI (10)	dppf	Toluene	60	16	-	23
11	Cu(SO ₄) ₂ (10)	dppf	Toluene	60	16	-	20
12	CuCN (10)	dppf	Toluene	60	16	-	18
13	Cu(acac) ₂ (10)	dppf	Toluene	60	16	-	19
14	TfOH (10)	-	Toluene	r.t	12	66	20
15	TfOH (10)	-	DCE	r.t	12	83	-
16	TfOH (10)	-	MeCN	r.t	12	-	-
17	TfOH (10)	-	THF	r.t	12	-	-
18	TfOH (10)	-	Dioxane	r.t	12	-	-
19	TfOH (10)	-	DMF	r.t	12	-	-
20	TfOH (5)	-	DCE	r.t	12	30	-

^aReactions run with 1 mmol 1, 0.5 mmol Phenylboronic acid, and 10mol% of catalyst in toluene(0.06M); Isolated yields after chromatography was reported. ^b2.5 equivalent of cinnamyl alcohol was used. ^c3 equivalent of cinnamyl alcohol was used.

alkene onto the protonated ether in an S_N^{2'}-type displacement of the boronic ester. The resulting benzylic carbocation is then trapped by the free boronic acid oxygen that was liberated

in the first cyclization step (Figure 4.8). To test this hypothesis, we synthesized the phenyl boronic acid bis cinnamyl ester and found that when treated with acid, the boronic ester converted cleanly to the dimerized product. Thus, we believe that the boronic acid is necessary for the transformation to occur because it templates the two cinnamyl alcohols and enables the

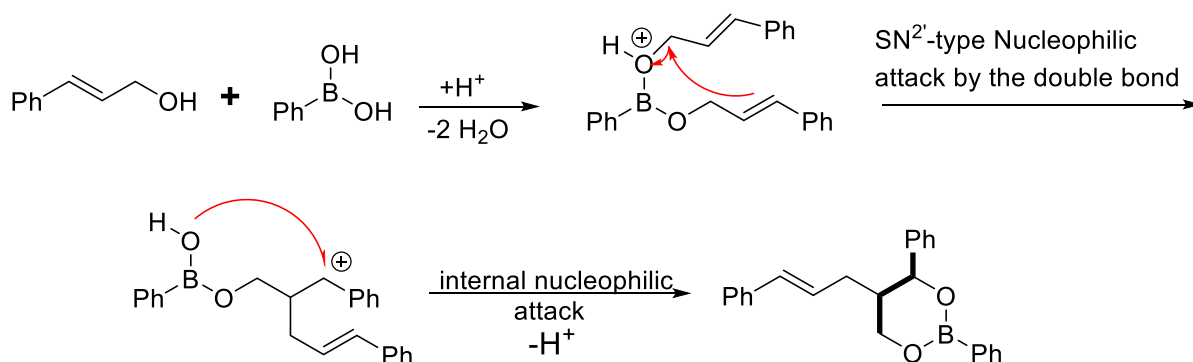


Figure 4.8 Plausible mechanism of acid catalyzed dimerization of cinnamyl alcohols

acid-catalyzed cyclization to occur. With optimized reaction conditions in hand, we next sought to demonstrate the functional group tolerance of the reaction. A library of electron-donating and electron-withdrawing groups on the phenyl ring of the cinnamyl alcohol were subjected to the reaction conditions (Figure 4.9). Although in each case the product was obtained with moderate to good yield, slight increase in the catalyst loading and temperature were necessary for the electron-withdrawing functional groups (**3a-3d**). While dimethyl-substituted allylic alcohol was amenable to the reaction condition and produced the desired product in moderate yield (**3n**), the diphenyl-substituted derivative did not show any reactivity due to the

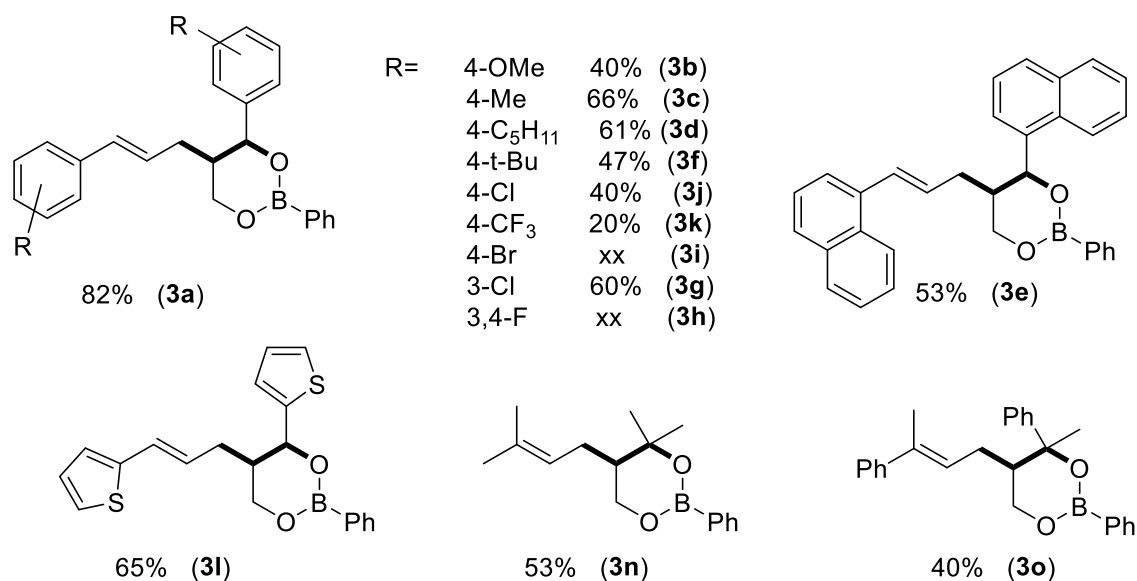


Figure 4.9 Substrate scope of dimerization of various allyl alcohols

high steric hinderance (**3f**). By replacing one of the phenyl groups on the double bond with a methyl group, the product was obtained with slightly lower yield indicating the importance of sterics (**30**). The applicability of our method was also tested for substrates containing various heteroatoms. Importantly, thiophene-containing allyl alcohol formed the dimer product in high yield (**31**). The cyclic boronic ester product obtained through this new acid-catalyzed transformation could prove to be a valuable intermediate in chemical synthesis. For example, the cyclic boronic ester structure represents a fully protected diol structure. In fact, we found that the free diol could be obtained by hydrolysis of the boronic ester under basic conditions (Figure 4.10). This hydrolysis reaction proceeds efficiently with various substrates to give the diol in good yield. Current efforts on this project include further exploration of the substrate scope of the reaction and applying this method to the total synthesis of (+)-Wutaienin. We are also currently investigating the possibility of incorporating chiral boronic acids as a way to induce enantioselectivity in the reaction through a diastereoselective process. If we observe high diastereoselectivity in the transformation, this will confirm the importance of the boronic acid in templating the two cinnamyl alcohols and enabling the cyclization reaction.

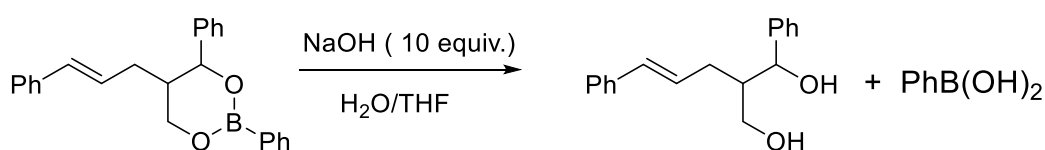


Figure 4.10 Hydrolysis of the cyclic boronic ester product to diol

In conclusion, we have developed a new method for selective dimerization of allylic alcohols to give cyclic boronic ester products. The boronic acid starting material is essential for the reaction and based on mechanistic studies, templates the two cinnamyl alcohols and enables the selective transformation. This new reaction represents a formal alkoxy allylation of a double bond where new C–C and C–O bond are formed in a single synthetic step. This difunctionalization reaction of alkenes could find much application in the synthesis of 1,3-diol-containing natural products.

4.3 References

1. Nicolaou, K.; Edmonds, D. J.; Bulger, P. G., Cascade reactions in total synthesis. *Angewandte Chemie International Edition* **2006**, *45* (43), 7134-7186.

2. Trost, B. M., Atom economy—a challenge for organic synthesis: homogeneous catalysis leads the way. *Angewandte Chemie International Edition in English* **1995**, *34* (3), 259-281.
3. Robinson, R., LXIII.—A synthesis of tropinone. *Journal of the Chemical Society, Transactions* **1917**, *111*, 762-768.
4. Johnson, W. S.; Gravestock, M. B.; McCarry, B. E., Acetylenic bond participation in biogenetic-like olefinic cyclizations. II. Synthesis of dl-progesterone. *Journal of the American Chemical Society* **1971**, *93* (17), 4332-4334.
5. Anderson, K. W.; Tepe, J. J., Trifluoromethanesulfonic acid catalyzed Friedel–Crafts acylation of aromatics with β -lactams. *Tetrahedron* **2002**, *58* (42), 8475-8481.
6. Rueping, M.; Antonchick, A. P., A highly enantioselective brønsted acid catalyzed reaction cascade. *Angewandte Chemie International Edition* **2008**, *47* (31), 5836-5838.
7. Li, C. J., Organic reactions in aqueous media—with a focus on carbon-carbon bond formation. *Chemical Reviews* **1993**, *93* (6), 2023-2035.
8. Nanda, L. N.; Rangari, V. A., TfOH catalyzed synthesis of 1-substituted tetrahydrocarbazoles. *Tetrahedron Letters* **2018**, *59* (33), 3194-3197.
9. Jacob, A.; Roy, T.; Kaicharla, T.; Biju, A. T., Metal-Free, Brønsted Acid-Catalyzed Formal [3+ 2] Annulation of Quinone Monoacetals with 2-Naphthols. *The Journal of organic chemistry* **2017**, *82* (20), 11269-11274.
10. Mothe, S. R.; Chan, P. W. H., Highly efficient synthesis of Tri-and tetrasubstituted conjugated enynes from brønsted acid catalyzed alkoxylation of 1-cyclopropylprop-2-yn-1-ols with alcohols. *The Journal of Organic Chemistry* **2009**, *74* (16), 5887-5893.
11. Laali, K. K.; Sarca, V. D.; Okazaki, T.; Brock, A.; Der, P., Triflic acid-catalyzed adamantylation of aromatics in [BMIM][OTf] ionic liquid; synthetic scope and mechanistic insight. *Organic & Biomolecular Chemistry* **2005**, *3* (6), 1034-1042.
12. Zhou, H.; Zeng, X.; Ding, L.; Xie, Y.; Zhong, G., Triflic Acid Catalyzed Formal [3+ 2] Cycloaddition of Donor–Acceptor Oxiranes and Nitriles: A Facile Access to 3-Oxazolines. *Organic Letters* **2015**, *17* (10), 2385-2387.
13. Snider, B. B., Lewis-acid catalyzed ene reactions. *Accounts of Chemical Research* **1980**, *13* (11), 426-432.
14. Kuci ski, K.; Hreczycho, G., S-Acetylation of thiols mediated by triflic acid: a novel route to thioesters. *Organic Process Research & Development* **2018**, *22* (4), 489-493.

15. Mandal, M.; Balamurugan, R., Triflic acid-Mediated Expedient Synthesis of Benzo [a] fluorenes and Fluorescent Benzo [a] fluorenones. *Advanced Synthesis & Catalysis* **2018**, *360* (7), 1453-1465.
16. Rupanwar, B. D.; Chavan, S. S.; Shelke, A. M.; Suryavanshi, G. M., Triflic acid-catalyzed metal-free synthesis of (E)-2-cyanoacrylamides and 3-substituted azetidine-2, 4-diones. *New Journal of Chemistry* **2018**, *42* (8), 6433-6440.
17. Liu, Y. M.; He, L.; Wang, M. M.; Cao, Y.; He, H. Y.; Fan, K. N., A General and Efficient Heterogeneous Gold-Catalyzed Hydration of Nitriles in Neat Water under Mild Atmospheric Conditions. *ChemSusChem* **2012**, *5* (8), 1392-1396.
18. Yamaguchi, K.; Matsushita, M.; Mizuno, N., Efficient hydration of nitriles to amides in water, catalyzed by ruthenium hydroxide supported on alumina. *Angewandte Chemie International Edition* **2004**, *43* (12), 1576-1580.
19. Mitsudome, T.; Mikami, Y.; Mori, H.; Arita, S.; Mizugaki, T.; Jitsukawa, K.; Kaneda, K., Supported silver nanoparticle catalyst for selective hydration of nitriles to amides in water. *Chemical Communications* **2009**, (22), 3258-3260.
20. Xin, X.; Xiang, D.; Yang, J.; Zhang, Q.; Zhou, F.; Dong, D., Homogeneous and Stereoselective Copper (II)-Catalyzed Monohydration of Methylenemalononitriles to 2-Cyanoacrylamides. *The Journal of Organic Chemistry* **2013**, *78* (23), 11956-11961.
21. Mori, K.; Umehara, N.; Akiyama, T., Highly diastereoselective synthesis of tricyclic fused-pyrans by sequential hydride shift mediated double C (sp³)-H bond functionalization. *Chemical Science* **2018**, *9* (37), 7327-7331.
22. Takahashi, M.; Suzuki, N.; Ishikawa, T.; Huang, H.-Y.; Chang, H.-S.; Chen, I.-S., Unprecedented 8, 9'-Neolignans: Enantioselective Synthesis of Possible Stereoisomers for Structural Determination. *Journal of Natural Products* **2014**, *77* (12), 2585-2589.
23. Cai, Y.; Jalan, A.; Kubosumi, A.; Castle, S.L., Microwave-promoted tin-free iminyl radical cyclization with TEMPO trapping: A practical synthesis of 2-acylpyrroles. *Organic Letters* **2015**, *17* (3), 488-491.
24. Brownlee, B.; Bahari, M.; Harb, J.; Claussen, J.C.; Iverson, B., Electrochemical Glucose Sensors Enhanced by Methyl Viologen and Vertically Aligned Carbon Nanotube Channels. *ACS Appl. Mater. Interfaces*, **2018**, *10* (34), 28351-28360.

Chapter 5 New Ligand Design for Bimetallic Catalysis

5.1 Introduction

C–H functionalization is a sustainable alternative to a wide range of synthetic transformations as it streamlines traditional strategies and obviates the need of pre-functionalization steps¹. However, the strong nature of C–H bonds in organic molecules has limited their manipulation as it usually requires state of the art catalytic systems for an efficient transformation². Initial discoveries on C(sp²)-H activation included the reaction of arenes and heteroarenes with transition metals. Volhard reported isolation of chloromercury thiophene in 1892 from a reaction between thiophene and mercury (II) chloride³ (Figure 5.1 A).

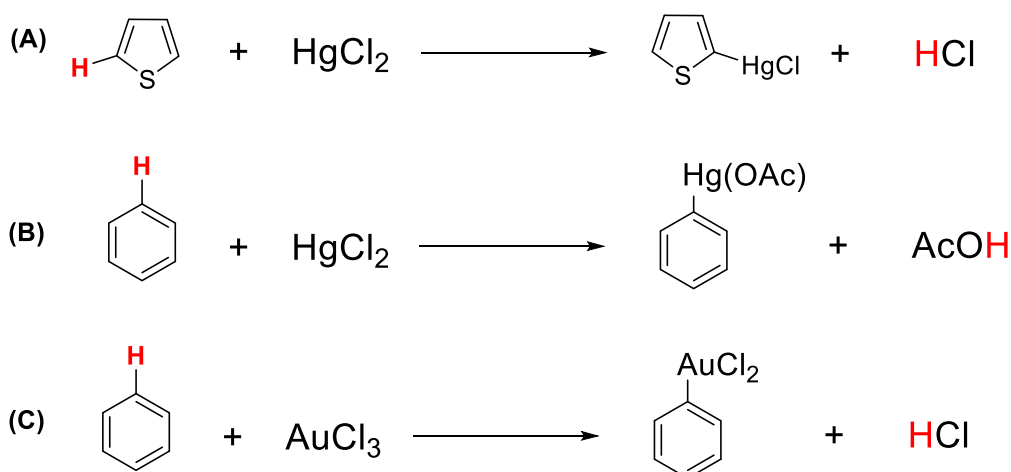


Figure 5.1 Early examples of C–H activation

A few years later, several aryl mercury acetates and aryl gold chlorides were synthesized from the reactions between benzene and mercury acetate and gold chloride, respectively⁴⁻⁵ (Figure 5.1 B, C). Distinguishing a C–H bond among numerous bonds of the same energy level is the biggest challenge in C–H bond activation strategy². Depending on the substrates used in the reaction and the catalyst, selective C–H functionalization reactions can occur either via substrate control⁶ (Sterics or a directing effect) or catalyst control⁷. The former approach, which has been widely investigated over the last decade, relies on the innate propensity of the substrate to bind a catalyst at a certain position and enable selective reaction with proximal C–H bonds. In the later approach, the specific properties of the catalyst drive the reaction in favor of a specific C–H bond. Initial data on site-selective aromatic C–H

activation were reported by Akita⁸ in 1982 where he functionalized indole at the 2-position (Figure 5.2). The reaction was believed to proceed through concerted protodemetalation.

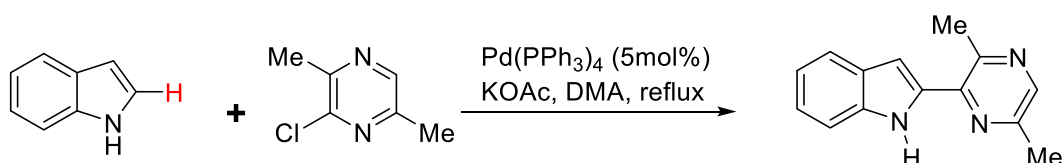


Figure 5.2 The first example of site selective C(sp²)-H activation

Recent advances in site-selective C–H functionalization of aromatic rings have led to the discovery of a new class of cross-coupling reactions named cross dehydrogenative coupling reactions (CDC). Early examples were reported by Fagnou and DeBoef on biaryl heterocoupling from unactivated arenes. Fangou⁹ reported the first example of coupling of protected indole with benzene, and DeBoef¹⁰ discovered site selective arylation of isooxazole (Figure 5.3 A, B). These reactions go through an oxidative coupling process that involves double C–H activation, followed by reductive elimination. Oxygen and copper salts proved to be efficient oxidants for this transformation. Also, elevated temperature was required for the best conversion.

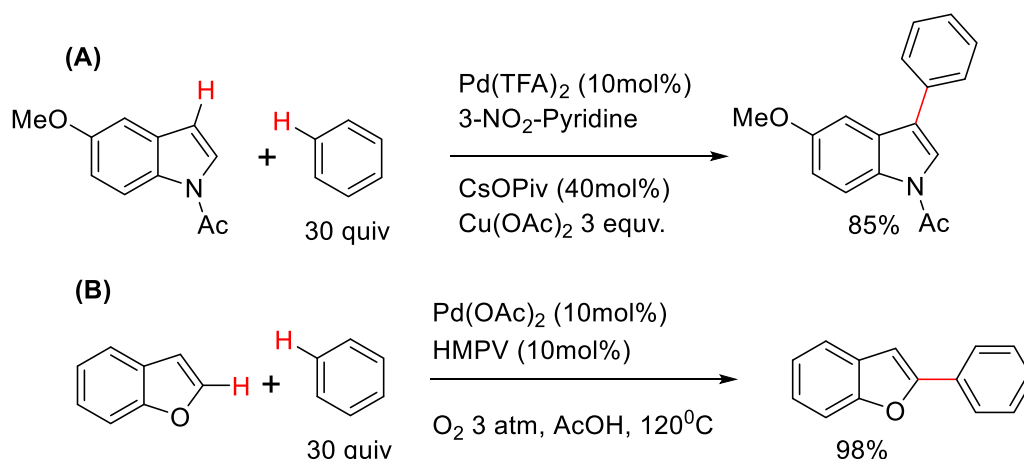


Figure 5.3 Regioselective cross dehydrogenative coupling

The breakthrough in the field of C–H functionalization happened with invention of new catalytic systems for regio-divergent C–H functionalization. A striking example in this area was presented by Carrow and coworkers, who designed new ancillary thioether ligands for regioselective arylation of heterocyclic compounds¹¹ (Figure 5.4). Using a thioether ligand, they alkenylated thiophene at the more hindered terminal position with high regioselectivity

(20:1). Traditional catalysts¹² prefer position 5 of thiophene, which is less-hindered. Their kinetic studies demonstrated that the thioether palladium complexes accelerated the reaction rate 800 times faster than other palladium catalysts. Moreover, they proposed the C–H bond cleavage as the rate-determining step, and that the rate acceleration upon coordination of thioether ligand happens through a change in the mechanism of the reaction from a neutral to

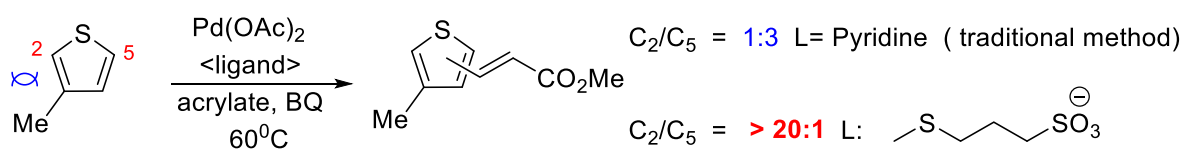


Figure 5.4 Regioselective arylation of heteroaryls using ancillary thioether ligands

a cationic pathway. Continuing efforts in this area have focused on the development of new strategies for regioselective functionalization of C–H bonds using auxiliary directing groups. The typical approach uses σ -chelating directing groups that facilitate ortho C–H functionalization through a rigid six-membered ring cyclic transition state¹³ (Figure 5.5 A). Despite the broad applications of this method, the inherent vicinal reactivity of these directing groups prevent access to the further C–H bonds. To overcome this challenge, the Yu¹⁴ group

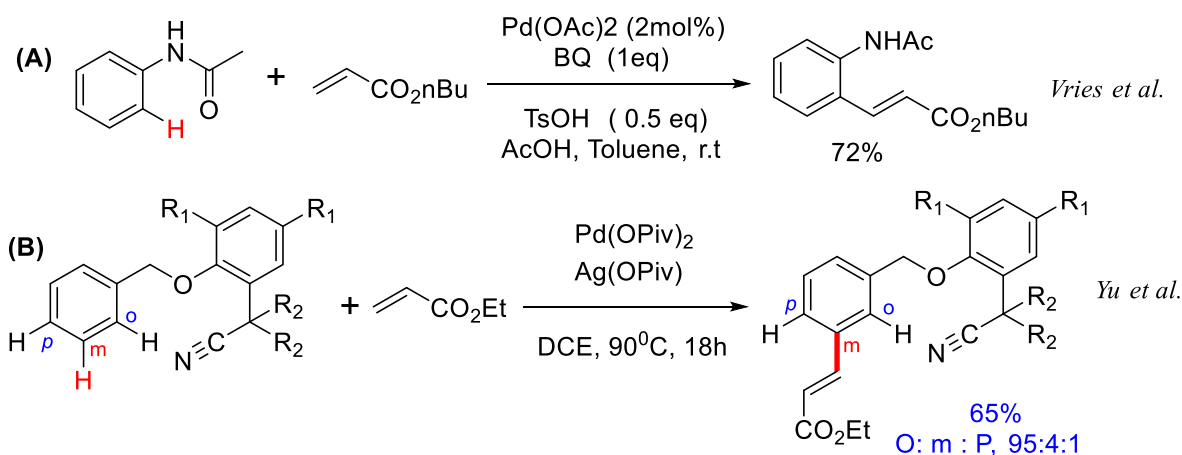


Figure 5.5 Auxiliary directed C–H functionalization at Ortho (A) and metha (B) positions

designed a nitrile-incorporated directing group that directs the activation of distal meta C–H bonds of the aryl group (Figure 5.5 B). The first classical example of C(sp³)-H functionalization dates back to the 1970s when Shilov reported C–H oxidation of methane¹⁵. This discovery inspired scientists to address challenge of storing methane gas by converting it to methanol using a variety of homogeneous¹⁶⁻¹⁷, heterogeneous¹⁸⁻¹⁹, or biomimetic

approaches²⁰⁻²¹. Over the past several decades, theoretical studies have highlighted new mechanistic insights about the C–H activation process²²⁻²⁴. These studies have provided chemists with new tools for addressing the challenge of C(sp³)-H functionalization. Numerous catalytic systems have been developed for a variety of transformations including halogenation²⁵⁻²⁶, arylation²⁷, alkenylation²⁸, and alkynylation²⁹ of C(sp³)-H bonds. However, existing methods usually employ palladium catalysts plus ancillary directing groups on the substrate to drive the cyclometallation mechanism to target the neighboring protons³⁰. Although ionic mechanisms for interception of distal protons is rare, several transition metal catalyzed radical [1,6]-H-abstractions have been reported for diverse C–H functionalization³¹⁻³². Copper-catalyzed functionalization of C(sp³)-H distal to the functional group is a quintessential example of this type of reaction²⁶ (Figure 5.6). Despite the radical mechanism, the reaction is sensitive to sterics and occurs at the less-hindered carbon.

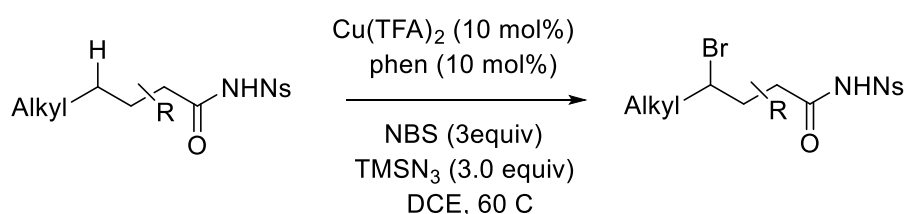


Figure 5.6 Distal C-H functionalization of aliphatic amide

Attempts to functionalize C(sp³)-H bonds with different selectivity and directing groups led to the exploration of amino acids as potential ligands for distal C–H functionalization²⁴. Jin Quan Yu has developed a variety of catalytic systems for C(sp³)-H activation using amino acid based ligands²⁴. His initial endeavors on C(sp³)-H activation included the use of derivatized carboxylic acids that incorporated an amide functionality as an X-type ligand³³. This sort of amide functional group can be manipulated to form a variety of useful products (Figure 5.7). The reactions typically need moderate to high temperatures and

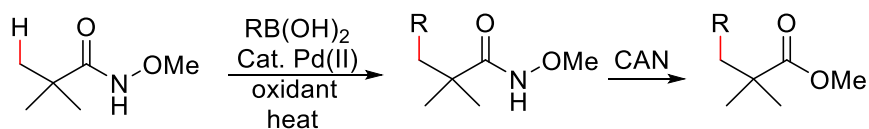


Figure 5.7 Distal beta C-H functionalization using removable directing group

strong oxidants plus expensive additives. Moreover, the use of a simple amino acid with at least one amide bond in the structure was also necessary. An elegant application of directing

group mediated C–H functionalization has been shown in the late stage manipulation of oligopeptides³⁴ (Figure 5.8).

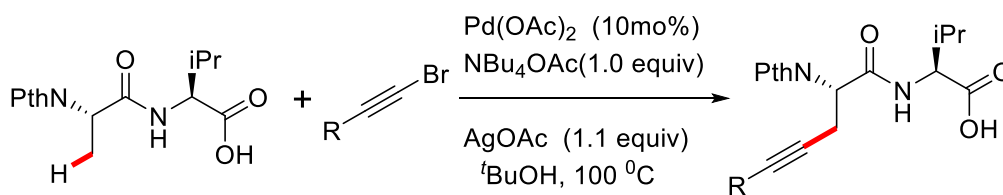


Figure 5.8 Late stage beta C–H functionalization of oligopeptide

This strategy is crucial for the success of peptide synthesis owing to the limitations associated with the non-proteinogenic amino acids. To increase the applicability of their catalytic system, Yu and coworkers designed a transient ligand for beta or gamma C–H functionalization of simple ketones and aldehydes^{27, 35} (Figure 5.9). To achieve selectivity, an amino acid ligand is

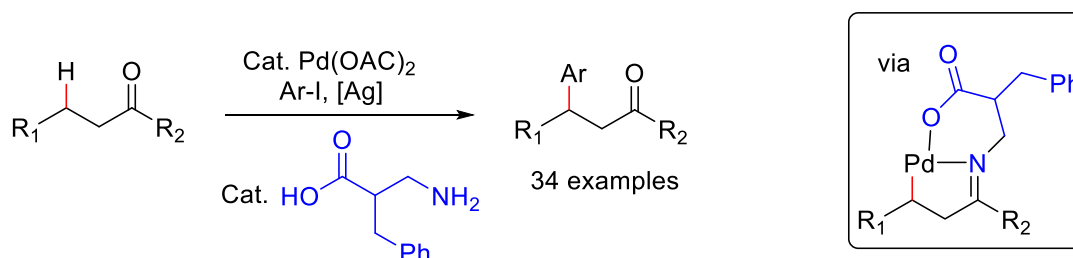


Figure 5.9 Beta functionalization of ketones using catalytic amount of transient directing group

used to condense with the carbonyl group, forming an imine derivative of the substrate that can bind and chelate palladium, leading to selective C–H activation. Using a chiral acetyl protected amino oxazoline ligand, The Yu group has also performed an enantioselective cross coupling of phenyl boronic acids with aliphatic amines²⁸. This transformation proceeds selectively to give the product arylated at the gamma position with respect to the amine. In this reaction

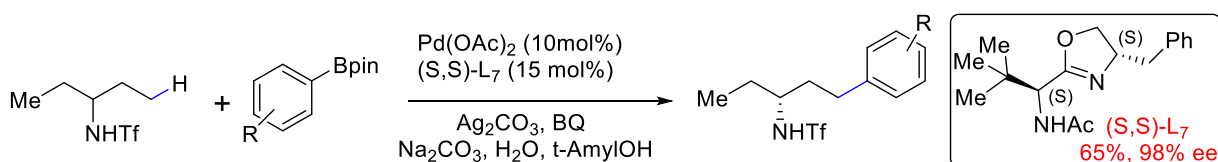


Figure 5.10 Enantioselective gamma functionalization desymmetrization using auxiliary ligand

desymmetrization of racemic starting material led to a chiral product with excellent enantiomeric excess (Figure 5.10).

Keywords: C-H bond activation, C-C bond activation, Palladium dimer, Boron ligand

5.1.1 New ligand design for regioselective transformations

In the Michaelis Laboratory, we are interested in the potential of heterobimetallic complexes as a tool for developing new organic reactions. In particular, we are developing new catalysts for enhanced reactivity and diverse selectivity in a variety of reactions, including for C–H functionalization. Our approach includes incorporation of a Lewis acid into the structure of a ligand that binds to the transition metal catalyst. The role of the Lewis acid is to bind to a heteroatom on our substrate and bring it into close proximity to the late transition metal. This proximity effect will improve reaction kinetics and selectivity by preorganizing the reacting substrate near the active catalyst. For example, a ligand for a transition metal catalyst that contains a titanium center could coordinate a Lewis Basic functional group such as a ketone and bring the substrate into close proximity to the metal catalyst (Figure 5.11). The substrate binding could then enable selective activation of a C–H bond by a palladium center. These

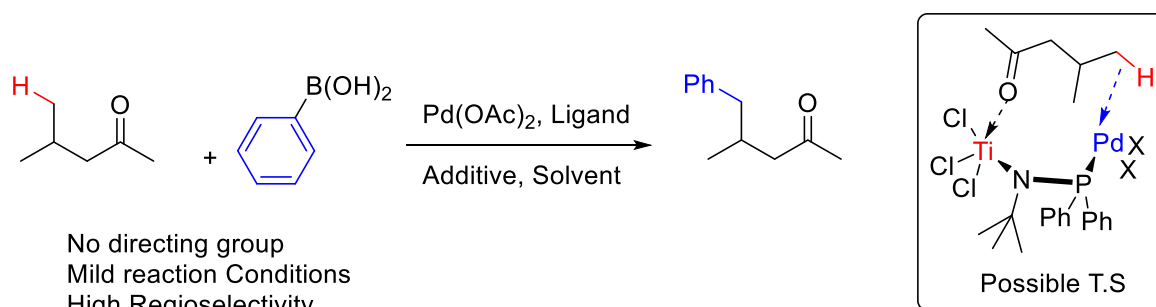


Figure 5.11 Cooperative heterobimetallic approach for C-H activation

proximity effects could also offset the harsh conditions that are generally required for this type of C–H activation catalyst. In addition, immobilization of the substrate between the Lewis acid and the late transition metal provides an opportunity to influence the regioselectivity of a reaction by holding specific reactive functionality, such as C–H bonds, in close proximity to the metal catalyst.

To this aim, this section will describe our efforts to synthesize new ligand frameworks that enable this type of cooperative catalysis. As a starting point, we designed and synthesized numerous ligands containing different Lewis acids and various organic tethers (Figure 5.12). Ligands A³⁶, B³⁶, E³⁶⁻³⁷, I³⁶, H³⁸, and K³⁸ have been previously reported and we prepared these complexes according to literature procedures from the corresponding phosphinoamine or diol precursor. The synthesis for new ligands structures is described below. These ligands gave us

a variety of coordination environments around both titanium and boron Lewis acids and the possibility to bind a second transition metal at the phosphine or amide functional groups. Our strategy for the synthesis of each of the new ligand frameworks is convenient and straightforward. Representative synthetic plans for these new ligands are shown in Figure 5.13.

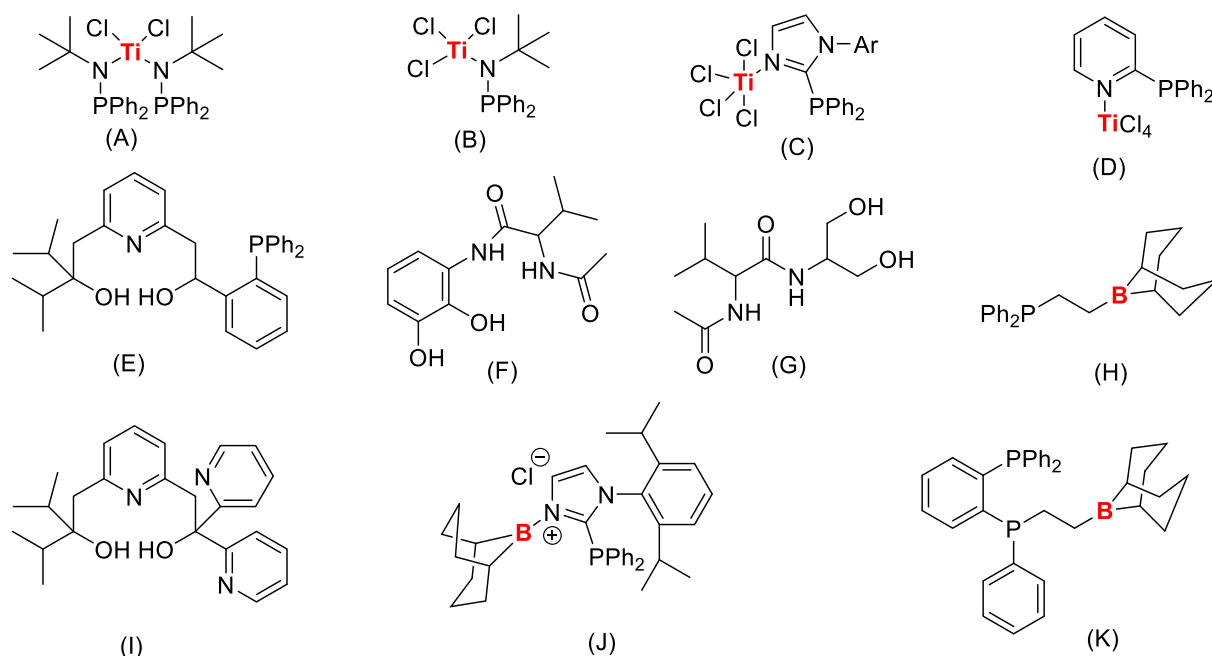


Figure 5.12 New ligand design for heterobimetallic catalysis

Ligands C and J have a common imidazolo-pyridine core, which is synthesized by deprotonation of an *N*-arylimidazole with *n*-butyl lithium at the 2-position followed by reaction of this anionic intermediate with chlorodiphenyl phosphine (Figure 5.13a). This 1-diphenylphosphinoimidazole is then reacted with either TiCl_4 or 9-BBN-Cl to give the final product in quantitative yield. Single crystals of the ligands C and J were grown via slow evaporation of benzene solution and the structure of each ligand was confirmed by X-ray crystallography (Figure 5.14). A noticeable difference between ligand C and J was detected by crystal structure analysis where the structures of the ligand J proved to be zwitterionic as opposed to ligand C which is neutral. The later was confirmed to form only a dative interaction between titanium and the nitrogen of the imidazole ring. The structure of the other newly made ligands were also fully identified by NMR analysis. Ligand D (Figure 5.13b) was also synthesized in a similar manner to ligand C. Diol-containing ligands F and G were synthesized following the procedure seen in Figure 5.13c and d. These diol ligands can bind a titanium center at the diol functional group, then enable binding of a palladium atom at the two amide

nitrogens. These ligands have been metallated with titanium and their metal-containing structures are currently being analyzed by NMR spectroscopy and we are attempting to grow X-ray quality single crystals to confirm their structure. The activity of each of the ligands in

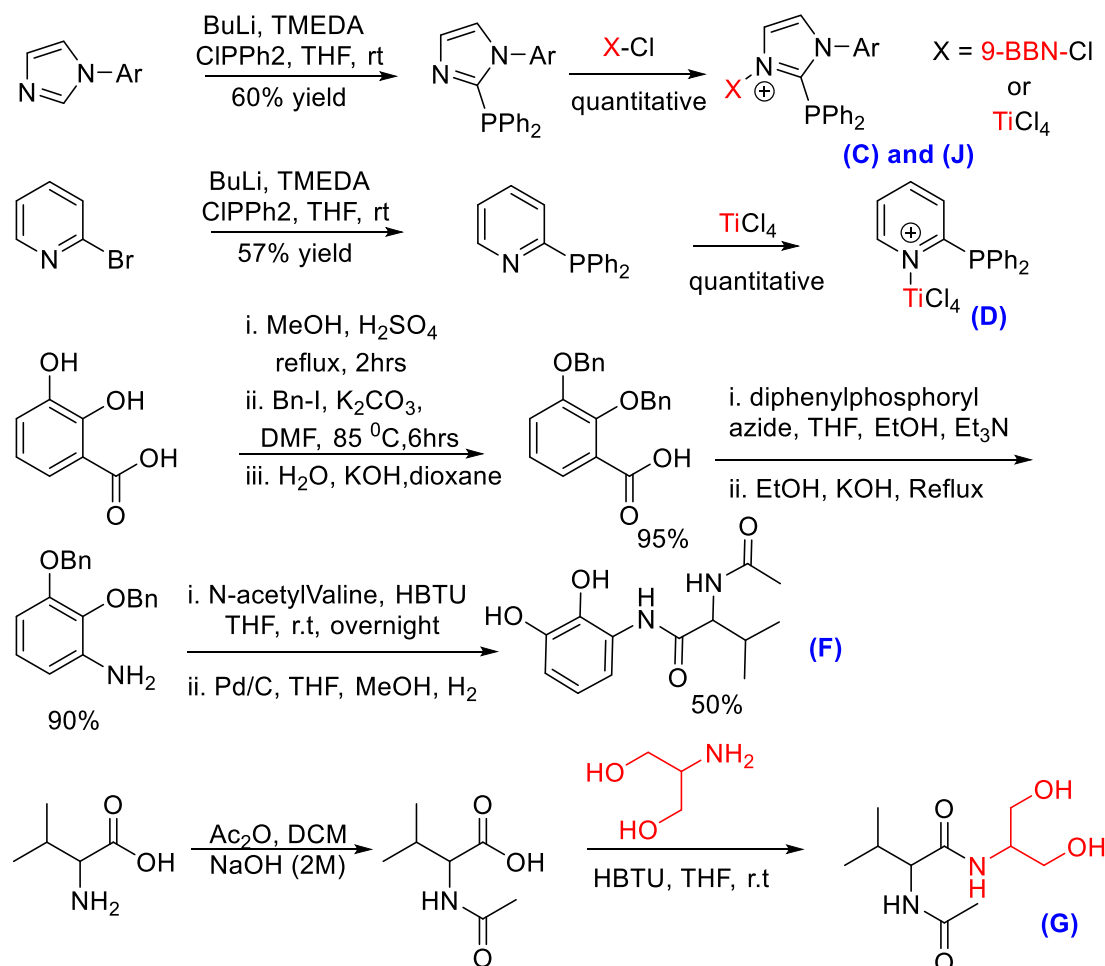


Figure 5.13 Synthesis pathway for newly designed ligands

Figure 5.13 was next tested in various organic reactions, including C (sp^3)-H activation. For ligands E, F, G, I, which do not have a Lewis acid in their structure, $\text{Ti}(\text{O}-i\text{Pr})_4$ was mixed with the ligands for *in situ* formation of the Lewis acid incorporated ligand. The formation of new titanium-containing species was confirmed by $^1\text{H-NMR}$ as the chemical shifts shifted distinctly in the aliphatic area. Addition of the second metal (palladium in this case) constructed the heterobimetallic complex. Although the structure of the heterobimetallic complexes have not been identified yet by crystallography, $^1\text{H-NMR}$ clearly showed they were assembled as the chemical shifts changed or became broad after addition of the second metal. After *in situ* formation of our heterobimetallic complexes, appropriate reagents were added to test the

reactivity of the complexes. Importantly, when octanol and phenyl iodide were used as the substrates and exposed to a reaction containing ligand (G) and Pd(OAc)₂, a mixture of arylation products were observed in moderate yield (Figure 5.15). Other ligands were not active in this reaction. This result is exciting because it represents the first example of C(sp³)-H

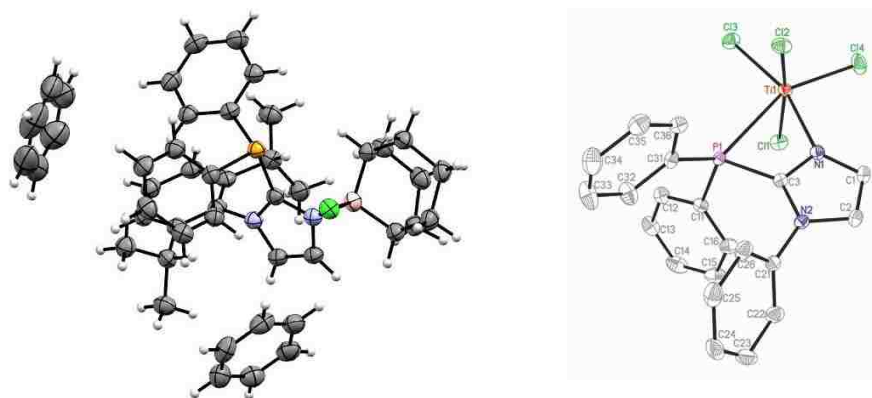


Figure 5.14 Crystal structure of the ligands (C) and (J)

activation where a simple alcohol acts as the directing group. Our hypothesis is that the titanium center binds to the alcohol functional group and holds the substrate in close proximity to the palladium center. This leads to C-H activation by the palladium, followed by arylation with phenyl iodide. We are currently optimizing this transformation both for yield and selectivity.

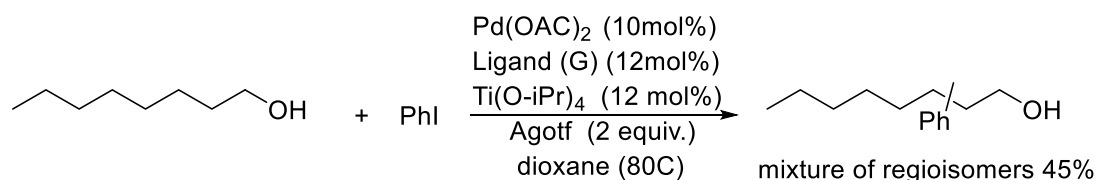


Figure 5.15 Activity of the ligand (G) in C(SP3)-H activation

In our attempts to develop C-H functionalization reactions with these new bimetallic ligand structures, we found new reactivity when using boron-containing ligand J (Figure 5.16). When 3-methyl-2-pentanone was employed as substrate for C(sp³)-H arylation using ligand J and Pd(OAc)₂, a new product was observed. Initial NMR analysis and mass spectrometry experiments on the structure of the product indicated that a C-C bond cleavage occurred on the ketone substrate. According to ¹H-NMR analysis, a doublet at δ=8.0 belongs to an aromatic proton adjacent to an electron withdrawing group (carbonyl or sulfonyl). Also, the methylene group on the sec-butyl group shows an abnormally high chemical shift at δ=3.0 indicating the

proximity to an electron withdrawing group. However, ^{13}C -NMR together with advanced 2D-NMR experiments like HMBC decline the possibility of every carbonyl group in the structure. IR studies also confirm the SO_2 group, but not the carbonyl group. The formation of these products suggest that the C-C bond between carbonyl and the bigger chain in the starting material has been cleaved and, surprisingly, the acetyl moiety is not present in the structure of the final product. Instead, the presumed product contains a sulfonyl group sandwiched between

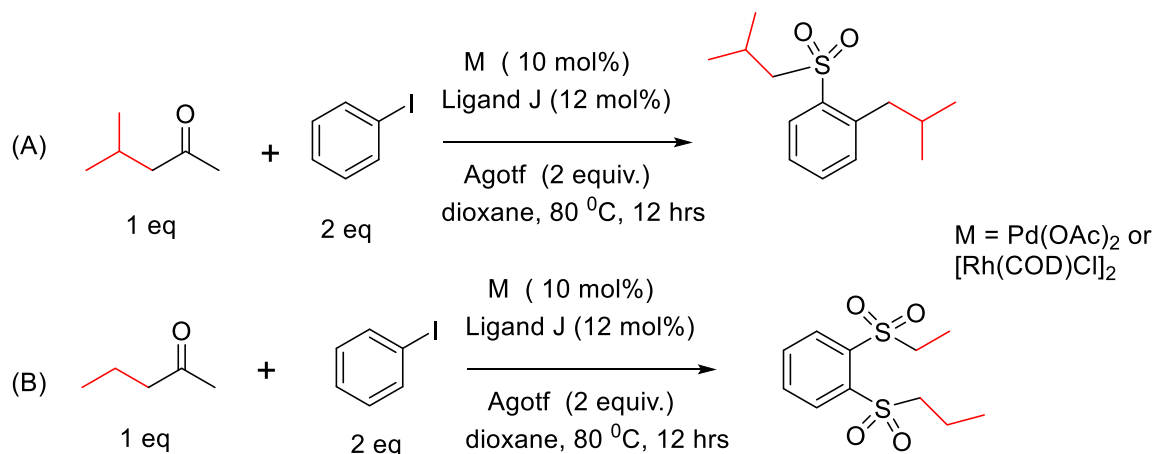


Figure 5.16 Activity of the ligand (J) in C(SP³)-H functionalization

the phenyl ring and sec-butyl moieties. Also one of the sec-butyl groups is directly bound to the phenyl ring (Figure 5.16a). In order to gain a better understanding of the structure of the product, we also tested 2-pentanone in the reaction. In this transformation, we observed products corresponding to incorporation of both sulfano propyl group and a butanosulfonyl group, suggesting a new type of mechanism for C–C bond activation and cross coupling (Figure 5.16b). Other ligands did not show any activity in this reaction. Our control experiment with different nonmetallic ligands and various reaction conditions revealed that the presence of borane in the structure of the ligand is necessary as we did not get any product under other reaction conditions. In an attempt to understand the reactivity of Ligand J under these reaction conditions, we crystalized various derivatives of Ligand J with both PdCl_2 and $\text{Pd}(\text{OAc})_2$ (Figure 5.17). Interestingly, when palladium acetate is employed as the precursor, a new Pd(I) dimer structure is obtained (Figure 5.17a). Alternatively, when PdCl_2 is used instead of $\text{Pd}(\text{OAc})_2$, a similar bimetallic complex is formed, but this time the palladium centers are both at the Pd(II) oxidation state with the overall complex being cationic (Figure 5.17b). In contrast, when the phosphino-imidazole ligand that lacks the boron center is used as the ligand precursor, a completely metal complex is obtained where the palladium has inserted between the

phosphorous and the imidazole ring (Figure 5.17c). Interestingly, in the reaction described in Figure 5.16, the boron atom is essential for reactivity; when the phosphino-imidazole ligand is used that does not contain boron, no product forms. This result suggests that formation of the bimetallic palladium species may be necessary for the transformation to occur³⁹. We are currently investigating the stoichiometric reactivity of these palladium dimer complexes and optimizing this new C–C bond activation reaction as a new synthetic approach to C–C bond activation for cross coupling.

We have also explored the reactivity of the ligand (J) in the Heck reactions with conjugated carboxylic acids. While the reaction of acrylic acid and phenyl iodide went to completion with ligand J, other ligands showed much lower reactivity (Figure 5.18 A-D). The results of the table in Figure 5.18 show significant enhancement in reactivity for our heterobimetallic complex (entry A) as compared to other ligands (entry B-D). While the reaction proceeds to 20% conversion when no ligand was used, triphenyl phosphine improved the conversion to 45% (entry B). The heterobimetallic Ti–Pd complex composed of ligand E reported by other groups provided 60% conversion under otherwise equal conditions (entry C). These results show the preference of our ligand in this reaction and suggest that the formation of bimetallic palladium dimers may serve to enhance reactivity in the Heck reaction as well.

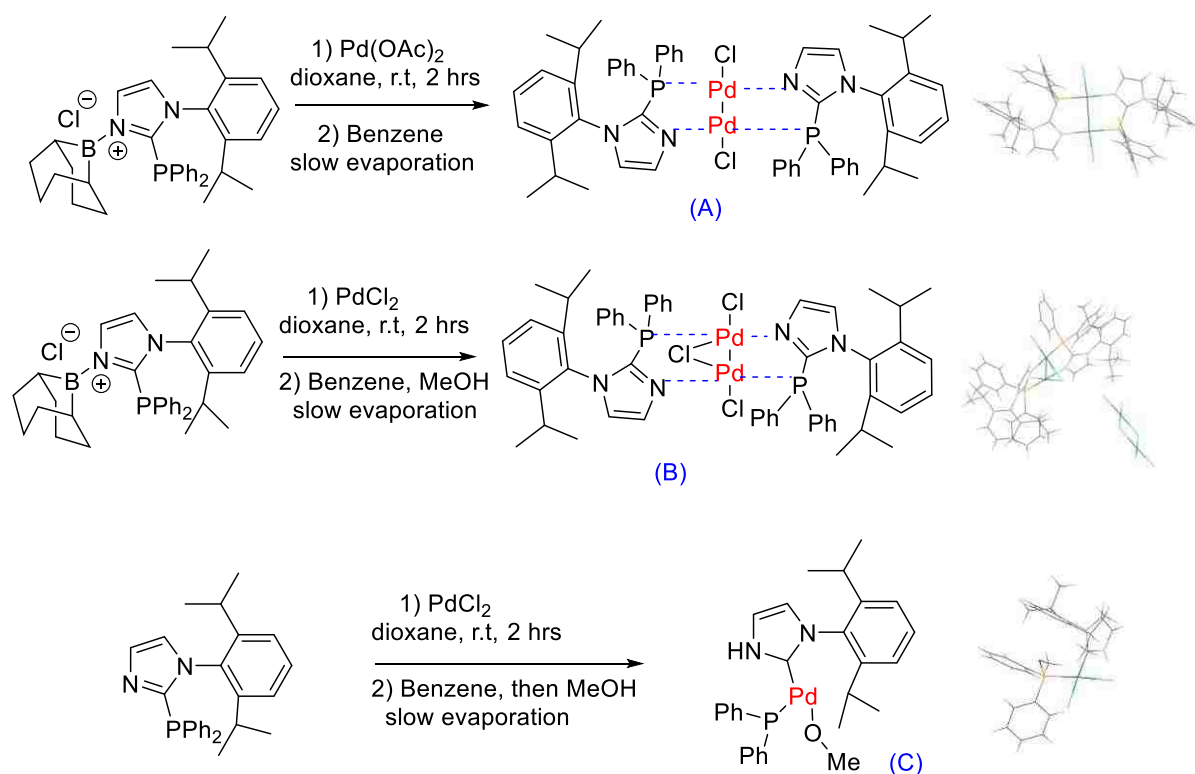


Figure 5.17 Synthetic route and the crystal structure of the bimetallic complexes using ligand (J) and different metal precursors (A) $\text{Pd}(\text{OAc})_2$, (B) PdCl_2 , and (C) phosphinoimidazole

Our future directions on this project include synthesis, crystallization, and study of the structure of the heterobimetallic and homobimetallic complexes with ligands G and J. With ligand G, we will optimize the reactivity of this complex in C–H arylation of simple alcohols and determine whether the ligand structure can help influence the reactivity of the arylation. We will also investigate the stoichiometric reactivity of the palladium dimers with each of the reagents in this transformation in an attempt to understand the new reactivity observed. These results will provide useful information about the potential of these bimetallic complexes to facilitate C–C activation processes⁴⁰.

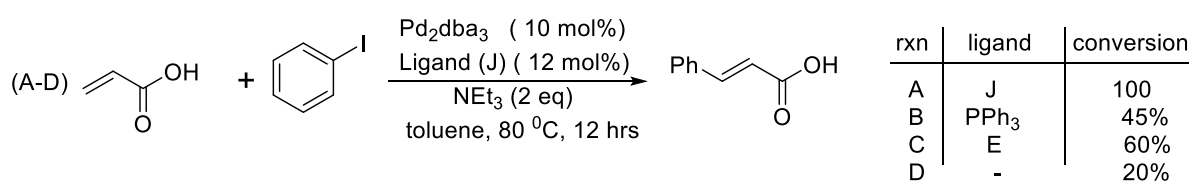


Figure 5.18 Activity of the ligand J in the Heck reaction and comparison with conventional methods

Our future directions on this project include synthesis, crystallization, and study of the structure of the heterobimetallic and homobimetallic complexes with ligands G and J. With ligand G, we will optimize the reactivity of this complex in C–H arylation of simple alcohols and determine whether the ligand structure can help influence the reactivity of the arylation. We will also investigate the stoichiometric reactivity of the palladium dimers with each of the reagents in this transformation in an attempt to understand the new reactivity observed. These results will provide useful information about the potential of these bimetallic complexes to facilitate C–C activation processes.

5.2 References

1. Roudesly, F.; Oble, J.; Poli, G., Metal-catalyzed CH activation/functionalization: The fundamentals. *Journal of Molecular Catalysis A: Chemical* **2017**, *426*, 275-296.
2. Xue, X.-S.; Ji, P.; Zhou, B.; Cheng, J.-P., The essential role of bond energetics in C–H activation/functionalization. *Chemical Reviews* **2017**, *117* (13), 8622-8648.
3. Volhard, J., Ueber Verbindungen des Thiophens, seiner Homologen und einiger Ketone mit Quecksilberchlorid. *Justus Liebigs Annalen der Chemie* **1892**, *267* (2-3), 172-185.
4. Dimroth, O., Ber. dtsh. chem. Ges. 1898, 31, 2154. *Wiley Online Library| CAS Ber. dtsh. chem. Ges* **1899**, *32*, 758.

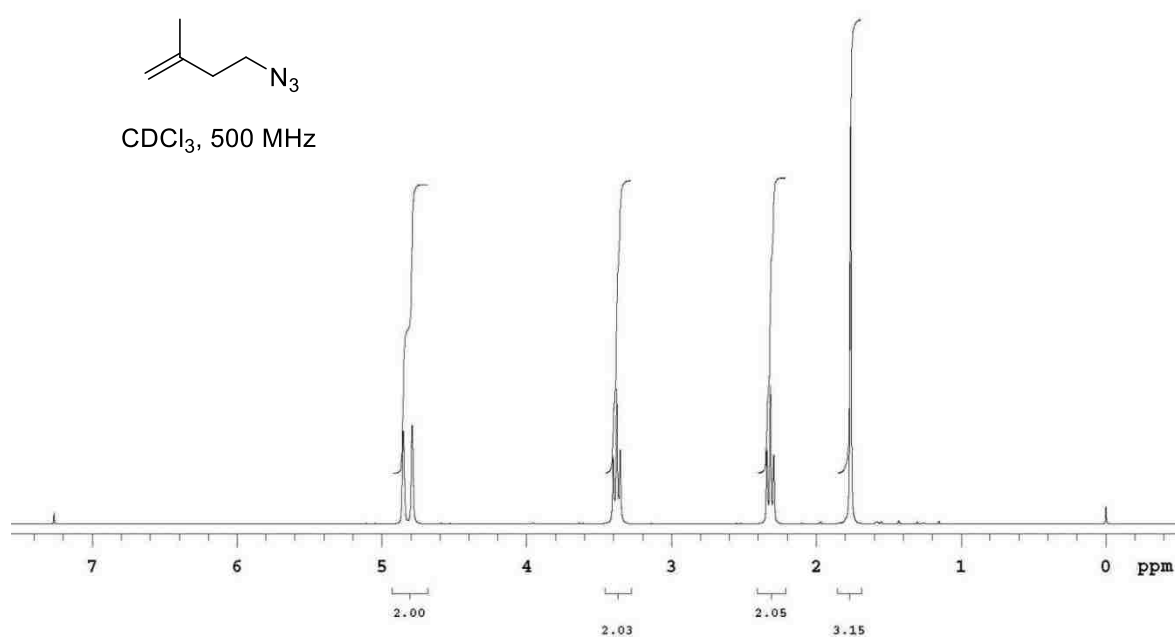
5. Kharasch, M.; Isbell, H. S., The chemistry of organic gold compounds. III. Direct introduction of gold into the aromatic nucleus (Preliminary communication). *Journal of the American Chemical Society* **1931**, *53* (8), 3053-3059.
6. Nakamura, N.; Tajima, Y.; Sakai, K., Direct Phenylation of Isoxazoles Using Palladium Catalysts Synthesis of 4-Phenylmuscimol. *Chemischer Informationsdienst* **1982**, *13* (33), no-no.
7. Neufeldt, S. R.; Sanford, M. S., Controlling site selectivity in palladium-catalyzed C–H bond functionalization. *Accounts of Chemical Research* **2012**, *45* (6), 936-946.
8. Akita, Y.; Ohta, A., Facile Synthesis Of (Z)-And (E)-2, 5-Dimethyl-3-Styrylpyrazine, Isolated From The Argentine Ants. *Chemischer Informationsdienst* **1982**, *13* (32), no-no.
9. Stuart, D. R.; Fagnou, K., The catalytic cross-coupling of unactivated arenes. *Science* **2007**, *316* (5828), 1172-1175.
10. Dwight, T. A.; Rue, N. R.; Charyk, D.; Josselyn, R.; DeBoef, B., C–C bond formation via double C–H functionalization: aerobic oxidative coupling as a method for synthesizing heterocoupled biaryls. *Organic Letters* **2007**, *9* (16), 3137-3139.
11. Gorsline, B. J.; Wang, L.; Ren, P.; Carrow, B. P., C–H Alkenylation of Heteroarenes: Mechanism, Rate, and Selectivity Changes Enabled by Thioether Ligands. *Journal of the American Chemical Society* **2017**, *139* (28), 9605-9614.
12. Yanagisawa, S.; Ueda, K.; Sekizawa, H.; Itami, K., Programmed Synthesis of Tetraarylthiophenes through Sequential C–H Arylation. *Journal of the American Chemical Society* **2009**, *131* (41), 14622-14623.
13. Boele, M. D.; van Strijdonck, G. P.; De Vries, A. H.; Kamer, P. C.; de Vries, J. G.; van Leeuwen, P. W., Selective Pd-catalyzed oxidative coupling of anilides with olefins through C–H bond activation at room temperature. *Journal of the American Chemical Society* **2002**, *124* (8), 1586-1587.
14. Jin, Z.; Chu, L.; Chen, Y.-Q.; Yu, J.-Q., Pd-Catalyzed Remote Meta-C–H Functionalization of Phenylacetic Acids Using a Pyridine Template. *Organic Letters* **2018**, *20* (2), 425-428.
15. Wang, V. C.-C.; Maji, S.; Chen, P. P.-Y.; Lee, H. K.; Yu, S. S.-F.; Chan, S. I., Alkane oxidation: methane monooxygenases, related enzymes, and their biomimetics. *Chemical Reviews* **2017**, *117* (13), 8574-8621.
16. Shilov, A. E.; Shul'pin, G. B., Activation of C–H bonds by metal complexes. *Chemical Reviews* **1997**, *97* (8), 2879-2932.

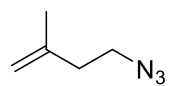
17. Periana, R. A.; Taube, D. J.; Gamble, S.; Taube, H.; Satoh, T.; Fujii, H., Platinum catalysts for the high-yield oxidation of methane to a methanol derivative. *Science* **1998**, *280* (5363), 560-564.
18. Liu, H.; Liu, R.; Liew, K. Y.; Johnson, R.; Lunsford, J., Partial oxidation of methane by nitrous oxide over molybdenum on silica. *Journal of the American Chemical Society* **1984**, *106* (15), 4117-4121.
19. Smeets, P. J.; Groothaert, M. H.; Schoonheydt, R. A., Cu based zeolites: A UV–vis study of the active site in the selective methane oxidation at low temperatures. *Catalysis today* **2005**, *110* (3-4), 303-309.
20. Sirajuddin, S.; Rosenzweig, A. C., Enzymatic oxidation of methane. *Biochemistry* **2015**, *54* (14), 2283-2294.
21. Tinberg, C. E.; Lippard, S. J., Dioxygen activation in soluble methane monooxygenase. *Accounts of Chemical Research* **2011**, *44* (4), 280-288.
22. Yu, J.-Q.; Shi, Z., *CH activation*. Springer: 2010; Vol. 292.
23. Ackermann, L.; Vicente, R.; Potukuchi, H. K.; Pirovano, V., Mechanistic insight into direct arylations with ruthenium (II) carboxylate catalysts. *Organic Letters* **2010**, *12* (21), 5032-5035.
24. Yang, Y.-F.; Hong, X.; Yu, J.-Q.; Houk, K., Experimental–Computational Synergy for Selective Pd (II)-Catalyzed C–H Activation of Aryl and Alkyl Groups. *Accounts of chemical Research* **2017**, *50* (11), 2853-2860.
25. Lyons, T. W.; Sanford, M. S., Palladium-catalyzed ligand-directed C–H functionalization reactions. *Chemical Reviews* **2010**, *110* (2), 1147-1169.
26. Liu, T.; Myers, M. C.; Yu, J. Q., Copper-Catalyzed Bromination of C (sp³)–H Bonds Distal to Functional Groups. *Angewandte Chemie* **2017**, *129* (1), 312-315.
27. Hong, K.; Park, H.; Yu, J.-Q., Methylene C (sp³)–H Arylation of Aliphatic Ketones Using a Transient Directing Group. *ACS catalysis* **2017**, *7* (10), 6938-6941.
28. Shao, Q.; Wu, Q.-F.; He, J.; Yu, J.-Q., Enantioselective γ -C (sp³)–H Activation of Alkyl Amines via Pd (II)/Pd (0) Catalysis. *Journal of the American Chemical Society* **2018**, *140* (16), 5322-5325.
29. Fu, H.; Shen, P. X.; He, J.; Zhang, F.; Li, S.; Wang, P.; Liu, T.; Yu, J. Q., Ligand-Enabled Alkynylation of C (sp³)–H Bonds with Palladium (II) Catalysts. *Angewandte Chemie* **2017**, *129* (7), 1899-1902.

30. Xu, H.-J.; Lu, Y.; Farmer, M. E.; Wang, H.-W.; Zhao, D.; Kang, Y.-S.; Sun, W.-Y.; Yu, J.-Q., Rh (III)-Catalyzed meta-C–H Olefination Directed by a Nitrile Template. *Journal of the American Chemical Society* **2017**, *139* (6), 2200-2203.
31. Barton, D.; Beaton, J.; Geller, L.; Pechet, M., A New Photochemical Reaction. *Journal of the American Chemical Society* **1961**, *83* (19), 4076-4083.
32. Barton, D.; Beaton, J.; Geller, L.; Pechet, M., A new photochemical reaction. *Journal of the American Chemical Society* **1960**, *82* (10), 2640-2641.
33. Wang, D.-H.; Wasa, M.; Giri, R.; Yu, J.-Q., Pd (II)-catalyzed cross-coupling of sp³ C–H bonds with sp² and sp³ boronic acids using air as the oxidant. *Journal of the American Chemical Society* **2008**, *130* (23), 7190-7191.
34. Liu, T.; Qiao, J. X.; Poss, M. A.; Yu, J. Q., Palladium (II)-Catalyzed Site-Selective C (sp³)–H Alkynylation of Oligopeptides: A Linchpin Approach for Oligopeptide–Drug Conjugation. *Angewandte Chemie International Edition* **2017**, *56* (36), 10924-10927.
35. Chen, Y.-Q.; Wang, Z.; Wu, Y.; Wisniewski, S. R.; Qiao, J. X.; Ewing, W. R.; Eastgate, M. D.; Yu, J.-Q., Overcoming the Limitations of γ - and δ -C–H Arylation of Amines through Ligand Development. *Journal of the American Chemical Society* **2018**, *140* (51), 17884-17894.
36. Sunada, Y.; Sue, T.; Matsumoto, T.; Nagashima, H., Titanium (IV) phosphinoamide as a unique bidentate ligand for late transition metals II: Ti Ru heterobimetallics bearing a bridging chlorine atom. *Journal of Organometallic Chemistry* **2006**, *691* (14), 3176-3182.
37. Suzuki, N.; Yoneyama, S.; Shiba, K.; Hasegawa, T.; Masuyama, Y., Synthesis of O, N, OP multidentate ligands and the formation of early–late heterobimetallic complexes. *Inorganica Chimica Acta* **2018**, *471*, 355-363.
38. Hirata, G.; Satomura, H.; Kumagae, H.; Shimizu, A.; Onodera, G.; Kimura, M., Direct Allylic Amination of Allylic Alcohol Catalyzed by Palladium Complex Bearing Phosphine–Borane Ligand. *Organic Letters* **2017**, *19* (22), 6148-6151.
39. Jalan, A.; Kastner, DW.; Webber, KGI.; Smith, MS.; Castle, SL., Bulky Dehydroamino Acids Enhance Proteolytic Stability and Folding in β -Hairpin Peptides. *Organic Letters* **2017**, *19* (19), 5190-5193.
40. Rigby, C.R.; Bhowmik, P.; Bahari, M.; Chang, A.; Harb, J.; Lewis, R.; Watt, J. Soluble viologen polymers as carbohydrate oxidation catalysts for alkaline carbohydrate fuel cells. *Journal of Electroanalytical Chemistry*, **2018**, *823*, 416-421.

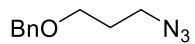
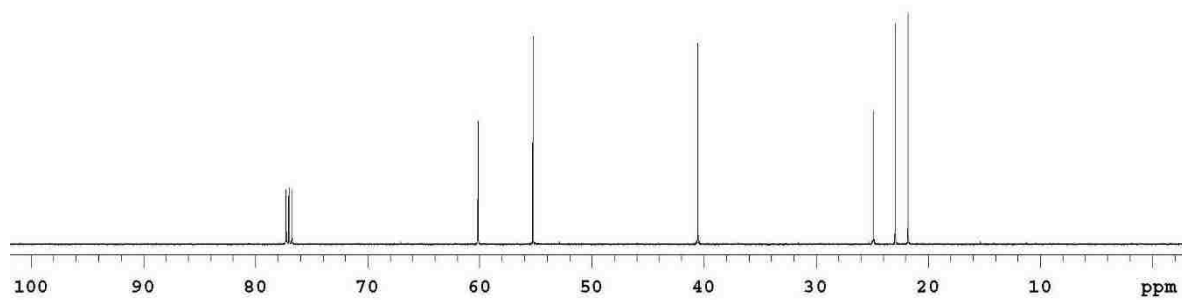
Appendix A

Spectral Images for Chapter 1, 2, and 3

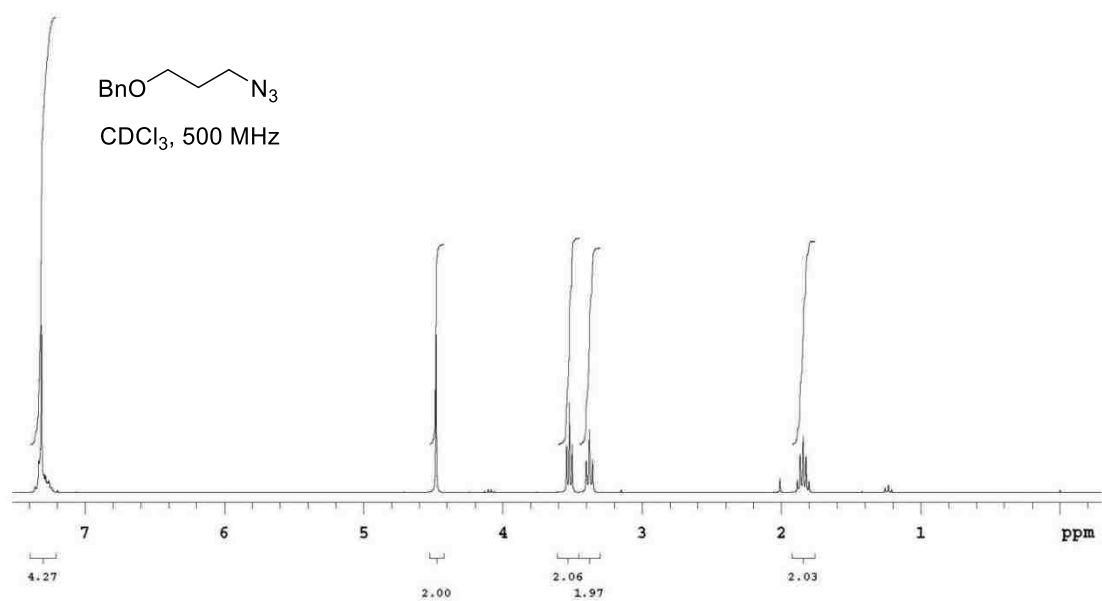


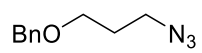


CDCl₃, 500 MHz

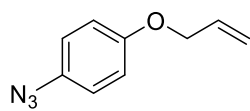
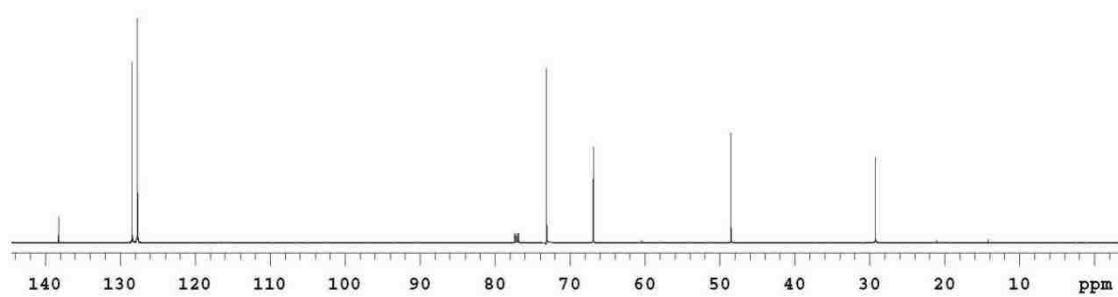


CDCl₃, 500 MHz

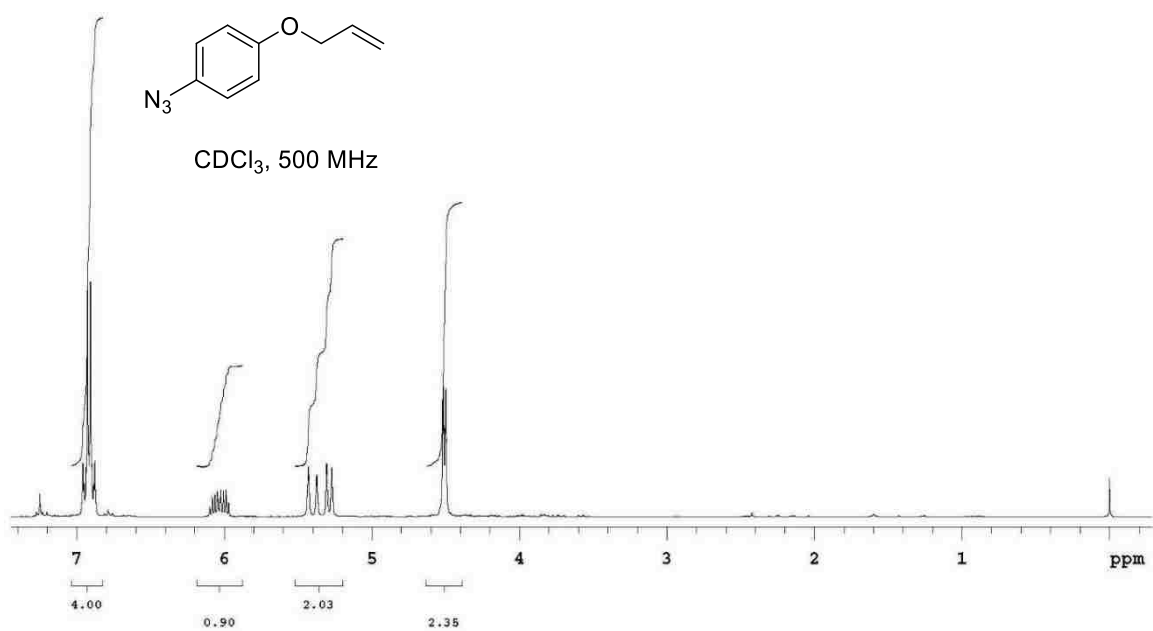


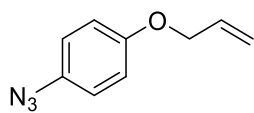


CDCl₃, 500 MHz

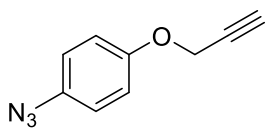
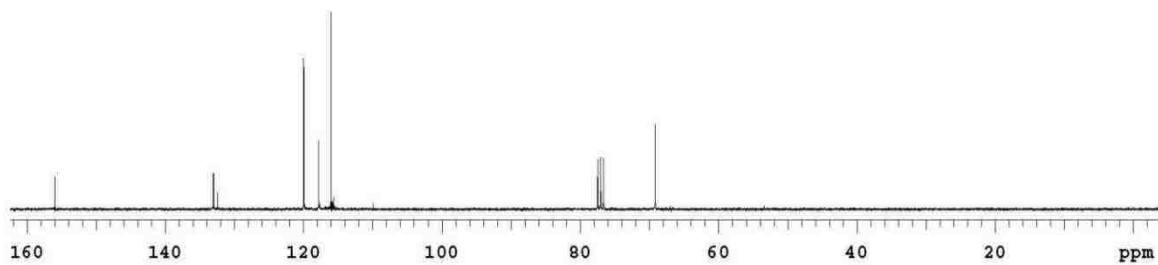


CDCl₃, 500 MHz





CDCl₃, 500 MHz



CDCl₃, 500MHz

